

Pertanika Journal of

SCIENCE &

TECHNOLOGY

JST

VOL. 33 (S3) 2025

A Special Issue devoted to

**Exploring Future Innovation and Sustainability in Engineering
and Computing Technologies**

Guest Editors

Mohd Sobri Takriff, Mazidah Puteh and Norulhidayah Isa



PERTANIKA
JOURNALS

A scientific journal published by Universiti Putra Malaysia Press

PERTANIKA JOURNAL OF SCIENCE & TECHNOLOGY

About the Journal

Overview

Pertanika Journal of Science & Technology is an official journal of Universiti Putra Malaysia. It is an open-access online scientific journal. It publishes original scientific outputs. It neither accepts nor commissions third party content.

Recognised internationally as the leading peer-reviewed interdisciplinary journal devoted to the publication of original papers, it serves as a forum for practical approaches to improve quality on issues pertaining to science and engineering and its related fields.

Pertanika Journal of Science & Technology currently publishes 6 issues a year (*January, March, April, July, August, and October*). It is considered for publication of original articles as per its scope. The journal publishes in **English** and it is open for submission by authors from all over the world.

The journal is available world-wide.

Aims and scope

Pertanika Journal of Science & Technology aims to provide a forum for high quality research related to science and engineering research. Areas relevant to the scope of the journal include: bioinformatics, bioscience, biotechnology and bio-molecular sciences, chemistry, computer science, ecology, engineering, engineering design, environmental control and management, mathematics and statistics, medicine and health sciences, nanotechnology, physics, safety and emergency management, and related fields of study.

History

Pertanika Journal of Science & Technology was founded in 1993 and focuses on research in science and engineering and its related fields.

Vision

To publish a journal of international repute.

Mission

Our goal is to bring the highest quality research to the widest possible audience.

Quality

We aim for excellence, sustained by a responsible and professional approach to journal publishing. Submissions can expect to receive a decision within 90 days. The elapsed time from submission to publication for the articles averages 180 days. We are working towards decreasing the processing time with the help of our editors and the reviewers.

Abstracting and indexing of Pertanika

Pertanika Journal of Science & Technology is now over 33 years old; this accumulated knowledge and experience has resulted the journal being abstracted and indexed in SCOPUS (Elsevier), Journal Citation Reports (JCR-Clarivate), EBSCO, ASEAN CITATION INDEX, Microsoft Academic, Google Scholar, and MyCite.

Citing journal articles

The abbreviation for Pertanika Journal of Science & Technology is *Pertanika J. Sci. & Technol.*

Publication policy

Pertanika policy prohibits an author from submitting the same manuscript for concurrent consideration by two or more publications. It prohibits as well publication of any manuscript that has already been published either in whole or substantial part elsewhere. It also does not permit publication of manuscript that has been published in full in proceedings.

Code of Ethics

The *Pertanika* journals and Universiti Putra Malaysia take seriously the responsibility of all of its journal publications to reflect the highest in publication ethics. Thus, all journals and journal editors are expected to abide by the journal's codes of ethics. Refer to *Pertanika's Code of Ethics* for full details, or visit the journal's web link at http://www.pertanika.upm.edu.my/code_of_ethics.php

Originality

The author must ensure that when a manuscript is submitted to *Pertanika*, the manuscript must be an original work. The author should check the manuscript for any possible plagiarism using any program such as Turn-It-In or any other software before submitting the manuscripts to the *Pertanika* Editorial Office, Journal Division.

All submitted manuscripts must be in the journal's acceptable similarity index range:
≤ 20% – PASS; > 20% – REJECT.

International Standard Serial Number (ISSN)

An ISSN is an 8-digit code used to identify periodicals such as journals of all kinds and on all media—print and electronic.

Pertanika Journal of Science & Technology: e-ISSN 2231-8526 (Online).

Lag time

A decision on acceptance or rejection of a manuscript is reached in 90 days (average). The elapsed time from submission to publication for the articles averages 180 days.

Authorship

Authors are not permitted to add or remove any names from the authorship provided at the time of initial submission without the consent of the journal's Chief Executive Editor.

Manuscript preparation

For manuscript preparation, authors may refer to *Pertanika*'s **INSTRUCTION TO AUTHORS**, available on the official website of *Pertanika*.

Editorial process

Authors who complete any submission are notified with an acknowledgement containing a manuscript ID on receipt of a manuscript, and upon the editorial decision regarding publication.

Pertanika follows a **double-blind peer-review** process. Manuscripts deemed suitable for publication are sent to reviewers. Authors are encouraged to suggest names of at least 3 potential reviewers at the time of submission of their manuscripts to *Pertanika*, but the editors will make the final selection and are not, however, bound by these suggestions.

Notification of the editorial decision is usually provided within 90 days from the receipt of manuscript. Publication of solicited manuscripts is not guaranteed. In most cases, manuscripts are accepted conditionally, pending an author's revision of the material.

The journal's peer review

In the peer-review process, 2 to 3 referees independently evaluate the scientific quality of the submitted manuscripts. At least 2 referee reports are required to help make a decision.

Peer reviewers are experts chosen by journal editors to provide written assessment of the **strengths and weaknesses** of written research, with the aim of improving the reporting of research and identifying the most appropriate and highest quality material for the journal.

Operating and review process

What happens to a manuscript once it is submitted to *Pertanika*? Typically, there are 7 steps to the editorial review process:

1. The journal's Chief Executive Editor and the Editor-in-Chief examine the paper to determine whether it is relevance to journal needs in terms of novelty, impact, design, procedure, language as well as presentation and allow it to proceed to the reviewing process. If not appropriate, the manuscript is rejected outright and the author is informed.
2. The Chief Executive Editor sends the article-identifying information having been removed, to 2 to 3 reviewers. They are specialists in the subject matter of the article. The Chief Executive Editor requests that they complete the review within 3 weeks.

Comments to authors are about the appropriateness and adequacy of the theoretical or conceptual framework, literature review, method, results and discussion, and conclusions. Reviewers often include suggestions for strengthening of the manuscript. Comments to the editor are in the nature of the significance of the work and its potential contribution to the research field.

3. The Editor-in-Chief examines the review reports and decides whether to accept or reject the manuscript, invite the authors to revise and resubmit the manuscript, or seek additional review reports. In rare instances, the manuscript is accepted with almost no revision. Almost without exception, reviewers' comments (to the authors) are forwarded to the authors. If a revision is indicated, the editor provides guidelines for attending to the reviewers' suggestions and perhaps additional advice about revising the manuscript.
4. The authors decide whether and how to address the reviewers' comments and criticisms and the editor's concerns. The authors return a revised version of the paper to the Chief Executive Editor along with specific information describing how they have addressed the concerns of the reviewers and the editor, usually in a tabular form. The authors may also submit a rebuttal if there is a need especially when the authors disagree with certain comments provided by reviewers.
5. The Chief Executive Editor sends the revised manuscript out for re-review. Typically, at least 1 of the original reviewers will be asked to examine the article.
6. When the reviewers have completed their work, the Editor-in-Chief examines their comments and decides whether the manuscript is ready to be published, needs another round of revisions, or should be rejected. If the decision is to accept, the Chief Executive Editor is notified.
7. The Chief Executive Editor reserves the final right to accept or reject any material for publication, if the processing of a particular manuscript is deemed not to be in compliance with the S.O.P. of *Pertanika*. An acceptance letter is sent to all the authors.

The editorial office ensures that the manuscript adheres to the correct style (in-text citations, the reference list, and tables are typical areas of concern, clarity, and grammar). The authors are asked to respond to any minor queries by the editorial office. Following these corrections, page proofs are mailed to the corresponding authors for their final approval. At this point, **only essential changes are accepted**. Finally, the manuscript appears in the pages of the journal and is posted on-line.

Pertanika Journal of
**SCIENCE
& TECHNOLOGY**

A Special Issue devoted to
**Exploring Future Innovation and Sustainability in Engineering
and Computing Technologies**

Vol. 33 (S3) 2025

Guest Editors
Mohd Sobri Takriff, Mazidah Puteh and Norulhidayah Isa



A scientific journal published by Universiti Putra Malaysia Press

UNIVERSITY PUBLICATIONS COMMITTEE

CHAIRMAN

Zamberi Sekawi

EDITOR-IN-CHIEF

Luqman Chuah Abdullah
Chemical Engineering

EDITORIAL STAFF

Journal Officers:

Ellyyanur Puteri Zainal
Kanagamalar Silvarajoo
Siti Zuhaila Abd Wahid

Editorial Assistants:

Siti Juridah Mat Arip
Zulinaardawati Kamarudin

English Editor:

Norhanizah Ismail

PRODUCTION STAFF

Pre-press Officers:

Ku Ida Mastura Ku Baharom
Nur Farrah Dila Ismail

WEBMASTER

IT Officer:

Kiran Raj Kaneswaran

EDITORIAL OFFICE

JOURNAL DIVISION

Putra Science Park
1st Floor, IDEA Tower II
UPM-MTDC Technology Centre
Universiti Putra Malaysia
43400 Serdang, Selangor Malaysia.

General Enquiry

Tel. No: +603 9769 1622

E-mail:

executive_editor.pertanika@upm.edu.my

URL: <http://www.pertanika.upm.edu.my>

PUBLISHER

UPM Press

Universiti Putra Malaysia
43400 UPM, Serdang, Selangor, Malaysia.
Tel: +603 9769 8855

E-mail: dir.penerbit@upm.edu.my

URL: <http://penerbit.upm.edu.my>



PENERBIT
UPM
UNIVERSITI PUTRA MALAYSIA
P R E S S



PERTANIKA
JOURNALS

ASSOCIATE EDITOR

2024-2026

Miss Laiha Mat Kiah

Security Services Sn: Digital Forensic, Steganography, Network Security, Information Security, Communication Protocols, Security Protocols
Universiti Malaysia, Malaysia

Saidur Rahman

Renewable Energy, Nanofluids, Energy Efficiency, Heat Transfer, Energy Policy
Sunway University, Malaysia

EDITORIAL BOARD

2024-2026

Abdul Latif Ahmad

Chemical Engineering
Universiti Sains Malaysia, Malaysia

Hsiu-Po Kuo

Chemical Engineering
National Taiwan University, Taiwan

Mohd. Ali Hassan

Bioprocess Engineering, Environmental Biotechnology
Universiti Putra Malaysia, Malaysia

Ahmad Zaharin Aris

Hydrochemistry, Environmental Chemistry, Environmental Forensics, Heavy Metals
Universiti Putra Malaysia, Malaysia

Ivan D. Rukhlenko

Nonlinear Optics, Silicon Photonics, Plasmonics and Nanotechnology
The University of Sydney, Australia

Nor Azah Yusof

Biosensors, Chemical Sensor, Functional Material
Universiti Putra Malaysia, Malaysia

Azlina Harun@

Kamaruddin
Enzyme Technology, Fermentation Technology
Universiti Sains Malaysia, Malaysia

Lee Keat Teong

Energy Environment, Reaction Engineering, Waste Utilization, Renewable Energy
Universiti Sains Malaysia, Malaysia

Norbahiah Misran

Communication Engineering
Universiti Kebangsaan Malaysia, Malaysia

Bassim H. Hameed

Chemical Engineering: Reaction Engineering, Environmental Catalysis & Adsorption
Qatar University, Qatar

Mohamed Othman

Communication Technology and Network, Scientific Computing
Universiti Putra Malaysia, Malaysia

Roslan Abd-Shukor

Physics & Materials Physics, Superconducting Materials
Universiti Kebangsaan Malaysia, Malaysia

Biswajeet Pradhan

Digital image processing, Geographical Information System (GIS), Remote Sensing
University of Technology Sydney, Australia

Mohd Shukry Abdul Majid

Polymer Composites, Composite Pipes, Natural Fibre Composites, Biodegradable Composites, Bio-Composites
Universiti Malaysia Perlis, Malaysia

Sodeifan Gholmosseini

Supercritical technology, Optimization, nanoparticles, Polymer nanocomposites
University of Kashan, Iran

Ho Yuh-Shan

Water research, Chemical Engineering and Environmental Studies
Asia University, Taiwan

Mohd Zulkifly Abdullah

Fluid Mechanics, Heat Transfer, Computational Fluid Dynamics (CFD)
Universiti Sains Malaysia, Malaysia

Wing Keong Ng

Aquaculture, Aquatic Animal Nutrition, Aqua Feed Technology
Universiti Sains Malaysia, Malaysia

INTERNATIONAL ADVISORY BOARD

2024-2027

Hiroshi Uyama

Polymer Chemistry, Organic Compounds, Coating, Chemical Engineering
Osaka University, Japan

Mohini Sain

Material Science, Biocomposites, Biomaterials
University of Toronto, Canada

Mohamed Pourkashanian

Mechanical Engineering, Energy, CFD and Combustion Processes
Sheffield University, United Kingdom

Yulong Ding

Particle Science & Thermal Engineering
University of Birmingham, United Kingdom

ABSTRACTING AND INDEXING OF PERTANIKA JOURNALS

Pertanika Journal of Science & Technology is indexed in Journal Citation Reports (JCR-Clarivate), SCOPUS (Elsevier), EBSCO, ASEAN Citation Index, Microsoft Academic, Google Scholar and MyCite.

The publisher of Pertanika will not be responsible for the statements made by the authors in any articles published in the journal. Under no circumstances will the publisher of this publication be liable for any loss or damage caused by your reliance on the advice, opinion or information obtained either explicitly or implied through the contents of this publication. All rights of reproduction are reserved in respect of all papers, articles, illustrations, etc., published in Pertanika. Pertanika provides free access to the full text of research articles for anyone, worldwide. It does not charge either its authors or author-institution for refereeing/publishing outgoing articles or user-institution for accessing incoming articles. No material published in Pertanika may be reproduced or stored on microfilm or in electronic, optical or magnetic form without the written authorization of the Publisher.

Copyright ©2021 Universiti Putra Malaysia Press. All Rights Reserved.

Pertanika Journal of Science & Technology
Vol. 33 (S3) 2025

Contents

Preface	i
<i>Mohd Sobri Takriff, Mazidah Puteh and Norulhidayah Isa</i>	
Full Factorial Design for Formulation and Optimisation of Polyvinyl Alcohol with Starch Composite Using Conventional Injection Moulding	1
<i>Mohd Shahrul Nizam Salleh, Roshafima Rasit Ali, Norzila Mohd, Fatahiya Mohamed Tap, Iswaibah Mustafa and Zatil Izzah Tarmizi</i>	
Weeds Detection for Agriculture Using Convolutional Neural Network (CNN) Algorithm for Sustainable Productivity	15
<i>Khairun Nisa Mohammad Nasir, Hasiah Mohamed, Norshuhani Zamin and Rajeswari Raju</i>	
Mathematical Modelling for Performance Prediction of Ex-Mining Lake Water Phytoremediation by <i>Scirpus Grossus</i>	37
<i>Norhaslina Mohd Sidek, Siti Rozaimah Sheikh Abdullah and Sarifah Fauziah Syed Draman</i>	
Modelling Heterogeneous Traffic Performance During Non-Recurrent Congestion (NRC): A Case Study of Tugu Bundaran Sweta Intersection	49
<i>Ahmad Muharror, Wardati Hashim, Noor Azreena Kamaluddin, Nor Izzah Zainuddin, Nur Ilya Farhana Md Noh and Ekarizan Shaffie</i>	
Enhancing Yolov8 Backbone Using Gradient Descent-based Method for Dental Segmentation	65
<i>Dhiaa Mohammed Abed, Shuzlina Abdul-Rahman and Sofianita Mutalib</i>	
Enhancing Recycling Collection Point Coverage in Seremban City, Malaysia: A Comprehensive Study on Adapting Integer Linear Programming Models with Fixed Capacity Levels	81
<i>Muhammad Zulhazwan Rosni, Zati Aqmar Zaharudin and Adibah Shuib</i>	
Public Sentiment on Awareness of Climate Change Based on Support Vector Machine	97
<i>Norlina Mohd Sabri, Izzatul Syahirah Ismail, Nik Marsyahariani Nik Daud and Nor Azila Awang Abu Bakar</i>	

Enhancing Leachate Treatment with Electrocoagulation: A Computational Approach Using Response Surface Methodology <i>Mahmoud A. M. Al-Alwani, Alia Atasha Arisucman, Zadariana Jamil and Azianabiha A Halip Khalid</i>	123
Elucidation of <i>Chromolaena odorata</i> Extract's Pharmacological Potential Through Integration of Network Pharmacology and Molecular Docking Study <i>Nur 'Ainun Mokhtar, Fatahiya Mohamed Tap, Iswaibah Mustafa, Mohd Shahrul Nizam Salleh, Norzila Mohd, Nurhannani Ahmad Rozani and Norazlan Mohmad Misnan</i>	141
Breast Cancer Prediction: A Random Forest-based System with Expert Validation <i>Sharifah Nurulhikmah Syed Yasin, Aiman Azhar and Rajeswari Raju</i>	157

Preface

The 4th International Conference on Engineering and Computing Technologies (ICECT IV) 2023 was successfully held at Permai Hotel, Kuala Terengganu, Malaysia, from 20th to 23rd October 2023. Hosted by Universiti Teknologi MARA Cawangan Terengganu, ICECT IV continued its tradition, established in 2018, as a platform for researchers, academicians, industry experts, and students to engage in meaningful discussions on engineering challenges and emerging technologies.

We are pleased to present this Special Issue of the PERTANIKA Journal, which features selected papers from ICECT IV. This collection highlights a multidisciplinary approach to sustainability in engineering and computing technologies, integrating mathematical and computational methods with sustainable materials and manufacturing innovations.

The ten articles in this edition showcase diverse research contributions across several key domains, including artificial intelligence and machine learning, medical and biological sciences, environmental engineering, traffic and transportation, materials science, and operations research. Each study provides valuable insights into contemporary challenges and advances in these fields, reflecting the conference's commitment to fostering innovation and interdisciplinary collaboration.

As editors, we believe this compilation will significantly contribute to the body of knowledge in engineering and computing sciences. We sincerely thank the authors for sharing their expertise and perspectives, as well as to the reviewers and editorial team for their dedication to ensuring the quality and relevance of the published works.

We hope this Special Issue will be a valuable resource for researchers and practitioners, inspiring further exploration and advancements in the field.

Warm regards.

Guest Editors

Mohd Sobri Takriff (Prof. Ir. Dr.)

Mazidah Puteh (Prof. Ts. Dr.)

Norulhidayah Isa (Dr.)

Full Factorial Design for Formulation and Optimisation of Polyvinyl Alcohol with Starch Composite Using Conventional Injection Moulding

Mohd Shahrul Nizam Salleh^{1,2*}, Roshafima Rasit Ali², Norzila Mohd¹, Fatahiya Mohamed Tap¹, Iswaibah Mustafa¹ and Zatil Izzah Tarmizi²

¹*School of Chemical Engineering, College of Engineering, Universiti Teknologi MARA Cawangan Terengganu, Kampus Bukit Besi, 23200 Dungun, Terengganu, Malaysia*

²*Chemical Environmental and Engineering Department, Malaysia-Japan International Institute of Technology, Universiti Teknologi Malaysia, 53200 Kuala Lumpur, Malaysia*

ABSTRACT

The combination of polyvinyl alcohol (PVOH) and starch composites leads to the production of biodegradable polymer composites. This polymer compound has good qualities for being used as a biodegradable material, which makes it easier to stop the buildup of synthetic substances made from petroleum. This study is intended to analyse the processability characteristics of PVOH-starch composites using actual injection moulding. The processability study of PVOH-starch found that the compound could be injection moulded. The name tag product (NTP) was used as a product outcome during the injection moulding. The verification of the optimisation was conducted by means of statistical analysis employing full-factorial design methodologies. In short, the statistical results have indicated that optimal processing techniques can contribute to the production of NTP with little volumetric shrinkage (as observed in short-shot scenarios) while maintaining acceptable levels of variability. Finally, the optimum injection moulding process parameters were found at 200°C and a pressure of 90 bar. This is because the NTP was produced at the lowest variation of the NTP's total weight in this set of parameters.

ARTICLE INFO

Article history:

Received: 22 August 2024

Accepted: 24 February 2025

Published: 24 April 2025

DOI: <https://doi.org/10.47836/pjst.33.S3.01>

E-mail addresses:

shahrulnizam@uitm.edu.my (Mohd Shahrul Nizam Salleh)

roshafima@utm.my (Roshafima Rasit Ali)

norzi085@uitm.edu.my (Norzila Mohd)

fatahiya@uitm.edu.my (Fatahiya Mohamed Tap)

iswaibahmustafa@uitm.edu.my (Iswaibah Mustafa)

zatil.izzah@utm.my (Zatil Izzah Tarmizi)

* Corresponding author

Keywords: Composite, full factorial design, injection moulding, polyvinyl alcohol, starch

INTRODUCTION

The composite of polyvinyl alcohol (PVOH) loaded starch was developed at the beginning of the 1980s as an alternative biodegradable polymer technology to the existing conventional polymers, such as polyethene,

polypropylene and other petroleum-based polymers (Ray et al., 2021; Wang et al., 2023). The utilisation of starch as a matrix for the advancement of biodegradable polymers has gained attention due to its complete biodegradability and cost-effectiveness in production (Chopra et al., 2013). Numerous researchers have extensively explored starch in the field of edible films and coatings to utilise it as a protective agent for food products (Flores et al., 2007).

The present research indicates that incorporating starch with synthetic polymers has enhanced the resulting material's biodegradability. Starch exhibits polarity, rendering it incompatible with non-polar synthetic polymers like polyethylene when combined. According to the findings of Jagannath et al. (2006), the mechanical characteristics of low-density polyethylene filled with starch were observed to deteriorate. Hence, to address this issue, incorporating an intrinsic polar polymer into the blending process will provide compatibility between the components. It is probable that a composite material consisting of both PVOH and starch, which are both polar polymers, will exhibit superior mechanical capabilities and barrier behaviour (Siddaramaiah et al., 2004). In the context of polymer films, incorporating glycerol as a plasticiser mitigates brittleness by disrupting the hydrogen bonding interactions between lipid and hydrocolloid molecules (Pan et al., 2022).

Currently, limited efforts have been made to develop processable injection-moulded starch composites using either native or modified starch. This study evaluated the processing parameters for the composites to be processed via conventional injection moulding. The comprehensive examination and determination of thermal and flow characteristics are crucial in optimising the processing parameters in order to facilitate the broad utilisation of these compounds across diverse industries, particularly in conventional polymer processing methods like injection moulding, extrusion, blown film, and thermoforming techniques (Ramesh, 2016). In addition, an investigation was conducted on the processing behaviour of PVOH/Starch using the injection moulding technique often employed in various industrial applications. This study's findings also have significant industrial implications. The optimised injection moulding parameters for PVOH/starch composites provide a cost-effective and environmentally friendly alternative for manufacturing biodegradable products, such as packaging and consumer goods.

Typically, if a new material is introduced to the injection moulding process, trial and error are required to determine the optimal processing parameters. Most of the time, personnel will resolve this issue based on their experience or with the aid of a processing troubleshooting guide (Gülçür et al., 2023). All variables except one are held constant in this task, and elements are tolerated through trial and error. This situation may have required hours or days to determine the optimisation parameter. More variables will bring more problems, squander time, and sometimes not detect the troublesome variables (Krantz et al., 2023). When this occurs, the operator must continually adjust the system to produce quality parts without resolving the underlying issue (Trotta et al., 2021). This will result in a loss of competitiveness in the long term. The optimal parameter is determined using a full factorial

design to encourage further development and enhancement of biodegradable starch-based polymer compounds for injection moulding (Moo-Tun et al., 2020). Compared to previous studies, which primarily focused on the mechanical properties of starch-based composites, this research uniquely integrates a full factorial design methodology to statistically optimise processing parameters for conventional injection moulding applications.

The optimised parameters demonstrated in this study align with recent advancements in biopolymer research but provide a novel focus on statistical optimisation. This sets the study apart from prior works relying on trial-and-error methods for parameter determination. As highlighted in Jung et al. (2023), statistical optimisation plays a pivotal role in improving process efficiency, which is directly addressed in this study (Jung et al., 2023). The study examined two process parameters using a 2-level full factorial design approach. The two process parameters involved in the injection moulding process are temperature and pressure. The variables of interest in the experiment were the weights of the samples. A complete factorial experiment includes all possible level combinations for each factor. According to Antony (2023), the total number of experiments for investigating factors at the 2-level was 2. In the early phases of experimentation, the full factorial design is particularly useful, especially when the number of process parameters or design parameters (or factors) is less than or equal to four (Antony, 2023). One of the assumptions for 2-level factors is that the response is approximately linear over the range of the selected factor setting.

MATERIALS AND METHODS

Injection Moulding

Polyvinyl alcohol-starch (PVOH/Starch) blends were successfully injected through the “JSW N100 BII” injection moulding machine, complete with a reciprocating unit. Testing specimen mound shape was used for the injection moulding process. On the other hand, name tag product shape (NTP) was used to optimise the product injection moulding processing parameter. The NTP was drawn using commercial computer-aided design (CAD) software. Figure 1 shows the details of the NTP drawn by CAD based on the mould, as shown in Figure 2. This process was done using the injection moulding machine Demag EL-EXISE 60/370, as shown in Figure 3.

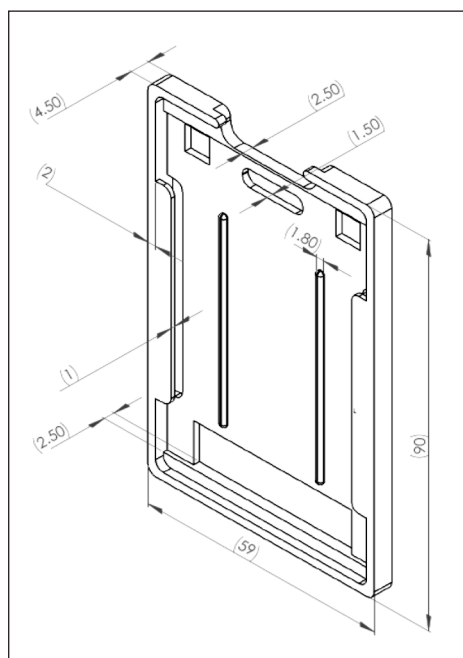


Figure 1. Drawing and measurement of NTP (unit in mm)

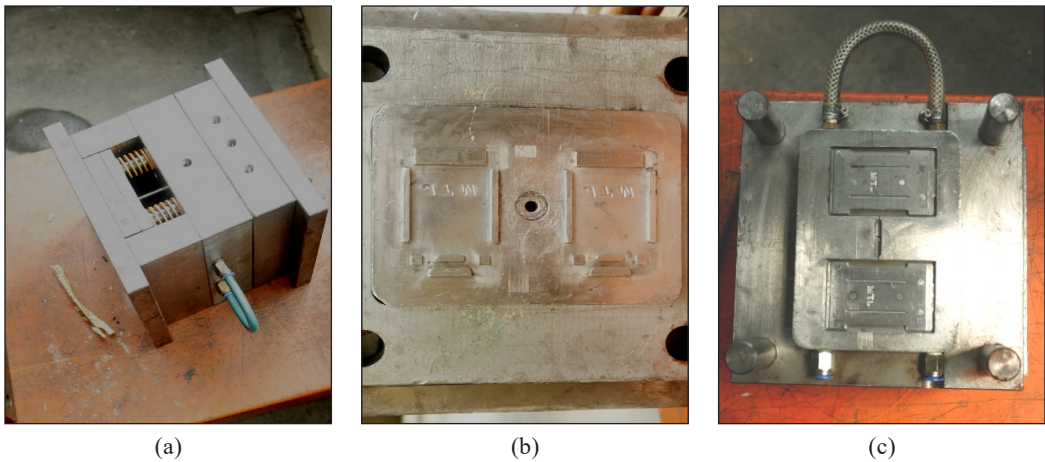


Figure 2. (a) NTP mould set; (b) Female mould of NTP; and (c) Male mould of NTP



Figure 3. Injection moulding machine Demag EL-EXISE 60/370

Full Factorial Design

The online investigations were carried out to identify the optimal processing parameters, namely the injection temperature and pressure. The 2-level full factorial design method was employed to investigate two process parameters. The variable of interest was the weight of the sample. Based on a 2-level full factorial design, 2^k trials must be conducted to provide a comprehensive statistical analysis. k represents the quantity of process parameters (Antony,

2023). Thus, in this scenario involving two process factors, four experiments were conducted to assess the impact of the process parameters on the weight of the samples. The arrangement of the experimental full factorial design layouts for PVOH/Starch is presented in Table 1.

The collected data was imported into the statistical software tool Minitab 15 for analysis to determine the impact of each process parameter on the weight of the sample. The main goal was to determine the most favourable process condition to maintain a consistent sample weight. Following the completion of the analysis of the outputs, an experiment validation was conducted to verify the reproducibility of the results. Ultimately, the specific processing parameters were documented for subsequent utilisation.

Table 1

Full factorial design of the experimental layout of PVOH/starch injection moulding process parameters

Trial	A	B	AB	Sample Weight (g)		
1	-1	-1	1	W1	W2	W3
2	-1	1	-1	W1	W2	W3
3	1	-1	-1	W1	W2	W3
4	1	1	1	W1	W2	W3

Note. A= Injection temperature (°C); B= Injection Pressure (Bar)

Differential Scanning Calorimetry (DSC) Analysis

Thermal analysis of the PPVA/TS blends was carried out using Differential Scanning Calorimetry (DSC-7 Perkin-Elmer) to determine the melting temperature (T_m) of the PVOH/starch blend. The samples were placed in sealed 10 mg aluminium pans under constant nitrogen flow. DSC was performed by heating a 5–12 mg blend sample from 30°C to 260°C. The heating rate used was at 10°C/min.

RESULTS AND DISCUSSION

The injection moulding processing parameters were optimised using the Demag EL-EXISE 60/370 machinery. The selection of the mould shape for the name tag product (NTP) was made as the final result for evaluating the processing parameters in the injection moulding process—the analysis aimed to determine the optimal injection moulding parameters for manufacturing NTP. The trial session was conducted to identify the range of settings for each parameter before determining the appropriate and optimised variable tuning using the full factorial design method.

Differential Scanning Calorimetry (DSC) Analysis

The particular thermal scanning range was selected to include the melting point of PVOH at 230°C but lower than 250°C to avoid dehydration of hydroxyl groups (Bercea, 2024).

In general, the melting stage can be detected through the presence of the endothermic peak in DSC thermograms (Sangthongdee et al., 2022). The onset temperature, end-point temperature, and melting temperature (T_m) are presented in Table 2. Incorporating starch into the PVOH has led to a decrease in the onset and end-point temperature as well as melting temperature (T_m) shown in Table 2. The melting properties of PVOH/starch blends are significantly affected by crystal formation within the blends, which depends on the starch composition in the matrix. The reduction in PVOH content significantly affects the amount and size of crystallites, weakening the interaction between PVOH and starch and consequently reducing the crystalline region (Othman & Azahari, 2011). The results indicated a melting range between 180°C and 240°C, which aligns with the experimental temperature settings. This data justifies the chosen temperature range and explains the formation of flashing and burn marks at higher temperatures (above 220°C).

Table 2
Onset and end-point melting temperature and melting temperature (T_m)

Sample	Onset (°C)	End-point (°C)	T_m (°C)
PVOH	183.41	200.00	196.03
SD	4.33	3.04	2.18
PVOH/starch	173.89	189.97	186.37
SD	1.25	1.78	2.28

*SD= Standard Deviation

Injection Moulding Start-up Setting

Two parameters were chosen for the optimisation process. Initially, the setting was established in the presence of pre-injected tensile bars. The NTP injection during the initialisation phase exhibited inconsistencies with respect to the samples' weight. Adjusting the setting was a viable solution to achieve the desired tolerance level. During the trial session, a list of parameters was established to determine the most optimal set for the subsequent validation experiment.

The two parameters subject to optimisation were injection temperature and injection pressure. Other parameters, including the mould temperature, holding time (comprising both cooling and packing time), injection speed, and packing pressure, were fixed at 45°C, 20 s, 60 mm/s, and 70 bar values, respectively. The experimental conditions employed during the trial injection moulding of NTP were recorded and organised in Table 3. The outcomes resulting from each alteration were carefully monitored and documented.

In the injection moulding of PVOH/starch composites, ensuring sufficient injection pressure is crucial to prevent short shots and situations where the mould cavity is inadequately filled, resulting in faulty components (Shogren, 1995). Pressures below 90 bar have been observed to induce such problems, highlighting the necessity of adequate

Table 3

Setting range injection temperature and injection pressure during trial run

Sample	Injection Temperature (°C)	Injection pressure (bar)	Remarks
PVOH/Starch	180	90	Short shot
	200	90	Fully moulded
	220	90	Fully moulded
	240	90	Fully moulded, but have burn marks
	180	110	Short shot
	200	110	Fully moulded
	220	110	Fully moulded
	240	110	Flashing and have burn marks
	180	130	Short shot
	200	130	Flashing
	220	130	Flashing
	240	130	Overpacking and having burn marks

injection pressure. Insufficient pressure prevents the molten polymer from fully occupying the mould cavity, leading to inadequate filling and diminished product (Liou et al., 2023).

Full Factorial Analysis and Actual Injection Moulding Verification

The study employed a full-factorial design methodology to examine the effectiveness of various processing parameters in producing NTP. The investigation of processing parameters by injection moulding was conducted using the design of experiment (DOE) methodology. The experimental design for the injection moulding validation experiment is presented in Table 4, which displays the process parameters and their corresponding levels. The chosen parameter ranges were further analysed using the full factorial design procedure.

Each set of combinations was repeated four times to calculate the NTP weight's standard deviation (SD). The standard variation was used to measure the level of variability in the process parameters. The remaining parameters, such as the mould's temperature, the duration of holding (which includes cooling and packing time), the speed of injection, and the pressure of packing, were set at 45°C, 20 seconds, 60 millimetres per second, and 70 bars, respectively.

Table 4

The level of process parameters utilised in the verification experiment

Sample	Process Factor	Low Level	High Level
PVOH/Starch	Injection temperature (°C)	200	210
	Injection pressure (bar)	90	110

Analysis of Process Factors: Effects on Total Weight of PVOH/Starch

This analysis aimed to investigate the influence that process factors had on the total weight of the sample in order to determine the ideal combination of process factors that would result in the highest possible sample weight. The analysis was performed by providing the PVOH/Starch compound, with the parameters established in line with the specifications in Table 4. The entire weight of NTP was the response to this analysis, tabulated in Table 5.

According to the data presented in Table 5, the maximum aggregate weight of NTP was observed at a temperature of 200°C and a pressure of 110 bar. The findings demonstrated that the diverse combinations of parameters led to significant variations in the total weight of NTP, suggesting interactions among the process components. In summary, a comprehensive statistical analysis can be employed to derive the optimal set of process parameters. The results were imported into Minitab 15 for analysis.

Figures 4 and 5 depict the normal probability plot and Pareto chart of the standardised effects based on the computed data in Minitab 15. Figure 4 depicts the reaction, represented by a red dot, which exhibits a similar pattern to the normal distribution condition, illustrated by a blue line. The scenario suggests that the reaction fell within the established parameters and can be subjected to additional examination using a Pareto chart, as depicted in Figure 5. The Pareto chart displayed the process factor along with its standardised effect. According to the information provided, when the standardised effect exceeds the threshold indicated by the red line in Figure 4, the specific process factor or the interaction of process factors has considerably influenced the total weight filled by PVOH/Starch in the NTP.

According to the Pareto Chart, it can be observed that both factor A (injection temperature) and component B (injection pressure) significantly impact the total weight of the NTP. The injection temperature factor influenced the overall weight, as the greater temperature facilitated the free movement of the polymer complex, enabling it to effectively occupy any available space (Moo-Tun et al., 2020; Ray et al., 2021). Therefore, the issue of premature solidification of material prior to complete cavity filling might be effectively mitigated (Ghazy et al., 2016). Furthermore, the use of increased injection pressure has resulted in the compression of the molten polymer compound, enabling a greater quantity

Table 5
Total weight of NTP filled by PVOH/Starch

Trial	Injection Temperature (°C)	Injection Pressure (bar)	Weight (g)				Mean
			1	2	3	4	
1	200	90	26.51	26.43	26.07	26.22	26.31
2	200	110	27.33	26.88	26.53	26.58	26.83
3	210	90	25.33	24.17	25.11	24.01	24.66
4	210	110	25.02	24.93	25.40	25.11	25.12

of molten PVOH/Starch compound to be injected into the mould (Liu et al., 2021). This is indicative of the larger overall weight of the final product. The investigation of the interaction of process factors was conducted comprehensively by generating a normal interaction plot, as depicted in Figure 6. In terms of the high total weight response, the interaction plot results indicated that the injection temperature and pressure should consistently be set at 200°C and 110 bar, respectively.

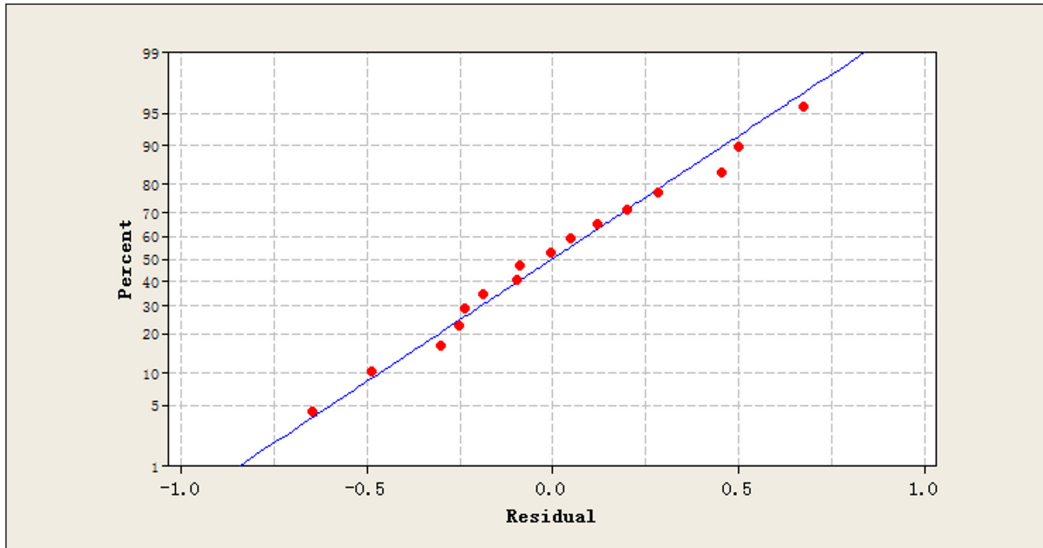


Figure 4. Normal probability plot of NTP (response is weight)

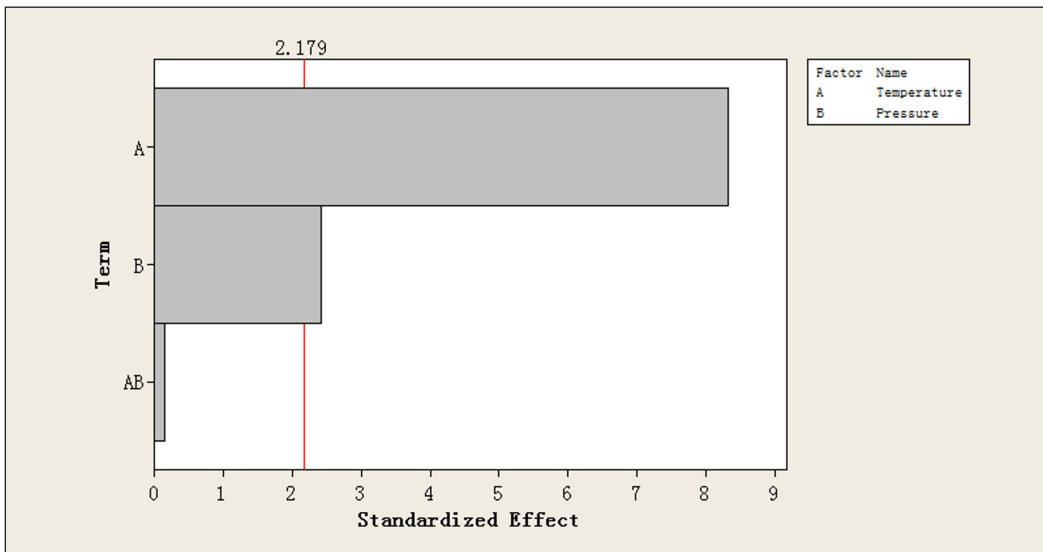


Figure 5. Pareto chart plot of NTP (response is weight, alpha= 0.05)

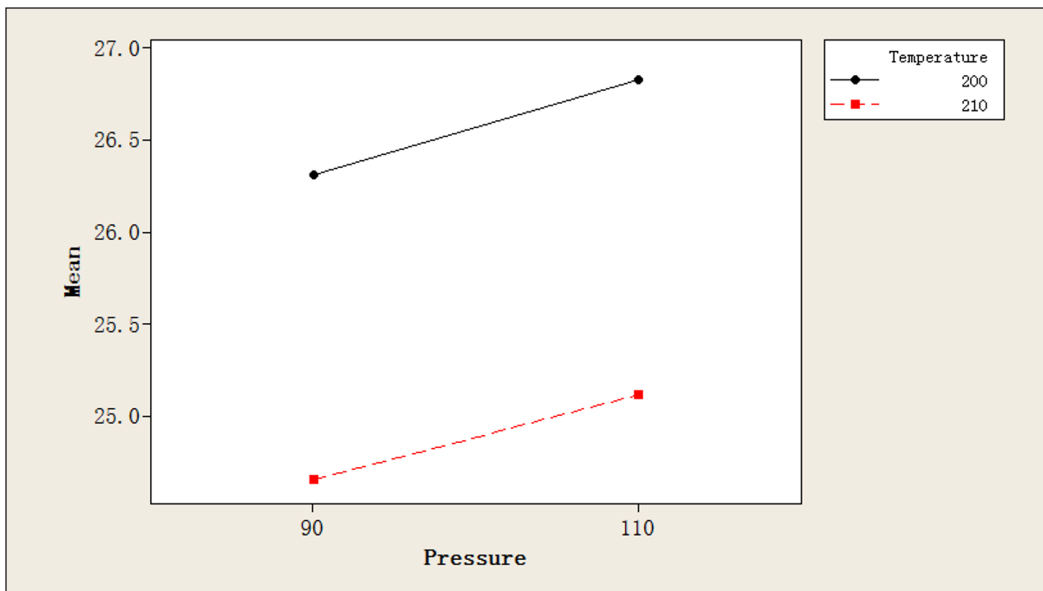


Figure 6. Interaction plot for a total weight of NTP (data means)

Analysis of Process Factors: Effects on the Variability of Total Weight of PVOH/Starch

This analysis aims to identify the process element affecting the variability of the NTP’s overall weight when filled with PVOH/Starch. The table marked as Table 6 contains standard deviations (SD) information. Standard deviation (SD) is a crucial factor in this analysis and is transformed into logarithmic form to bring the standard deviations closer to a normal distribution (Antony, 2023). A high standard deviation of the individual process parameters results in a significant variability in the quantity of NTP generated. As a result, there was a lack of uniformity in the manufacturing of NTP, potentially resulting in deviations from the specified product requirements. The Pareto chart depicted in Figure 7 indicates that the injection temperature (A) and pressure (B) do not exert a substantial impact on the variability of NTP’s total weight. Furthermore, there has been an interaction between these two process elements (AB).

Figure 8 illustrates the fluctuation in the weight of the total NTP (Nucleotide Triphosphate) at an injection temperature of 200°C and an injection pressure of 90 bar. These findings suggest that the largest total weight of NTP occurred at a temperature of 200°C and a pressure of 110 bar, resulting in a greater variance compared to the conditions set at 200°C and 90 bar. These findings indicate that the injection temperature and pressure do not have a substantial impact on the fluctuation in the production of NTP. Despite possessing the greatest overall weight, it exhibited the second-highest degree of variability at a temperature of 200°C and a pressure of 110 bar. Currently, the most favourable

Table 6
SD of NTP filled by PVOH/Starch

Trial	Injection Temperature (°C)	Injection Pressure (bar)	Weight (g)				Mean	SD
			1	2	3	4		
1	200	90	26.51	26.43	26.07	26.22	26.31	0.200062
2	200	110	27.33	26.88	26.53	26.58	26.83	0.367423
3	210	90	25.33	24.17	25.11	24.01	24.66	0.661791
4	210	110	25.02	24.93	25.40	25.11	25.12	0.203715

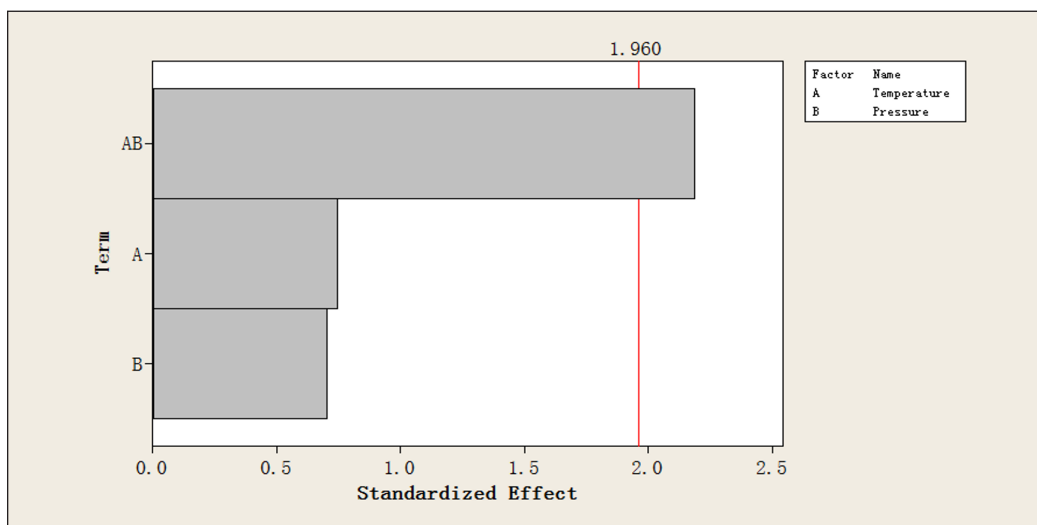


Figure 7. Pareto chart of NTP-filled PVOH/Starch (response is ln of weight SD, alpha= 0.05)

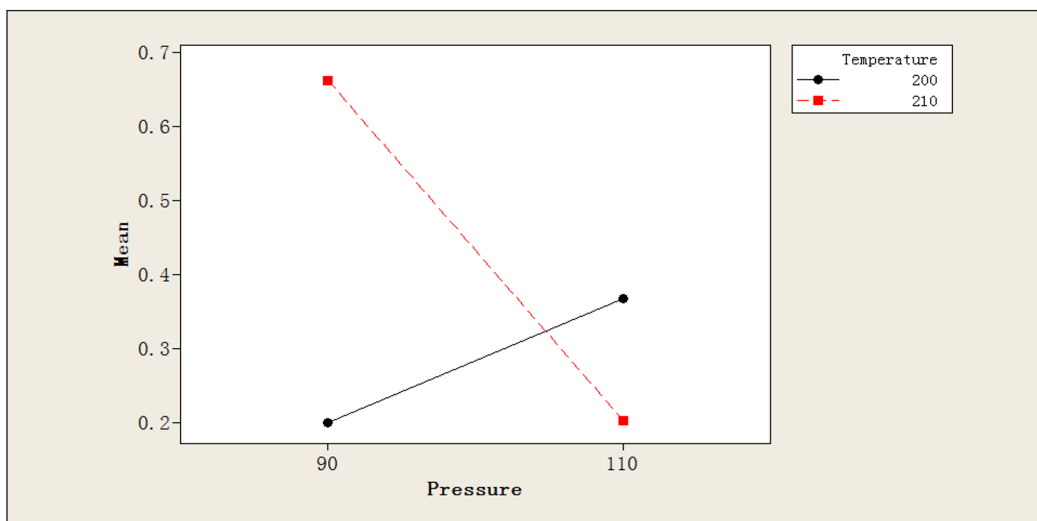


Figure 8. Interaction plot for a total weight of NTP (data means)

condition for generating NTP is observed at a temperature of 200°C and a pressure of 90 bar. This condition significantly impacts the quality of the resulting product. Additionally, by reducing variance, it is possible to mitigate the inconsistency that may arise during the production of NTP (Moo-Tun et al., 2020).

A validation experiment was undertaken to ensure the reproducibility of the process parameter acquired for the PVOH/starch blend. The experiment validated the feasibility of doing the analyses in a real-world conventional injection moulding process. The findings are documented in Table 7. The statistical study confirmed that the findings obtained from optimising processing parameters for producing NTP filled with PVOH/Starch are reproducible. These findings also validate the reproducibility of the optimal parameters in a real-world injection moulding process. These results underscore the practicality of employing biodegradable composites in industries aiming to reduce reliance on petroleum-based materials.

Table 7
NTP's lower variation validation experiment

Sample	Injection Temperature (°C)	Injection Pressure (bar)	Weight (g)				Mean	SD
			1	2	3	4		
PVOH/Starch	200	90	26.37	26.38	26.61	26.12	26.37	0.200167

CONCLUSION

A combination of polyvinyl alcohol (PVOH) and starch has been effectively developed and established. The development of PVOH/Starch blends for injection moulded applications was evaluated. The reproducibility of optimal parameters at 200°C and 90 bar reinforces their industrial applicability for producing consistent, high-quality biodegradable products. This work provides a foundation for scaling up PVOH/starch composites in environmentally sustainable applications. Under these conditions, the NTP exhibited higher precision because of reduced variation. Additionally, by reducing variance, it is possible to mitigate the inconsistency that may arise during the manufacture of NTP. The selected set of parameters was subsequently validated to assess its reproducibility, which exhibited a comparable trend to that observed in standard injection moulding practices in the industry.

ACKNOWLEDGEMENTS

We thank the School of Chemical Engineering, College of Engineering, UiTM Cawangan Terengganu, Kampus Bukit Besi, for providing the facilities and administrative support. The authors also express their appreciation for the resource assistance provided by the

Ministry of Higher Education Malaysia (MOHE) under the Fundamental Research Grant Scheme (FRGS) (FRGS/1/2020/STG05/UTM/02/9) and Universiti Teknologi Malaysia under the UTM Fundamental Research Grant (Q.K130000.3843.22H72).

REFERENCES

- Antony, J. (2023). 6 - Full factorial designs. In J. Antony (Ed.), *Design of experiments for engineers and scientists* (3rd ed., pp. 65-87). Elsevier. <https://doi.org/https://doi.org/10.1016/B978-0-443-15173-6.00009-3>
- Bercea, M. (2024). Recent advances in poly(vinyl alcohol)-based hydrogels. *Polymers*, *16*(14), 2021. <https://doi.org/10.3390/polym16142021>
- Chopra, P., Garg, S., & Jana, A. K. (2013). Study on the performance of starch / PVA blend films modified with SiO₂ Nanoparticles. *International Journal of Research in Mechanical Engineering & Technology*, *3*(2), 36-40.
- Flores, S., Famá, L., Rojas, A. M., Goyanes, S., & Gerschenson, L. (2007). Physical properties of tapioca-starch edible films: Influence of filmmaking and potassium sorbate. *Food Research International*, *40*(2), 257-265. <https://doi.org/https://doi.org/10.1016/j.foodres.2006.02.004>
- Ghazy, O. A., Nabih, S., Abdel-moneam, Y. K., & Senna, M. M. (2016). Polyvinyl alcohol-modified Pithecellobium Clypearia Benth herbal residue fiber/polypropylene composites. *Polymer Composites*, *37*(1), 915-924. <https://doi.org/10.1002/pc>
- Gülçür, M., Brown, E., Gough, T., & Whiteside, B. (2023). Characterisation of microneedle replication and flow behaviour in ultrasonic micro-injection moulding through design of experiments. *Journal of Manufacturing Processes*, *102*, 513-527. <https://doi.org/https://doi.org/10.1016/j.jmapro.2023.07.068>
- Jagannath, J. H., Nadanasabapathi, S., & Bawa, A. S. (2006). Effect of starch on thermal, mechanical, and barrier properties of low density polyethylene film. *Journal of Applied Polymer Science*, *99*(6), 3355-3364. <https://doi.org/https://doi.org/10.1002/app.22358>
- Jung, J., Park, K., Cho, B., Park, J., & Ryu, S. (2023). Optimization of injection molding process using multi-objective bayesian optimization and constrained generative inverse design networks. *Journal of Intelligent Manufacturing*, *34*(8), 3623-3636. <https://doi.org/10.1007/s10845-022-02018-8>
- Krantz, J., Nieduzak, Z., Kazmer, E., Licata, J., Ferki, O., Gao, P., Sobkowicz, M. J., & Masato, D. (2023). Investigation of pressure-controlled injection molding on the mechanical properties and embodied energy of recycled high-density polyethylene. *Sustainable Materials and Technologies*, *36*, e00651. <https://doi.org/https://doi.org/10.1016/j.susmat.2023.e00651>
- Liou, G.-Y., Su, W.-J., Cheng, F.-J., Chang, C.-H., Tseng, R.-H., Hwang, S.-J., Peng, H.-S., & Chu, H.-Y. (2023). Optimize injection-molding process parameters and build an adaptive process control system based on nozzle pressure profile and clamping force. *Polymers*, *15*(3), 610. <https://doi.org/10.3390/polym15030610>
- Liu, D., Dang, S., Zhang, L., Munsop, K., & Li, X. (2021). Corn starch/polyvinyl alcohol based films incorporated with curcumin-loaded Pickering emulsion for application in intelligent packaging. *International Journal of Biological Macromolecules*, *188*, 974-982. <https://doi.org/https://doi.org/10.1016/j.ijbiomac.2021.08.080>

- Moo-Tun, N. M., Iñiguez-Covarrubias, G., & Valadez-Gonzalez, A. (2020). Assessing the effect of PLA, cellulose microfibrils and CaCO₃ on the properties of starch-based foams using a factorial design. *Polymer Testing*, 86, 106482. <https://doi.org/https://doi.org/10.1016/j.polymertesting.2020.106482>
- Othman, N., & Azahari, N. (2011). Thermal properties of polyvinyl alcohol (PVOH)/corn starch blend film. *Malaysian Polymer Journal*, 6(6), 147-154.
- Pan, W., Liang, Q., & Gao, Q. (2022). Preparation of hydroxypropyl starch/polyvinyl alcohol composite nanofibers films and improvement of hydrophobic properties. *International Journal of Biological Macromolecules*, 223, 1297-1307. <https://doi.org/https://doi.org/10.1016/j.ijbiomac.2022.11.114>
- Ramesh, M. (2016). Kenaf (*Hibiscus cannabinus* L.) fibre based bio-materials: A review on processing and properties. *Progress in Materials Science*, 78–79, 1-92. <https://doi.org/10.1016/j.pmatsci.2015.11.001>
- Ray, R., Narayan Das, S., & Das, A. (2021). Mechanical, thermal, moisture absorption and biodegradation behaviour of date palm leaf reinforced PVA/starch hybrid composites. *Materials Today: Proceedings*, 41, 376-381. <https://doi.org/https://doi.org/10.1016/j.matpr.2020.09.564>
- Sangthongdee, M., Phattarateera, S., & Threepopnatkul, P. (2022). The effect of pregelatinized starch on the properties of poly (vinyl alcohol) film for the water-soluble laundry bag. *Chiang Mai Journal of Science*, 49(6), 1604-1617. <https://doi.org/10.12982/CMJS.2022.096>
- Shogren, R. L. (1995). Poly(ethylene oxide)-coated granular starch-poly(hydroxybutyrate-co-hydroxyvalerate) composite materials. *Journal of Environmental Polymer Degradation*, 3(2), 75-80. <https://doi.org/10.1007/BF02067483>
- Siddaramaiah, Raj, B., & Somashekar, R. (2004). Structure–property relation in polyvinyl alcohol/starch composites. *Journal of Applied Polymer Science*, 91(1), 630-635. <https://doi.org/https://doi.org/10.1002/app.13194>
- Trotta, G., Stampone, B., Fassi, I., & Tricarico, L. (2021). Study of rheological behaviour of polymer melt in micro injection moulding with a miniaturized parallel plate rheometer. *Polymer Testing*, 96, 107068. <https://doi.org/https://doi.org/10.1016/j.polymertesting.2021.107068>
- Wang, S., Zhang, P., Li, Y., Li, J., Li, X., Yang, J., Ji, M., Li, F., & Zhang, C. (2023). Recent advances and future challenges of the starch-based bio-composites for engineering applications. *Carbohydrate Polymers*, 307, 120627. <https://doi.org/https://doi.org/10.1016/j.carbpol.2023.120627>

Weeds Detection for Agriculture Using Convolutional Neural Network (CNN) Algorithm for Sustainable Productivity

Khairun Nisa Mohammad Nasir¹, Hasiah Mohamed^{1*}, Norshuhani Zamin² and Rajeswari Raju¹

¹College of Computing, Informatics, and Mathematics, Universiti Teknologi MARA Cawangan Terengganu, 21080 Kuala Terengganu, Terengganu, Malaysia

²College of Computer Studies, De La Salle University, 2401 Taft Avenue, Manila 0922, Philippines

ABSTRACT

This project aims to develop a weed detection prototype for agricultural settings using the Convolutional Neural Networks (CNN) algorithm. The project thoroughly analyses and optimises CNN hyperparameters to improve accuracy and efficiency, empowering efficient weed control practices. The potential of this algorithm in weed detection is immense, offering a promising future for sustainable productivity in agriculture. Adopting innovative and sustainable agricultural practices is essential for building a robust and productive agriculture sector that can meet future food demands while protecting the environment. The research then assesses how well the CNN model generalises to various agricultural environments that support multiple crop situations. The dataset comprises 360 images of weeds, broadleaf, maize plants, soil and cotton crops. The images underwent four preprocessing phases: image scaling, normalisation, filtering, and segmentation. The proposed model achieved an accuracy of 89.82% utilizing the Convolutional Neural Network (CNN) algorithm, with the dataset partitioned into 80% for training and 20% for testing. Furthermore, the model attained an F1 score of 88.08%, indicating a high degree of alignment between predicted positive instances and actual positive samples. In addition to technological innovations in agriculture, this CNN-based weed detection prototype is a reliable resource for agriculturalists. AI-driven weed detection optimizes resource use, ensuring that pesticides and herbicides are applied only where necessary, reducing chemical overuse. This is in line with the United Nation Sustainable Development Goal (SDG) No. 12.

ARTICLE INFO

Article history:

Received: 22 August 2024

Accepted: 24 February 2025

Published: 24 April 2025

DOI: <https://doi.org/10.47836/pjst.33.S3.02>

E-mail addresses:

2022930669@student.uitm.edu.my (Khairun Nisa Mohammad Nasir)

hasiahm@uitm.edu.my (Hasiah Mohamed)

norshuhani.zamin@dlsu.edu.ph (Norshuhani Zamin)

rajes332@uitm.edu.my (Rajeswari Raju)

* Corresponding author

Keywords: Agriculture, CNN, detection, hyperparameters, performance, weed

INTRODUCTION

Artificial intelligence (AI) and machine learning deal with image recognition, commonly called computer vision (CV) or

object recognition, which is exciting and is developing quickly (Dosovitskiy et al., 2020). Image recognition is a vital technology with many practical applications since it allows machines to recognise and identify objects, patterns, and features inside digital images (Zoph et al., 2018). It focuses on creating models and algorithms that allow computers to observe, examine, and comprehend visual data from pictures and videos precisely like people do (Hu et al., 2021). Image recognition is essential for improving automation and understanding the world around us in various fields, including autonomous vehicles, healthcare, surveillance systems, and augmented reality (Dosovitskiy et al., 2020).

Various techniques are used in the expanding field of image recognition. Researchers and engineers have created a variety of methods over the years to handle diverse picture recognition problems (Henaff et al., 2020). Firstly, Traditional CV Techniques (Xie et al., 2020). These methods include picture segmentation, feature extraction, and corner and edge detection (Qiao et al., 2018). Next is Convolutional Neural Networks (CNN), a type of deep learning model created expressly for image identification applications (Qiao et al., 2018). They have revolutionised the CV field and are motivated by the structure of the visual cortex in animals (Xie et al., 2020). For image classification, object recognition, and segmentation, CNN automatically learns hierarchical features from raw pixel data (Xie et al., 2020). CNN and deep learning techniques are frequently used for image recognition. These methods have revolutionised the field in recent years because of their capacity to learn intricate patterns and hierarchies from images. CNN is made to automatically and hierarchically learn complex patterns and features from images or other kinds of grid-like input (Sarvini et al., 2019).

Agriculture activities include cultivating crops, raising livestock, and manufacturing food, textiles, and other goods vital for expanding the global population (Ukaegbu et al., 2021). Unwanted weeds have proven to be a detrimental factor in the agricultural industry as they contribute immensely to reducing crop yields, leading to severe economic losses for farmers worldwide (Lottes et al., 2018). These pesky plants can adversely affect crops, depriving them of essential nutrients, water, and sunlight, reducing productivity and quality (Razfar et al., 2022). The agriculture sector faces several significant obstacles that limit its capacity to meet the rising demands and uphold environmental stewardship. The inability to determine the precise location of weeds has led to excessive usage and low utilisation rate of pesticides, causing severe pollution (Xu et al., 2023). Agricultural professionals, including agriculture officers and agronomists, encounter substantial challenges in effectively controlling weeds due to the inherent difficulty in accurately identifying and distinguishing between weeds and crop plants (Wu et al., 2019; Razfar et al., 2022). Traditional agricultural methods often involve manual weed extraction, where farmers use handheld tools such as machetes and hoes to meticulously remove undesired plants from the soil (Asad & Bais, 2020). The motivation for this project stems from the recent use of CNNs in agricultural research, particularly for the early detection of weeds, which can help increase production and reduce costs for farmers.

LITERATURE REVIEW

In the following literature review, this study explores the landscape of the agricultural industry and weeds, focusing on how weed detection can be implemented by utilising computer science advancements.

Agricultural Industry

The agricultural sector is essential in many nations, contributing significantly to their economies' growth and creating many employment possibilities (Wu et al., 2019). Food production, economic growth, and environmental sustainability are all significantly impacted by agriculture, a crucial industry that directly impacts people's lives (Komarek et al., 2020). Several research projects have used machine learning to identify and eradicate weeds. Machine learning algorithms techniques have been used to analyse photos taken in agricultural areas to discriminate between crops and weeds (Xiao et al., 2020). These algorithms develop the ability to identify and correctly classify the visual characteristics of various weed species, but the research's accuracy is still poor (Li et al., 2020). Farming fields are intricate, dynamic settings with various distractions like crop canopy, soil, shadows, and occlusions (Hamuda, 2019). Weed recognition algorithms must consider these elements and differences in lighting, weather, and plant growth stages (Darwin et al., 2021). The difficulty of managing such complexity can affect the detection algorithms' accuracy, and the need for further research in weed detection is urgent and crucial (Ramli et al., 2024).

The need for further research in weed detection is urgent and crucial. The researchers can still learn a lot from these unsuccessful trials and pinpoint areas that need improvement and more research. The improved weed detection research spurs new developments and increases the overall accuracy of weed detection systems. Agriculture has changed dramatically throughout time, utilising technological developments to boost productivity, sustainability, and efficiency (Komarek et al., 2020). According to a United Nations Food and Agriculture Organization (FAO) study, global food production has been rising over time (Boliko, 2019). Approximately 2.76 billion metric tons of cereals were produced worldwide in 2020, with corn, rice, and wheat being the most widely grown crops (Katel et al., 2023). Other than that, it is believed that there are roughly 4.9 billion hectares of agricultural land in the world (Otsuka & Fan, 2021). This land is utilised for farming, including the breeding of cattle and the cultivation of crops (Komarek et al., 2020).

Weeds

Any plant growing where it is not wanted is called a "weed", and the definition of a "weed" is an undesirable plant, out of place, or a problem because it hinders the growth of crops or cattle (De Clercq et al., 2018). Weeds invaded crop-designated regions and were later

discovered to possess qualities that were not initially suspected. As a result, they were taken under cultivation and removed from the category of weeds (De Clercq et al., 2018). Weeds frequently display quick growth, a high capacity for reproduction, and the ability to adapt to diverse environmental conditions (Cox et al., 2019). They propagate through seeds, rhizomes, stolons, or other vegetative structures, and they can be annuals, biennials, or perennials (Cox et al., 2019). Three major categories of weeds, in general, are plants with broad leaves and frequently distinguishable flower structures known as broadleaf weeds, and some examples are dandelions, thistles, and plantains (Klerkx et al., 2019). Grass weeds are next and these are weeds that are related to grass and look like them and some examples are crabgrass, foxtail, and barnyard grass (Klerkx et al., 2019). The third categories are Sedges, grass-like weeds, but they may be identified by their solid, three-sided leaves and triangular stems (Klerkx et al., 2019). Nutsedge and yellow nutsedge are two examples (Klerkx et al., 2019). Weeds are close competitors of crops as they constantly devour water, air, nutrients, and sunlight, which helps the maturation of crops. For better cultivation and good quality production of crops, weed detection at the appropriate time is an essential stride (Singh et al., 2023). Next is grass weeds. These weeds are related to grasses and look like them, and some examples of grass weeds include crabgrass, foxtail, and barnyard grass (Patton, 2023). Lastly, sedges resemble grass but are not the same as grasses because they grow in damp or moist environments and have triangle stems. Nutsedge, yellow nutsedge and kyllinga are typical sedge weeds (Patton, 2023).

Weeds frequently cause farmers to worry that agricultural production may suffer, and, in many cases, weeds consume crop plants' equivalent amounts of nutrients (De Clercq et al., 2018). Additionally, they consume resources like water, sunlight, and space that could have been used for agriculture (Cox et al., 2019). The more similar a crop's needs are to those of weeds, the more they will fight for the same resources, and crop yields will decrease because weeds aggressively compete with them (Anwar et al., 2021). If weeds gain an advantage over the crop, crop yields will be most negatively impacted. Four significant factors are density, timing, size, and chemistry (Lowry & Smith, 2018).

In addition, misusing herbicides or relying too heavily on chemical weed management techniques might harm the environment (Harwood, 2020). Herbicides can affect non-target organisms, such as beneficial insects, wildlife, and aquatic life, contaminate soil and seep into water bodies and herbicide use for weeding management can negatively affect the environment (Ustuner et al., 2020). It can also be expensive and time-consuming for farmers to control weeds (Cox et al., 2019). Herbicide application, manual weed control, and other weed management techniques all demand time, effort, and financial investment (Westwood et al., 2018). For small-scale farmers, weed control can be a significant financial strain, and weeding requires much labour (Woyessa, 2022).

Role of Computer Science in Weed Management

Weed management is a critical aspect of precision agriculture, and computer science plays a vital role in enhancing efficiency, accuracy, and sustainability in this domain. Weed control is vital to modern agriculture to ensure the best crop development and output (Chegini et al., 2023). However, conventional weed control methods can entail lengthy, labour-intensive procedures and excessive pesticide use, which can harm the environment (Pervaiz, 2024). The fusion of computer science and weed management has been a potential area for creating novel and long-lasting solutions in recent years (Prathima & Varshini, 2024). With its wide range of algorithms, machine learning methods, and cutting-edge sensing technologies, computer science has enormous potential to transform weed management practices (Jinglei et al., 2017). Researchers and practitioners can improve weed management practices' effectiveness, accuracy, and sustainability by utilising computational tools, which will increase agricultural productivity and have less negative impact on the environment (Vasileiou et al., 2023).

Innovative weed detection, classification, mapping, and targeted removal methods can be developed using computer scientific methodologies like machine learning, image processing, robotics, and data analytics (Jinglei et al., 2017). Machine learning techniques have much potential for weed detection (Islam et al., 2021). These algorithms may learn to distinguish between crops and weeds by being trained on large datasets of annotated weed photos, accurately recognising and outlining weed-infested areas inside agricultural fields (Shorewala et al., 2021). CV techniques can help with weed detection and create automated robotic systems that selectively recognise and remove weeds (Haichen et al., 2020). These autonomous robots can walk through fields, recognising and mechanically eradicating weeds while sparing important crops since they are outfitted with machine-learning algorithms (Vasileiou et al., 2023).

Computer science approaches can be used to analyse and interpret high-resolution imaging and spectral data, enabling prompt and precise weed species identification, growth stage monitoring, and forecast (Ghazal et al., 2024). Although there is great potential for combining computer science and weed management, several issues must be resolved (Dong et al., 2021). These include the necessity for interdisciplinary partnerships between agronomists, computer scientists, and engineers, algorithm robustness in shifting environmental circumstances, computing constraints for real-time applications, and data collection and annotation (Voutos et al., 2019).

Image Recognition

A CV technique called image recognition, commonly referred to as object detection, is used to find occurrences of objects in pictures or movies (Hall et al., 2020). Image detection algorithms frequently use machine learning or deep learning to generate

valuable results. Humans can quickly identify and pinpoint objects of interest when viewing photos or videos (Hall et al., 2020). Image detection aims to automate the replication of this intelligence, and it involves locating and detecting objects or features inside an image or a video (Mohan & Poobal, 2018). It is crucial in numerous applications, such as augmented reality, surveillance systems, driverless vehicles, and facial recognition (Li et al., 2020).

A deep learning-based method, notably those based on CNN, has become extremely popular and has attained outstanding results in recent years. Due to its high computational requirements, implementation in edge devices becomes challenging. Cloud computing serves as an enabler, allowing devices with limited resources to perform deep learning (Tan et al., 2022). Furthermore, developing frameworks like TensorFlow, PyTorch, and OpenCV offers significant tools and resources for creating image detection systems (Hall et al., 2020). These frameworks include pre-trained models for object detection in pictures or videos, which can be adjusted or applied immediately (Murthy et al., 2020). They also offer Application Programming Interfaces (API) and GUI to make it easier to incorporate picture-detecting capabilities into various applications (Li et al., 2020).

Every object class has unique characteristics that aid in identifying the class. For instance, searching for circles is expected to seek items a specific distance from the circle's axis (Traore et al., 2018). Similar to searching for squares, finding items with equal side lengths and perpendicular corners is necessary (Traore et al., 2018). Object detection techniques typically fall into two categories: neural network-based or non-neural methods (Xiao et al., 2020). For non-neural approaches, it is required first to define features using one of the techniques listed below and then perform the classification using a method like Support Vector Machine (SVM) (Li et al., 2020). On the other hand, neural approaches, which are frequently based on CNN, can do end-to-end object detection without directly defining features (Li et al., 2020).

Image Recognition Techniques

In the realm of image recognition, conventional machine learning methods rely on approaches such as Histogram of Oriented Gradients (HOG), Scale-Invariant Feature Transform (SIFT), and Local Binary Patterns (LBP) to extract pertinent features from images. CNN has revolutionised the field by autonomously learning intricate hierarchical representations directly from pixel data via convolutional, pooling, and fully connected layers. CNN is proof of the evolution of Artificial Neural Networks (ANN), which are mainly used to extract features from datasets with grid-like matrixes (Li et al., 2020). Examples of visual datasets where data patterns play a significant role are images and videos (Gu et al., 2018). Artificial neurons, also known as units, are found in artificial neural networks, and units are connected from one layer to another (Yamashita et al.,

2018). Each linkage has weights that control how much one unit influences another, and the neural network learns more and more about the data as it moves from one unit to another, eventually producing an output from the output layer (Tan & Le, 2019).

Although there are different kinds of neural networks in deep learning, CNN is the preferred network architecture for identifying and recognising objects (Tan & Le, 2019). Therefore, they are ideally suited for CV activities and applications where accurate object recognition is crucial, such as facial and self-driving automobile systems (Tan & Le, 2019). CV, which uses one or more video cameras, analogue-to-digital conversion (ADC), and digital signal processing (DSP), is the ability of a computer to see (Li et al., 2020). Machine vision's complexity is comparable to speech recognition (Zhou, 2020). Cameras are used by machine vision to collect visual data from the environment and then prepare the data for usage in various applications by processing the photos using a combination of hardware and software (Gu et al., 2018). Specialised optics are frequently used in machine vision technology to capture images; with these methods, specific aspects of the image can be processed, examined, and assessed (Zhou, 2020). The implication of the convergence of weed control and computer science is the intriguing potential to revolutionise agricultural practices. We can develop more precise, effective, and sustainable weed management strategies by embracing cutting-edge technologies and computational tools.

MATERIALS AND METHODS

This study divided the methodology into three phases: data preparation, algorithm implementation, and performance evaluation. Figure 1 visually represents the three phases: Phase 1: Dataset preparation, Phase 2: Algorithm Implementation, and Phase 3: Performance Evaluation.

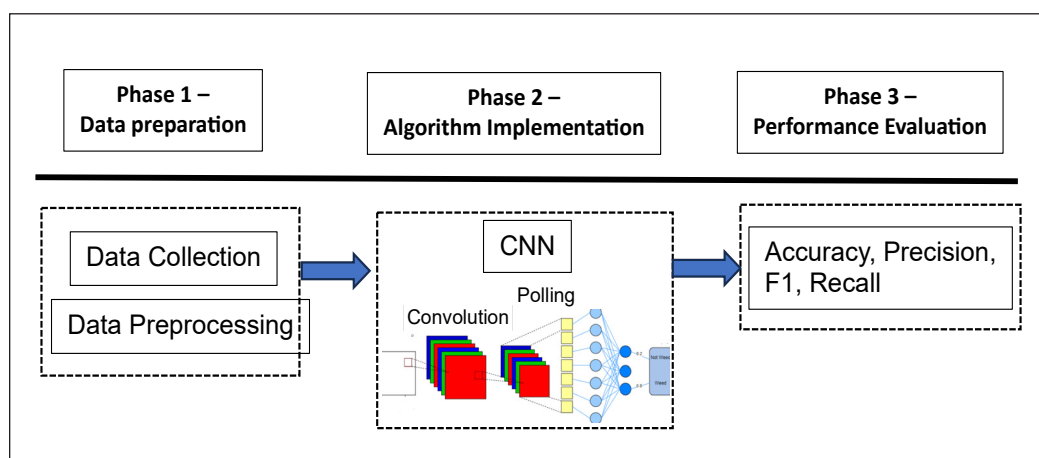


Figure 1. Research methodology

Phase 1: Data Preparation

Data Collection

It is crucial to ensure that the dataset accurately depicts real-life situations that can be anticipated when running into them during inference. It should include a variety of weed species, stages of growth, lighting, backgrounds, and viewpoints. A dataset was chosen based on research conducted by Uchechi F. Ukaegbu at the University of Johannesburg in South Africa. The dataset collection for automatic weed detection and identification came from Yuzhen Lu of the Department of Agricultural and Biological Engineering. The annotated visual dataset for this dataset is now accessible via Kaggle and the repository. The dataset of images of cotton crops, weeds, maize and wheat crops, chilli and jute crops was collected using unmanned aerial vehicles (UAVs) with an input shape of $224 \times 224 \times 3$ and a batch size of 20. This data collection has 360 images and a total size of 83 MB. There are 360 total images in the dataset. 80% of the dataset are images used for training, while the remaining 20% are used for testing and evaluation. Based on research by Hosein Chegini from the University of Auckland, who used a training dataset of 77% and a testing dataset of 23% from 500 photos and achieved an accuracy of 95%, this division was created.

Data Preprocessing

Raw data is subjected to several techniques and activities known as dataset preprocessing before being utilised to train a machine-learning model. It requires transforming and altering the data to guarantee that it is in an appropriate format for analysis and modelling. Enhancing the data's quality, consistency, and usefulness for training a CNN model requires dataset preparation. This enhances the model's capacity to discover significant patterns, generalise fresh data well, and produce reliable forecasts in practical situations. The goal of dataset preparation is to format the data for training a machine learning model. It helps improve model evaluation, enhances feature representation, reduces noise or inconsistencies, and ensures data quality.

Image resizing is a common preprocessing step in machine learning projects. It involves changing the image's dimensions while keeping its aspect ratio to avoid distortion. A typical method for resizing is scaling, which adjusts the width and height, using interpolation techniques like bilinear or bicubic to maintain quality. Another method is cropping, where a region of interest (ROI) is selected and resized. Image normalisation helps standardise pixel values, making the model more resilient to lighting or colour changes and aiding training. One type of normalisation is min-max normalisation, which scales pixel values to a specific range, usually between 0 and 1. Histogram equalisation improves image contrast by redistributing pixel values to a new range. This technique is useful for images with low contrast or uneven lighting.

Image filtering is a common technique in image processing used to enhance or modify an image's visual qualities. It involves applying a filter or kernel to each pixel using methods like convolution or correlation. Image filtering is used for noise reduction, edge detection, smoothing, sharpening, and feature extraction. A Gaussian filter smooths the image by reducing high-frequency noise while preserving its structure. It gives higher weight to pixels near the centre, creating a blurring effect. Sobel and Prewitt filters are often used for edge detection by calculating the gradient's size and direction at each pixel, highlighting areas with rapid intensity changes. Image segmentation divides an image into meaningful sections. Thresholding is a basic segmentation method that assigns pixels to different segments based on intensity values, best used when objects stand out from the background. Edge-based segmentation finds the borders between different regions by detecting sudden changes in pixel intensity. Popular edge detection techniques include the Laplacian of Gaussian (LoG) and the Sobel operator.

Phase 2: Algorithm Implementation

The dataset consists of images of weeds, broadleaf, maize plants, soil, and cotton crops that go through a few processes, based on Figure 2. The 360-image dataset was split into two categories: 80% dataset for training and 20% dataset for testing. This partition was based on research by Dong Hu using data from 22177 images of 12 rice weeds. Dong Hu from Shanghai Ocean University in China selected to use a 74% training and 26% testing dataset for his study (Dong et al., 2021). The result showed that the accuracy was 81% (Dong et al., 2021).

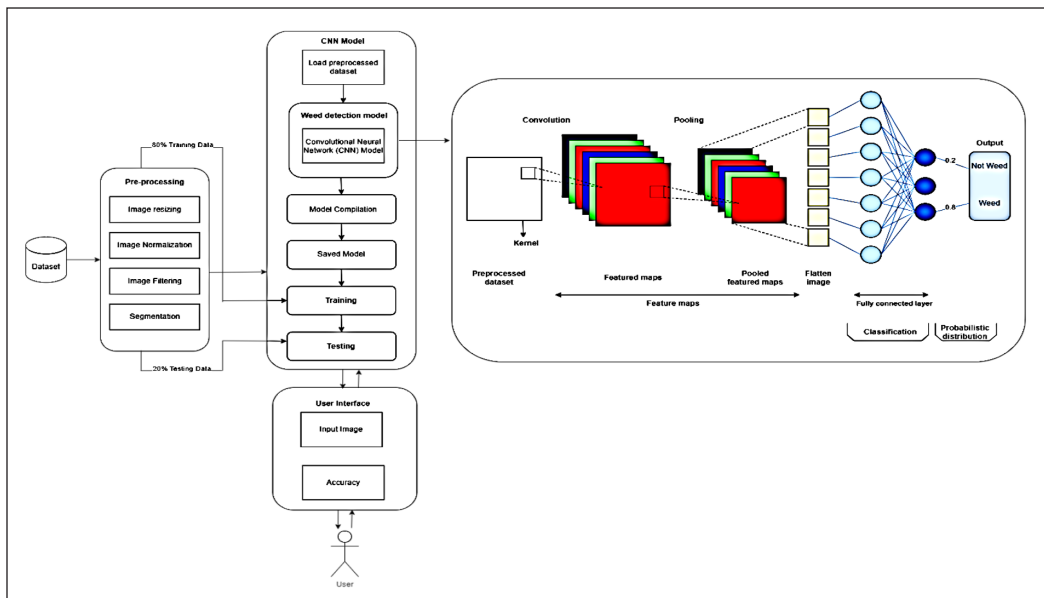


Figure 2. Prototype architecture of weed detection for agriculture using CNN algorithm

After preprocessing the weed image successfully, it will move on to the CNN model training. Using the preprocessed dataset to train a machine-learning model is a practice known as “Dataset training.” The major source of information for the model is that it discovers patterns and relationships in the input data and their associated labels. The goal is to enable the model to accurately predict or categorise novel, unanticipated inputs. The model can generalise and predict cases it has not encountered before due to the training process, which teaches it the data’s underlying patterns, relationships, and representations. The CNN model includes taking the dataset photos. It applies a filter or kernel to the input image during the convolution process to identify and extract specific characteristics. The pooling layer then reduces the spatial dimensions of the feature maps produced by the convolutional layer. It down-sampled the data to reduce the size of the feature maps and the computational difficulty.

The activation layer then applies a non-linear activation function, such as the ReLU function, to the output of the pooling layer. The nonlinearity generated by this function allows the model to learn increasingly complex representations of the input data. Next is the layer that is entirely interconnected. In a typical neural network layer, every neuron in the layer before is connected to every neuron in the layer after. This layer combines the learned information from the convolutional and pooling layers to provide a prediction (Goodfellow, 2016). The dense layer can then merge the features that the convolutional and pooling layers combined to extract from the input image, producing the final prediction. The dense layer in a CNN is often the last used to generate the output predictions. The dense layer conducts a weighted sum of the inputs. It employs an activation function to generate the final output after flattening and passing the activations from the layers before it as inputs. The dataset will be tested when the CNN model has been built. The goal of dataset testing is to gauge how effectively the model works with unknown data and predict how effective it will be in practical situations. During this phase, the accuracy of the CNN model will be calculated and analysed using the confusion matrix.

Finally, the user interface will display the accuracy to be analysed, whether there is an image of a weed. Typically, accuracy is given as a percentage. A model score is a number or statistic used to determine the degree to which a prediction model works. These results show how effectively the model can predict outcomes based on brand-new, unforeseen data. For instance, an accuracy of below 50% denotes that the system cannot detect any weed’s presence in the input data. However, the weeds are detected if the accuracy is above 50%.

Pseudocode

Before the CNN algorithms are implemented in a programming language, the weed detection prototype pseudocode is primarily intended to simplify the design, planning, and communication of the CNN algorithms inside the prototype. By offering a more

accessible and intelligible representation of an algorithm than formal programming language syntax, pseudocode plays a crucial role in software development. It enables programmers to pay attention to the logic and flow of the algorithm rather than becoming sidetracked by language-specific features. The pseudocode is shown in Figure 3.

This pseudocode describes how to train a CNN model to recognise weeds in photographs of crop fields and how to use the model to forecast the presence of weeds in fresh images supplied by the user. The accuracy score determines weed detection, and the results are printed accordingly. Weeds datasets are the prototype's inputs (images). The weed detection algorithm will be trained and tested using these images. Weed detection is the prototype's output. The main objective of the pseudocode is to

detect weeds in the input crop field images. The system will determine whether weeds are present in the input images. The pseudocode's primary goal for the input images is to detect weeds. The prototype will determine whether weeds are visible in the supplied dataset.

The dataset is divided into two parts: 20% is used to test the model's performance, and 80% is used to train the model. With this split, the model is trained on a sizable dataset and given access to unused data for evaluation. The CNN training model then starts. CNNs are particularly well-suited for image-related tasks due to their ability to learn and recognize spatial feature hierarchies. The CNN model will be trained using the provided dataset, where the training data is fed into the model during the training phase. The model discovers weed-related patterns and traits through an iterative optimisation procedure. The model's performance is assessed following training using the testing dataset. This process enables evaluation of the model's ability to generalise to unseen data. The model is prepared to be utilised for weed detection on user-provided input photos after it has been trained and tested.

The model gives accuracy by reflecting its confidence level in a prediction when it produces one based on an image the user has provided. The pseudocode interprets a positive detection of weeds as one for which the accuracy is greater than or equal to 50%. This message ("Weeds detected in the image.") will be printed if the model finds

```

Input:
  Crop field images

Output:
  Weed Detection

Start
  1. Input Weeds Dataset
  2. Data preprocessing
    - Image resizing
    - Image normalization
    - Image filtering
    - Image segmentation
  3. Dataset splitting
    - 80% training set
    - 20% testing set
  4. Training the CNN model
  5. Testing CNN model
  6. Detecting weed from the user input
    if accuracy >=50%
      print("Weeds detected in the image.")
      print (accuracy)
    else
      print("No weeds detected in the image.")
      print (accuracy)

End

```

Figure 3. Pseudocode

weeds in the input image. The accuracy score, which expresses how confident it is in detecting weeds, is printed to provide further details. The pseudocode classifies weed detection as negative if the accuracy of finding it is lower than 50%. This message (“No weeds detected in the image.”) will be printed if the model determines that there are no weeds in the input image in this circumstance. Additionally, the model’s rating for the negative detection is printed.

Evaluation Phase

The performance of the model was tested throughout the evaluation phase. The evaluation phase is a step in the machine learning process when evaluation metrics and methodologies are used to gauge the performance of a trained model. The objectives of the evaluation phase are to gain knowledge of the model’s performance, comprehending its advantages and disadvantages, and assessing its suitability for the intended job or application. The evaluation of a CNN model’s performance on a test dataset is called a CNN accuracy test. The accuracy with which the CNN model predicts the classes for the test samples is what is measured. Since accuracy clearly indicates the model’s general correctness, it is a crucial evaluation statistic. The number of accurate forecasts divided by the total number of predictions is used to compute it. High accuracy means the model correctly predicts values from the testing dataset. As a result, the confusion matrix might offer more profound perceptions about the model’s effectiveness. The confusion matrix is illustrated in Figure 4.

A confusion matrix evaluates the performance of a classification model by presenting its predictions, including true positives, true negatives, false positives, and false negatives

	POSITIVE	NEGATIVE	
POSITIVE	True Positive (TP)	False Negative (FN)	SENSITIVITY TP $\frac{TP}{(TP + FN)}$
NEGATIVE	False Positive (FP)	True Negative (TN)	SPECIFICITY TN $\frac{TN}{(TN + FP)}$
	PRECISION TP $\frac{TP}{(TP + FP)}$	NEGATIVE PREDICTIVE VALUE TN $\frac{TN}{(TN + FN)}$	ACCURACY TP + TN $\frac{TP + TN}{(TP + TN + FP + FN)}$

Figure 4. Confusion matrix

(Powers, 2011). It includes details on both actual and anticipated classifications. The number of accurately anticipated positive instances or observations is measured by the term “True Positive” (TP). The number of accurately anticipated negative occurrences or observations is True Negative (TN). False Positive (FP) counts the number of instances or observations wrongly projected to be positive. These are situations that the model mistook for positive ones, even if they are genuinely harmful. Finally, False Negative (FN) displays how many negative data instances or observations were mispredicted. This refers to instances where the model incorrectly classified positive cases as negative.

It indicates how many instances of positivity the classifier has classified as such. The outcome ought to be better. The following term for specificity is the True Negative Rate. It measures how many negative examples the classifier is classified as such. There needs to be much specificity. The ratio of the total number of positively classified positive examples to the total number of positively forecasted positive examples is known as precision. It demonstrates that a favourable prediction was accurate. The accuracy formula then multiplies the total number of instances, equal to the sum of the true positives, false positives, true negatives, and false negatives, by the number of true positives and true negatives. Concerning the overall number of cases, it measures how effectively the model predicts positive and negative examples.

RESULTS AND DISCUSSIONS

The first step is evaluating the accuracy of the CNN algorithm that has been put into practice and analysing how well it performs in weed detection. The second part thoroughly examines the CNN model to determine its general effectiveness and accuracy in weed identification. The third and final section tests the weed detection prototype interface, examining its workings and ensuring everything works.

Evaluation of the CNN Model

A crucial aspect of evaluating the CNN model for weed detection is evaluating the model through dataset splitting. A split of 70–30 is commonly employed, where 70% of the data is designated for training, and the remaining 30% is reserved for testing. This approach ensures that the model’s performance generalises effectively to new, unseen data. Table 1 provides a comprehensive overview of accuracy results obtained from different splitting configurations, including 70–30, 80–20, and 90–10, executed over 15 epochs. Upon analysis of the table, it becomes evident that the optimal dataset splitting for the best accuracy is achieved when 80% of the data is allocated for training and 20% is set aside for testing. This configuration produces an accuracy of 89.82% for training and 94.37% for testing after 15 epochs. The findings suggest that the 80–20 split strikes the right balance, facilitating good model performance in weed detection.

Table 1
Evaluate the CNN model with different splits

Total dataset	Data splitting				Epochs	Training accuracy	Testing accuracy
	Training		Testing				
	Percentage	Number of datasets	Percentage	Number of datasets			
360 images	70%	252	30%	108	15	88.37%	97.2%
	80%	288	20%	72		89.82%	94.37%
	90%	324	10%	36		89.16%	97.14%

As Figure 5 demonstrates, the model outperformed the results obtained with the 70–30 and 80–20 splits, achieving an accuracy of 89.82% with 15 epochs. Considering that this specific model’s training process took several hours is relevant. Because of the significant size of the datasets and technological limitations, the maximum number of epochs tested was limited to 15. Despite these limitations, the accuracy of 89.82% attained with the 15-epoch configuration demonstrates the model’s performance under the specified circumstances.

Figure 6 presents a graphical representation of the accuracy achieved with an 80% training dataset, utilising 15 epochs for 360 image datasets. The graph portrays an upward trend, indicating a consistent increase in accuracy over the training period. This visual representation is a valuable tool for assessing the model’s performance, demonstrating its ability to learn and improve accuracy as the training epochs progress. The graph’s ascending

```

Epoch 1/15
8/8 [=====] - 3s 75ms/step - loss: 0.6735 - accuracy: 0.6195 - val_loss: 0.6476 - val_accuracy: 0.8070
Epoch 2/15
8/8 [=====] - 0s 20ms/step - loss: 0.6220 - accuracy: 0.7920 - val_loss: 0.6017 - val_accuracy: 0.8070
Epoch 3/15
8/8 [=====] - 0s 19ms/step - loss: 0.5816 - accuracy: 0.8319 - val_loss: 0.5670 - val_accuracy: 0.8246
Epoch 4/15
8/8 [=====] - 0s 18ms/step - loss: 0.5497 - accuracy: 0.8186 - val_loss: 0.5434 - val_accuracy: 0.8070
Epoch 5/15
8/8 [=====] - 0s 18ms/step - loss: 0.5143 - accuracy: 0.8186 - val_loss: 0.5131 - val_accuracy: 0.8596
Epoch 6/15
8/8 [=====] - 0s 19ms/step - loss: 0.4798 - accuracy: 0.8451 - val_loss: 0.4797 - val_accuracy: 0.8421
Epoch 7/15
8/8 [=====] - 0s 18ms/step - loss: 0.4489 - accuracy: 0.8451 - val_loss: 0.4538 - val_accuracy: 0.8421
Epoch 8/15
8/8 [=====] - 0s 19ms/step - loss: 0.4191 - accuracy: 0.8540 - val_loss: 0.4275 - val_accuracy: 0.8246
Epoch 9/15
8/8 [=====] - 0s 20ms/step - loss: 0.3965 - accuracy: 0.8717 - val_loss: 0.4106 - val_accuracy: 0.8246
Epoch 10/15
8/8 [=====] - 0s 22ms/step - loss: 0.3795 - accuracy: 0.8761 - val_loss: 0.4001 - val_accuracy: 0.8421
Epoch 11/15
8/8 [=====] - 0s 17ms/step - loss: 0.3675 - accuracy: 0.8673 - val_loss: 0.3987 - val_accuracy: 0.8421
Epoch 12/15
8/8 [=====] - 0s 19ms/step - loss: 0.3514 - accuracy: 0.8628 - val_loss: 0.3851 - val_accuracy: 0.8421
Epoch 13/15
8/8 [=====] - 0s 18ms/step - loss: 0.3404 - accuracy: 0.8761 - val_loss: 0.3746 - val_accuracy: 0.8421
Epoch 14/15
8/8 [=====] - 0s 18ms/step - loss: 0.3310 - accuracy: 0.8982 - val_loss: 0.3682 - val_accuracy: 0.8421
Epoch 15/15
8/8 [=====] - 0s 18ms/step - loss: 0.3229 - accuracy: 0.8982 - val_loss: 0.3666 - val_accuracy: 0.8421
INFO:tensorflow:Assets written to: saved_model/my_model/assets
    
```

Figure 5. Training epoch

trajectory indicates the model’s effectiveness in capturing patterns and features within the dataset, ultimately improving accuracy. Furthermore, it is observed that increasing the number of training epochs tends to enhance accuracy. The highest accuracy recorded is 89.82%, achieved with 15 epochs. The model still delivers commendable accuracy at 86.01% for a more time-efficient approach with five epochs. Interestingly, utilising ten epochs does not significantly alter the performance, maintaining accuracy levels akin to those achieved with five epochs.

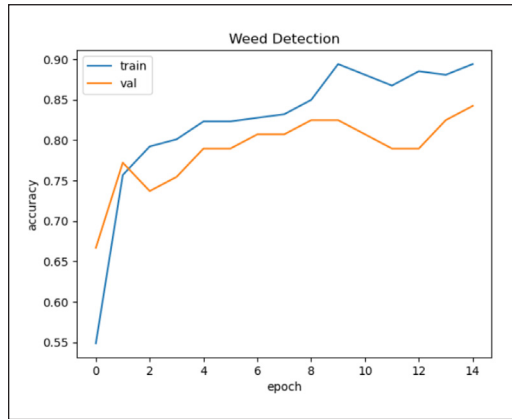


Figure 6. Graph of accuracy for 80% training dataset

Table 2 illustrates this comparison across different epoch configurations. The results indicate that an 80–20 dataset split, coupled with a judicious choice of epochs, significantly contributes to the model’s accuracy and efficiency in identifying weeds.

Table 2
Evaluate the CNN model with different epochs

Total dataset	Data splitting				Epochs	Testing accuracy
	Training		Testing			
	Percentage	Number of datasets	Percentage	Number of datasets		
360 images	80%	288	20%	72	5	86.01%
					10	86.71%
					15	89.82%

Model Performance

Figure 7 shows that the accuracy of the CNN model is 0.9014, indicating that 90.14% of the model’s predictions are correct. Precision, measured at 0.9394, signifies that 93.94% of the samples identified as weeds by the model were indeed weeds. The recall of 0.8611 indicates that the model accurately identifies weeds 86.11% of the time when predicting a sample as a weed. The F1 score, an average of accuracy and

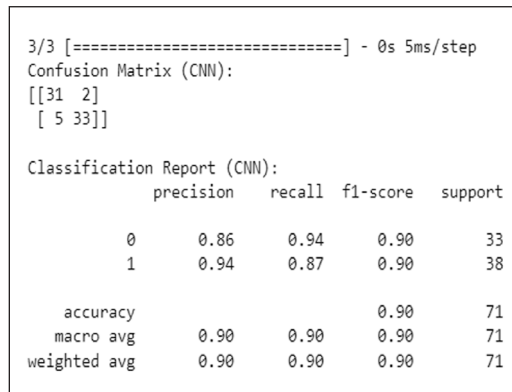


Figure 7. Calculation of accuracy by the prototype

recall, is computed at 88.08%, serving as a comprehensive measure of the model’s overall performance.

Prototype Interface

The user interface for the weed detection prototype was developed using Tkinter, providing a visually intuitive and user-friendly experience. Figure 8 illustrates the graphical user interface (GUI) that comprises three main buttons. The “Upload Image” button allows users to select and upload an image displayed within a designated box on the interface. The “Start” button initiates the weed detection algorithm, leveraging a pre-trained CNN model (new_model) previously trained on a weed detection dataset. The accuracy of the detection process is showcased, providing valuable insights into the model’s performance. As shown in Figure 8, if a user inputs an image containing weeds, the system successfully detects the weeds and displays the accuracy of the CNN model.

Conversely, in Figure 9, if a non-weed image is selected, the system accurately identifies the absence of weeds and presents the corresponding model accuracy.

DISCUSSION

The evaluation of our weed detection system, employing CNN algorithms, reveals an accuracy of 89.51%. To contextualise our findings, we compare notable studies in the field. Table 3 presents a summarised comparison of the findings with previous research. This indicates that the research conducted in this project is in line with previous studies, achieving an accuracy of 89.82%. This highlights the effectiveness of the CNN-based

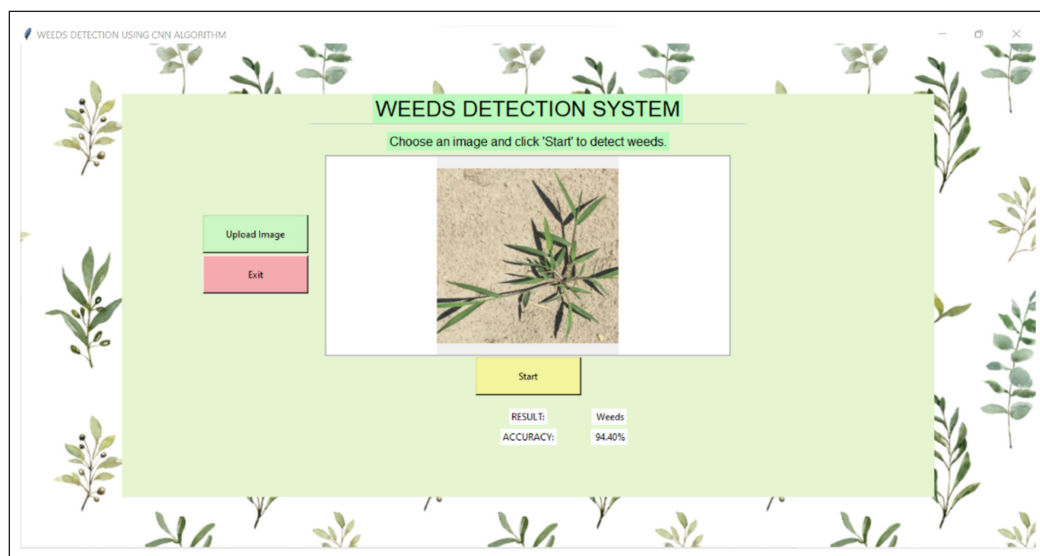


Figure 8. User interface with weeds as input User interface with weeds as input

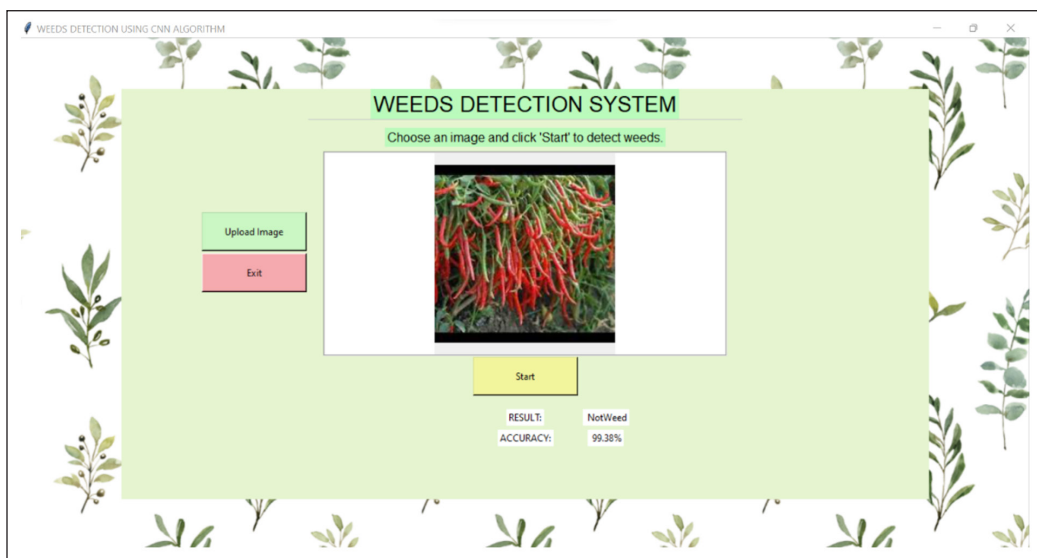


Figure 9. User interface with weeds as input, User interface with no weeds as input

Table 3

Discussion on previous research

No.	Title	Year	Result	Reference
1.	Weed Detection in Farm Crops Using Parallel Image Processing	2018	91.1%	Umamaheswari et al. (2018)
2.	Weed Classification in Hyperspectral Remote Sensing Images Via Deep Convolutional Neural Network	2018	88%	Farooq et al. (2018)
3.	Weed Seedling Detection Using Mask Regional Convolutional Neural Network	2020	98%	Patidar et al. (2020)
4.	Designing and Developing a Weed Detection Model for California Thistle	2023	95%	Chegini et al. (2023)

weed detection system and places it in a favourable position among notable endeavours in the field. As we delve into the details of our methodology, it becomes clear that our approach has yielded promising outcomes, making a valuable contribution to the continuous advancement of weed detection technologies.

CONCLUSION

To summarise, the project highlights the significant potential of Convolutional Neural Networks (CNN) in weed detection for precision agriculture. The successful accomplishment of the project demonstrates the robustness of the implemented CNN algorithms and their application in addressing the intricacies associated with weed identification in agricultural settings. The model architecture, input representation, and user-friendly graphical interface

are all seamlessly integrated into the prototype of the CNN model. A user-friendly prototype successfully identified weeds in agricultural images and functioned as a valuable tool for agriculturalists. A thorough evaluation demonstrated how accurate CNN's weed detection algorithms are. Specific testing procedures, such as confusion matrix analysis and dataset splitting, were used. Along with precision, recall, and F1 score metrics, the accuracy of 89.87% indicates the effectiveness of the developed CNN model in accurately identifying weeds in various agricultural contexts.

The effective CNN-based weed detection prototype solved another problem highlighted: the challenges of accurately identifying and managing weeds. The prototype's accuracy of 89.87% for splitting 80–20, proven by thorough evaluation metrics, allows weed control in agriculture to be effectively and practically addressed. CNN's demonstrates potential performance underscores its relevance in precision agricultural research. The outcome of this project fosters agricultural innovation by integrating AI and machine learning into farming practices, encouraging technological advancements in the agricultural sector. Future research can explore the integration of CNN and LSTM algorithms, specifically for weed detection, with the goal of enhancing model performance and accuracy.

ACKNOWLEDGEMENTS

The authors sincerely express their gratitude to Universiti Teknologi MARA Cawangan Terengganu, Malaysia and De La Salle University, Philippines for their support and encouragement in this research. Additionally, they extend their appreciation to everyone who contributed, either directly or indirectly, to the success of this study.

REFERENCES

- Anwar, M. P., Islam, A. M., Yeasmin, S., Rashid, M. H., Juraimi, A. S., Ahmed, S., & Shrestha, A. (2021). Weeds and their responses to management efforts in a changing climate. *Agronomy*, *11*(10), 1921. <https://doi.org/10.3390/agronomy11101921>. <https://www.mdpi.com/2073-4395/11/10/1921>
- Asad, M. H., & Bais, A. (2020). Weed detection in canola fields using maximum likelihood classification and deep convolutional neural network. *Information Processing in Agriculture*, *7*(4), 535-545. <https://doi.org/10.1016/j.inpa.2019.12.002>
- Bolico, M. C. (2019). FAO and the situation of food security and nutrition in the world. *Journal of Nutritional Science and Vitaminology*, *65*(Supplement), S4-S8. <https://doi.org/10.3177/jnsv.65.s4>
- Chegini, H., Beltran, F., & Mahanti, A. (2023). Designing and developing a weed detection model for California Thistle. *ACM Transactions on Internet Technology (TOIT)*, *23*(3), 1-9. <https://doi.org/10.1145/3544491>
- Cox, G., Lowe, P., & Winter, M. (2019). *Agriculture: People and policies (Vol. 5)*. Routledge. <https://doi.org/10.4324/9780429340949>

- Darwin, B., Dharmaraj, P., Prince, S., Popescu, D. E., & Hemanth, D. J. (2021). Recognition of bloom/yield in crop images using deep learning models for smart agriculture: A review. *Agronomy*, *11*(4), 646. <https://doi.org/10.3390/agronomy11040646>
- De Clercq, M., Vats, A., & Biel, A. (2018). Agriculture 4.0: The future of farming technology. *Proceedings of the World Government Summit*, 1-30.
- Dong, H., Zhang, L., & Zou, B. (2021). Exploring vision transformers for polarimetric SAR image classification. *IEEE Transactions on Geoscience and Remote Sensing*, *60*, 1-15. <https://doi.org/10.1109/TGRS.2021.3137383>
- Dosovitskiy, A., Beyer, L., Kolesnikov, A., Weissenborn, D., Zhai, X., Unterthiner, T., Dehghani, M., Minderer, M., Heigold, G., & Gelly, S. (2020). An image is worth 16x16 words: Transformers for image recognition at scale. *arXiv preprint arXiv:2010.11929*
- Edwards, N. (2024). *Weeds*. Reaktion Books.
- Farooq, A., Hu, J., & Jia, X. (2018). Weed classification in hyperspectral remote sensing images via deep convolutional neural network. In *IGARSS 2018-2018 IEEE International Geoscience and Remote Sensing Symposium* (pp. 3816-3819). IEEE. <https://doi.org/10.1109/IGARSS.2018.8518541>
- Ghazal, S., Munir, A., & Qureshi, W. S. (2024). Computer vision in smart agriculture and precision farming: Techniques and applications. *Artificial Intelligence in Agriculture*, *13*, 64-83. <https://doi.org/10.1016/j.aiaa.2024.06.004>
- Goodfellow, I., Bengio, Y., & Courville, A. (2016). *Deep learning*. MIT Press.
- Gu, J., Wang, Z., Kuen, J., Ma, L., Shahroudy, A., Shuai, B., Liu, T., Wang, X., Wang, G., & Cai, J. (2018). Recent advances in convolutional neural networks. *Pattern Recognition*, *77*, 354-377. <https://doi.org/10.1016/j.patcog.2017.10.013>
- Haichen, J., Qingrui, C., & Zheng Guang, L. (2020). Weeds and crops classification using deep convolutional neural network. In *Proceedings of the 3rd International Conference on Control and Computer Vision* (pp. 40-44). Association for Computing Machinery. <https://doi.org/10.1145/3425577.3425585>
- Hall, D., Dayoub, F., Skinner, J., Zhang, H., Miller, D., Corke, P., Carneiro, G., Angelova, A., & Sünderhauf, N. (2020). Probabilistic object detection: Definition and evaluation. In *Proceedings of the IEEE/CVF Winter Conference on Applications of Computer Vision* (pp. 1031-1040). IEEE. <https://doi.org/10.1109/WACV45572.2020.9093599>
- Hamuda, E. A. (2019). *Signal and image processing technology for smart agriculture*. NUI Galway.
- Harwood, R. R. (2020). A history of sustainable agriculture. In *Sustainable agricultural systems* (pp. 3-19). CRC Press. <https://doi.org/10.1201/9781003070474-2>
- Henaff, O. J., Srinivas, A., De Fauw, J., Razavi, A., Doersch, C., Eslami, S. M. A., & Van Den Oord, A. (2020). Data-efficient image recognition with contrastive predictive coding. In *Proceedings of the 37th International Conference on Machine Learning* (pp. 4182-4192). JMLR.org.
- Hu, D., Ma, C., Tian, Z., Shen, G., & Li, L. (2021). Rice weed detection method on YOLOv4 convolutional neural network. In *2021 International Conference on Artificial Intelligence, Big Data and Algorithms (CAIBDA)* (pp. 41-45). IEEE. <https://doi.org/10.1109/CAIBDA53561.2021.00016>

- Islam, N., Rashid, M. M., Wibowo, S., Xu, C.-Y., Morshed, A., Wasimi, S. A., Moore, S., & Rahman, S. M. (2021). Early weed detection using image processing and machine learning techniques in an Australian chilli farm. *Agriculture*, *11*(5), 387. <https://doi.org/10.3390/agriculture11050387>
- Jinglei, T., Ronghui, M., Zhiyong, Z., Jing, X., & Dong, W. (2017). Distance-based separability criterion of ROI in classification of farmland hyper-spectral images. *International Journal of Agricultural and Biological Engineering*, *10*(5), 177-185. <https://doi.org/10.25165/j.ijabe.20171005.2264>
- Katel, S., Yadav, S. P. S., Khadka, A., Karki, N., & Neupane, S. (2023). Cereal import and consumption patterns in Nepal—Analysis of rice, wheat, maize, and millet: A review. *Russian Journal of Agricultural and Socio-Economic Sciences*, *139*(7), 16-32. <https://doi.org/10.18551/rjoas.2023-07.03>
- Klerkx, L., Jakku, E., & Labarthe, P. (2019). A review of social science on digital agriculture, smart farming, and Agriculture 4.0: New contributions and a future research agenda. *NJAS - Wageningen Journal of Life Sciences*, *90*, 100315. <https://doi.org/10.1016/j.njas.2019.100315>
- Komarek, A. M., De Pinto, A., & Smith, V. H. (2020). A review of types of risks in agriculture: What we know and what we need to know. *Agricultural Systems*, *178*, 102738. <https://doi.org/10.1016/j.agsy.2019.102738>
- Li, K., Wan, G., Cheng, G., Meng, L., & Han, J. (2020). Object detection in optical remote sensing images: A survey and a new benchmark. *ISPRS Journal of Photogrammetry and Remote Sensing*, *159*, 296-307. <https://doi.org/10.1016/j.isprsjprs.2019.11.023>
- Lottes, P., Behley, J., Milioto, A., & Stachniss, C. (2018). Fully convolutional networks with sequential information for robust crop and weed detection in precision farming. *IEEE Robotics and Automation Letters*, *3*(4), 2870-2877. <https://doi.org/10.1109/LRA.2018.2846289>
- Lowry, C. J., & Smith, R. G. (2018). Weed control through crop plant manipulations. In K. Jabran & B. S. Chauhan (Eds.), *Non-chemical weed control* (pp. 73-96). Academic Press. <https://doi.org/10.1016/B978-0-12-809881-3.00005-X>
- Mohan, A., & Poobal, S. (2018). Crack detection using image processing: A critical review and analysis. *Alexandria Engineering Journal*, *57*(2), 787-798. <https://doi.org/10.1016/j.aej.2017.01.020>
- Murthy, C. B., Hashmi, M. F., Bokde, N. D., & Geem, Z. W. (2020). Investigations of object detection in images/videos using various deep learning techniques and embedded platforms—A comprehensive review. *Applied Sciences*, *10*(9), 3280. <https://doi.org/10.3390/app10093280>
- Otsuka, K., & Fan, S. (Eds.) (2021). *Agricultural development: New perspectives in a changing world*. International Food Policy Research Institute. <https://doi.org/10.2499/9780896293830>
- Patidar, S., Singh, U., & Sharma, S. K. (2020). Weed seedling detection using mask regional convolutional neural network. In *2020 International Conference on Electronics and Sustainable Communication Systems (ICESC)* (pp. 311-316). IEEE. <https://doi.org/10.1109/ICESC48915.2020.9155701>
- Patton, B. A. (2023). *Control of annual grasses using new Sorghum Herbicides* [Master's thesis, Texas Tech University]. <https://ttu-ir.tdl.org/server/api/core/bitstreams/b44e9489-b099-4944-84da-95140f3e15d9/content>

- Pervaiz, R. (2024). Herbicide strategies for weed control in rice cultivation: Current practices and future directions. *Haya: Saudi Journal of Life Sciences*, 9(4), 114-129. <https://doi.org/10.36348/sjls.2024.v09i04.004>
- Powers, D. M. W. (2011). Evaluation: From precision, recall and F-measure to ROC, informedness, markedness & correlation. *Journal of Machine Learning Technologies*, 2(1), 37–63.
- Prathima, S. Y., & Varshini, V. (2024). Integrating IoT sensors and deep learning for robust crop and weed discrimination in dynamic agricultural environments. In *2024 2nd International Conference on Networking and Communications (ICNWC)* (pp. 1-6). IEEE. <https://doi.org/10.1109/icnwc60771.2024.10537300>
- Qiao, S., Shen, W., Zhang, Z., Wang, B., & Yuille, A. (2018). Deep co-training for semi-supervised image recognition. In V. Ferrari, M. Hebert, C. Sminchisescu & Y. Weiss (Eds.), *Proceedings of the European Conference on Computer Vision (ECCV)* (pp. 142-159). Springer. https://doi.org/10.1007/978-3-030-01267-0_9
- Ramli, Z., Juraimi, A. S., Motmainna, M., Che' Ya, N. N., Roslim, M. H. M., Noor, N. M., & Ahmad, A. (2024). Weed management using UAV and remote sensing in Malaysia paddy field: A review. *Pertanika Journal of Science & Technology*, 33(3), 1219-1241. <https://doi.org/10.47836/pjst.32.3.13>
- Razfar, N., True, J., Bassiouny, R., Venkatesh, V., & Kashef, R. (2022). Weed detection in soybean crops using custom lightweight deep learning models. *Journal of Agriculture and Food Research*, 8, 100308. <https://doi.org/10.1016/j.jafr.2022.100308>
- Saleh, A. Y., Chin, C. K., & Rosdi, R. A. (2024). Transfer learning for lung nodules classification with CNN and random forest. *Pertanika Journal of Science & Technology*, 32(1), 463-479. <https://doi.org/10.47836/pjst.32.1.25>
- Sarvini, T., Sneha, T., GS, S. G., Sushmitha, S., & Kumaraswamy, R. (2019). Performance comparison of weed detection algorithms. In *2019 International Conference on Communication and Signal Processing (ICCSP)* (pp. 0843-0847). IEEE. <https://doi.org/10.1109/iccsp.2019.8698094>
- Shorewala, S., Ashfaque, A., Sidharth, R., & Verma, U. (2021). Weed density and distribution estimation for precision agriculture using semi-supervised learning. *IEEE Access*, 9, 27971-27986. <https://doi.org/10.1109/ACCESS.2021.3057912>
- Singh, V., Gourisaria, M. K., GM, H., & Choudhury, T. (2023). Weed detection in soybean crop using Deep Neural Network. *Pertanika Journal of Science & Technology*, 31(1), 401-423. <https://doi.org/10.47836/pjst.31.1.24>
- Tan, K. K. H., Wong, Y. W., & Nugroho, H. (2022). Image classification for edge-cloud setting: A comparison study for OCR application. *Pertanika Journal of Science & Technology*, 30(2), 157-1170. <https://doi.org/10.47836/pjst.30.2.17>
- Tan, M., & Le, Q. (2019). Efficientnet: Rethinking model scaling for convolutional neural networks. In *International Conference on Machine Learning* (pp. 6105-6114). PMLR.
- Traore, B. B., Kamsu-Foguem, B., & Tangara, F. (2018). Deep convolution neural network for image recognition. *Ecological Informatics*, 48, 257-268. <https://doi.org/10.1016/j.ecoinf.2018.10.002>
- Ukaegbu, U. F., Tartibu, L. K., Okwu, M. O., & Olayode, I. O. (2021). Deep learning application in diverse fields with plant weed detection as a case study. In *Proceedings of the International Conference on*

- Artificial Intelligence and its Applications* (pp. 1-9). Association for Computing Machinery. <https://doi.org/10.1145/3487923.3487926>
- Umamaheswari, S., Arjun, R., & Meganathan, D. (2018). Weed detection in farm crops using parallel image processing. In *2018 Conference on Information and Communication Technology (CICT)* (pp. 1-4). IEEE. <https://doi.org/10.1109/INFOCOMTECH.2018.8722369>
- Ustuner, T., Sakran, A., & Almhemed, K. (2020). Effect of herbicides on living organisms in the ecosystem and available alternative control methods. *International Journal of Scientific and Research Publications*, *10*(8), 633-641. <https://doi.org/10.29322/IJSRP.10.08.2020.p10480>
- Vasileiou, M., Kyriakos, L. S., Kleisiari, C., Kleftodimos, G., Vlontzos, G., Belhouchette, H., & Pardalos, P. M. (2023). Transforming weed management in sustainable agriculture with artificial intelligence: A systematic literature review towards weed identification and deep learning. *Crop Protection*, *176*, 106522. <https://doi.org/10.1016/j.cropro.2023.106522>
- Voutos, Y., Mylonas, P., Katheriotis, J., & Sofou, A. (2019). A survey on intelligent agricultural information handling methodologies. *Sustainability*, *11*(12), 3278. <https://doi.org/10.3390/su11123278>
- Westwood, J. H., Charudattan, R., Duke, S. O., Fennimore, S. A., Marrone, P., Slaughter, D. C., Swanton, C., & Zollinger, R. (2018). Weed management in 2050: Perspectives on the future of weed science. *Weed Science*, *66*(3), 275-285. <https://doi.org/10.1017/wsc.2017.78>
- Woyessa, D. (2022). Weed control methods used in agriculture. *American Journal of Life Science and Innovation*, *1*(1), 19-26. <https://doi.org/10.54536/ajlsi.v1i1.413>
- Wu, J., Li, B., & Wu, Z. (2019). Detection of crop pests and diseases based on deep convolutional neural network and improved algorithm. In *Proceedings of the 2019 4th International Conference on Machine Learning Technologies* (pp. 20-27). Association for Computing Machinery. <https://doi.org/10.1145/3340997.3341010>
- Xiao, Y., Tian, Z., Yu, J., Zhang, Y., Liu, S., Du, S., & Lan, X. (2020). A review of object detection based on deep learning. *Multimedia Tools and Applications*, *79*, 23729-23791. <https://doi.org/10.1007/s11042-020-08976-6>
- Xie, C., Tan, M., Gong, B., Wang, J., Yuille, A. L., & Le, Q. V. (2020). Adversarial examples improve image recognition. In *Proceedings of the IEEE/CVF Conference on Computer Vision and Pattern Recognition* (pp. 816-825). IEEE. <https://doi.org/10.1109/CVPR42600.2020.00090>
- Xu, K., Shu, L., Xie, Q., Song, M., Zhu, Y., Cao, W., & Ni, J. (2023). Precision weed detection in wheat fields for agriculture 4.0: A survey of enabling technologies, methods, and research challenges. *Computers and Electronics in Agriculture*, *212*, 108106. <https://doi.org/10.1016/j.compag.2023.108106>
- Yamashita, R., Nishio, M., Do, R. K. G., & Togashi, K. (2018). Convolutional neural networks: An overview and application in radiology. *Insights into Imaging*, *9*, 611-629. <https://doi.org/10.1007/s13244-018-0639-9>
- Zhou, D.-X. (2020). Theory of deep convolutional neural networks: Downsampling. *Neural Networks*, *124*, 319-327. <https://doi.org/10.1016/j.neunet.2020.01.018>
- Zoph, B., Vasudevan, V., Shlens, J., & Le, Q. V. (2018). Learning transferable architectures for scalable image recognition. In *Proceedings of the IEEE Conference on Computer Vision and Pattern Recognition* (pp. 8697-8710). IEEE. <https://doi.org/10.1109/CVPR.2018.00907>

Mathematical Modelling for Performance Prediction of Ex-mining Lake Water Phytoremediation by *Scirpus Grossus*

Norhaslina Mohd Sidek^{1,2}, Siti Rozaimah Sheikh Abdullah¹ and Sarifah Fauziah Syed Draman^{2*}

¹Department of Chemical and Process Engineering, Faculty of Engineering and Build Environment, Universiti Kebangsaan Malaysia, 43600 Bangi, Selangor, Malaysia

²School of Chemical Engineering, College of Engineering, Universiti Teknologi MARA Cawangan Terengganu, Kampus Bukit Besi, 23200 Dungun, Terengganu, Malaysia

ABSTRACT

This study explores the use of *Scirpus grossus* for phytoremediation of ex-mining lake water, offering a potential low-cost alternative to conventional wastewater treatment. The focus is on removing contaminants such as total iron, total nitrate, total sulfate, total phosphorus, electrical conductivity, chemical oxygen demand, turbidity, and pH. Over 28 days, the ex-mining lake water was treated with *S. grossus* to assess contaminant removal, with the results analyzed using a mathematical model in Microsoft Excel. The model simulated exponential reductions in pollutants and increases in pH, with absorption coefficients calculated for each parameter. The study found that *S. grossus* effectively reduced contaminants, with the most significant removal of total iron at 95.45%. The pH of the water increased from 2.61 (acidic) to 6.29 (neutral), improving its suitability for aquatic life. The predicted removal rates closely matched the observed data, suggesting that the model is reliable for forecasting phytoremediation outcomes. Overall, the study confirms that *S. grossus* is a highly effective species for cleaning ex-mining lake water, offering a sustainable and cost-effective solution for industrial wastewater treatment. The findings encourage further research into the scalability, long-term effectiveness, and integration of this technique with other wastewater management strategies.

Keywords: Abandoned mine lake water, mathematical computing, plant-based remediation, *Scirpus grossus*, simulation

ARTICLE INFO

Article history:

Received: 22 August 2024

Accepted: 24 February 2025

Published: 24 April 2025

DOI: <https://doi.org/10.47836/pjst.33.S3.03>

E-mail addresses:

norhaslinamohdsidek@gmail.com (Norhaslina Mohd Sidek)

rozaimah@ukm.edu.my (Siti Rozaimah Sheikh Abdullah)

sfauziah@uitm.edu.my (Sarifah Fauziah Syed Draman)

* Corresponding author

INTRODUCTION

Phytoremediation, using plants to remove, degrade, or stabilize contaminants from soil and water, has emerged as a promising, eco-friendly approach for environmental

cleanup. This technique leverages the natural abilities of plants and their associated microorganisms to absorb, transform, and detoxify pollutants, including heavy metals, radionuclides, and organic compounds (Almaamary et al., 2017). Despite its potential, the practical application of phytoremediation poses several challenges, including variability in contaminant removal efficiency, environmental conditions, and plant species performance. Mathematical modeling has become invaluable in optimizing and predicting the outcomes of phytoremediation efforts to address these complexities (Tangahu et al., 2022).

S. grossus (locally known as *Rumput Menderong*), as shown in Figure 1, holds great promise as a phytoremediation agent for contaminated water bodies, particularly those affected by industrial activities. Its robust growth, high tolerance to pollutants, and ability to enhance microbial degradation of contaminants make it a valuable tool in sustainable and effective water quality management (Almaamary et al., 2022). As research continues to explore and optimize the use of *S. grossus* in phytoremediation, this plant may become an integral part of efforts to restore and protect our water resources.



Figure 1. *Scirpus grossus* (*Rumput Menderong*) (Tangahu et al., 2015)

Sordes et al. (2023) reported that mathematical modeling in phytoremediation involves the development of theoretical frameworks and computational algorithms to simulate the interactions between plants, contaminants, and environmental variables. These models can predict the behavior of contaminants in different scenarios, evaluate the effectiveness of various plant species, and optimize the design and management of phytoremediation projects. By integrating data from laboratory experiments, field studies, and environmental monitoring, mathematical models provide insights into the dynamics of phytoremediation processes, allowing for more precise and efficient remediation strategies (Alvarez-Vazquez et al., 2019).

The use of mathematical models offers several advantages in phytoremediation. They can reduce the need for extensive and costly field trials by simulating different remediation scenarios, thus saving time and resources. According to Darajeh et al. (2016), models can also identify the most effective plant species for specific contaminants and environmental conditions, enhancing the overall efficiency of phytoremediation. Furthermore, they help understand the complex interactions between plants and contaminants, providing a deeper insight into pollutant uptake, transformation, and stabilization mechanisms.

Kamalu et al. (2017) mentioned that mathematical modeling can play a crucial role in managing and mitigating environmental risks in the context of contaminated sites, particularly

those affected by mining activities. For instance, ex-mining lake waters often contain high concentrations of heavy metals and other pollutants, posing significant ecological and human health risks. Modeling the phytoremediation processes in such environments can help predict the long-term behavior of contaminants, assess the potential impact of remediation activities, and design effective remediation plans (Simha & Achyuth, 2015).

Jaskulak et al. (2020) stated that mathematical modeling is crucial in optimizing and predicting the effectiveness of phytoremediation processes, providing valuable insights into the interactions between plants, contaminants, and environmental conditions. However, many limitations in this field still hinder the full realization of phytoremediation's potential. Therefore, it is essential to explore the various aspects of mathematical modeling in phytoremediation, including model development, validation, and application in real-world scenarios, as studied by Shi et al. (2023). By harnessing the power of computational techniques to develop a suitable predictive system, we can enhance the effectiveness of phytoremediation and contribute to sustainable environmental management. Mathematical modeling in phytoremediation lies in its ability to enhance the efficiency, precision and applicability of phytoremediation techniques. The models can simulate contaminant uptake, translocation, and degradation over time, providing accurate remediation rates and time frame predictions.

MATERIALS AND METHODS

Experimental Setup

Seedling *S. grossus* collected from the natural pond at Bukit Besi was thoroughly washed with tap water to remove any surface contamination and then placed in a plastic vessel containing tap water. Two constructed wetland (CW) chambers were set up for two replicates, each approximately 50 cm in length (L), 35 cm in width (W), and 34 cm in depth (D), as shown in Figure 2. Each chamber was filled with approximately 13 cm height of river sand and lake water (approximately 28 liters). The CWs were placed in a greenhouse exposed to ambient conditions but shielded from direct sunlight to prevent water evaporation. Twelve plants were allowed to grow in each tub for 28 days (Sidek et al., 2020).

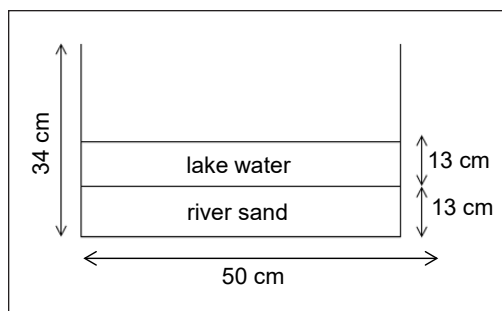


Figure 2. CW setup dimension

Plant Physical Observation

Plant physical observation was also recorded on each monitoring date, as reported by Ismail et al. (2017). Visual stress symptoms, including chlorosis, wilting, necrosis and stunted

growth, were observed on each of the sampling days. This is crucial for assessing plant health, growth and tolerance during remediation.

Lake Water Analysis

Analysis of total iron (TI), total nitrate (TN), total sulfate (TS), total phosphorus (TP), electrical conductivity (EC), chemical oxygen demand (COD), turbidity and pH. of the lake water drawn from experimental treatments was done on 0th, 7th, 14th, 21st and 28th of sampling days using standard methods outlined in APHA11 (Kumari et al., 2015; Kutty & Al-Mahaqeri, 2016). All selected parameters considered the possible characteristics of contaminants in the ex-mining lake water.

Mathematical Modelling Hypothesis

The parameter variation is attributed to the phytoremediation of ex-mining lake water by *S. grossus*, which contains high organic and inorganic compounds. This study assumes that the concentration of pollutants and/or effectiveness decreases over time as aquatic plants decrease inorganic and some organic compounds from wastewater (Jyotsna et al., 2015). However, once equilibrium is reached (when the plants' capacity for pollutant sequestration is maximized), the plants no longer contribute to pollution removal—noted that the parameter variation due to the phytoremediation of ex-mining lake water is limited and reaches its peak on the first day of the experiment.

Phytoremediation Prediction Model

According to Jyotsna et al. (2015), let P (phytoremediation parameter) be at the time of the initial day of the experiment for the phytoremediation potential of the *S. grossus*. The rate of change in P from the first day of the experiment until the plants reach equilibrium is directly proportional to P ; then,

$$\frac{dp}{dt} \propto P = \mu P \quad [1]$$

Where μ is a constant. Integrating Equation 1.

$$\ln P = \mu t + C \quad [2]$$

Where C is the constant of integration. To determine the value of C , apply the initial condition to Equation 2 by setting $t=0$ on the starting day of the experiment, where P will be at its maximum value, denoted as P_0 . Then,

$$\ln P_0 = \mu 0 + C$$

$$\text{Or } C = \ln P_0$$

Putting the value of C in Equation 2,

$$\ln P = \mu t + \ln P_0$$

$$\text{Or } \ln P - \ln P_0 = \mu t$$

$$\text{Or } \ln(P/P_0) = \mu t$$

$$\text{Or } P/P_0 = \exp(\mu t)$$

$$\text{Or } P = P_0 \exp(\mu t) \quad [3]$$

Now, when the plant reaches equilibrium after 28 days, the change in P with respect to t approaches zero.

$$\frac{dp}{dt} = 0$$

This indicates that,

$$P = b \quad [4]$$

Where b is a constant. Now, merging Equations 3 and Equation 4,

$$\begin{aligned} P &= P_0 \exp(\mu t) \text{ (before reaching steady-state)} \\ &= b \text{ (after reaching steady-state)} \end{aligned} \quad [5]$$

For the condition before reaching equilibrium, Equation 3 should be applied and denoted as Equation 5 to find the P values at the interval. At the same time, P is equal to b (constant) after reaching equilibrium.

Now consider t at an identical interval, let these be $t_1, t_2, t_3, \dots, t_N$.

$$\mu = \{ \ln(P_i / P_0) / t_i \}, \text{ where } i = 1, 2, 3, \dots, N$$

$$\mu = \frac{\sum_1^N \mu_i}{N}$$

The activity can be predicted by substituting the value of μ into Equation 3 (Kumar et al., 2005).

Mathematical Model Application

The method previously discussed was used to apply the model to the observed data. Observations were taken at three equidistant time intervals: on the 0th, 7th, 14th, 21st,

and 28th days. The value of μ was calculated using these observations, and the predicted value of P for *S. grossus* was compared with the observed values (Figures 3–10) (Jyotsna et al., 2015). The prediction simulation task was performed using the developed predictive system in Microsoft Excel.

RESULTS AND DISCUSSION

Plant Growth Observation

The plants show symptoms of yellowing leaves, root impairment, brown spots, and reduced metabolic activity. According to Sidek et al. (2018), this initial plant behavior (up to 28 days) for nutrient absorption from the lake water could be due to the plants reaching their carrying capacity, as all binding sites in the root zone were occupied. Additionally, the high elemental concentration in the plant bodies may have negatively impacted plant growth, resulting in relatively poor growth beyond 28 days (Table 1). This stunted growth likely halted the absorption of organic and inorganic contents from the lake water (Ismail et al., 2020).

Table 1
Scirpus grossus physical observation

Observation day	Initial day (0 th day)	Final day (28 th day)
Observation result	 <p>All healthy</p>	 <p>A few withered and dead</p>

Lake Water Parameters Analysis

All parameters showed an exponential decrease in P of *S. grossus* from the start of the experiment up to 28 days, after which the decrease became negligible until the experiment’s conclusion. A comparison between the estimated and observed values of a given parameter of the lake water (Figures 3–10) shows minimal variation. This finding strongly agrees with previous studies by Jyotsna et al. (2015) and Kumar et al. (2005), evident from the values of μ and the percentage reduction of different parameters with respect to the observed and estimated values. However, some inconsistency between observed and estimated values can be attributed to the subjectivity inherent in the experiment (Darajeh et al., 2016). Additionally, as the duration of phytoremediation increases, the pH values rise exponentially towards neutral.

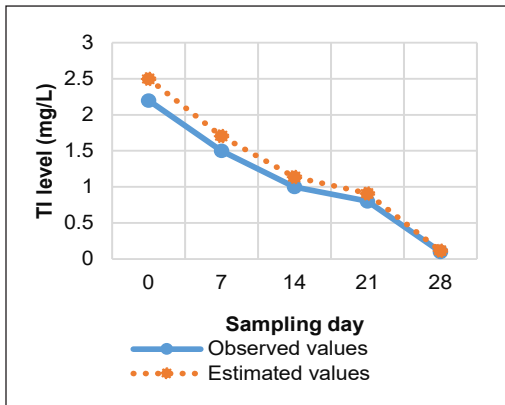


Figure 3. Comparison between the estimated value and observed value of TI

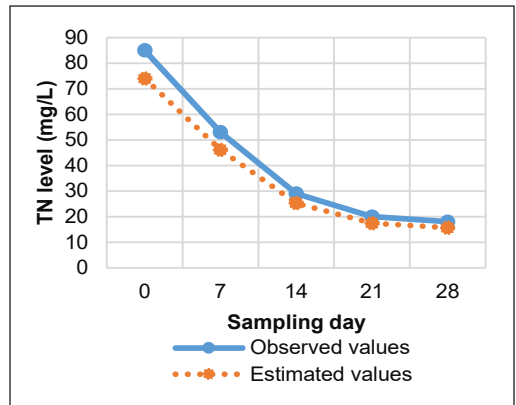


Figure 4. Comparison between the estimated value and the observed value of TN

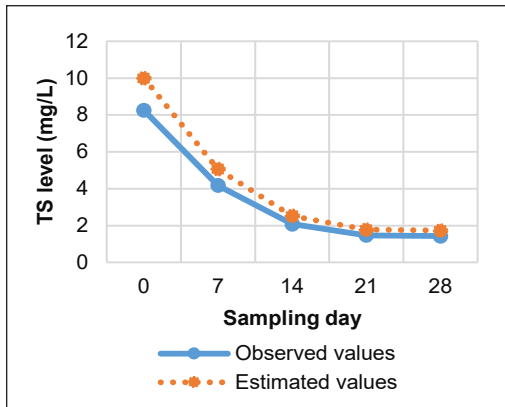


Figure 5. Comparison between the estimated value and the observed value of TS

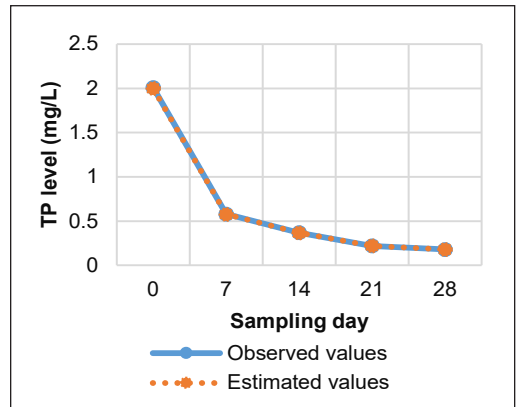


Figure 6. Comparison between the estimated value and the observed value of TP

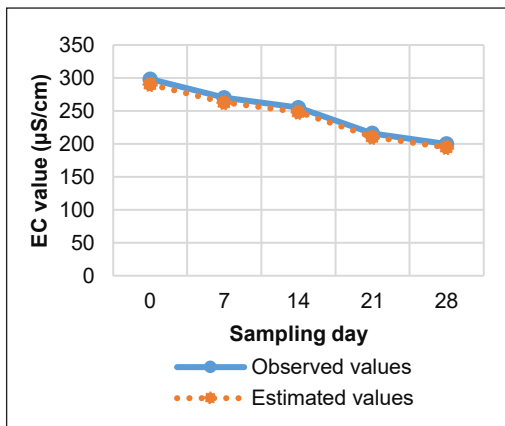


Figure 7. Comparison between the estimated value and the observed value of EC

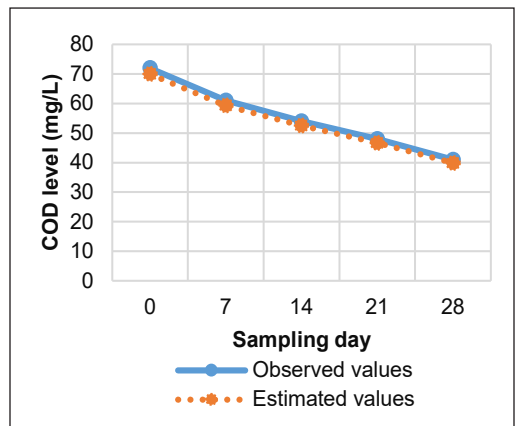


Figure 8. Comparison between the estimated value and the observed value of COD

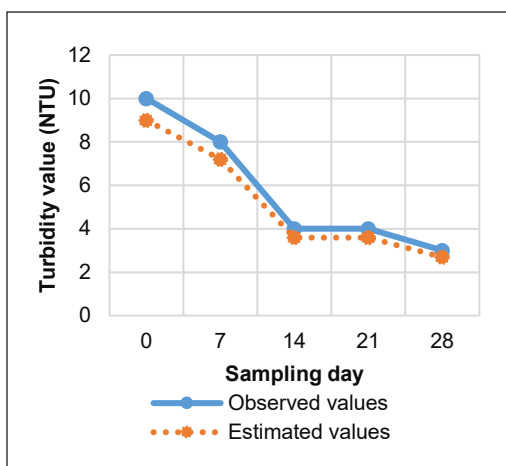


Figure 9. Comparison between the estimated value and observed value of turbidity

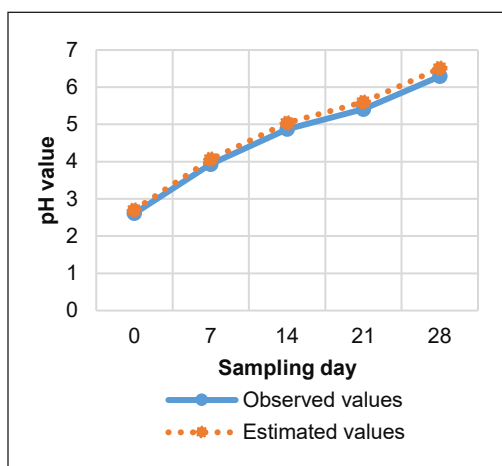


Figure 10. Comparison between the estimated value and observed value of pH

Mathematical Modelling

The trend of contaminant reduction is dependent on the value of μ (equilibrium constant) calculated using the mathematical model and the developed predictive system as shown in Table 2 as the highest value is 0.19358 ($R=95.45\%$) for TI and the lowest is 0.02949 ($R=32.89\%$) for EC neglecting the (-ve) signs which exhibit decrement values. This indicates that with extended phytoremediation, the phytoremediator reaches an equilibrium level of absorption

and/or degradation of the pollutants in the lake water, resulting in a halt in the reduction of the studied parameters beyond that point (Wang & Delavar, 2024). Figure 11 displays the window of the phytoremediation predictive system, which consists of the observed values, estimated values and contaminants removal graphs developed in Microsoft Excel.

Mathematical and computing techniques offer several advantages in phytoremediation technology, enhancing the efficiency, accuracy, and effectiveness of remediation processes. The advantages of this approach are beneficial for optimized plant selection, optimized plant selection, and cost and time efficiency (Jaskulak et al., 2020). Mathematical models can predict which plant species are most effective for specific contaminants, helping to select the best candidates for phytoremediation based on factors like growth rate, tolerance, and uptake capacity. Computational techniques enable the simulation of

Table 2

Calculated mean μ for eight physico-chemical parameters of *Scirpus grossus*

Parameters	Removal/Reduction	μ
TI	95.45%	-0.19358
TN	78.82%	-0.09256
TS	82.67%	-0.07106
TP	91.04%	-0.12235
EC	32.89%	-0.02949
COD	43.06%	-0.05247
Turbidity	70.00%	-0.06525
pH	+3.68	0.04591

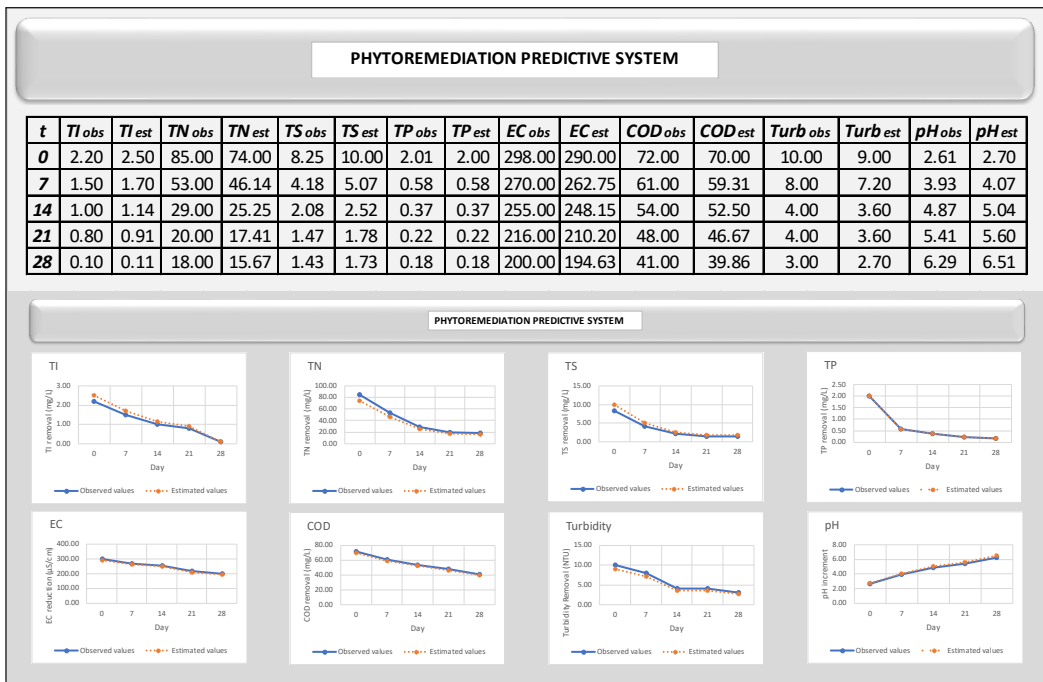


Figure 11. Phytoremediation predictive system

different scenarios, predicting the outcomes of phytoremediation efforts under various conditions. This helps in planning and optimizing remediation strategies. By simulating different phytoremediation strategies, mathematical models can identify the most cost-effective and time-efficient approaches, reducing the need for extensive field trials, as reported by Mohammadi et al. (2019).

As a practical technique for further research, an integrated phytoremediation model should account for the influence of agronomic practices, soil amendments, and native plants (Alvarez-Vazquez et al., 2019). In real-world settings, industries and environmental agencies can use phytoremediation mathematical models to optimize the selection of plant species, predict pollutant uptake, scale remediation efforts, and ensure long-term sustainability. Proper calibration, monitoring, and consideration of site-specific conditions (like soil type, climate, and contaminant type) are essential for successfully implementing these models. With the right combination of data, models, and field validation, phytoremediation can become an effective and cost-efficient strategy for addressing environmental contamination (Jaskulak et al., 2020).

According to Wang and Delavar (2024), phytoremediation modeling is valuable for predicting and optimizing environmental cleanup using plants. However, its limitations can impact its accuracy, applicability, and scalability in real-world settings. These limitations stem from the inherent complexity of biological, ecological, and environmental systems.

Phytoremediation mathematical modeling can be highly applicable when certain conditions are met, ensuring that predictions and recommendations are robust and realistic. These conditions include access to site-specific data, knowledge of contaminant-plant interactions, the environmental and climatic context, and a solid understanding of soil-plant feedback mechanisms (Jaskulak et al., 2020). Additionally, the model should consider the economic feasibility and practical constraints of applying phytoremediation on a large scale, as well as include tools for uncertainty analysis to ensure that decision-makers can manage risks effectively. When these conditions are met, phytoremediation models can be a powerful tool for optimizing remediation strategies, ensuring sustainable and cost-effective environmental cleanup.

CONCLUSION

Based on the current investigation, the proposed model effectively predicts the phytoremediation potential of *S. grossus* for ex-mining lake water and similar industrial effluents over time. TI parameter shows the highest percentage removal at $R=95.45\%$ with μ value of -0.19358 . This model is particularly useful for the fast observation of industrial pollution treatment. The mathematical model demonstrates a reasonably accurate remediation method for industrial wastewater pollution using plants such as *S. grossus*. This approach could be effectively utilized to remediate the effects of ex-mining lake water, at least on an experimental basis.

ACKNOWLEDGEMENTS

The authors express their appreciation to the Faculty of Engineering and Built Environment (FKAB), Universiti Kebangsaan Malaysia (UKM) and the College of Engineering, Universiti Teknologi MARA (UiTM) Cawangan Terengganu, Bukit Besi Campus, for providing technical facilities and financial funding for this project.

REFERENCES

- Almaamary, E. A. S., Abdullah, S. R. S., Hasan, H. A., Rahim, R. A. A., & Idris, M. (2017). Treatment of methylene blue in wastewater using *Scirpus grossus*. *Malaysian Journal of Analytical Sciences*, 21(1), 182-187. <http://dx.doi.org/10.17576/mjas-2017-2101-21>
- Almaamary, E. A. S., Abdullah, S. R. S., Ismail, N. I., Idris, M., Kurniawan, S. B., & Imron, M. F. (2022). Comparative performance of *Scirpus grossus* for phytotreating mixed dye wastewater in batch and continuous pilot subsurface constructed wetland systems. *Journal of Environmental Management*, 307, 114534. <https://doi-org.uitm.idm.oclc.org/10.1016/j.jenvman.2022.114534>
- Alvarez-Vazquez, L. J., Martínez, A., Rodríguez, C., Vazquez-Mendez, M. E., & Vilar, M. A. (2019). Mathematical analysis and optimal control of heavy metals phytoremediation techniques. *Applied Mathematical Modelling*, 73, 387-400. <https://doi-org.uitm.idm.oclc.org/10.1016/j.apm.2019.04.011>

- Darajeh, N., Idris, A., Masoumi, H. R. F. M., Nourani, A., Truong, P., & Sairi, N. A. (2016). Modelling BOD and COD removal from palm oil mill secondary lake water in floating wetland by *Chrysopogon zizanioides* (L.) using response surface methodology. *Journal of Environmental Management*, 181, 343-352. <https://doi.org/10.1016/j.jenvman.2016.06.060>
- Ismail, N. I., Abdullah, S. R. S., Idris, M., Hasan, H. A., Halmi, M. I. E., Al Sbani, N. H., Jehawi, O. H., Sanusi, S. N. A., & Hashim, M. H. (2017). Accumulation of Fe-Al by *Scirpus grossus* grown in synthetic bauxite mining wastewater and identification of resistant rhizobacteria. *Environmental Engineering Science*, 34(5), 367-375. <http://dx.doi.org/10.1089/ees.2016.0290>
- Ismail, N. I., Abdullah, S. R. S., Idris, M., Kurniawan, S. B., Halmi, M. I. E., Al Sbani, N. H., Jehawi, O. H., & Hasan, H. A. (2020). Applying rhizobacteria consortium for the enhancement of *Scirpus grossus* growth and phytoaccumulation of Fe and Al in pilot constructed wetlands. *Journal of Environmental Management*, 267, 1110643. <https://doi.org/10.1016/j.jenvman.2020.110643>
- Jaskulak, M., Grobelak, A., & Vandenbulcke, F. (2020). Modelling assisted phytoremediation of soils contaminated with heavy-metals: Main opportunities, limitations, decision making and future prospects. *Chemosphere*, 249, 126196. <https://doi.org/10.1016/j.chemosphere.2020.126196>
- Jyotsna, K., Bhasin, S. K., & Punit, B. (2015). Mathematical approach to assess phytoremediation potential of *Lemna Minor* for pulp and paper mill lake water—A case study. *International Research of Advance Research in Science and Engineering*, 4, Special Issue (01), 707-714. <http://data.conferenceworld.in/ICSTM2/P2397-2404.pdf>
- Kamalu, C. I. O., Okere, P. C., Egbufor, U. C., Nwandikom, G. I., Obijiaku, J. C., & Asomugha, C. C. (2017). Modelling and optimization of phytoremediation kinetics of metals in soil by a plant hyperaccumulator. *American Journal of Engineering Research*, 6(11), 196-207.
- Kumar, S., Dube, K. K., & Rai, J. P. N. (2005). Mathematical model for phytoremediation of pulp and paper industry wastewater. *Journal of Scientific & Industrial Research*, 64(October 2005), 717-721.
- Kumari, S. B., Kumar, M. M., Kumar, K. V., Juginu, M. S., Kavithamani, N., & Hema, S. (2015). Phytoremediation of industrial lake water and reduction of physico-chemical parameters from pond water using aquatic weeds. *IOSR Journal of Environmental Science, Toxicology and Food Technology*, 9(11), Special Issue(I), 54-55. <https://doi.org/10.6084/M9.FIGSHARE.1603361.V1>
- Kutty, A. A., & Al-Mahaqeri, S. A. (2016). An investigation of the levels and distribution of selected heavy metals in sediments and plant species within the vicinity of ex-iron mine in Bukit Besi. *Journal of Chemistry*, 2016(1), 1-12. <http://dx.doi.org/10.1155/2016/2096147>
- Mohammadi, F., Samaei, M. R., Azhdarpoor, A., Teiri, H., Badeenezhad, A., & Rostami, S. (2019). Modelling and optimizing pyrene removal from the soil by phytoremediation using response surface methodology, artificial neural networks, and genetic algorithm. *Chemosphere*, 237, 124486. <https://doi.org/10.1016/j.jece.2020.103985>
- Shi, L., Li, J., Palansooriya, K. N., Chen, Y., Hou, D., Meers, E., Tsang, D. C. W., Wang, X., & Ok, Y. S. (2023). Modelling phytoremediation of heavy metal contaminated soils through machine learning. *Journal of Hazardous Materials*, 441, 129904. <https://doi-org.uitm.idm.oclc.org/10.1016/j.jhazmat.2022.129904>

- Sidek, N. M., Abdullah, S. R. S., Draman, S. F. S., & Ahmad, N. 'U. (2020). Phytoremediation of ex-mining lake water in constructed wetland by perennial plants. *Chiang Mai University Journal of Natural Sciences*, 19(3), 580-594. <https://doi.org/10.12982/CMUJNS.2020.0038>
- Sidek, N. M., Abdullah, S. R. S., Draman, S. F. S., Ahmad, N. 'U, Rosli, M. M. M., & Sanusi, M. F. (2018). Phytoremediation of abandoned mining lake by water hyacinth and water lettuces in constructed wetlands. *Jurnal Teknologi*, 80(5), 87-93. <https://doi.org/10.11113/jt.v80.10992>
- Simha, L. U., & Achyuth, K. N. (2015). Mathematical modelling of household water treatment by duckweed batch reactor. *International Research of Advance Research in Science and Engineering*, 4, Special Issue (01), 1-6.
- Sordes, F., Pellequer, E., Sahli, S., Sarzynski, T., Denes, M., & Techer, I. (2023). Phytoremediation of chloride from marine dredged sediments: A new model based on a natural vegetation recolonization. *Journal of Environmental Management*, 344, 118508. <https://doi-org.uitm.idm.oclc.org/10.1016/j.jenvman.2023.118508>
- Tangahu, B.V. (2015). Growth rate measurement of *Scirpus Grossus* plant as preliminary step to apply the plant in wastewater treatment using reedbed system. *Journal of Civil & Environment Engineering*, 2015, 5(6), 100192. <http://dx.doi.org/10.4172/2165-784X.1000192>
- Tangahu, B.V., Abdullah S. R. S., Basri, H., Idris, M., Anuar, N., & Mukhlisin, M. (2022). Lead (Pb) removal from contaminated water using constructed wetland planted with *Scirpus grossus*: Optimization using Response Surface Methodology (RSM) and assessment of rhizobacterial addition. *Chemosphere*, 291, 132952. <https://doi-org.uitm.idm.oclc.org/10.1016/j.chemosphere.2021.132952>
- Wang, J., & Delavar, M. A. (2024). Modelling phytoremediation: Concepts, methods, challenges and perspectives. *Soil & Environmental Health*, 2, 100062. <https://doi.org/10.1016/j.seh.2024.100062>

Modelling Heterogeneous Traffic Performance During Non-Recurrent Congestion (NRC): A Case Study of Tugu Bundaran Sweta Intersection

Ahmad Muharror¹, Wardati Hashim^{2*}, Noor Azreena Kamaluddin²,
Nor Izzah Zainuddin², Nur Ilya Farhana Md Noh² and Ekarizan Shaffie³

¹Transport Agency of West Nusa Tenggara, Mataram, 83125, Indonesia

²School of Civil Engineering, College of Engineering, Universiti Teknologi MARA, 40450 Shah Alam, Selangor, Malaysia

³Institute for Infrastructure Engineering and Sustainable Management, Universiti Teknologi MARA, 40450 Shah Alam, Selangor, Malaysia

ABSTRACT

This research delves into the intricate dynamics of traffic performance during non-recurrent congestion (NRC), specifically focusing on the Lebaran Topat festival in Lombok. Utilising sophisticated transport modelling software, namely PTV Vissim, the study systematically models real-world traffic scenarios and calibrates and validates the simulation model's accuracy. The calibration of driver behaviour parameters, guided by the Wiedemann 74 model, is pivotal in comprehending nuanced vehicle interactions. Data collected from field observation was analysed in preparation for the calibration process, which employed maximum queue length as the parameter and an innovative trial and error method for optimisation. Specific values were assigned for each vehicle type during this calibration, exemplified by an average standstill distance. The validation of the NRC traffic performance model using the chi-square test stands as a testament to its reliability, boasting a chi-square value of 0.12, lower than the critical value of 0.18, at a significance level of 98%. Field assessment shows that during Lebaran Topat, the Level of Service (LOS) for signalised intersections based on the field maximum queue length is F, improved to D after simulated through PTV Vissim.

ARTICLE INFO

Article history:

Received: 22 August 2024

Accepted: 24 February 2025

Published: 24 April 2025

DOI: <https://doi.org/10.47836/pjst.33.S3.04>

E-mail addresses:

ahmadmuharror1@gmail.com (Ahmad Muharror)

wardati@uitm.edu.my (Wardati Hashim)

azreena@uitm.edu.my (Noor Azreena Kamaluddin)

norizzah@uitm.edu.my (Nor Izzah Zainuddin)

nurilya@uitm.edu.my (Nur Ilya Farhana Md Noh)

eka@uitm.edu.my (Ekarizan Shaffie)

* Corresponding author

Keywords: Maximum queue length, Non-Recurrent Congestion (NRC), PTV Vissim, Wiedemann 74 Model

INTRODUCTION

Non-Recurrent Congestion (NRC) presents a significant challenge in transportation research, characterised by abrupt and unforeseeable traffic disruptions triggered by various factors like holidays, festivals,

or accidents. These disruptions escalate traffic volume, posing considerable challenges to traffic performance. An illustrative example is evident during the Lebaran Topat celebration in Lombok, West Nusa Tenggara (NTB), Indonesia, a week after Eid al-Fitr. During this time, a substantial influx of visitors flocked to regional tourist destinations, notably increasing traffic volume (Rianti et al., 2018). Additionally, individuals from middle to low-income groups, predominantly engaged in manual occupations such as farming, labour, and fishing, use this opportunity to visit beaches, parks, and other recreational areas. Due to their affordability and versatility, pick-up vehicles become the primary mode of transportation during this period, further contributing to the heterogeneous traffic composition.

This highlights the need to comprehensively understand traffic behaviour and performance during NRC. Addressing the complexities of NRC requires accurate simulation and modelling of traffic conditions. Advanced traffic simulation tools like PTV Vissim are crucial in achieving this. PTV Vissim offers a robust platform to replicate real-world traffic scenarios by simulating heterogeneous vehicle interactions and assessing traffic performance under varying conditions. Hence, PTV Vissim is hypothetically expected to be able to simulate NRC's traffic performance.

This study focuses on understanding traffic behaviour during NRC through rigorous model calibration in PTV Vissim. Previous studies emphasise the importance of accurate calibration in traffic simulation models to reflect realistic traffic conditions. Building upon this foundation, questions arise about how traffic performance during NRC can be calibrated and validated using the PTV Visim. By calibrating driver behaviour parameters for diverse vehicle types, including pick-ups, motorcycles, and heavy vehicles, this research aims to provide insights into traffic performance during the Lebaran Topat festival and serve as a foundation for formulating effective traffic management strategies with the main objective to develop a reliable and validated traffic simulation model.

The influx of visitors and heightened traffic volume during the festive celebration of Lebaran Topat in Lombok precipitates NRC, exerting profound impacts on traffic performance and causing diverse traffic disruptions. Modelling this heterogeneous traffic and evaluating its performance during NRC is crucial for understanding the challenges of such events and formulating effective traffic management strategies. Previous studies underscore the significance of addressing NRC and advocate for research focusing on traffic performance in this context. This research endeavours to contribute to this area by employing the software PTV Vissim to model and analyse heterogeneous traffic performance during NRC to enhance traffic management during similar events.

BACKGROUND OF RESEARCH

NRC Analysis

A study by Boonserm and Wiwatwattana (2021) examined road traffic crashes during New Year festivals in Thailand. The findings revealed a significant increase in crash rates during

the festive period. The congestion and higher vehicle volumes led to an elevated risk of collisions and reduced overall traffic safety.

Furthermore, a study by Lin and Yan (2011) investigated the impact of major events on traffic performance. The results showed a substantial decrease in intersection capacity and increased queue lengths and delays. These findings emphasised the adverse effects of non-recurrent congestion during the festive season, highlighting the need for effective traffic management strategies.

Another study by Isa et al. (2018) reviewed the impact of non-recurrent traffic congestion on traffic flow and traffic density. The study revealed a significant decrease in traffic performance and proposed several approaches to handle NRC. One of the findings underscored that adjusting the traffic signal time could mitigate drivers' challenges.

This study would like to evaluate how Lebaran Topat compares to other festive celebrations in terms of traffic performance. It would provide insights into Lebaran Topat's unique characteristics and identify specific challenges that need to be addressed.

Makarova et al. (2020) found that simulation modelling emerges as the most effective means of exploring and discovering the optimal solutions within the domain of traffic safety. By creating virtual representations of real-world traffic scenarios, simulation modelling empowers transportation professionals and researchers to delve into various factors and variables under controlled conditions. This approach allows for a comprehensive understanding of the intricate dynamics within traffic systems, enabling the assessment of different safety measures and identifying the most efficient strategies to enhance overall traffic safety. With the ability to replicate real-world scenarios, modify variables, and analyse complex interactions, simulation modelling provides a safe, cost-effective, and versatile platform to test and refine safety interventions, ultimately paving the way for improved traffic safety outcomes.

In the PTV Vissim manual, three essential parameters are introduced for fine-tuning driver behaviour within the context of the Wiedemann 74 car-following model. These parameters play a pivotal role in shaping the dynamics of vehicle interactions and influencing the distances between vehicles during traffic simulations. The key parameters include the Average Standstill Distance (referred to as $w74ax$), the Additive Part of Safety Distance ($w74bxAdd$), and the Multiplicative Part of Safety Distance ($w74bxMult$).

Calibration Practice

Researchers employ diverse parameter calibration criteria to tailor Vissim models to real-world conditions, as shown in Table 1 below:

The selection of parameter calibration in this study is based on the chi-square test, reflecting a statistical approach to parameter determination. The optimisation procedure involves trial and error, systematically exploring parameter values. The chosen Measure

Table 1
Calibration methods from researchers

Source	Selection of parameter calibration	Optimisation procedure	MOE of Calibration
Zhou & Huang (2013)	MAPE	Trial and error	Traffic conflict
Manjunatha et al. (2013)	2-way Annova	Genetic algorithm	Delay
Siddharth & Ramadurai (2013)	Annova	Genetic algorithm	Flow
Mehar et al. (2014)	Literature review, 2-way Annova	Trial and error	Capacity
Prabhu & Sarkar (2016)	2-way Annova	Manual adjustment	Vehicle flow, pedestrian flow
Salgado et al. (2016)	Coefficient of determination (R^2)	Manual adjustment	Turning movement
Karakikes et al. (2017)	GEH	Genetic algorithm	Travel time
Yu & Fan (2017)	GRE, PMAE, PMRE	Genetic algorithm, Tabu Search	Flow
Gallelli et al. (2019)	RMSE	Genetic algorithm	Speed
Bhattacharyya et al. (2020)	Kolmogorov– Smirnov test (K–S test) Smirnov test (K–S	Genetic algorithm	Travel time
Arafat et al. (2020)	Kolmogorov– test), Shapiro-Wilk test	Non-inbuilt attribute	Saturation headway, saturation flow
Maheshwary et al. (2020)	One-way Annova	Genetic algorithm	Vehicle class
Preston & Pulugurtha (2021)	Ensure a minimum error ($\leq 15\%$)	Trial and error	Speed
Mistry et al. (2022)	MAPE	Manual adjustment	Traffic volume, Travel time
Jehad et al. (2022)	MAPE	Paired t-test	Traffic flow
Severino et al. (2022)	GEH	Trial and error	Traffic flow
Kvašňovská et al. (2023)	Deviation percentage	Trial and error	Average travel time
This Study	Chi Square Test	Trial and error	Max queue length

of Effectiveness (MOE) for calibration is the maximum queue length, underscoring the significance of accurately representing and managing queue lengths in Vissim simulations. This unique combination of parameter selection, optimisation, and MOE contributes to a comprehensive understanding of the calibration process within the Vissim framework. By using the maximum queue length as an MOE, this study ensures that evaluating traffic performance is both practical and meaningful, particularly in the context of non-recurrent congestion, while also contributing to an underexplored area of traffic research.

METHODS

Research Framework

The research framework shown in Figure 1 involves inserting primary and secondary traffic data into PTV Vissim to develop a traffic model. The model is initially built using

default Wiedemann 74 parameters and then validated against real-world data. If the model does not adequately represent the observed traffic conditions, calibration of the Wiedemann 74 parameters is conducted to improve its accuracy.

Data Collection

Data collection techniques in transportation studies involve primary and secondary methods. Primary data collection encompasses classified traffic counting surveys, turning movement counting surveys, spot speed surveys, and queue length surveys.

- (i) **Traffic Counting Survey:** This survey collects data on the number of vehicles passing through a particular location over a specified period. It helps understand traffic volumes, identify peak periods, and evaluate the overall traffic flow.
- (ii) **Classified Turning Movement Counting Survey:** Focused on analysing specific movements of vehicles at intersections. It involves identifying and classifying different turning movements, such as right turns, left turns, and through movements, to assess the traffic distribution and demand at the intersection approaches.
- (iii) **Spot Speed Survey:** This survey aims to determine the speed of vehicles at specific locations on a roadway network.
- (iv) **Queue Length Survey:** This survey involves measuring the length of queues or lines of vehicles at specific locations, such as signalised intersections or toll plazas. It helps in understanding congestion levels, assessing the performance of traffic control measures, and identifying areas where queue lengths exceed acceptable limits.

Secondary data collection methods include literature reviews to gather relevant information on traffic performance evaluation during festive periods and obtaining historical traffic data from relevant authorities, which supplements primary data to enrich analysis and decision-making processes in transportation planning and management.

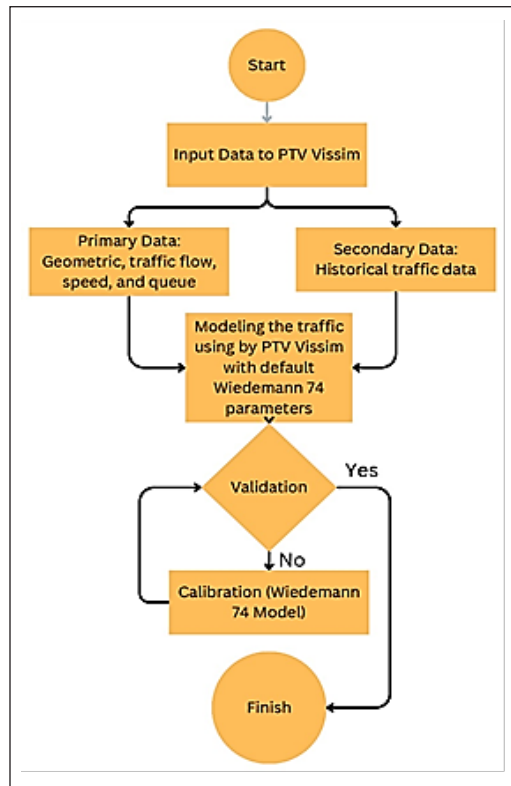


Figure 1. Research methodology framework

Sampling Procedures

The sampling procedure involves purposefully selecting the signalised intersection in Lombok and the link representing Non-Recurrent Congestions (NRC). This targeted selection allows us to obtain primary data from areas most likely to experience traffic congestion challenges during Lebaran Topat while also considering secondary data sources that provide historical context.

Location Selection and Considerations

The chosen signalised intersection, as shown in Figure 2, was strategically selected to align with the research objectives, considering factors such as traffic volume, its location at a primary junction with mixed land use, including shopping centres, residential areas, and office buildings, and its role in connecting the districts of West Lombok, Central Lombok, and East Lombok to the city of Mataram. This makes it a highly strategic point for community travel, especially during the Lebaran Topat festivities, as it links several areas with popular tourist attractions in Lombok. Additionally, the study focused on this single intersection due to the limited time available for research, enabling a more detailed and focused analysis of traffic behaviour during the event.

Table 2 shows the intersection dimensions, which are the location of this research. Table 3 shows the field survey results regarding traffic volumes at the intersection. As illustrated in Figure 3, the cycle time of this intersection remains consistent on weekdays, weekends, and even during the Lebaran Topat period.

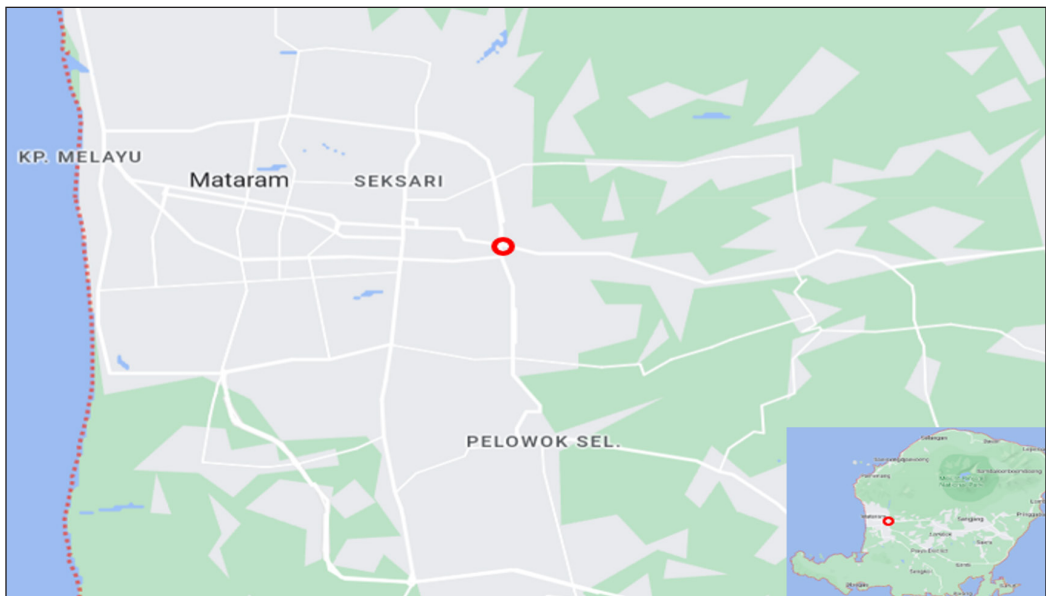


Figure 2. Study location (node)

Table 2
Detail geometry of the intersection

Approach	Type	Lane	Approach width (m)
North	Divided	4	26
East	Undivided	2	22
South	Divided	4	21.4
West	Undivided	4	19

Table 3
Traffic count for each movement

Direction	Motor cycle	Car/ Small Vans	Lorries/Large Vans	Large Lorry	Buses	Pick Up
NORTH						
Left	273	109	15	0	0	29
Straight	454	137	22	0	0	36
Right	183	64	2	0	0	26
SOUTH						
Left	368	66	2	0	0	22
Straight	356	72	23	5	0	24
Right	853	160	20	3	0	57
EAST						
Left	627	232	26	0	4	67
Straight	847	373	23	1	2	127
Right	713	232	30	0	0	74
WEST						
Left	316	100	2	0	0	39
Straight	1172	465	14	0	0	96
Right	614	87	1	0	0	21

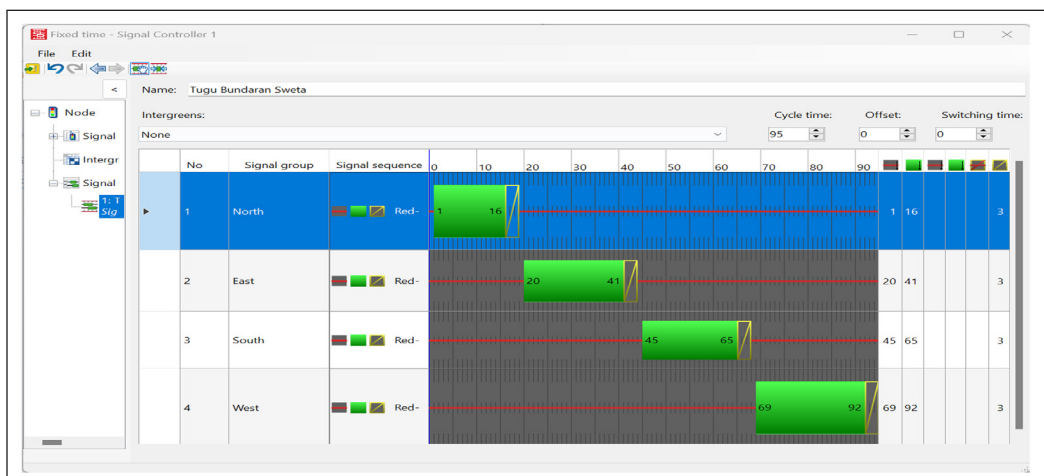


Figure 3. Cycle time of intersection

Data Analysis

Differences in maximum queue length between Vissim output and observed field data during Lebaran Topat are analysed. This ensures that the parameter selection for the modelling process is made accordingly. The datasets are appropriately prepared for analysis, which includes addressing outliers, managing missing data, and confirming data distribution assumptions. Hypothesis testing is conducted to observe any significant difference between the observed field data and the Vissim output. A chi-square test is necessary to assess the statistical significance of the difference in maximum queue length between the two datasets through the p-value obtained.

Modelling and Validation

The modelling process is done through the calibration of modelling parameters. The calibration includes selecting parameters pivotal in determining how vehicles interact and respond to traffic conditions. Then, an iterative process is conducted, with the default parameter values set based on available literature and standard settings. Subsequently, these parameters are fine-tuned to align the modelled traffic with observed field data. The calibration process is data-driven, relying on a data analysis process.

Model validation is carried out to prove whether the model used follows the field data. The validation model used is the Chi-square test. The decision is accepted (H_0 is born) based on calculations if $\chi_{count}^2 < \chi_{table}^2$, where χ_{count}^2 is obtained by the Equation 1 below:

$$\sum \chi_{count}^2 = \sum \frac{(Q_o - Q_m)^2}{Q_o} \quad [1]$$

Where: Q_o : max queue length (observed); Q_m : max queue length (model)

Employing the appropriate statistical method, such as the chi-square test, the difference in maximum queue length between Vissim output and observed field data during Lebaran Topat is rigorously evaluated.

RESULTS AND DISCUSSION

Calibration of NRC Traffic Model

We utilize data collected during the Lebaran Topat festival to investigate the calibration process in detail. The analysis includes adjustments to driver behaviour parameters within the PTV Vissim simulation model, which guarantees the model's accuracy in replicating real-world traffic conditions.

Bhattacharyya et al. (2020) and Severino et al. (2022) have calibrated models in urban contexts using approaches divergent from the Vissim manual yet successfully yielded statistically validated models. Similarly, Mistry et al. (2022) and Preston and Pulugurtha

(2021) found that calibrating Wiedemann 74 parameters produced Vissim outputs consistent with field conditions, enabling them to propose improved traffic management strategies.

These studies further support the planned adjustment of Wiedemann 74 parameters in this research. Despite variations in approaches and parameters utilised, these investigations collectively underscore the efficacy of calibrating driver behaviour parameters in the car-following model, particularly through applying Wiedemann 74 parameters, in producing accurate and reliable Vissim models reflective of real-world traffic conditions. Thus, the proposed parameter re-adjustment aligns to enhance the accuracy and validity of Vissim traffic simulation models.

Table 4 shows the default parameters of Wiedemann 74 in PTV Vissim before undergoing calibration. The parameters employed for calibrating PTV Vissim encompass the “max queue length,” Table 5 delineates the outcomes of field measurements for this length.

After conducting the initial run using the Wiedemann 74 parameter values under default conditions specified in Table 6, the maximum queue length generated by PTV Vissim is compared with the field measurement results.

The substantial disparities between the measured field data and the PTV Vissim outputs, as evident in the maximum queue lengths at the intersection in Table 5 and Table 6, underscore the necessity for calibrating the driver behaviour parameters, specifically those related to the car following model. The divergence in these results suggests that the existing parameterisation may not accurately capture the intricacies of real-world traffic conditions. A meticulous calibration process is imperative to align the PTV Vissim outputs with the observed field measurements. This calibration will involve refining the driver behaviour parameters, ensuring that the simulated outcomes closely mirror the on-site conditions.

The Wiedemann 74 parameters were calibrated using a systematic trial-and-error approach from the first to the 28th iteration

Table 4
Default parameters for Wiedemann 74

VehClass	W74ax	W74bxAdd	W74bxMult
Car	2	2	3
HGV	2	2	3
Bus	2	2	3
MC	2	2	3
Pick Up	2	2	3
Lorries	2	2	3

Table 5
Observed maximum queue length during Lebaran Topat

Approach	Queue length max, Q (meter)
North	60.4
East	215.5
South	184.5
West	242.0

Table 6
Maximum queue length from PTV Vissim using default parameters

Approach	Queue length max, Q (meter)
North	214.7
East	219.0
South	269.4
West	246.0

to achieve an appropriate level of validity. The process involved incrementally adjusting key parameters, and at each iteration, the model’s output from PTV Vissim was scrutinised for its alignment with observed field data. The calibration details, including parameter adjustments and corresponding model outputs at each iteration, are documented in Tables 7 and 8.

Table 7
28th iteration of adjusting Wiedemann 74 parameters

Vehicle type	W74ax	W74bxAdd	W74bxMult
Car	0.8	1	1.2
HGV	1.5	1.5	1.6
Bus	1.4	1.4	1.7
M	0.2	0.5	1.2
Pick Up	0.8	0.8	1
Lorries	1	0.9	1.2

Table 8
Maximum queue length comparison between existing conditions vs PTV Vissim output from 1st iteration to 28th iteration

Existing condition	Iteration 1	Iteration 2	Iteration 27	Iteration 28
60.4	156.4	203.4	63.2	59.5
215.5	218.1	218.9	218.1	218.0
184.5	242.0	268.6	199.3	183.3
242.0	246.1	246.1	246.1	246.0
$\sum \chi^2_{count}$	170.50	377.18	1.42	0.12

The parameter values at the 28th iteration (final) in Table 8 have exhibited disparities compared to the suggested range provided in both the VDOT Vissim Manual (2020) and the Vissim User Manual (2023). This finding aligns with previous research conducted by Bhattacharyya et al. (2020) and Severino et al. (2022), who calibrated models in urban contexts using approaches divergent from the Vissim manual yet successfully yielded statistically validated models. Specifically, in the case of Lebaran Topat, the utilised parameters have values smaller than the recommended ranges outlined in both manuals. This discrepancy indicates that the calibrated parameters, particularly during the festive period of Lebaran Topat, deviate from the default settings recommended by the Vissim manuals. The reduction in parameter values suggests nuanced variations in vehicle behaviour and traffic dynamics during Lebaran Topat, underscoring the importance of meticulous calibration to capture the unique characteristics of real-world scenarios within the simulation framework.

Validation of the NRC Traffic Model

Validation is made by comparing simulated outputs and observed field data using chi-square analysis. This validation process aims to establish the model’s predictive accuracy and robustness through a systematic comparison between simulated outputs and observed field data. Table 9 compares the field and simulated data with a chi-square value of 0.12, whereas the critical chi-square value (χ^2) for a significance level of 98% is 0.18. This indicates that the model used aligns with a validity level of 98%, as the obtained chi-square value falls below the critical value. The model’s performance is deemed consistent with the observed data, affirming its reliability and suitability for the specified level of significance.

Contrastingly, other researchers, such as Jehad et al. (2022), found in their study that the validity of their Vissim model, assessed through MAPE and paired t-test analysis, demonstrated no significant differences at a validity level of 98.5%. This indicates a robust alignment between their model and the observed data, albeit using different validation metrics. Similarly, Maheshwary et al. (2020) explored the use of genetic algorithms to optimise driving behaviour parameters for different vehicle classes, achieving a validity level of 95%. Their findings highlight the importance of tailored parameter optimisation for improving model accuracy. Additionally, Karakikes (2017) reported on their model’s systematic calibration and validation, which encompassed a vast network of links, nodes, and origin-destination pairs. Their approach yielded highly satisfactory results, with a validation level of 96.5%, underscoring the effectiveness of comprehensive calibration techniques.

NRC Traffic Model at Field Assessment

Evaluation of traffic performance is a critical aspect of transportation management and urban planning. Therefore, we investigate assessing traffic conditions at Tugu Bundaran Sweta, a pivotal junction in the study area. The selection of these two approaches is based on considerations of the smallest volume from the approaches and the presence of a central intersection protector in the form of a monument that separates vehicle flows from the north approach to the west approach and the south approach to the east approach.

Understanding the intricacies of traffic flow and congestion at this location is paramount for devising effective strategies to alleviate congestion, enhance safety, and optimise traffic operations. Table 10 shows that the Level of Service (LOS) value during the occurrence of

Table 9
Comparison between observed field data and PTV Vissim output after calibration

Approach	$Q_o(m)$	$Q_m(m)$	$\frac{(Q_o - Q_m)^2}{Q_o}$
North	60.4	59.5	0.013104
East	215.5	218.0	0.028858
South	184.5	183.3	0.00828
West	242.0	246.0	0.067391
$\sum \frac{(Q_o - Q_m)^2}{Q_o}$			0.117633

Lebaran Topat is rated as F. This underscores the critical need for management intervention and subsequent actions.

Table 11 shows the node performance results after running the model using PTV Vissim. The results show a reduction in maximum queue length and delays in every approach, thereby improving the overall LOS to become D by using the average of all delays for all approaches.

Previous studies analysing the performance of signalised intersections, such as those by Sofia et al. (2018), Jiang and Wang (2019), Wu et al. (2015), and Maripini et al. (2022), which adjusted cycle times, reported improved LOS after optimising signal timings. Sofia et al. (2018) coordinated signal cycles at multiple intersections in Karbala using Synchro and Sidra. Jiang and Wang (2019) adjusted inter-green times using a Monte-Carlo simulation approach. Wu et al. (2015) optimised cycle lengths at three signalised intersections in urban areas in China, Maripini et al. (2022) implemented a traffic-responsive signal control system that adjusts signal timings according to traffic volume fluctuations.

Table 10
Node performance during Lebaran Topat

Approach	Queue length max (m)	Delay (s)	Level of Service
North	60,4	61,57	E
East	215,5	123,09	F
South	184,5	118,45	F
West	242,0	138,01	F

Table 11
Node performance during Lebaran Topat after running PTV Vissim

Approach	Queue length max, Q (m)	Delay (s)	Level of Service
North	33.97	23.02	C
East	139.23	60.6	E
South	51.6	29.75	C
West	178.7	79.27	E

CONCLUSION

The modelling of NRC traffic performance through PTV Vissim calibration is integral to ensuring the accuracy and realism of simulation models. Parameters such as average standstill distance, the additive part of safety distance, and the multiplicative part of safety distance, following the Wiedemann 74 standards, were meticulously adjusted to account for the unique characteristics of different vehicle types, with values like 0.8 for Cars, 1.5 for HGVs, and 1.4 for Buses and despite variations from suggested ranges in manuals, particularly evident during Lebaran Topat, the trial-and-error method, supported by the

chi-square test, proved effective in optimising these parameters, underscoring their direct influence on vehicle behaviour within the simulated environment.

The validation assessed the NRC simulation model's accuracy in predicting traffic performance, focusing on maximum queue length at critical signalised junctions. Statistical analysis, utilising a chi-square test with a 98% significance level, showed high validity, with a chi-square value of 0.12, which is lower than the critical value of 0.18, and a p-value of 0.02, indicating no significant difference between Vissim output and observed field data. This robust validation enhances the credibility of simulation outcomes. It underscores the model's capability to inform traffic management strategies, which are crucial during non-recurrent congestions like cultural festivals such as Lebaran Topat.

ACKNOWLEDGEMENT

Special thanks to the School of Civil Engineering, College of Engineering, Universiti Teknologi MARA, for the invaluable support throughout the process. Their assistance has facilitated various aspects of this endeavour, ensuring its smooth progress and completion. Also, thanks to the Transport Agency of West Nusa Tenggara's constant support.

REFERENCES

- Arafat, M., Nafis, S. R., Sadeghvaziri, E., & Tousif, F. (2020). A data-driven approach to calibrate microsimulation models based on the degree of saturation at signalized intersections. *Transportation Research Interdisciplinary Perspectives*, 8, 100231. <https://doi.org/10.1016/j.trip.2020.100231>
- Bhattacharyya, K., Maitra, B., & Boltze, M. (2020). Calibration of micro-simulation model parameters for heterogeneous traffic using mode-specific performance measure. *Transportation Research Record*, 2674(1), 135-147. <https://doi.org/10.1177/0361198119900130>
- Boonserm, E., & Wiwatwattana, N. (2021). Using machine learning to predict injury severity of road traffic accidents during new year festivals from Thailand's open government data. *Proceeding of the 2021 9th International Electrical Engineering Congress, IEECON 2021*, 464-467. <https://doi.org/10.1109/IEECON51072.2021.9440287>
- Gallelli, V., Guido, G., Vitale, A., & Vaiana, R. (2019). Effects of calibration process on the simulation of rear-end conflicts at roundabouts. *Journal of Traffic and Transportation Engineering (English Edition)*, 6(2), 175-184. <https://doi.org/10.1016/j.jtte.2018.03.006>
- Isa, N., Mohamed, A., & Yusoff, M. (2018). A review of the non-recurrent traffic congestion problem. *Researchgate*. <https://www.researchgate.net/publication/350513939>
- Jehad, A. E., Al-Msari, H., & Ismail, A. (2022). Calibration and validation of Vissim microscopic model of contraflow operation system of Silk Highway, Malaysia. *Journal of Engineering Science and Technology*, 17(1), 640-653.
- Jiang, Z. H., & Wang, T. (2019). Intergreen time calculation method of signalized intersections based on safety reliability theory: A Monte-Carlo simulation approach. *Journal of Advanced Transportation*, 2019, 1-9. <https://doi.org/10.1155/2019/1941405>

- Karakikes, I., Spangler, M., & Margreiter, M. (2017). Designing a Vissim-Model for a motorway network with systematic calibration on the basis of travel time measurements. *Transportation Research Procedia*, 24, 171-179. <https://doi.org/10.1016/j.trpro.2017.05.086>
- Kvašňovská, E., Striegler, R., Pelikan, L., & Havlickova, E. (2023). Capacity and emission evaluation of new interchange designs using microsimulation. *Transportation Research Procedia*, 69(Tis 2022), 61-68. <https://doi.org/10.1016/j.trpro.2023.02.145>
- Lin, L., & Yan, W. (2011). Transportation characteristics and analysis of management measures of expressways during holidays. In *ICCTP 2011: Towards Sustainable Transportation Systems* (pp. 1094-1102). [https://doi.org/10.1061/41186\(421\)107](https://doi.org/10.1061/41186(421)107)
- Maheshwary, P., Bhattacharyya, K., Maitra, B., & Boltze, M. (2020). A methodology for calibration of traffic micro-simulator for urban heterogeneous traffic operations. *Journal of Traffic and Transportation Engineering (English Edition)*, 7(4), 507-519. <https://doi.org/10.1016/j.jtte.2018.06.007>
- Makarova, I., Khabibullin, R., Pashkevich, A., & Shubenkova, K. (2020). Modelling as a method to improve road safety during mass events. *Transportation Research Procedia*, 20(September 2016), 430-435. <https://doi.org/10.1016/j.trpro.2017.01.070>
- Manjunatha, P., Vortisch, P., & Mathew, T. (2013). Methodology for the calibration of VISSIM in mixed traffic. *Transportation Research Board 92nd Annual Meeting*, 11, 1-10. <https://www.researchgate.net/publication/281290567>
- Maripini, H. B., Vanajakshi, L., & Chilukuri, B. R. (2022). Optimal signal control design for isolated intersections using sample travel-time data. *Journal of Advanced Transportation*, 2022, 1-16. <https://doi.org/10.1155/2022/7310250>
- Mehar, A., Chandra, S., & Velmurugan, S. (2014). Passenger car units at different levels of service for capacity analysis of multilane interurban highways in India. *Journal of Transportation Engineering*, 140(1), 81-88. [https://doi.org/10.1061/\(ASCE\)TE.1943-5436.0000615](https://doi.org/10.1061/(ASCE)TE.1943-5436.0000615)
- Mistry, J., Chaudhari, P., Arkatkar, S., & Antoniou, C. (2022). Examining traffic operations at multi-legged intersection operating under heterogeneous traffic: A case study in India. *Transportation Research Procedia*, 62(2021), 83-90. <https://doi.org/10.1016/j.trpro.2022.02.011>
- Prabhu, T. D., & Sarkar, P. K. (2016). Pedestrian warrants for developing countries by simulation approach. *Procedia Computer Science*, 83(Ant), 665-669. <https://doi.org/10.1016/j.procs.2016.04.148>
- Preston, A., & Pulugurtha, S. S. (2021). Simulating and assessing the effect of a protected intersection design for bicyclists on traffic operational performance and safety. *Transportation Research Interdisciplinary Perspectives*, 9(February), 100329. <https://doi.org/10.1016/j.trip.2021.100329>
- PTV Vision. (2023). *PTV Vissim 2023 Manual*. Haid-und-Neu-Str. 15, 76131 Karlsruhe, Germany: PTV Group.
- Rianti, A., Novenia, A. E., Christopher, A., Lestari, D., & Parassih, E. K. (2018). Ketupat as traditional food of Indonesian culture. *Journal of Ethnic Foods*, 5(1), 4-9. <https://doi.org/10.1016/j.jef.2018.01.001>
- Salgado, D., Jolovic, D., Martin, P. T., & Aldrete, R. M. (2016). Traffic microsimulation models assessment - A case study of International Land Port of Entry. *Procedia Computer Science*, 83(Ant), 441-448. <https://doi.org/10.1016/j.procs.2016.04.207>

- Severino, A., Pappalardo, G., Olayode, I. O., Canale, A., & Campisi, T. (2022). Evaluation of the environmental impacts of bus rapid transit system on turbo roundabout. *Transportation Engineering*, 9(April), 100130. <https://doi.org/10.1016/j.treng.2022.100130>
- Siddharth, S. M. P., & Ramadurai, G. (2013). Calibration of VISSIM for Indian heterogeneous traffic conditions. *Procedia - Social and Behavioural Sciences*, 104, 380-389. <https://doi.org/10.1016/j.sbspro.2013.11.131>
- Sofia, G., Al-haddad, A., & Al-haydari, I. S. (2018). Improvement of traffic performance at intersections in Karbala City. *MATEC Web of Conferences*, 162, 1-10. <https://doi.org/10.1051/mateconf/201816201032>
- Virginia Department of Transportation. (2020). *VDOT Vissim User Guide Version 2.0*. Traffic Engineering Division.
- Wu, Y., Lu, J., Chen, H., & Yang, H. (2015). Development of an optimization traffic signal cycle length model for signalized intersections in China. *Mathematical Problems in Engineering*, 2015, 1-9. <https://doi.org/10.1155/2015/954295>
- Yu, M., & Fan, W. D. (2017). Calibration of microscopic traffic simulation models using metaheuristic algorithms. *International Journal of Transportation Science and Technology*, 6(1), 63-77. <https://doi.org/10.1016/j.ijtst.2017.05.001>
- Zhou, H., & Huang, F. (2013). Development of traffic safety evaluation method based on simulated conflicts at Signalized Intersections. *Procedia - Social and Behavioural Sciences*, 96(Cictp), 881-885. <https://doi.org/10.1016/j.sbspro.2013.08.100>

Enhancing Yolov8 Backbone Using Gradient Descent-based Method for Dental Segmentation

Dhiaa Mohammed Abed^{1,2}, Shuzlina Abdul-Rahman^{2*} and Sofianita Mutalib²

¹Faculty of Biomedical Engineering, University of Technology, Baghdad, Iraq

²School of Computer Sciences, College of Computing, Informatics and Mathematics, Universiti Teknologi MARA, 40450 Shah Alam, Selangor, Malaysia

ABSTRACT

This research addresses the challenge of dental segmentation in computer vision, a task focused on accurately outlining dental structures in images. The traditional methods, particularly convolution neural networks (CNNs), often suffer from suboptimal performance and computational inefficiency. Our study introduces an enhanced approach by applying the YOLOv8 algorithm, known for its effectiveness in object detection, for dental segmentation. Our proposed model improves YOLOv8's feature extraction capability by integrating additional layers into its backbone architecture, primarily focusing on the Coordinates-To-Features (C2f) module. This C2f-based feature extraction technique is designed to optimize gradient descent, reducing loss and maximizing prediction accuracy. By incorporating adaptive weights, the model effectively enhances the propagation of gradients, allowing for a more precise focus on dental structures. The adapted model, comprising 29 layers, is trained on a large-scale real-color dental dataset. Experimental evaluation demonstrates that the proposed model achieves exceptional performance, attaining 99.6% precision and recall in dental segmentation tasks. These results highlight the potential of YOLOv8 for specialized segmentation challenges and mark a significant contribution to automated dental analysis, offering direct benefits for clinical diagnostics and treatment planning in dentistry.

Keywords: Computer vision, deep learning, dental segmentation, image processing, YOLOv8

ARTICLE INFO

Article history:

Received: 22 August 2024

Accepted: 24 February 2025

Published: 24 April 2025

DOI: <https://doi.org/10.47836/pjst.33.S3.05>

E-mail addresses:

Dhiaa.M.Alfyadh@uotechnology.edu.iq (Dhiaa Mohammed Abed)

shuzlina@uitm.edu.my (Shuzlina Abdul-Rahman)

sofianita@uitm.edu.my (Sofianita Mutalib)

* Corresponding author

INTRODUCTION

Image segmentation is a major task in computer vision that divides an image into meaningful and semantically cohesive parts or segments. Its purpose is to distinguish pixels or regions with similar visual features, like color, texture, intensity, or spatial proximity, from the surrounding regions.

Image segmentation is essential for a variety of applications, including object recognition, scene interpretation, medical image analysis, autonomous cars, and more (Elyan et al., 2022).

The primary objective of image segmentation is to allocate a label or identifier to each pixel or region of the image, effectively partitioning the image into distinct regions based on the underlying visual characteristics. These labeled regions can then be used for further analysis, feature extraction, object detection, and other computer vision-related tasks (Bi et al., 2022).

Semantic segmentation assigns every pixel in an image to a definite class label, demonstrating the object or section it goes to. The goal is to achieve pixel-level labeling, where all pixels belonging to the same object share the same label. For example, in an image containing a person, a car, and a tree, semantic segmentation would label each pixel as belonging to the person, car, tree, or background (El Bsat et al., 2022).

Instance Segmentation is a particular type of segmentation. It differs from semantic segmentation by assigning a class label to each pixel and distinguishing between individual instances of a given class. In other words, it identifies and distinguishes various objects or instances of the same class. For example, in a photograph with numerous people, such segmentation would not just label all the pixels belonging to people but also assign a unique identifier to each person, separating them as individual instances (Almalki & Latecki, 2023).

Various approaches to image segmentation exist, ranging from traditional methods based on handcrafted features to advanced techniques leveraging deep learning models. Deep learning procedures in actual convolutional neural networks (CNNs) have recently gained popularity and demonstrated superior performance in image segmentation tasks. Models like U-Net, FCN, SegNet, and Mask R-CNN have become popular for semantic and instance segmentation responsibilities due to their aptitude to learn multifaceted spatial features and patterns from the data (Hou et al., 2023).

Despite the progress made with deep learning, image segmentation remains challenging, especially in complex scenes, occlusions, and varying lighting conditions. Researchers and developers continue to discover new techniques and architectures to improve image segmentation methods' precision, efficiency, and robustness for a wide range of uses (Wu et al., 2023).

Dental segmentation using deep learning is an advanced technique in the domain of medical image analysis, besides computer vision. The aim of dental segmentation is to recognize and delineate the boundaries of dental in an image, which can be suitable for numerous uses, including dental diagnosis, treatment planning, and orthodontic analysis. It is essential to note that dental image segmentation can be an inspiring task because of the differences in image quality, lighting, and occlusions. Consequently, having a robust and diverse dataset is crucial to training a successful deep-learning model. Additionally,

in the medical domain, it is essential to ensure that the segmentation model is accurate and reliable before applying it to real-world applications (Lee & Kim, 2022).

As with any medical-related AI application, it's crucial to validate the model's performance with the help of dental professionals and conduct extensive testing and validation to ensure its accuracy and safety in clinical practice (Chandrashekar et al., 2022).

Related Works

Many previous research works have been based on dental segmentation, where many different algorithms have been used to obtain high accuracy. The most important of this research are:

- (a) Im et al. (2022) assessed the effectiveness and accuracy of deep learning-based automatic teeth segmentation in digital dental models. Consuming 516 digital dental models, it created a method for autonomous teeth segmentation and classification based on a dynamic graph convolutional neural network (DGCNN). Thirty digital dental models were segmented using three different methods for comparison: (1) landmark-based tooth segmentation (LS) using OrthoAnalyzer software, (2) tooth designation and segmentation (DS) using Autalign software, and (3) automatic teeth segmentation (AS) utilizing the DGCNN-based algorithm from LaonSetup software. The clinical crown height (CCH), segmentation duration, mesiodistal (MD) width, and segmentation success rate were all assessed. A digital dental model's automatic tooth segmentation utilizing deep learning has a high segmentation achievement rate, precision and efficiency, making it suitable for orthodontic diagnosis and usage production.
- (b) Tian et al. (2019) suggested a novel method for segmenting and classifying tooth kinds on 3D dental models based on 3D convolution neural networks (CNNs) and the sparse voxel octree. A dental classification approach constructed on two-level hierarchical features learning is first suggested to address the misclassification issue in extremely similar tooth classes. Second, individual teeth-gingiva and interteeth segments are segmented using an upgraded three-level hierarchical segmentation approach based on deep convolution features. The interteeth fusion zone and gingival margin borders are refined using the conditional random field model. The experiment results indicate that the Level_1 network has a classification accuracy of 95.96%, the Level_2 network has an average classification accuracy of 88.06%, and the tooth segmentation accuracy of 89.81%. The suggested method has more potential for application in computer-assisted orthodontic treatment diagnosis and is more widely applicable and exact than current state-of-the-art methodologies.
- (c) Rashid et al. (2022) delivered a diverse sample for the dental (colored or X-ray) images and implemented a deep learning method to improve carious area

localization. They also applied a comprehensive program that uses basic dental scans to automatically identify carious areas. In order to identify dental carious areas, the instantiation principally uses a pre-trained hybrid Mask RCNN in conjunction with a heterogeneous dataset of dental photos (colored photographs or X-rays) obtained from diverse causes. Dentists' examinations revealed that annotated datasets have an accuracy of up to 96%, while the precision of the suggested method ranges from 78% to 92%. Furthermore, the approach received more than 80% general acceptance among dentists.

- (d) Fatima et al. (2023) suggested model has two parts: (1) for periapical disease localization on a limited dataset, a region-based network (RBN) and (2) a lightweight modified MobileNet-v2 backbone. The lightweight Mask-RCNN is assessed on a specially marked dataset that includes pictures of five distinct kinds of periapical wounds to gauge the efficacy of the suggested model. The results show that the model has a total precision of 94%, a mean average precision of 85%, and a mean inspection above a separation of 71.0% in identifying and identifying periapical lesions. Compared to current techniques, the suggested model greatly increases recognition and classification, and localization precision consumes fewer photos and outperforms state-of-the-art approaches.
- (e) Zhao et al. (2020) proposed a Two-Stage Attention Segmentation Network (TSASNet) used for dental panoramic X-ray images to improve tooth boundary and root segmentation due to small differences and uneven intensity supply. First, a framework for attention in the initial stage and employing global and local attention modules will be employed to approximate the tooth placement. The attention model can automatically detect coarse tooth borders and gather contextual information pixel by pixel without an interaction operator. Second, they utilize a fully convolutional network to extract the real tooth area from the responsiveness maps gained in the first stage, obtaining more accurate final boundary information. The usefulness of TSASNet is demonstrated using a benchmark dataset of 1,500 dental panoramic X-ray images. Their suggested solution outperforms the state-of-the-art methods, achieving 96.94% precision, 92.72% dice, and 93.77% recall.
- (f) Al Nassan et al. (2022) modified CNNs to segment the bitewing image in this investigation. Before segmenting, the bitewing radiographs are imported into MATLAB and improved to produce a binary mask image that removes the background from the original images. This image will be fed into the CNN model. Those masks are the aim of the deep learning model. We were able to attain the greatest accuracy on hidden images after training the provided method with 456 bitewing shots, 88.27% F1-score and 97.3% accuracy.

- (g) Sivagami et al. (2020) UNet architecture using convolutional neural networks was presented to accurately separate dental panoramic x-ray pictures, which radiographic pictures assist medical professionals in accurately identifying and diagnosing diseases. Radiographic pictures contain X-rays, computed tomography (CT), and magnetic resonance imaging (MRI). In general, X-ray images are complicated. Noise makes it more difficult to distinguish between different portions of the teeth. This makes the segmentation process extremely tough. Dental image segmentation assists dentists in detecting damaged teeth, determining the proper position for dental implant insertion, and determining the direction of the tooth structure. The UNet architectural model is a contemporary method for medical image segmentation. In this paper, they achieved a Dice score of 94% and an accuracy of 97% in dental X-ray picture segmentation using UNet architecture. Furthermore, a comparison is made between the performance of the UNet architecture and other image segmentation techniques for the segmentation of dental X-ray pictures.

Through previous research and deep learning algorithms, note that increasing segmentation accuracy depends on several criteria: extracting the largest number of features from the image, selecting the most important features, and deleting the rest. One of the most important of these algorithms is CNN, which is one of the most important deep learning algorithms. This algorithm is characterized by high accuracy in segmenting, detecting, and classifying images due to layers of extracting features from images and selecting the best features, which greatly affect the decision. Some research has added a technique with the CNN algorithm to increase the number of features extracted; the structure of the U-Net or Mask R-CNN algorithms was combined with the CNN architecture to increase accuracy by increasing the number of features. Note that the greater the amount of features extracted from the images and selecting the best among them leads to an increase in the accuracy of the segmentation. However, these layers may lead to slow execution due to their size compared to the entered images, and to obtain a proposed model. The accuracy of the segmentation and the execution time must be taken into account.

MATERIALS AND METHODS

The YOLO algorithm is considered one of the modern algorithms as it has shown its efficiency in many areas. For this reason, it was chosen as a proposal for dental segmentation. This research used and modified YOLOv8 of the algorithm to display its increased accuracy in dental segmenting. Modifications were made to the model's layers by increasing the cumulative number of backbone layers to enhance the number of features extracted from the image. Additionally, the sizes of the layers were modified to make the proposed model suitable for the process of the dental segmentation and isolating it from the rest of the mouth. Figure 1 illustrates the proposed YOLOv8 segmentation model.

The proposed model consists of 29 layers, and the specifications of each layer have been accurately determined to suit the process of dental segmentation. Table 1 illustrates the specification of the proposed YOLOv8 segmentation model.

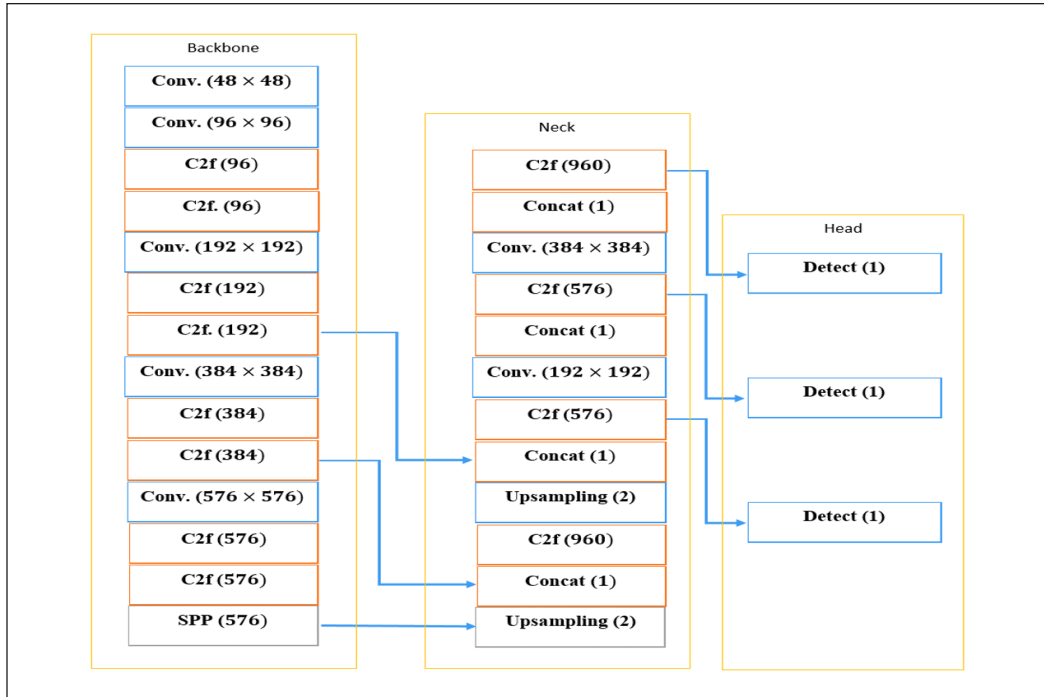


Figure 1. Proposed YOLOv8 segmentation model

Table 1
Specification of proposed YOLOv8 segmentation model

Layer No.	Part	Layer	Specification
1	Backbone	Conv.	[3, 48, 3, 2]
2		Conv.	[48, 96, 3, 2]
3		C2f	[96, 96, 2, True]
4		C2f	[96, 96, 2, True]
5		Conv.	[96, 192, 3, 2]
6		C2f	[192, 192, 4, True]
7		C2f	[192, 192, 4, True]
8		Conv.	[192, 384, 3, 2]
9		C2f	[384, 384, 4, True]
10		C2f	[384, 384, 4, True]
11		Conv.	[384, 576, 3, 2]
12		C2f	[576, 576, 2, True]
13		C2f	[576, 576, 2, True]
14		SPP	[576, 576, 5]

Table 1 (continue)

Layer No.	Part	Layer	Specification
15		Upsampling	[None, 2, 'nearest']
16		Concat	[1]
17		C2f	[960, 384, 2]
18		Upsampling	[None, 2, 'nearest']
19		Concat	[1]
20	Neck	C2f	[576, 192, 2]
21		Conv.	[192, 192, 3, 2]
22		Concat	[1]
23		C2f	[576, 384, 2]
24		Conv.	[384, 384, 3, 2]
25		Concat	[1]
26		C2f	[960, 576, 2]
27		Conv.	[1]
28	Head	Conv.	[1]
29		Conv.	[1]

The C2f layer is important in extracting features from images, significantly contributing to teeth identification. While the C2f layer is highly efficient in determining teeth, it can be improved from the mathematical side. In the proposed model to improve Adaptive Cross-Stage Partial Connections, this layer has been improved based on the introduction of adaptive weights, through which the grid is allowed to modify and integrate features more efficiently and improve the flow of the gradient through the next layers. Let x_i represent the output of the i^{th} layer, and w_i be an adaptive weight associated with the connection from layer i . The output of C2f is y can be as shown in Equation 1:

$$y = \sum x_i \times w_i \quad [1]$$

Now, the summation of weight must be 1, and the SoftMax activation function must be used to ensure Equation 2.

$$w_i = \text{SoftMax}(z_i) \quad [2]$$

where z_i is a learnable parameter for each connection.

Minimizing the loss function, which measures the discrepancy between the predictions made by the model, maximizes the model's performance by optimizing weights, which can be described in Equation 3:

$$L(w) = \text{Loss}(y(w)) \quad [3]$$

where Loss is a suitable loss function, such as mean squared error or cross-entropy loss.

Gradient descent-based methods can be employed to optimize the weights. The gradient of the loss function for the weights can be calculated using the chain rule in Equation 4:

$$\frac{dL}{dw_i} = \frac{dL}{dy} \times \frac{dy}{dw_i} \quad [4]$$

Where dL/dy is the gradient of the loss function with output y , and dy/dw_i is the derivative of the output weight w_i .

This improvement allows the proposed model to focus more on dental features and more efficiently facilitate the spread of gradients through adaptive weights.

The process of building a dataset is of high importance for building an intelligent system. AI algorithms need a number of different types of images to obtain high accuracy in training. In this dissertation, the dataset (top view) was taken from a dental clinic where 100 images were taken of dental patients from different patients. The images taken from the dental clinic are in different sizes and were divided into two parts: (1) 70% for training and (2) 30% for testing. Figure 2 illustrates samples of the dataset. These images were taken through real cases in a dental clinic in Iraq.

Two main parts of preparing the dataset before the proposed system uses it are dental dataset augmentation and dental dataset annotation. Image augmentation was used to transform the original images to increase the size of the dental dataset. This helps improve the model's generalization and robustness by exposing it to a wider range of variations in the input data. Image augmentation is particularly useful when the available labeled dataset is limited (Figure 3). Here are image augmentation techniques used to increase dental dataset: Rotate the image by a certain angle, flip the image horizontally or vertically, zoom in or out of the image, apply shift transform to the left or right, apply shift transform to the up or down, and apply a shear transformation to the image.

This step increased the number of images in the dataset from 100 to 600, which is highly suitable for training and testing the enhanced YOLOv8 algorithm and increasing its accuracy in dental segmentation.

The dental annotation step includes the work of image segmentation annotation and involves labeling individual regions within an image to delineate dental. This

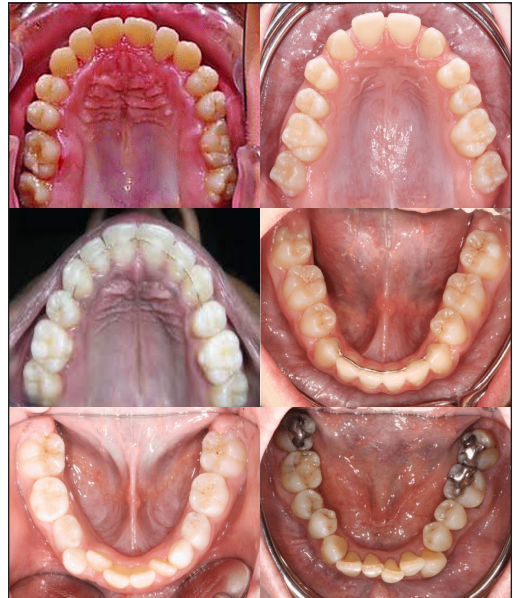


Figure 2. Samples of dataset

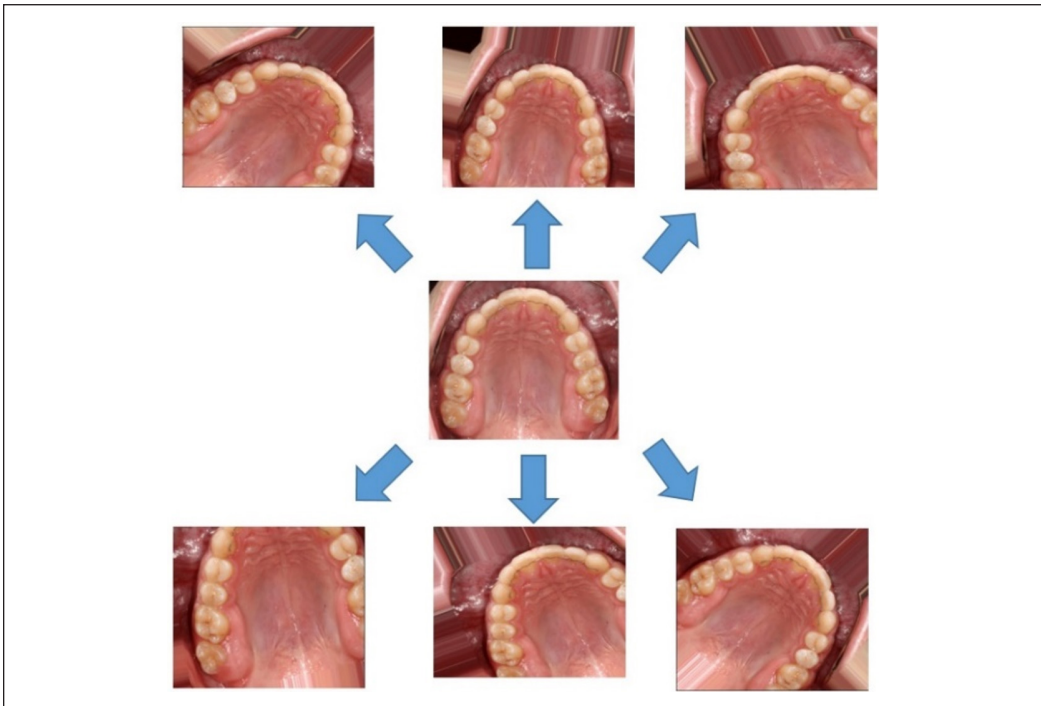


Figure 3. Dental dataset augmentation

annotation is commonly used in computer vision tasks, such as training models for semantic segmentation. Annotators draw polygons around the dental. Each polygon defines a segment of the image. The vertices of the polygon represent the boundary of the annotated dental. Masks are binary images where pixels inside the dental are labeled as foreground (1) and pixels outside as background (0). A LabelMe program was used to create dental annotation (Figure 4).

RESULTS AND DISCUSSION

The practical experiments conducted to train the proposed YOLOv8 segmentation model in dental segmentation reached high accuracy in segmenting dental from oral parts. Many experiments have been conducted to demonstrate the precision of the proposed model. The experiment's trained model uses an epoch of 50, with Figure 5 illustrating the performance measurement.

The train/box_loss scale of the lower value indicates better performance, as it represents the loss associated with the model's ability to accurately predict the boxes surrounding the detected teeth. Here, its value reached 0.38524 because the shapes of the teeth are not rectangular. For this reason, the determination will be the tooth and part of its surroundings. As for the train/seg_loss scale, it is related to the loss of dental segmentation, and note

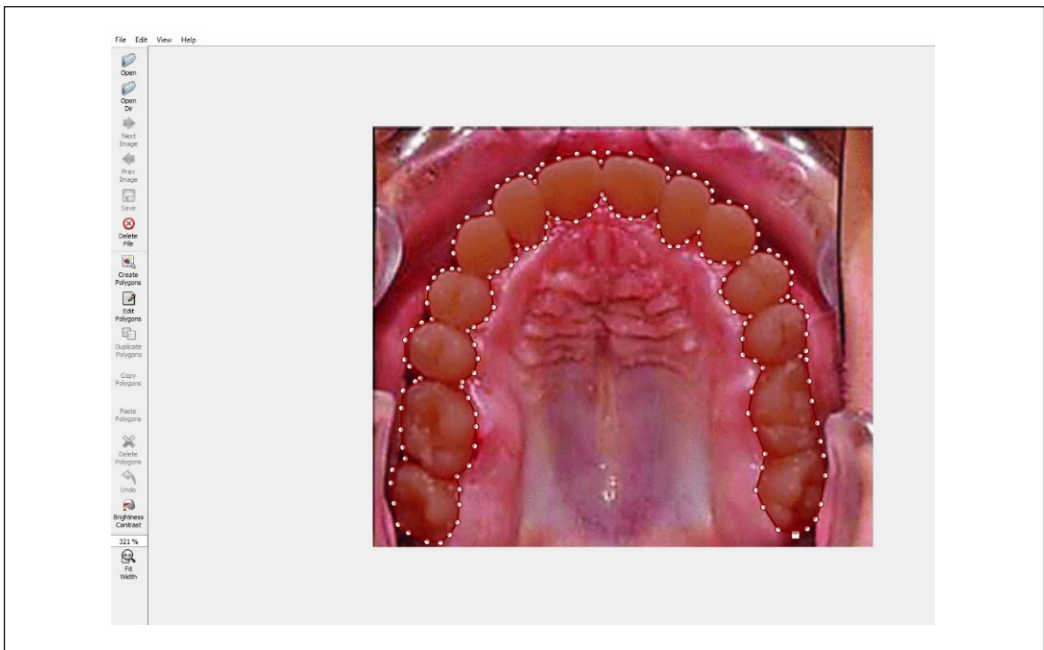


Figure 4. Dental annotation

that its value reached 0.35353 because it takes a determination of the tooth in a way that surrounds the tooth and does not take from the surrounding parts. Its value is less than the scale train/box_loss . Train/cls_loss scale represents the loss represented by the classification of the teeth, and we note that its value is high, 0.87865, because the model is for the segmentation of the teeth and not their classification. Train/dfl_loss measure is related to the process of augmentation of dental images, and in the absence of repetition, its value rises because the dental images are not duplicated, and its value reaches 1.0683. Everything mentioned is specific to the images of the model's training.

The following metrics are specific to validation and these scales are similar to the previous scales. However, they are applied to data on which the proposed model has not been trained, where val/box_loss is similar to train/box_loss , but val/box_loss represents the loss of the boxes that surround the images of teeth that the model has not been trained on. This applies to other measures where train/seg_loss , train/cls_loss , and train/dfl_loss like val/seg_loss , val/cls_loss , and val/dfl_loss . $\text{metrics/precision(B)}$, metrics/recall(B) , metrics/mAP50(B) , $\text{metrics/mAP50-95(B)}$. These metrics evaluate the model's performance in tooth detection. The $\text{metrics/precision(B)}$ scale reached 0.9761, representing the ratio of true tooth detection to the total number of expected teeth. The metrics/recall(B) reached 0.996, representing the ratio of true tooth detection to the total number of true teeth. As for metrics/mAP50(B) , it reached 0.995, which is the average resolution at the IoU threshold by 50%. In addition to scale $\text{metrics/mAP50-95(B)}$, the average accuracy calculated on IoU thresholds, ranging

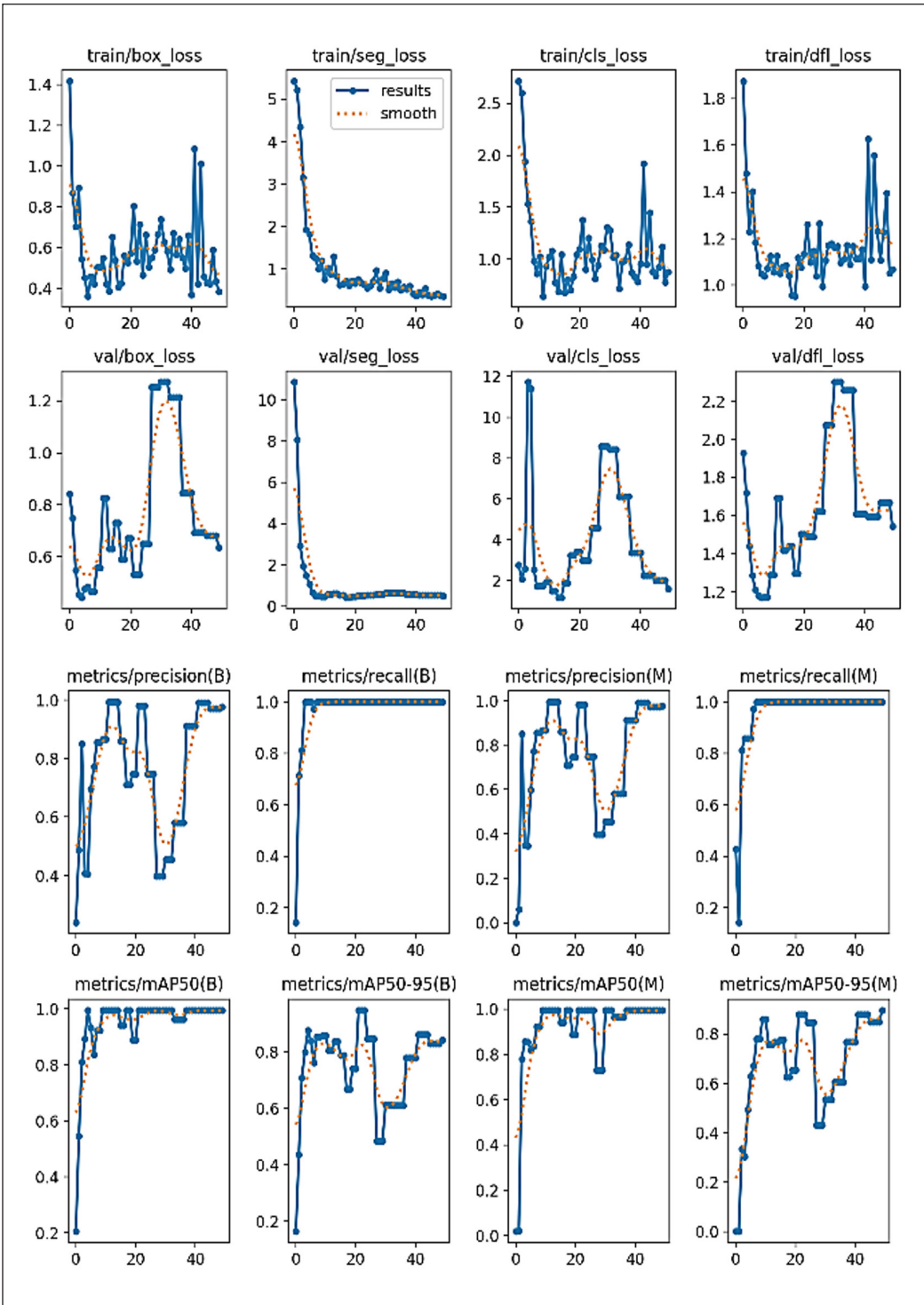


Figure 5. Illustrate performance measurement

from 50% to 95%, reached 0.84186. metrics/precision(M), metrics/recall(M), metrics/mAP50(M), metrics/mAP50-95(M). These scales are like the detection scales, but these are for segmentation. For this reason, note that the values of the segmentation scales are higher. Table 2 illustrates the values of measurement.

Many images were tested to evaluate the proposed model, as the images were of different lighting and sizes. Figure 6 illustrates the mask detection results, and Figure 7 explains the segmentation results.

The proposed model for dental segmentation will be compared with some segmentation algorithms. Many algorithms can be referred to and get good results in dental segmentation. The dataset used in the

Table 2
Values of measurement

Measure	Value
train/box_loss	0.38524
train/seg_loss	0.35353
train/cls_loss	0.87865
train/df_l_loss	1.0683
metrics/precision(B)	0.9761
metrics/recall(B)	0.996
metrics/mAP50(B)	0.995
metrics/mAP50-95(B)	0.84186
metrics/precision(M)	0.9761
metrics/recall(M)	0.996
metrics/mAP50(M)	0.995
metrics/mAP50-95(M)	0.8955
val/box_loss	0.63554
val/seg_loss	0.48883
val/cls_loss	1.5975
val/df_l_loss	1.5415

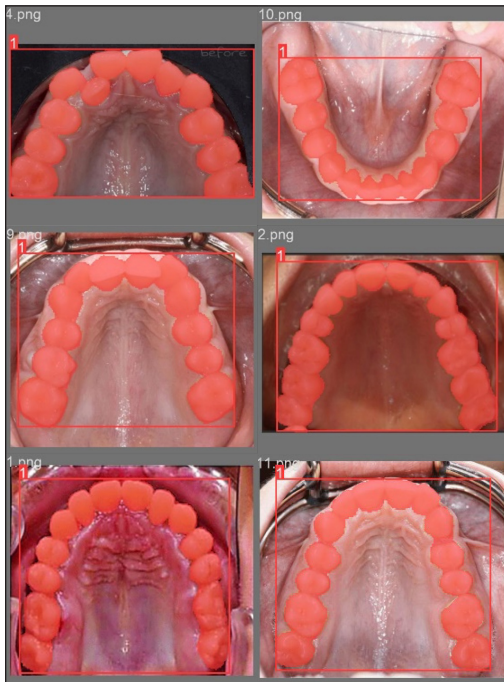


Figure 6. Show the mask detection results



Figure 7. Illustrate segmentation results using the YOLOv8 segmentation model

paper will be applied to compare its results with the results of the model proposed in this paper. The comparison results are summarized in Table 3.

Table 3 shows the difference between the previous algorithms compared to the enhanced model, where the proposed model outperformed the rest of the algorithms by comparing it in terms of accuracy in dental segmentation due to the equation that has been improved to reduce loss and reach the best features. In addition, it takes less time to segment the teeth because the algorithm of YOLOv8 has been reduced to complex equations, which take a long time to calculate, as in U-Net and R-CNN.

Table 3
Comparison with segmentation algorithms

Method	Accuracy	Precision	Recall	F1-Score	Time Per Frame
U-Net	0.8150	0.8247	0.8421	0.8333	100 ms
R-CNN	0.8667	0.8900	0.8725	0.8812	87 ms
ASF-YOLO	0.9512	0.9674	0.9468	0.9570	78 ms
YOLO2U-Net	0.9571	0.9674	0.9570	0.9622	76 ms
Our Work	0.9950	0.9761	0.9964	0.9861	66 ms

CONCLUSION

Dental isolation remains a critical challenge in modern dentistry, with various technological advancements aiding dentists in diagnosing dental conditions. Tooth segmentation is particularly challenging due to the similarity in characteristics among dental structures, necessitating the development of a fast and highly precise system. In this study, an enhanced YOLOv8-based model was proposed and optimized for dental segmentation, incorporating a gradient descent-based approach to refine feature extraction and improve segmentation accuracy. The proposed model achieved an unprecedented accuracy of approximately 99.6% when tested on real-world dental images. These results demonstrate the model's high efficiency and reliability in accurately isolating teeth. Given its superior performance, the enhanced YOLOv8 algorithm presents a promising automated dental analysis and segmentation solution. Future research can explore further refinements and adaptations of this model to improve its generalizability across diverse dental imaging datasets and clinical applications.

ACKNOWLEDGEMENT

The authors express their gratitude to the College of Computing, Informatics and Mathematics, the Institute of Postgraduate Studies (IPSiS) and the Research Management Centre, Universiti Teknologi MARA, Shah Alam, Selangor, Malaysia, for supporting the publication of this paper.

REFERENCES

- Al Nassan, W., Bonny, T., Obaideen, K., & Hammal, A. A. (2022). A customized convolutional neural network for dental bitewing images segmentation. In *2022 International Conference on Electrical and Computing Technologies and Applications (ICECTA)* (pp. 347-351). IEEE. <https://doi.org/10.1109/ICECTA57148.2022.9990564>
- Almalki, A. & Latecki, L. J. (2023). Self-supervised learning with masked image modeling for teeth numbering, detection of dental restorations, and instance segmentation in dental panoramic radiographs. In *Proceedings of the IEEE/CVF Winter Conference on Applications of Computer Vision* (pp. 5594-5603). IEEE. <https://doi.org/10.1109/WACV56688.2023.00555>
- Bi, Y., Xue, B., Mesejo, P., Cagnoni, S., & Zhang, M. (2022). A survey on evolutionary computation for computer vision and image analysis: Past, present, and future trends. *IEEE Transactions on Evolutionary Computation*, 27(1), 5-25. <https://doi.org/10.1109/TEVC.2022.3220747>
- Chandrashekar, G., AlQarni, S., Bumann, E. E., & Lee, Y. (2022). Collaborative deep learning model for tooth segmentation and identification using panoramic radiographs. *Computers in Biology and Medicine*, 148, 105829. <https://doi.org/10.1016/j.compbiomed.2022.105829>
- El Bsar, A. R., Shamma, E., Asmar, D., Sakr, G. E., Zeno, K. G., Maxari, A. T., & Ghafari, J. (2022). Semantic segmentation of maxillary teeth and palatal Rugae in two-dimensional images. *Diagnostics*, 12(9), 2176. <https://doi.org/10.3390/diagnostics12092176>
- Elyan, E., Vuttipittayamongkol, P., Johnston, P., Martin, K., McPherson, K., Moreno-Garcia, C. F., Jayne, C., & Sarker, M. M. K. (2022). Computer vision and machine learning for medical image analysis: Recent advances, challenges, and way forward. *Artificial Intelligence Surgery*, 2, 24-45. <https://doi.org/10.20517/ais.2021.15>
- Fatima, A., Shafi, I., Afzal, H., Mahmood, K., Diez, I. D. L. T., Lipari, V., Ballester, J. B., & Ashraf, I. (2023). Deep learning-based multiclass instance segmentation for dental lesion detection. *Healthcare* 2023, 11, 347. <https://doi.org/10.3390/healthcare11030347>
- Hou, S., Zhou, T., Liu, Y., Dang, P., Lu, H., & Shi, H. (2023). Teeth U-Net: A segmentation model of dental panoramic X-ray images for context semantics and contrast enhancement. *Computers in Biology and Medicine*, 152, 106296. <https://doi.org/10.1016/j.compbiomed.2022.106296>
- Im, J., Kim, J. Y., Yu, H. -S., Lee, K. -J., Choi, S. -H., Kim, J. -H., Ahn, H. -K., & Cha, J. -Y. (2022). Accuracy and efficiency of automatic tooth segmentation in digital dental models using deep learning. *Scientific Reports*, 12(1), 9429. <https://doi.org/10.1038/s41598-022-13595-2>
- Lee, S., & Kim, J. E. (2022). Evaluating the precision of automatic segmentation of teeth, gingiva and facial landmarks for 2d digital smile design using real-time instance segmentation network. *Journal of Clinical Medicine*, 11(3), 852. <https://doi.org/10.3390/jcm11030852>
- Rashid, U., Javid, A., Khan, A. R., Liu, L., Ahmed, A., Khalid, O., Saleem, K., Meraj, S., Iqbal, U., & Nawaz, R. (2022). A hybrid mask RCNN-based tool to localize dental cavities from real-time mixed photographic images. *PeerJ Computer Science*, 8, e888. <https://doi.org/10.7717/peerj-cs.888>
- Sivagami, S., Chitra, P., Kailash, G. S. R., & Muralidharan, S. R. (2020). UNet architecture based dental panoramic image segmentation. In *2020 International Conference on Wireless Communications*

Signal Processing and Networking (WiSPNET) (pp. 187-191). IEEE. <https://doi.org/10.1109/WiSPNET48689.2020.9198370>

- Tian, S., Dai, N., Zhang, B., Yuan, F., Yu, Q., & Cheng, X. (2019). Automatic classification and segmentation of teeth on 3D dental model using hierarchical deep learning networks. *IEEE Access*, 7, 84817-84828. <https://doi.org/10.1109/ACCESS.2019.2924262>
- Wu, Y., Li, Z., Wang, J., He, M., Zhou, W., & Lin, P. (2023). Application study on the recognition of oral obstructed tooth images using semantic segmentation. *Second International Conference on Biomedical and Intelligent Systems (IC-BIS 2023)* (Vol. 12724, pp. 610-614). SPIE. <https://doi.org/10.1117/12.2687389>
- Zhao, Y., Li, P., Gao, C., Liu, Y., Chen, Q., Yang, F., & Meng, D. (2020). TSASNet: Tooth segmentation on dental panoramic x-ray images by two-stage attention segmentation network. *Knowledge-Based Systems*, 206, 106338. <https://doi.org/10.1016/j.knosys.2020.106338>

Enhancing Recycling Collection Point Coverage in Seremban City, Malaysia: A Comprehensive Study on Adapting Integer Linear Programming Models with Fixed Capacity Levels

Muhammad Zulhazwan Rosni¹, Zati Aqmar Zaharudin^{1*} and Adibah Shuib²

¹College of Computing, Informatics and Mathematics, Universiti Teknologi MARA Cawangan Negeri Sembilan, Kampus Seremban, 70300 Seremban, Negeri Sembilan, Malaysia

²College of Computing, Informatics and Mathematics, Universiti Teknologi MARA, 40450 Shah Alam, Selangor, Malaysia

ABSTRACT

This study introduces an integer linear programming (ILP) model as an effective strategy to address the problem of facility location and allocation. The implemented model incorporated the concept of covering and finding optimal sites for facility locations to effectively satisfy demand at its optimum level. Identifying strategic and optimal locations for recycling bins, essential for maximizing the effectiveness of recycling initiatives, remains an area that requires substantial improvement, particularly within the context of Malaysia. The study used a mathematical model based on the Maximal Expected Covering Location Problem, with modifications including a fixed capacity level for each recycling facility. The model is applied to households in Seremban, the capital city of Negeri Sembilan in Peninsular Malaysia. The results indicate that three recycling facilities successfully covered the demand locations based on the performance of the modified model.

Keywords: Covering model, facility locations, recycling, waste management

INTRODUCTION

Municipal solid waste (MSW) is commonly defined as daily trash and garbage, which includes waste from households, businesses and institutional sources but does not include industrial, construction, or hazardous waste (Hemidat et al., 2022). The amount of waste has grown massively worldwide in recent decades, mainly due to increased urbanization and industrialization. MSW

ARTICLE INFO

Article history:

Received: 22 August 2024

Accepted: 24 February 2025

Published: 24 April 2025

DOI: <https://doi.org/10.47836/pjst.33.S3.06>

E-mail addresses:

hazwan3005@gmail.com (Muhammad Zulhazwan Rosni)

zati@uitm.edu.my (Zati Aqmar Zaharudin)

adibah253@uitm.edu.my (Adibah Shuib)

*Corresponding author

must be collected regularly, recycled, or treated and disposed of properly to maintain healthy and sanitary living conditions and have less impact on the environment.

Kaza et al. (2018) estimate that by 2050, there will be 3.40 billion tonnes of waste produced globally, with each person producing between 0.11 and 4.54 kilograms per day on average. Malaysia is the third-largest ASEAN waste producer after Singapore and Brunei, producing 1.17 kilograms per person daily and increasing by 5.19% between 2015 and 2020 (Ghani, 2021). By 2030, these landfills are expected to reach their full capacity as 89% of MSW is sent to landfills (Yong et al., 2019). Despite increased waste segregation activity, Malaysian waste generation is at a high volume (Rangga et al., 2022), indicating that a mechanism for sustainable waste management is urgently required in Malaysia. The practice of waste segregation is an essential step in fostering recycling. However, in the current context, as public engagement in waste separation remains insufficient, over 80% of recyclable waste in Malaysia continues to be improperly disposed of, exacerbating environmental challenges (Daim & Mohamed Radhi, 2023).

Recycling contributes to environmental preservation, resource efficiency, and the general well-being of present and future generations by tackling waste creation holistically. It is also part of the sustainable development goal (SDG) 12, i.e., substantially reducing waste generation through prevention, reduction, recycling and reuse (3Rs), which must be achieved by 2030 (United Nations Environment Programme, 2023). Specifically, target 12.5 (Substantially reduce waste generation) of SDG 12 aims to "substantially reduce waste generation through prevention, reduction, recycling and reuse by 2030." Recycling also underpins the concept of zero-waste management.

Malaysia's current recycling rate is 31.5%, and the government plans to increase it to 40% by 2025 (Shakil et al., 2023). Although Malaysia's recycling rates have increased dramatically over the years, the need to cater to household waste is extremely important. Recycling practice must be part of their moral norm to encourage separation-at-source activity among householders (Razali et al., 2019). However, Malaysia still lacks of recycling infrastructures (Mustafa et al., 2022; Rodzi et al., 2023), which is an obstacle to the Malaysian community to practice recycling (Tiew et al., 2019). This is a particularly challenging problem for the local authority to solve, given the sporadic nature and restricted route options of households, especially within an urban congested area. Moreover, strategically located recycling facilities are believed to reach target users and effectively encourage recycling behavior (Azri et al., 2023; Rodzi et al., 2023).

Studies concerned about determining the strategic and optimal locations for recycling bins for more impactful results in recycling efforts, particularly in Malaysia, still lack of mathematical models to improve recycling facilities' location. Recently, mathematical programming models and set-covering location methodologies have become less common. Nevertheless, these techniques continue to retain significant importance across a variety of sectors.

Past Studies Covering Models of Recycling Facility Location

Standard covering models are based on *demand*-based objective functions. The covering concept occurs when a decision-maker strives to maximize a specific amount of demand within pre-specified distances (or travel times) between facilities and demand points. Problems with coverage arise in many real-life situations where location-specific services are unable to satisfy demand outside pre-specified coverage regions (Blanco & Gázquez, 2023). There were renowned basic covering-like models, the Location Set Covering Model (LSCM) and the Maximal Covering Location Problem (MCLP). The LSCM, introduced by Toregas et al. (1971), focuses on identifying the minimum number of facilities and their optimal locations to ensure complete coverage, whereby all demand points are served by at least one facility (Sitepu et al., 2019). In contrast, the MCLP, developed by Church and ReVelle (1974), aims to maximize the population coverage within a specified service distance by strategically locating a fixed number of facilities (Wang et al., 2021).

Several studies have applied mathematical programming (MP) models rooted in the covering conceptual framework to solve location-allocation problems, including identifying strategic locations and determining the optimal number of recycling facilities. Much recent work in utilizing a set covering framework was proposed by Zaharudin et al. (2024) for recycling facility locations and bin allocations. While some numerical analyses were presented, the study has yet to be applied to real-life cases. Additionally, Zaharudin et al. (2023) solved drop-off points for recyclable materials in a satellite city in Malaysia. The proposed model aims to maximize demand coverage by identifying the optimal sites for recycling drop-off points and determining the appropriate number of containers to be installed at these locations. Rosni et al. (2022) and Jamiron et al. (2021) modified a variant of the covering model, namely, the maximum expected covering location problem (MEXCLP) model of Daskin (1983) to position to identify and distribute recycling bins in Malaysia. However, both studies focused on different urban areas that exhibit varying levels of complexity in terms of route networks. Both studies utilized calibration values obtained from Shuib and Zaharudin (2011) to determine the allocation of recycling containers based on the likelihood of bin utilization. Rosni et al. (2022) do not restrict the allocation of containers at each chosen facility, while Jamiron et al. (2021) subsequently relaxed this constraint. On the other hand, Wang et al. (2021) introduced an element of uncertainty into the MCLP to determine the optimal location for a recycling facility in Tongji, China. The model incorporates the cost of service to characterize the uncertainty in demand variation. Meanwhile, Cubillos and Wøhlk (2020) proposed a bi-objective model that integrates cost elements to address the location and routing problem. The purpose is to identify the optimal locations for recyclable drop-off facilities in five specific regions of Denmark.

Certain types of waste, such as electronic waste (e-waste), batteries, and waste cooking oil (WCO), can also be recycled, but a diligent handling process is required. Therefore,

collecting these recyclable materials is of utmost importance due to their hazardous and detrimental environmental effects. Sari et al. (2021) investigated the Yogyakarta e-waste network system to determine the quantity and spatial distribution of collection facilities, as well as the optimal transportation route for e-waste disposal. A study on selecting the optimal WCO collection points was conducted by Hartini et al. (2021). The authors used the MCLP model to locate the WCO collection point within Semarang, Indonesia. As a recyclable material, batteries encompass certain types that are classified as hazardous. Guan and Yang (2020) developed a bi-objective linear programming model to effectively identify the optimal placement of recycling facilities for power battery waste. The model takes into account the adverse social effects, which are directly proportional to the quantity of transport power batteries located between the facility nodes. Table 1 provides a summary of selected prior studies that focus on recycling facility location and allocation.

Table 1
Summary of the selected past study covering models of recycling facility location

Authors (year)	Objective Functions	Capacity Integration	Application To Real-Life Problem	Case Study Area
Guan and Yang (2020)	Minimize adverse social effects of battery recycling based on transport distance	✓	Power battery recycling	-
Cubillos and Wöhlk (2020)	Minimize the cost of facility location	✓	Recycling drop-off facilities	Denmark
Sari et al. (2021)	Minimize the total cost of the number of facilities to be established	-	E-waste collection and transportation	Yogyakarta, Indonesia
Hartini et al. (2021)	Maximize coverage for waste cooking oil (WCO) collection	-	Waste cooking oil collection	Semarang, Indonesia
Wang et al. (2021)	Maximize coverage of demand under uncertain demand variations	✓	Recycling facility location	Tongji, China
Jamiron et al. (2021)	Maximize expected coverage of demand locations	✓	Recycling bin location and allocation	Johor Bahru, Malaysia
Rosni et al. (2022)	Maximize expected coverage of demand locations	-	Recycling bin location and allocation	Seremban, Malaysia
Zaharudin et al. (2023)	Maximize the coverage of recyclable waste	✓	Recycling drop-off points	Nilai, Malaysia
Zaharudin et al. (2024)	Maximize expected coverage of recyclable waste	✓	Recycling facility location and bin allocation	-

Table 1 highlights that while significant progress has been made in research on recycling facility location and container allocation, only two studies have explicitly prioritized expected recyclable waste generation as their primary focus. This underscores the need for greater emphasis on the coverability of recyclable waste generated. Addressing this research gap is vital for enhancing the efficiency of waste management systems by optimizing the utilization of existing facilities. Establishing new facilities often entails substantial financial costs and land requirements, which may not always be feasible.

This study introduces an ILP model to address the critical challenge of facility location and allocation within the context of recycling collection points. Incorporating the concept of covering, the ILP model seeks to identify optimal locations for recycling collection facilities to efficiently meet demand levels. A fixed capacity level is introduced in the ILP model to ensure full coverage of demand locations. The set capacity subsequently determines the bin allocations. We applied the proposed method to the urban area of Seremban using data from Rosni et al. (2022) through parameter calibration techniques to achieve optimal results.

MATERIALS AND METHODS

The framework in this paper describes the proposed study, referencing the MEXCLP model for the variables and outlining the objective functions, parameters, decision variables, and constraints of the existing covering model. The mathematical model for locating recycling facilities in this study adapts the model proposed by Rosni et al. (2022). By adopting this model, the paper aims to leverage its proven reliability and effectiveness in addressing the specific requirements of recycling facility location and capacity assessment. This paper has both modified and employed reliability measures, and it currently utilizes these adapted measures to assess a fixed capacity level simultaneously.

The application involved implementing a real-world case study. First, a case study of the recycling facilities in Seremban, Negeri Sembilan, was chosen. Second, the model was applied using data from Rosni et al. (2022). However, due to limited data, a weight is assigned to represent capacity levels. If actual capacity data is available, this weight can be adjusted. Third, the optimal solution for a recycling facility location was identified by calibrating the parameters and using the CPLEX solver.

There were variables for the formulation of a mathematical model. Thus, assume a network with a set of nodes (N) and arcs (A), namely as a graph, $G = (N, A)$. Let a set of demand, $D = \{d_i\}$, where $i = 1, 2, \dots, n$ and a set of facilities, $j = 1, 2, \dots, m$, be located at these nodes, with travel times between nodes being the weight for the arcs, i.e., t_{ij} . Let the maximum travel times between these nodes be defined as T . A parameter, namely the s_{ij} , is the value to one of $t_{ij} \leq T$, and zero otherwise. In the proposed ILP model, two decision variables are introduced. First, the x_j that is a binary variable assigned a value of 1 if site j is activated (i.e., a facility is located at site j) and 0 otherwise. Second,

the y_{ij} is the binary variable, whose value is 1 if demand at location i is covered with j facilities and 0 otherwise. The main objective of the proposed model is presented by [1], which maximizes the total demand served by activated recycling facilities.

$$\text{Maximize} \quad \sum_i^n \sum_j^m d_i x_j \quad [1]$$

Subject to:

$$\sum_{j=1}^m s_{ij} x_j \geq 1; \quad \forall i = 1, 2, \dots, n \quad [2]$$

$$y_{ij} \leq s_{ij} x_j; \quad \forall i = 1, 2, \dots, n; \forall j = 1, 2, \dots, m \quad [3]$$

$$\sum_{i=1}^n y_{ij} \geq x_j; \quad \forall j = 1, 2, \dots, m \quad [4]$$

$$\sum_{i=1}^n d_i y_{ij} \leq q_j x_j; \quad \forall j = 1, 2, \dots, m \quad [5]$$

$$\sum_{j=1}^m x_j \leq \sigma; \quad [6]$$

$$x_j, y_{ij} \in \{0,1\}; \quad \forall j = 1, 2, \dots, m; \forall i = 1, 2, \dots, n \quad [7]$$

Constraints of the proposed mathematical model are shown from [2] until [7]. Constraint [2] ensures that the demand at location i is served by the nearest activated recycling facility at site j , addressing the accessibility issue. To assign the demand from location i to the activated facility at location j , Constraint [3] is introduced, ensuring alignment with the proximity requirement specified in Constraint [2]. Constraint [4] guarantees that all demands within the proximity of the facilities are assigned to at least one operational site, ensuring the availability of services to all demand locations. To confirm that facilities can accommodate the assigned demand, Constraint [5] is implemented, ensuring that all facilities have sufficient capacity levels, q_j . Additionally, Constraint [6] sets an upper limit on the number of activated recycling facilities, restricting them to a maximum of σ locations. Lastly, Constraint [7] defines the domains of the decision variables, providing the necessary structure for solving the model.

The proposed method is grounded in the set covering framework, with the constraints designed to address the practical challenges of real-life recycling facility location and allocation problems, particularly in inadequate or less favorable locations. Furthermore, a capacity constraint is incorporated into the model to ensure that each facility has sufficient capacity to meet the assigned demand.

Implementation Process: Data Collections and Parameters Setting

Seremban is a densely populated region situated in the southern region of Malaysia. There are approximately 630,299 people residing in 221,529 households within 93.5 thousand square kilometers. Figure 1 depicts the geographic area of Seremban, visually denoted by the color red.

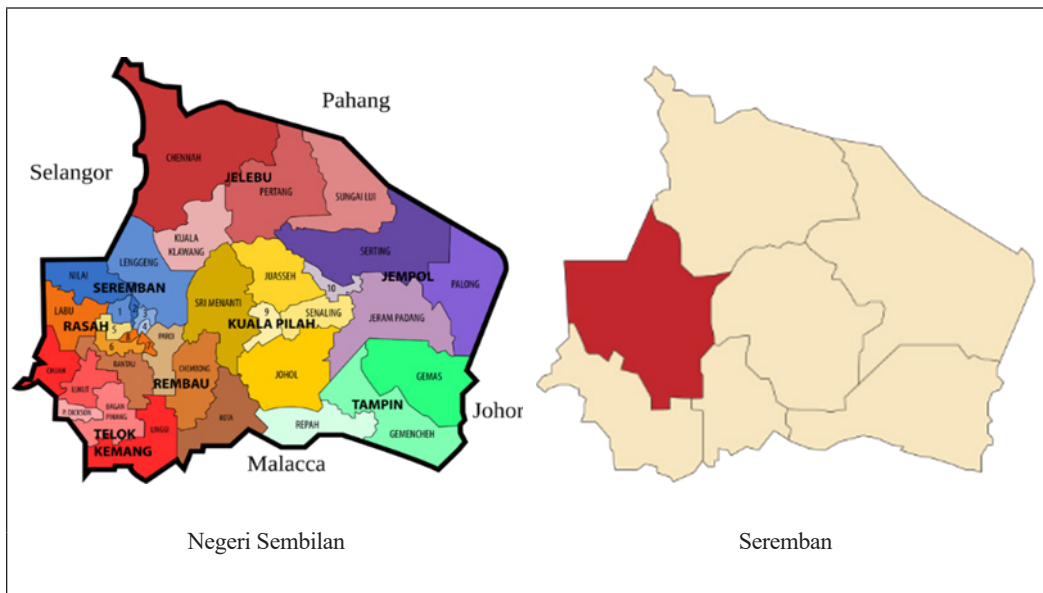


Figure 1. The area of study is Seremban, Malaysia

Figure 2 is the study area that was extracted from Rosni et al. (2022), with the number of households in area (i) being six and five potential locations for the recycling facilities (j). The potential location facilities consist of three shopping centers, one community center and one petrol center, namely, AEON Mall in Seremban 2 ($j=1$), Pall Mall in Seremban ($j=2$), CenterPoint in Seremban ($j=3$), Petronas Petrol Station in Senawang ($j=4$), and Youth and Sports Complex in Paroi ($j=5$). These locations can be depicted in the form of a graph network. Figure 2 also depicts an illustration of the interconnectedness between the demand locations and the potential locations for recycling facilities. The interconnectedness is measured by the travel distance between locations i and j , which is measured in minutes

using Google Maps. This study assumed there is no traffic congestion along the routes and that these locations are always accessible to the public at any time on all days.

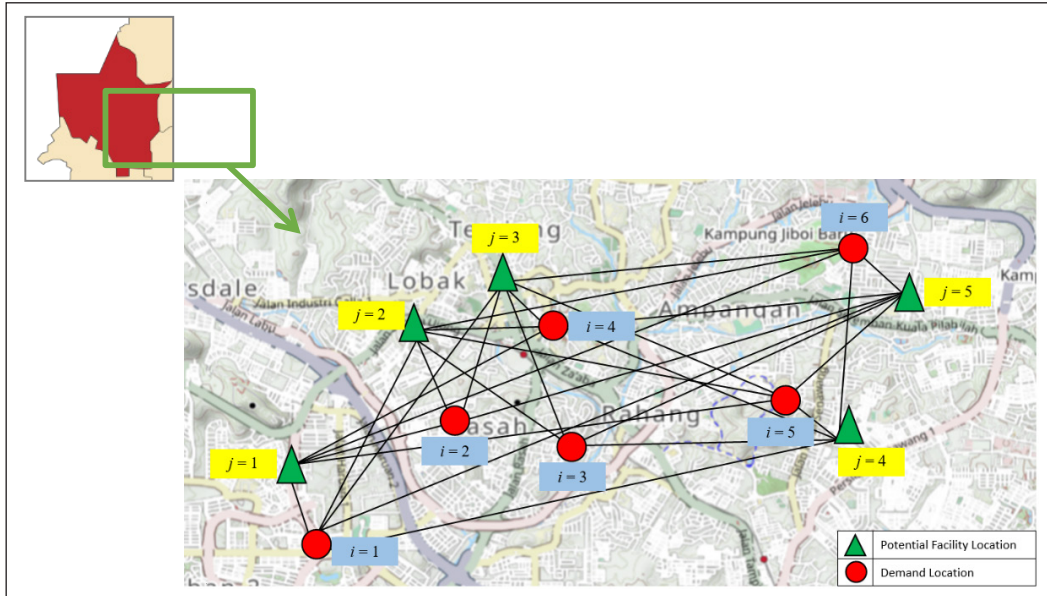


Figure 2. Area of study and network between demand locations and potential facility locations

The amount of waste generated in Seremban was approximated using the average number of persons per household. According to Ghani (2021), the mean waste generation rate for individuals in Malaysia is reported to be 1.17 kilograms per day. This means that for the Seremban area, almost 737,450 kilograms of waste are produced, or almost 3 kilograms per household per day. Currently, the Malaysian government is targeting a recycling rate of 40% for the entire nation. Hence, it is assumed that all users will actively participate in recycling practices that align with the established rate. The term "demand" can be interpreted as the expected amount of recyclable waste generated within a given household area. The data are shown in Table 2.

Table 2
Amount of demand and estimated recyclable waste generation

Household Area (<i>i</i>)	1	2	3	4	5	6	TOTAL
Expected amount of waste generation (kilograms/day)	60229	20885	12136	12668	36182	17610	159710
Expected recyclable waste generations (kilograms/day)	24092	8354	4855	5067	14473	7044	63884

Table 2 presents the data regarding waste generation amounts in various household areas (i), assuming a daily waste generation rate of 3 kilograms per household. Based on the figures in Table 2, it is possible to make an estimation regarding the generation of recyclable waste. Even though more than 80% of recyclable waste is found in landfills (Baba-Nalikant et al., 2023), for this study, we estimate the amount of recyclable waste generation by using the Malaysian government's target of 40% recycling rates. From this target, it is estimated that the amount of recyclable waste generated by households is almost 64,000 kilograms. The highest expected amount of recyclable waste is at $i = 1$. This is anticipated because the area consists of the household area of Seremban 2. Meanwhile, the least expected amount of recyclable waste is generated at area $i = 3$ since the area consists of a commercial area.

The remaining parameter values, including T , q_j , and σ , can be found in Table 3. The values of T are selected based on the permissible travel times between each demand location and each potential facility location. We randomly choose 10, 13, and 17 minutes to encompass the full spectrum of allowable travel durations. The parameter denotes the fixed potential capacity allocation of each recycling center q_j . In general, the values are gathered from the municipalities. However, due to limited data availability, we allocate a weight, denoted as δ , to the q_j , which signifies the dimensions of the recycling facility's capacity level. However, the weightage can be relaxed if the capacity data is known.

Table 3
List of parameter values

T	δ	q_j	σ
10, 13, and 15 minutes	1.0, 1.5, 2.0, 2.5, 3.0	12,776.8, 19,165.2, 25,553.6, 31,942, and 38,330.3 units	1–5 units

Subsequently, the acquired total capacity is evenly distributed among all prospective recycling establishments situated at location j . In this study, the total expected quantity of waste generated is estimated at 63,884 kilograms. To analyze the impact of varying capacity levels, the parameter δ , which serves as the multiplier for the capacity, is set to values ranging from 1.0 to 3.0, incrementing by 0.5 in each iteration. This approach allows for a systematic evaluation of the model's performance under different capacity scenarios. For example, if the value of $\delta = 1.5$, then the total capacity of all facilities amounts to 95,826 kilograms, resulting in an average of 19,165.2 kilograms per facility. Meanwhile, the values of parameter σ are systematically varied from 1 to 5 units, representing the range of permissible recycling facility locations to be operating in the study area. The maximum value of 5 indicates the maximum number of locations of potential recycling facilities. Table 4 presents the indices that we use to test the proposed model. The proposed model is solved using CPLEX 20.0 on a personal computer with a 3.2 GHz processor and 16 GB of RAM.

Table 4
List of data values

Total Expected Waste (kg)	Capacity Multiplier, δ	Total Capacity of All Facilities (kg)	Average Capacity per Facility (kg)	Maximum Number of Facility Locations, σ
63,884	1.0	63,884	12,776.8	5
	1.5	95,826	19,165.2	
	2.0	127,768	25,553.6	
	2.5	159,710	31,942	
	3.0	191,652	38,330.3	

RESULTS AND DISCUSSION

This study identifies the optimal locations for the recycling facilities based on the results obtained using CPLEX solver. This involved calibrating the parameters and running the model to find the optimal solutions. The validation and verification processes confirmed the reliability and effectiveness of the changes to the variable models. This paper successfully provides a robust and reliable framework for locating recycling facilities and assessing their capacity levels.

For this study, the value of the objective function is measured with the variations of travel times between the facility and the demand locations (T) being $T = 10, 13,$ and 17 minutes, the maximum number of operational facilities (σ) and the capacity multiplier (δ). We discovered that even though capacity multiplier (δ) increases, the objective function value remains unaffected because the total demand remains constant across all scenarios. Meanwhile, the relationship between objective function values across the travel times (T) and the maximum number of operational facilities (σ) is presented in Figure 3. The figure shows that across all T variations, the objective function consistently increases as σ rises. This trend indicates that as more facilities become operational or capacity levels increase, it incurs greater costs or significantly impacts system performance. At the same time, the objective function value remains stable regardless of T and δ ; the number of operating facilities changes with these constraints. A detailed analysis of operational facilities based on $T, \sigma,$ and δ is provided in Table 5.

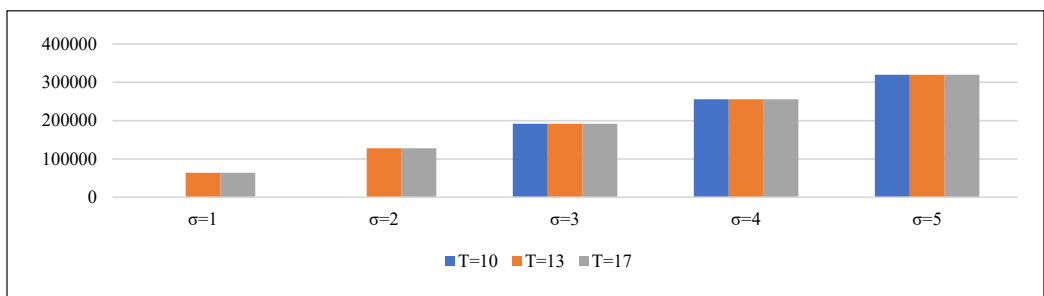


Figure 3. Variation of objective function values based on the values of $T, \sigma,$ and δ

Table 5 presents the total number of demand locations covered based on the variations of travel times between the facility and demand locations (T), the maximum allowance of operational facilities (σ) and the weight of the capacities level (δ). Table 4 presents the total number of demand locations covered based on the variations of travel times between the facility and demand locations (T), the maximum allowance of operational facilities (σ) and the weight of capacities level (δ). As observed, when T is 10 minutes, 100% of demand locations are covered when a maximum of three facilities are operational. Notably, as the T increases, the percentage of demand locations that can be covered is consistently below 100%, except when T is equal to 13 minutes, and the weight assigned to the capacity level is 3.0. As the weightage values (δ) assigned to the capacity level increase, the corresponding percentage of covered demand locations also increases. However, the increase would reach a threshold covering level, which further increases in δ do not guarantee that more demand locations can be covered. For example, from Table 5, when δ is 3.0 units, and T is at 13 minutes, 100% of the covering level can be reached. However, not all demand locations are covered when the δ is 2.5 units. This happens because the model prioritized facilities that can handle a greater amount of demand over the location of demand (i.e., the i). Instead, when the values of the maximum allowance of operational facilities (σ) increase, the total locations of demand covered also increase. This implies that the model exhibits less sensitivity towards the values of T and δ , and instead, has greater emphasis on the values of σ .

Table 5
The number of demand locations covered based on T , σ , and δ

T	σ	δ				
		1.0	1.5	2.0	2.5	3.0
10	1	-	-	-	-	-
	2	-	-	-	-	-
	3	2	4	3	6	6
	4	3	5	4	6	6
	5	3	5	4	6	6
13	1	2	1	1	1	1
	2	1	4	1	1	1
	3	2	1	1	4	4
	4	2	4	2	4	4
	5	3	4	3	5	6
17	1	1	1	1	1	1
	2	1	1	1	1	1
	3	2	1	1	1	1
	4	2	4	1	1	1
	5	3	4	4	5	4

The results presented in Table 5 demonstrate that the proposed model effectively identifies the optimal locations for recycling facilities, ensuring that the demand can be served at its maximum possible level. Based on the results, to get full coverage of demand locations, it is necessary to establish three recycling facilities with a weightage of δ is 2.5 units of capacity expansion, all of which should be located within a travel time, T is 10 minutes. The locations of the selected recycling facilities are depicted in Figure 4.

Based on Figure 4, the star-shaped icon represents the optimal location for a recycling facility computed using the proposed model, i.e., the ILP with covering approach. Therefore, the three optimal locations of the facility that have been identified are AEON Mall in Seremban 2 ($j=1$), Pall Mall in Seremban ($j=2$), and CenterPoint in Seremban ($j=3$). As shown, the demand locations 1 ($i=1$) are designated to the facility at location 1 ($j=1$), and the demand locations 2 ($i=2$) are assigned to the facility at location 2 ($j=2$). Demand locations 3, 4, 5, and 6 ($i=3, i=4, i=5, i=6$) are allocated to the facility at location 3 ($j=3$). From these results, clearly, all demand locations are assigned to one facility, and it is expected that all recyclable waste will be covered.

The proposed ILP model illustrated that increasing the number of operating recycling facilities will improve the level of service. Additionally, for the area chosen as the case study, the model explicitly demonstrates that an increase in travel time from the demand area to the recycling facility location and capacity expansion would not guarantee an improvement in the amount of recyclables collected. Therefore, even with minimal adjustments, the local municipality may improve its recycling service by adding more operational facilities within its jurisdiction.

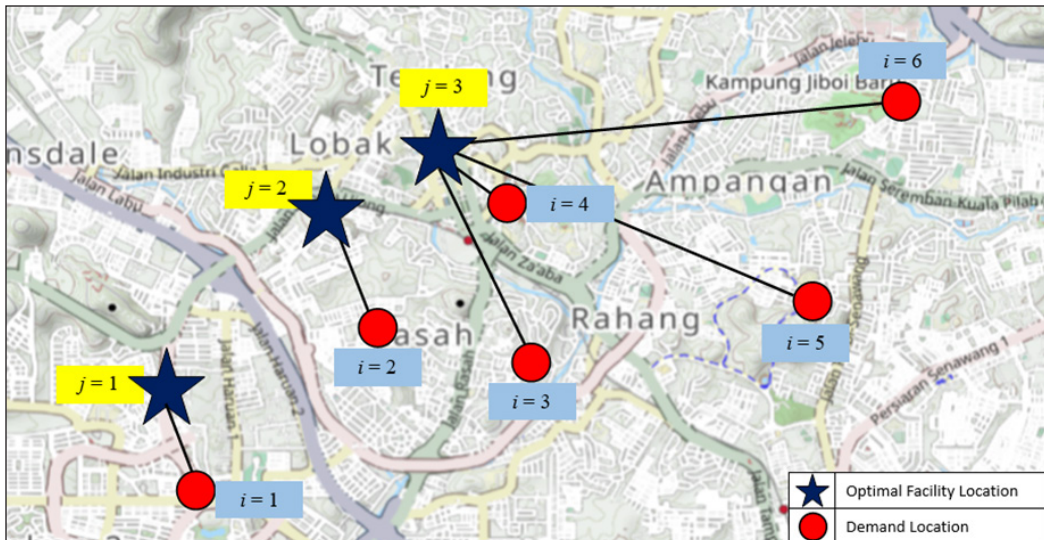


Figure 4. Three optimal facility locations with demand location assignments

The proposed model effectively captures the interaction between the expected amount of collected recyclables, facility capacity, service level, and user travel times. Changes in any of these variables are adequately accounted for within the proposed model. Therefore, it is imperative for decision-makers to implement suitable strategies to optimize users' coverage levels while ensuring optimal service delivery.

CONCLUSION

This study contributes to advancing sustainable regional waste management practices by offering a formal framework for optimizing recycling infrastructure and coverage. An ILP model with a covering concept was proposed to determine the optimal locations for a collection of recycling facilities while considering their restricted capacity levels. We utilized the data from Seremban, Malaysia, extracted from Rosni et al. (2022). Based on the results, to get full coverage of demand locations, it is necessary to establish three recycling facilities with a weightage of 2.5 units of capacity expansion ($\delta = 2.5$), all of which should be located within a travel time of 10 minutes ($T = 10$). On the other hand, there is a clear correlation between the total locations of demand covered and the maximum allowance of operational facilities provided in the model. As the value of the allowance expands, so does the total number of locations covered. This suggests that the model is more sensitive to changes in the maximum allowance of operational facilities (σ) than to changes in capacity level (δ) or maximum travel time (T).

This study addresses Malaysia's challenge of insufficient recycling infrastructure by introducing an ILP model to optimize the location and allocation of recycling bins. It fills a research gap in using mathematical programming and maximally covering locations' problems for this purpose, aiming to enhance recycling efforts in the country. For future work, it is suggested that demand clustering techniques be implemented as the initial step so that potential locations can be selected based on the cluster's centroid. This approach also implies that a system for collecting recyclable waste can be implemented once the locations of recycling facilities have been identified. One possible method for achieving this is to use the dynamic element to determine the inconsistency of waste generation over time.

ACKNOWLEDGEMENT

The authors express our gratitude to the Universiti Teknologi MARA (UiTM) for research support under the grant of Geran Insentif Penyelidikan (Project Code: 600-RMC/GIP 5/3 (083/2022)).

REFERENCES

Azri, S., Ujang, U., & Abdullah, N. S. (2023). Within cluster pattern identification: A new approach for optimizing recycle point distribution to support policy implementation on waste management in Malaysia.

- Waste Management & Research: The Journal for a Sustainable Circular Economy*, 41(3), 687-700. <https://doi.org/10.1177/0734242X221123489>
- Baba-Nalikant, M., Syed-Mohamad, S. M., Husin, M. H., Abdullah, N. A., Mohamad Saleh, M. S., & Abdul Rahim, A. (2023). A Zero-Waste Campus Framework: Perceptions and practices of university campus community in Malaysia. *Recycling*, 8(1), 21. <https://doi.org/10.3390/recycling8010021>
- Blanco, V., & Gázquez, R. (2023). Fairness in maximal covering location problems. *Computers and Operations Research*, 157(May), 106287. <https://doi.org/10.1016/j.cor.2023.106287>
- Church, R., & ReVelle, C. (1974). The maximal covering location problem. *Papers of the Regional Science Association*, 32(1), 101-118. <https://doi.org/10.1007/BF01942293>
- Cubillos, M., & Wøhlk, S. (2020). Solution of the maximal covering tour problem for locating recycling drop-off stations. *Journal of the Operational Research Society*, 72(8), 1898-1913. <https://doi.org/10.1080/01605682.2020.1746701>
- Daim, N., & Mohamed Radhi, N. A. (2023). Separating waste at source to boost recycling rate. *New Straits Times*. <https://www.nst.com.my/news/nation/2023/03/888284/separating-waste-source-boost-recycling-rate>
- Daskin, M. S. (1983). Maximum Expected Covering Location Model: Formulation, properties and heuristic solution. *Transportation Science*, 17(1), 48-70. <https://doi.org/10.1287/trsc.17.1.48>
- Ghani, L. A. (2021). Exploring the municipal solid waste management via MFA-SAA approach in Terengganu, Malaysia. *Environmental and Sustainability Indicators*, 12, 100144. <https://doi.org/10.1016/j.indic.2021.100144>
- Guan, Q., & Yang, Y. (2020). Reverse logistics network design model for used power battery under the third-party recovery mode. *Proceedings - 2020 16th International Conference on Computational Intelligence and Security, CIS 2020*, 293-297. <https://doi.org/10.1109/CIS52066.2020.00069>
- Hartini, S., Puspitasari, D., & Utami, A. A. (2021). Design of waste cooking oil collection center in Semarang City using maximal covering location problem: A finding from Semarang, Indonesia. *IOP Conference Series: Earth and Environmental Science*, 623(1), 012100. <https://doi.org/10.1088/1755-1315/623/1/012100>
- Hemidat, S., Achouri, O., Fels, L. El, Elagroudy, S., Hafidi, M., Chaouki, B., Ahmed, M., Hodgkinson, I., & Guo, J. (2022). Solid waste management in the context of a circular economy in the MENA Region. *Sustainability (Switzerland)*, 14(1), 480. <https://doi.org/10.3390/su14010480>
- Jamiron, N. F. H., Sarif, N. A. S., Abdul Rahman, N. S., & Zaharudin, Z. A. (2021). Establishing recycling bins location and allocation for sustainable urban municipalities of Johor Bahru in Malaysia. *International Journal of Academic Research in Economics and Management Sciences*, 10(3), 459-472. <https://doi.org/10.6007/IJAREMS/v10-i3/11344>
- Kaza, S., Yao, L. C., Bhada-Tata, P., & Van Woerden, F. (2018). What a Waste 2.0: A global snapshot of solid waste management to 2050. In *What a Waste 2.0: A Global Snapshot of Solid Waste Management to 2050*. World Bank. <https://doi.org/10.1596/978-1-4648-1329-0>

- Mustafa, M. A. S., Mohd Noor, N. H., Mohd Saharom, N. A., & Shamsol Kamal, N. S. S. (2022). Understanding Malaysian household waste separation: An extended theory of planned behaviour. *Malaysian Journal of Sustainable Environment*, 9(1), 19. <https://doi.org/10.24191/myse.v9i1.17285>
- Rangga, J. U., Ismail, S. N. S., Rasdi, I., & Karuppiah, K. (2022). Waste management costs reduction and the recycling profit estimation from the segregation programme in Malaysia. *Pertanika Journal of Science and Technology*, 30(2), 1457-1478. <https://doi.org/10.47836/pjst.30.2.34>
- Razali, F., Weng Wai, C., & Daud, D. (2019). A review of Malaysia solid waste management policies to improve recycling practice and waste separation among households. *International Journal of Built Environment and Sustainability*, 6(1-2), 39-45. <https://doi.org/10.11113/ijbes.v6.n1-2.381>
- Rodzi, Z. M., Hazri, A. N., Mohd Azri, N. A. S., Sharul Rhmdan, N. D. F., Zaharudin, Z. A., & Uttunggadewa, S. (2023). Uncovering obstacles to household waste recycling in Seremban, Malaysia through Decision-Making Trial and Evaluation Laboratory (DEMATEL) analysis. *Science and Technology Indonesia*, 8(3), 422-428. <https://doi.org/10.26554/sti.2023.8.3.422-428>
- Rosni, M. Z., Ishak, M. I., Mohd Shah, A. Z., & Zaharudin, Z. A. (2022). Location-Allocation Model of recycling facilities – A case study of Seremban, Malaysia. *International Journal of Academic Research in Economics and Management and Sciences*, 11(1), 56-69. <https://doi.org/10.6007/IJAREMS/v11-i1/12119>
- Sari, D. P., Masruroh, N. A., & Asih, A. M. S. (2021). Extended maximal covering location and vehicle routing problems in designing smartphone waste collection channels: A case study of Yogyakarta Province, Indonesia. *Sustainability*, 13(16), 8896. <https://doi.org/10.3390/su13168896>
- Shakil, N. S. M., Azhar, N. A. Z. M., & Othman, N. (2023). Solid waste management in Malaysia: An overview. *Information Management and Business Review*, 15(1(I)SI), 86-93. [https://doi.org/10.22610/imbr.v15i1\(I\)SI.3410](https://doi.org/10.22610/imbr.v15i1(I)SI.3410)
- Shuib, A., & Zaharudin, Z. A. (2011). TAZ_OPT: A goal programming model for ambulance location and allocation. *2011 IEEE Colloquium on Humanities, Science and Engineering*, 945-950. <https://doi.org/10.1109/CHUSER.2011.6163878>
- Sitepu, R., Puspita, F. M., Romelda, S., Fikri, A., Susanto, B., & Kaban, H. (2019). Set covering models in optimizing the emergency unit location of health facility in Palembang. *Journal of Physics: Conference Series*, 1282(1), 012008. <https://doi.org/10.1088/1742-6596/1282/1/012008>
- Tiew, K. G., Basri, N. E. A., Deng, H., Watanabe, K., Zain, S. M., & Wang, S. (2019). Comparative study on recycling behaviours between regular recyclers and non regular recyclers in Malaysia. *Journal of Environmental Management*, 237(February 2019), 255-263. <https://doi.org/10.1016/j.jenvman.2019.02.033>
- Toregas, C., Swain, R., ReVelle, C., & Bergman, L. (1971). The location of emergency service facilities. *Operations Research*, 19(6), 1363-1373. <https://doi.org/10.1287/opre.19.6.1363>
- United Nations Environment Programme. (2023). *The Sustainable Development Goals Report 2023: Special Edition*. <https://unstats.un.org/sdgs/report/2023/The-Sustainable-Development-Goals-Report-2023.pdf>
- Wang, Z., Duan, Y., & Huo, J. (2021). Maximal covering location problem of smart recycling infrastructure for recyclable waste in an uncertain environment. *Waste Management & Research: The Journal for a Sustainable Circular Economy*, 39(2), 396-404. <https://doi.org/10.1177/0734242X20967090>

- Yong, Z. J., Bashir, M. J. K., Ng, C. A., Sethupathi, S., Lim, J. W., & Show, P. L. (2019). Sustainable waste-to-energy development in Malaysia: Appraisal of environmental, financial, and public issues related with energy recovery from municipal solid waste. *Processes*, 7(10), 676. <https://doi.org/10.3390/pr7100676>
- Zaharudin, Z. A., Shuib, A., Hadiani, R., & Rodzi, Z. M. (2023). Towards sustainable city: A covering model for recycling facility location-allocation in Nilai, Malaysia. *Science and Technology Indonesia*, 8(4), 570-578. <https://doi.org/10.26554/sti.2023.8.4.570-578>
- Zaharudin, Z. A., Shuib, A., Hadiani, R., & Rodzi, Z. M. (2024). A preliminary model for recycling facility location-allocation problem. *AIP Conference Proceedings*, 2895(1), 70001. <https://doi.org/10.1063/5.0193367>

Public Sentiment on Awareness of Climate Change Based on Support Vector Machine

Norlina Mohd Sabri^{1*}, Izzatul Syahirah Ismail², Nik Marsyahariani Nik Daud³
and Nor Azila Awang Abu Bakar³

¹Research and Industrial Linkages Unit, Universiti Teknologi MARA Cawangan Terengganu, Kampus Kuala Terengganu, 21080 Kuala Terengganu, Terengganu, Malaysia

²Yayasan Hasanah Level 2, Blok A, Dataran PHB Saujana Resort, Seksyen U2, 40150 Shah Alam, Selangor, Malaysia

³College of Computing, Informatics and Mathematics, Universiti Teknologi MARA Cawangan Terengganu, Kampus Kuala Terengganu, 21080 Kuala Terengganu, Terengganu, Malaysia

ABSTRACT

Climate change has threatened human society and natural ecosystems, yet public opinion surveys have found that public awareness and concern are very deficient. If society is unaware of climate change, activities such as open burning, deforestation, and releasing excessive carbon dioxide gases would not be reduced. There are several methods to detect public opinion on climate change, and one of the convenient and efficient methods is conducting sentiment analysis on Twitter. This study uses machine learning techniques to collect and analyze public opinion on climate change from Twitter. Due to the increasing occurrences of natural disasters worldwide, understanding public awareness of climate change is crucial. The objective of the study is to analyze public sentiment on the awareness of climate change based on the Support Vector Machine (SVM) algorithm. The methodology for the study consists of several phases: data collection, pre-processing, labeling, feature extraction and classifier evaluation. The evaluation results indicated that SVM achieved a high accuracy of 91% with an 80:20 data split. The SVM classifier model has also produced high precision, F1-score, and recall results. The government could use the study results and non-

governmental organizations (NGOs) to help them spread awareness on climate change issues. Future work will improve the classifier by analyzing non-English tweets and using SentiWordNet to handle word ambiguity in the messages.

ARTICLE INFO

Article history:

Received: 22 August 2024

Accepted: 24 February 2025

Published: 24 April 2025

DOI: <https://doi.org/10.47836/pjst.33.S3.07>

E-mail addresses:

norli097@uitm.edu.my (Norlina Mohd Sabri)

izzatul.syahirah@hasanah.org.my (Izzatul Syahirah Ismail)

nikma944@uitm.edu.my (Nik Marsyahariani Nik Daud)

azila268@uitm.edu.my (Nor Azila Awang Abu Bakar)

*Corresponding author

Keywords: Awareness, climate change, public sentiment, Support Vector Machine

INTRODUCTION

Climate change is one of the important issues today and has often been associated with global warming. This association makes sense since one of the effects of climate change is global warming. According to an encyclopedic entry from National Geographic, climate change refers to long-term shifts in global temperatures and atmospheric characteristics, including typical weather patterns in a specific region (National Geographic Society, 2019). Today, the climate is evolving, with temperatures rising worldwide. Climate change can bring a lot of harm and difficulties to all the living things on this earth if this issue is always ignored. For example, the farmers will face difficulties maintaining and growing crops because of the expected temperature and rainfall levels. Other than that, climate change can cause a rise in sea level and damage the land due to increased flooding and erosion. Therefore, climate change has become a major concern because the impact of climate change is big and irreversible. Climate change is undeniably one of the threats to humans, animals, and the environment today.

Even though the effects of climate change are very obvious today, many people are still ignorant due to many factors, such as economic factors. People all over the world are still lacking awareness and concern for climate change. There is a need to know the public perception periodically on this matter to educate and warn the world. Humans must be aware of this issue and be prepared to prevent climate change. Knowing the public perception of this issue can help boost the preparation to prevent climate change and bring awareness to humans. One of the most convenient and efficient methods to detect public opinion on climate change is sentiment analysis on social media. In general, sentiment analysis focuses on systematic identification, extraction, quantification, and research of subjective data. It also belongs to the broader research area of social media content analysis. Sentiment analysis requires using a range of tools, principally, computational linguistics (Alkhatib et al., 2020; Yogi et al., 2024). Sentiment analysis helps track emotional trends over time and analyze information shared on social networks (Ramanathan et al., 2024; Singleton et al., 2019). In this context, sentiment analysis is used to analyze public opinion on climate change and determine if social media users are falling behind or are aware of the conversation about climate change.

Social media, such as Facebook, Twitter, and Tumblr, have become the trends and the most admired communication medium used on the internet. Each day, millions of texts appear on these micro-blogging sites. Social media serves as a valuable source of information, enabling users to share their opinions on various topics and engage in discussions on current issues without restrictions (Joseph et al., 2024; Loureiro & Alló, 2020). This study has chosen Twitter as one of the most popular microblogging sites, with more than 330 million monthly users worldwide. Twitter has increasingly become a top choice to raise awareness on a variety of topics (Otero et al., 2021; Ram et al., 2024). Analyzing the real-

time monitoring of public opinion about climate change on social media can be utilized for decision-making in problematic situations. Social media can be a valuable source of information to the debate on current issues and allow individuals from different cultures, backgrounds, and preferences to share their opinions and concerns with no restrictions (Alkhatib et al., 2020; Singh et al., 2024). Based on this motivation, the objective of the study is to analyze the public sentiment on the awareness of climate change over Twitter based on the Support Vector Machine (SVM) algorithm. The SVM classifier should be able to classify the tweets into positive (aware) or negative (not aware) sentiments. Machine learning-based sentiment analyses have proven reliable, and the techniques can produce good performance (Singh et al., 2024; Sudhir & Suresh, 2021). Previous studies have classified climate change sentiments tweets from the public using SVM and other algorithms such as Random Forest, Logistic Regression, Naive Bayes, Decision Tree, Neural Network, CNN and also RNN (Ahnsori & Shidik, 2024; Anoop et al., 2024; Baguio et al., 2023; Ray & Kumar, 2023; Thenmozhi et al., 2024; Varshney et al., 2022; Wang et al., 2020). In this study, the Support Vector Machine (SVM) algorithm has been chosen due to its exceptional capability in solving various problems related to regressions and classifications (Kumar, 2020; Reddy et al., 2022). Analyzing the public's opinion can help to spread climate change awareness, and sentiment analysis is one of the methods that is convenient and efficient in detecting public views on climate change. Based on similar works that had been conducted on climate change sentiment analysis, many approaches have been proposed. Even with the emergence of new algorithms such as CNN and RNN, algorithms such as SVM are still being applied for text analysis, as seen in the latest works (Ahnsori & Shidik, 2024; Thenmozhi et al., 2024). Thus, for this work, SVM is chosen to solidify the arguments that SVM is still relevant for text analysis.

MATERIALS AND METHODS

The study's methodology consists of data collection, pre-processing, sentiment annotation, feature extraction, classifier training and evaluation phases. This study has proposed the SVM algorithm to solve the climate change sentiment classification problem. The core principle of SVM is to identify linear separators within the search space, which separate the different classes. Figure 1 shows the phases of the methodology for this study. The following discussion explains the research methodology phases.

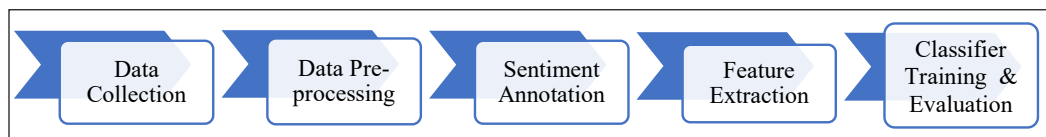


Figure 1. Research methodology phases

Data Collection

In this project, the Twitter API was accessed using Tweepy to scrape data from Twitter. Tweepy is an open-source Python package that facilitates interaction with the Twitter API. It provides a collection of classes and methods representing Twitter's models and API endpoints. Additionally, Tweepy manages various implementation aspects, including data encoding and decoding, HTTP requests, and OAuth authentication. In this project, Tweepy scraped 9244 rows of data using keywords, which were #ActonClimate, #ClimateEmergency, #ClimateReality, #ClimateCrisis, #ClimateChaos and #ClimateAction. Then, the data were stored in a CSV file to proceed to the next phase. This study scraped the Twitter data from March until August 2022. This was the period after the Covid-19 restriction orders were slowly lifted all over the world.

Data Pre-processing

Data pre-processing involves transforming raw data into a structured format, enabling the extraction of valuable information for training the model. It helps to get rid of unhelpful parts of the data. In machine learning processes, data pre-processing is important to ensure that large datasets are formatted so that learning algorithms can interpret and process their data content. Several steps have been taken to process the raw data before continuing with the data labeling. Text Cleaning, Tokenization, Normalization, Lemmatization, and Remove Duplicates are steps.

Text Cleaning

The first step in the text cleaning was lowercasing all the tweets to maintain the flow consistency during the NLP tasks and text mining (Singhal, 2020). Twitter tweets could be labeled or unlabeled, and these tweets are noisy. In order to remove the noise, the tweets must be cleaned first. Twitter usually contains informal sentences, URLs, and emojis, as most Twitter users use spoken language when posting a tweet (Otero et al., 2021) Cleaning is required to help analyze the dataset. Figure 2 shows the code fragment to lowercase all the tweets, including the output.

The second step was to remove any URL links and HTML reference characters in the tweets. Then, the next task was to remove placeholders such as 'LINK,' 'VIDEO' and any filler text that temporarily held any URL and HTML link for typesetting and layout. The following step was to remove Twitter handles and non-letter characters such as punctuation, question marks, symbols such as hashtag (#), slash (/) and other unwanted entities such as â, € and more. Next, stop words were removed to eliminate low-value information from tweets and emphasize essential content. This process helps reduce the dataset size, leading to shorter training times by minimizing the number of tokens involved. Afterward, the

Lowercasing all the tweets	
1	<code>df_clean = pd.DataFrame()</code>
2	<code>df_clean['tweet_text'] = tweets.tweet_text.str.lower()</code>
3	<code>df_clean.head()</code>
tweet_text	
0	rt @jinnieeee_274: @strwberissa here are the little things but has a big help to save the earth... #lettheearthbreath #climatecrisis https://
1	rt @trsrupdates: â€œeveryday is earth day, letâ€™s restore our earth!â€ - @treasuremembers #scienceprotest #lettheearthbreath #climatechangeawâ€
2	rt @walwrites_: instead of using google, you can use ecosiaâ€¦ ja search app just like google, but the difference is for every search you do inâ€
3	rt @sassiesahi: [#lettheearthbreath]\n\nhi, everyone ! you can donate your plastic wastes here. there are places where you can drop-off. yoâ€
4	rt @gyuubie: how to save mother earth\nâ€¢save water\nâ€¢save electricity\nâ€¢plant some trees\nâ€¢ unplug some appliances\nâ€¢delete emails\nâ€¢reduce the usâ€

Figure 2. The code fragment to lowercase the tweets and the output

cleaned data were ready to proceed to the next steps: tweet normalization, tokenization and lemmatization.

Tokenization

Tokenization separates a piece of text into smaller units called tokens to build blocks of Natural Language (Pai, 2022). The following tokens are then used to prepare vocabulary for the count vectorizer and boost the purpose of the SVM model. Figure 3 shows the code snippet for tokenization using the TweetTokenizer function from the nltk.tokenize library. The figure also shows the tokenized words column in the output.

Tokenization			
1	<code>from nltk.tokenize import TweetTokenizer</code>		
2	<code>from nltk.stem import WordNetLemmatizer</code>		
3	<code>tknznr = TweetTokenizer()</code>		
4	<code>df_clean['tokenized'] = df_clean['remove_short'].apply(tknznr.tokenize)</code>		
5	<code>df_clean.head()</code>		
	tweet_text	remove_short	tokenized
0	here are the little things but has big help sa...	little things big help save earth lettheearthb...	[little, things, big, help, save, earth, letth...
1	everyday earth day let restore our earth scie...	everyday earth day let restore earth sciencepr...	[everyday, earth, day, let, restore, earth, sc...
2	instead using google you can use ecosia search...	instead using google use ecosia search app lik...	[instead, using, google, use, ecosia, search, ...
3	lettheearthbreath hi everyone you can donate ...	lettheearthbreath hi everyone donate plastic w...	[lettheearthbreath, hi, everyone, donate, plas...
4	how save mother earth save water save electric...	save mother earth save water save electricity ...	[save, mother, earth, save, water, save, elect...

Figure 3. Code snippet for tokenization and the output

Normalization

Data normalization aims to improve the cohesion of entry types and organize the data to make it consistent across all contents. Since tweets often contain non-standard words such

as acronyms and misspelled words, normalization is helpful in reducing the number of unique tokens in the data. Figure 4 shows the output after the data is normalized.

	tweet_text	remove_short	tokenized	normalized_tweet
0	here are the little things but has big help save the earth lettheearthbreath climatecrisis https	little things big help save earth lettheearthbreath climatecrisis https	[little, things, big, help, save, earth, lettheearthbreath, climatecrisis, https]	[big, help, save, earth, lettheearthbreath, climatecrisis, http]
1	everyday earth day let restore our earth scienceprotest lettheearthbreath climatechangeaw	everyday earth day let restore earth scienceprotest lettheearthbreath climatechangeaw	[everyday, earth, day, let, restore, earth, scienceprotest, lettheearthbreath, climatechangeaw]	[day, let, restore, earth, scienceprotest, lettheearthbreath, climatechangeaw]
2	instead using google you can use ecosia search app just like google but the difference for every search you	instead using google use ecosia search app like google difference every search	[instead, using, google, use, ecosia, search, app, like, google, difference, every, search]	[google, use, ecosia, search, app, like, google, difference, every, search]
3	lettheearthbreath hi everyone you can donate your plastic wastes here there are places where you can drop off	lettheearthbreath hi everyone donate plastic wastes places drop	[lettheearthbreath, hi, everyone, donate, plastic, wastes, places, drop]	[everyone, donate, plastic, waste, place, drop]
4	how save mother earth save water save electricity plant some trees unplug some appliances delete emails reduce the	save mother earth save water save electricity plant trees unplug appliances delete emails reduce	[save, mother, earth, save, water, save, electricity, plant, trees, unplug, appliances, delete, emails, reduce]	[earth, save, water, save, electricity, plant, tree, unplug, appliances, delete, email, reduce]

Figure 4. The output after the data is normalized

Lemmatization

Lemmatization is a technique used in NLP to switch words to their base root form. The process removes inflectional suffixes and prefixes to return a word to its dictionary form (Wali, 2022). According to Singhal (2022), lemmatization is better than stemming. Sometimes, stemming loses the actual meaning of the words even though lemmatization and stemming have the same goal: returning the base or dictionary form of a word. Therefore, this study adopted the lemmatization over stemming technique.

Remove Duplicates

The last step in data pre-processing was to remove duplicates. Duplicate tweets can disrupt the division of train, validation, and test sets, potentially causing biased performance in the Support Vector Machine model (Chorev, 2021). After removing duplicates, 4037 rows of tweets were left. Figure 5 shows the tweets after the data pre-processing phase was completed.

Sentiment Annotation

Sentiment annotation, or data labeling, involves identifying raw data and assigning meaningful and informative labels to provide context for the machine learning model to learn effectively. Labeled data is also used to train the NLP models to make predictions or understand the text. This study used a Python library called Textblob to label the data. Firstly, the sentiment polarity function was called to return the polarity of the TextBlob. Figure 6 shows the code snippet for labeling using the sentiment polarity function and the output.

	tweet_text	remove_short	normalized_tweet	grams	tokenized	pos_tags	wordnet_pos	lemmatized
0	here are the little things but has big help save the earth lettheearthbreath climatecrisis https	little things big help save earth lettheearthbreath climatecrisis https	[strwberissa, little, thing, big, help, save, earth, lettheearthbreath, climatecrisis, https]	[strwberissa little, little thing, thing big, big help, help save, save earth, earth lettheearthbreath, lettheearthbreath climatecrisis, climatecrisis http, strwberissa little thing, little thing big, thing big help, big help save, help save earth, save earth lettheearthbreath, earth lettheearthbreath climatecrisis, lettheearthbreath climatecrisis http]	[little, things, big, help, save, earth, lettheearthbreath, climatecrisis, https]	[(little, JJ), (things, NNS), (big, JJ), (help, NN), (save, VB), (earth, JJ), (lettheearthbreath, JJ), (climatecrisis, NN), (https, NN)]	[(little, a), (things, n), (big, a), (help, n), (save, v), (earth, a), (lettheearthbreath, a), (climatecrisis, n), (https, n)]	[little, thing, big, help, save, earth, lettheearthbreath, climatecrisis, https]
1	everyday earth day let restore our earth scienceprotest lettheearthbreath climatechangeaw	everyday earth day let restore earth scienceprotest lettheearthbreath climatechangeaw	[everyday, earth, day, let, restore, earth, treasuremembers, scienceprotest, lettheearthbreath, climatechangeaw, everyday earth day, earth day let, day let restore, let restore earth, restore earth treasuremembers, earth treasuremembers scienceprotest, treasuremembers scienceprotest lettheearthbreath, scienceprotest lettheearthbreath climatechangeaw]	[everyday earth, earth day, day let, let restore, restore earth, earth treasuremembers, treasuremembers scienceprotest, lettheearthbreath, lettheearthbreath climatechangeaw, everyday earth day, earth day let, day let restore, let restore earth, restore earth treasuremembers, earth treasuremembers scienceprotest, treasuremembers scienceprotest lettheearthbreath, scienceprotest lettheearthbreath climatechangeaw]	[everyday, earth, day, let, restore, earth, scienceprotest, lettheearthbreath, climatechangeaw]	[(everyday, JJ), (earth, DT), (day, NN), (let, VBD), (restore, VB), (earth, JJ), (scienceprotest, JJS), (lettheearthbreath, NN), (climatechangeaw, NN)]	[(everyday, a), (earth, n), (day, n), (let, v), (restore, v), (earth, a), (scienceprotest, a), (lettheearthbreath, n), (climatechangeaw, n)]	[everyday, earth, day, let, restore, earth, scienceprotest, lettheearthbreath, climatechangeaw]
2	instead using google you can use ecosia search app just like google but the difference for every search you	instead using google use ecosia search app like google difference every search	[instead, using, google, use, ecosia, search, app, like, google, difference, every, search]	[instead using, using google, google, google use, use ecosia, ecosia search, search app, app like, like google, google difference, difference every, every search, instead using google, using google use, google use ecosia, use ecosia search, ecosia search app, search app like, app like google, like google difference, google difference every, difference every search]	[instead, using, google, use, ecosia, search, app, like, google, use, ecosia, search, app, like, google, difference, every, search]	[(instead, RB), (using, VBG), (google, NN), (use, NN), (ecosia, JJ), (search, NN), (app, NN), (like, IN), (google, NN), (difference, NN), (every, DT), (search, NN)]	[(instead, r), (using, v), (google, n), (use, n), (ecosia, a), (search, n), (app, n), (like, n), (google, n), (difference, n), (every, n), (search, n)]	[instead, use, ecosia, search, app, like, google, difference, every, search]

Figure 5. The results after data pre-processing

```

1 df_clean.lemmatized= df_clean.lemmatized.astype(str)
2 df_clean['label'] = ''
3 for i,x in df_clean.lemmatized.iteritems():
4     label = TextBlob(x)
5     df_clean['label'][i] = label.sentiment.polarity
6     print("Index: ", i , "label" , label.sentiment.polarity)

```

Index: 0 label 0.0
Index: 1 label 0.0
Index: 2 label 0.0
Index: 3 label -0.2
Index: 4 label 0.0
Index: 5 label -0.075
Index: 6 label 0.2
Index: 7 label 0.0
Index: 8 label 0.5
Index: 9 label 0.0
Index: 10 label 0.0

Figure 6. Code snippet for labeling data and the output

In Figure 6, the 'label' contains a float from -1 to 1 corresponding to each text. This label column will be transformed into a categorical column using the code in Figure 7.

```

1 df_clean.lemmatized= df_clean.lemmatized.astype(str)
2 def polarity_to_label(x):
3     if(x >= -1 and x < 0):
4         return 'neg'
5     if(x == 0):
6         return 'neutral'
7     if(x > 0 and x <= 1):
8         return 'pos'
9 df_clean.label = df_clean.label.apply(polarity_to_label)
    
```

Figure 7. Code snippet to categorize the label floats

If the polarity is between -1 and 0, it is labeled as negative; if the polarity ranges between 0 and 1, it is positive. Otherwise, it is neutral. Figure 8 below shows the counts of each data set based on their classes.

```

1 df_clean.label.value_counts()
neutral    2167
pos        1273
neg         598
Name: label, dtype: int64
    
```

Figure 8. Counts of each data based on their classes

However, this study does not require data that was labeled as neutral. Only positive and negative data were used in this classification problem. Therefore, the neutral-labeled data were removed, leaving only 1870 rows of data to proceed to the next step.

Figure 9 shows the labeled data with an additional column ‘sentiment’ that changes the negative label to -1 and the positive label to 1. Value 1 indicates that the public is aware of climate change, while value -1 indicates that the public is unaware of climate change.

	tweet_text	remove_short	tokenized	normalized_tweet	pos_tags	wordnet_pos	lemmatized	label	sentiment
3	lettheearthbreath hi everyone you can donate your plastic wastes here there are places where you can drop off	lettheearthbreath hi everyone donate plastic wastes places drop	[lettheearthbreath, hi, everyone, donate, plastic, wastes, places, drop]	[everyone, donate, plastic, waste, place, drop]	[(everyone, NN), (donate, NN), (plastic, NN), (waste, NN), (place, NN), (drop, NN)]	[(everyone, n), (donate, n), (plastic, n), (waste, n), (place, n), (drop, n)]	['everyone', 'donate', 'plastic', 'waste', 'place', 'drop']	neg	-1
5	ways prevent climate change all can something about small action can help lot you can	ways prevent climate change something small action help lot	[ways, prevent, climate, change, something, small, action, help, lot]	[climate, change, something, small, action, help, lot]	[(climate, NN), (change, NN), (something, NN), (small, JJ), (action, NN), (help, NN), (lot, NN)]	[(climate, n), (change, n), (something, n), (small, a), (action, n), (help, n), (lot, n)]	['climate', 'change', 'something', 'small', 'action', 'help', 'lot']	neg	-1
6	shit getting real lettheearthbreath scientistprotest	shit getting real lettheearthbreath scientistprotest	[shit, getting, real, lettheearthbreath, scientistprotest]	[real, lettheearthbreath, scientistprotest]	[(real, JJ), (lettheearthbreath, NN), (scientistprotest, NN)]	[(real, a), (lettheearthbreath, n), (scientistprotest, n)]	['real', 'lettheearthbreath', 'scientistprotest']	pos	1
8	look the hashtag lettheearthbreath tops twitter trending list the philippines today april fil	look hashtag lettheearthbreath tops twitter trending list philippines today april fil	[look, hashtag, lettheearthbreath, tops, twitter, trending, list, philippines, today, april, fil]	[lettheearthbreath, top, twitter, trending, list, philippine, today, april, fil]	[(lettheearthbreath, NN), (top, JJ), (twitter, NN), (trending, VBG), (list, NN), (philippine, NN), (today, NN), (april, VBP), (fil, NN)]	[(lettheearthbreath, n), (top, a), (twitter, n), (trending, v), (list, n), (philippine, n), (today, n), (april, v), (fil, n)]	['lettheearthbreath', 'top', 'twitter', 'trending', 'list', 'philippine', 'today', 'april', 'fil']	pos	1

Figure 9. Labeled data

Feature Extraction

Feature extraction converts raw data into numerical features while retaining the essential information from the original dataset. The process can be accomplished manually or automatically using either method, such as Term Frequency-Inverse Document Frequency (TF-IDF) or Bag of Words (BOW). This study has implemented the TF-IDF method using sklearn. TF-IDF is used to calculate the weight of each word. In this technique, words with higher TF-IDF weights are regarded as more representative and kept, while those with lower weights will be discarded. The Term Frequency (TF) of a particular term (t) is calculated as the number of times a term occurs in a document and is divided by the total number of words. Inverse Document Frequency (IDF) is used to calculate the importance of a term because some terms occur frequently but are not important such as “is,” “are,” “also,” “the,” and many more (Ahuja et al., 2019). In other words, TF measures how frequently a word occurs in the text, while IDF decreases the weight of terms that occur very frequently and increases the weight of terms that rarely occur instead (Shofiya & Abidi, 2021). The output is shown in Figure 10 to get a clearer glimpse of the IDF values. The word ‘climate’ is expected to have the lowest IDF values since this word appears in every document in the tweets collection. The lower the IDF value of a word, the less unique the word.

	idf_weights
climate	2.844403
climateaction	3.009310
climateemergency	3.319827
climatecrisis	3.738972
climatechange	3.781172

Figure 10. IDF values for the most frequent words

Support Vector Machine Implementation

Support Vector Machine (SVM) is a supervised machine learning algorithm capable of addressing regression and classification problems (Arora, 2020). The SVM algorithm has been particularly prominent in text classification performance in recent years. In this study, after the data has been processed and divided, the data is ready to be processed by the SVM classifier. SVM is an algorithm that constructs a line or hyperplane to divide data into distinct classes. The objective of SVM is to establish an optimal decision boundary that separates an n-dimensional space into distinct classes, enabling accurate classification of new data in the future. The first step is defining the kernel matrix. A kernel in SVM is a function that simplifies complex computations, efficiently solving classification problems. The SVM kernel in this project can be defined by the K matrix shown in Equation 1.

$$K_{jk} = k(\vec{x}_j, \vec{x}_k) = \vec{x}_j \cdot \vec{x}_k \quad [1]$$

The kernel matrix defining the transformation is symmetric. Figure 11 shows the K matrix construction to be used in the SVM classifier of this project, and Figure 12 shows the K values obtained. The structure of the kernel matrix is an array.

```
1 k_value = np.array(X_train @ X_train.T + np.identity(len(y_train))*1e-12)
2 pd.set_option('display.max_columns', None)
3 k_value
```

Figure 11. Code snippet for finding K matrix

```
array([[ 1.00000000e+00,  0.00000000e+00,  0.00000000e+00, ...,
         0.00000000e+00,  0.00000000e+00,  0.00000000e+00],
       [ 0.00000000e+00,  1.00000000e+00,  0.00000000e+00, ...,
         0.00000000e+00,  0.00000000e+00,  0.00000000e+00],
       [ 0.00000000e+00,  0.00000000e+00,  1.00000000e+00, ...,
         0.00000000e+00,  0.00000000e+00,  0.00000000e+00],
       ...,
       [ 7.47161478e-02,  0.00000000e+00,  0.00000000e+00, ...,
         1.24410253e-06,  0.00000000e+00,  0.00000000e+00],
       [ 0.00000000e+00,  6.81259001e-02,  0.00000000e+00, ...,
         1.06596945e-12,  1.09194231e-06,  0.00000000e+00],
       [ 0.00000000e+00,  3.85339450e-02,  0.00000000e+00, ...,
        -3.70580822e-14, -5.02160834e-13,  1.14222655e-06]])
```

Figure 12. K -values obtained

Then, the next step is to set up and minimize the dual function given the constraints using cvxpy tools. The tools allow the user to express a convex optimization problem in a readable form, convert it into a format that can be used to call a solver and translate the result into a readable form. This step is crucial before recreating the hyperplane of the SVM classifier. The code snippet is shown in Figure 13 below.

```
1 alpha = cp.Variable(shape=y_train.shape) # Create optimization variables.
2
3 beta = cp.multiply(alpha, y_train) # to simplify notation
4
5 K = cp.Parameter(shape=k_value.shape, PSD=True, value=k_value)
6
7 # objective function
8 obj = .5 * cp.quad_form(beta, K) - np.ones(alpha.shape).T @ alpha
9
10 # constraints
11 const = [np.array(y_train.T) @ alpha == 0,
12          -alpha <= np.zeros(alpha.shape),
13          alpha <= 10*np.ones(shape=alpha.shape)]
14 prob = cp.Problem(cp.Minimize(obj), const)
15 result = prob.solve()
```

Figure 13. Code snippet to minimize the dual function

The next step is to recreate the hyperplane. The code to recreate the hyperplane is shown in Figure 14.

```

1 w = np.multiply(y_train, alpha.value).T @ X_train

1 S = (alpha.value > 1e-4).flatten()
2 b = y_train[S] - X_train[S] @ w
3 b = b[0]
4 b = np.mean(b)

```

Figure 14. Code snippet to recreate the hyperplane

Equation 2 shows how the plane's parameter is modified to fulfill the SVM plane's formula.

$$\vec{w} \cdot \vec{x} - b = 0 \quad [2]$$

The above formula is also equivalent to $\vec{w} \cdot \vec{x} = b$, which is the equation of the separating hyperplane (Siong, 2019). \vec{w} is the normal direction of the plane, and b is a form of threshold. If $\vec{w} \cdot \vec{x}$ is calculated to be bigger than b , it belongs to a class. If not, then it belongs to another class. Ultimately, after the hyperplane is created, the SVM classifier is built by deploying the obtained hyperplane. Figure 15 shows the code snippet to build the SVM classifier.

```

1 def classify(x):
2     result = w @ x + b
3     return np.sign(result)

1 correct = 0
2 incorrect = 0
3 predictions = []
4 for i in X_test:
5
6     my_svm = classify(i)
7
8     predictions.append(my_svm)
9
10 predictions = np.array(predictions)

```

Figure 15. Code to build the SVM classifier

Classifier Training and Performance Evaluation

Classifier training is an important phase in which the SVM classifier learns to distinguish between positive and negative sentiments. Before the training, the dataset has to be split

into the training and testing ratios based on the hold-out method. The classifier is then evaluated using the appropriate performance measurements. The performance evaluation plays a significant role in accuracy measurement through a sentiment analysis word level (Mohamed & El-din, 2017). The performance of the SVM classifier can be evaluated based on accuracy, precision, recall, F1-Score, and receiver operating characteristic (ROC). One of the common techniques used to evaluate the performance of sentiment analysis is the Confusion Matrix.

Confusion Matrix

The confusion matrix is a tool used to evaluate the performance of machine learning classification models, accommodating two or more output classes. It is particularly valuable for assessing recall, precision, and accuracy. This matrix is commonly employed to illustrate how well a classification model performs on a test dataset with known actual values (Markham, 2020). A confusion matrix is also used to summarize the prediction results of a classification problem (Brownlee, 2020). Figure 16 shows the confusion matrix. The rows represent the instances in an actual class, while the columns represent the instances in a predicted class.

		Actual Values	
		Positive (1)	Negative (0)
Predicted Values	Positive (1)	True Positive (TP)	False Positive (FP)
	Negative (0)	False Negative (FN)	True Negative (TN)

Figure 16. Confusion matrix

The basic terms in the confusion matrix are true positive (TP), true negative (TN), false positive (FP), and false negatives (FN). These basic terms are used to calculate the rates often computed from a confusion matrix. The first-rate that can be computed from a confusion matrix is accuracy. Accuracy measures how often a sentiment rating is correct. The accuracy can be calculated using Equation 3.

$$Accuracy = \frac{TP + TN}{(TP + FP + TN + FN)} \quad [3]$$

Next, the second rate is precision, which measures the exactness of a classifier. Higher precision means fewer false positives. Otherwise, lower precision means more false positives. Equation 4 shows how the precision of the project can be obtained.

$$Precision = \frac{TP}{(TP + FP)} \quad [4]$$

The confusion matrix can also compute the recall rate and F-measure. Recall rates measure the completeness or sensitivity of a classifier. A higher recall means fewer false negatives, while a lower recall means more false negatives. The F1 Score estimates the accuracy of a test by considering Precision and Recall. The Recall and F1 Score can be calculated using Equations 5 and 6.

$$Recall = \frac{TP}{(TP + FN)} \quad [5]$$

$$F1 \text{ Measure} = \frac{2 (Precision * Recall)}{(Precision + Recall)} \quad [6]$$

ROC Curve

The ROC curve is a metric used to evaluate classification models across different threshold settings, indicating the model's ability to distinguish between classes (Narkhede, 2021). It can also be described as a graphical representation that assesses the diagnostic performance of binary classifiers (Chan, 2020). The ROC curve is constructed by plotting the True Positive Rate (TPR) on the y-axis against the False Positive Rate (FPR) on the x-axis. To summarize the performance of a classifier, the common approach is to calculate the area under the ROC curve (AUC). An excellent model has a value of AUC near 1. It means it has a good measure of separability (Narkhede, 2021).

RESULTS AND DISCUSSION

This section provides the results of the SVM classifier model performance evaluation. It covers the Confusion Matrix evaluation, the hold-out method, and the AUC calculation results. The elaboration of results also includes data exploration, which has been done through word cloud generation.

Confusion Matrix Results

One suitable tool for evaluating behavior and understanding the effectiveness of a categorical classifier is the confusion matrix. The confusion matrix is a 2-dimensional

array comparing predicted labels to the true label. For binary classification, the categories are True Positive (TP), True Negative (TN), False Positive (FP) and False Negative (FN). Figure 17 shows this study's confusion matrix results based on the 80:20 split of data training and testing.

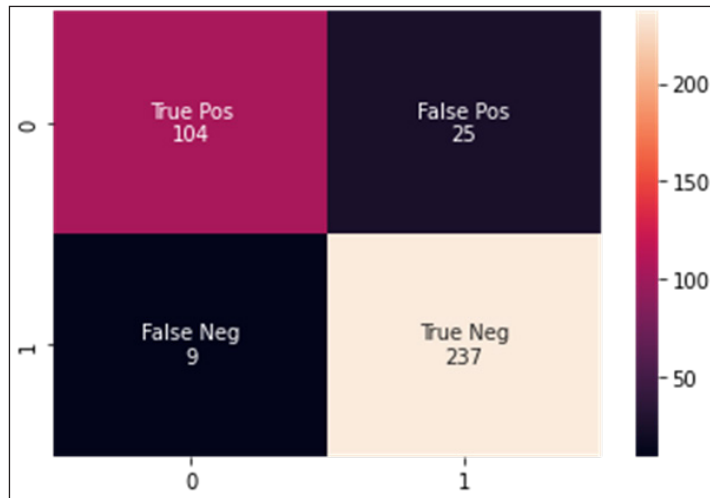


Figure 17. Confusion matrix of the classifier

Based on Figure 17, the diagonal from the top left to the bottom right contains the correctly predicted observations. Based on the confusion matrix above, the total predictions are 375. TP shows that there are 104 correctly predicted positive instances, while FP shows that there are 25 incorrectly predicted positive instances by the model. There are nine instances where the model incorrectly predicted the negative class (FN). On the contrary, the classifier model has correctly predicted 237 negative instances (TN). The total number of correct predictions is 341 (TP+TN), while the incorrect predictions are 34 (FN+FP). The confusion matrix shows that the SVM model performs well overall, with high accuracy and recall. Although the confusion matrix gives a detailed view of the total number of predictions, understanding how good the model is at classifying awareness of climate change samples is complicated. Therefore, the classification report is built to show the metrics that quantify the model's performance.

Classification Report

A classification report is a performance evaluation metric that shows the SVM classifier model's precision, recall, F1 Score, and support. In this project, the classification report also represents the confusion matrix. Table 1 shows all the metrics in the classification report to better understand the result obtained.

Table 1

Metrics in classification report (Kharwal, 2021)

Metrics	Definition
Precision	Describes how well the model can predict the labels correctly.
Recall	Describes how the model can retrieve all of the labels correctly.
F1 Score	The weighted average of precision and recall.
Support	The number of actual occurrences of the class in the dataset.

A function from the `sklearn.metrics` library called `classification_report` is used to generate the classification report. Figure 18 shows the code fragment to view this project's machine learning model's classification report, and Figure 19 shows the output.

```
1 from sklearn.metrics import accuracy_score, f1_score, precision_score, recall_score,
2 classification_report, confusion_matrix
3 print(classification_report(y_test, predictions))
```

Figure 18. Code to display the classification report on the classifier

	precision	recall	f1-score	support
-1	0.92	0.81	0.86	129
1	0.90	0.96	0.93	246
accuracy			0.91	375
macro avg	0.91	0.88	0.90	375
weighted avg	0.91	0.91	0.91	375

Figure 19. Classification report on the classifier

Figure 19 displays the classification report, which summarizes the performance of the SVM classification model across two classes, positive (class 1) and negative (class -1), based on an 80:20 data split. For the positive class (class 1), the precision shows that 90% of predictions were correct, and the recall shows that 96% of actual instances were correctly classified. The value of 0.93 of the F1-score shows a very strong performance for the positive class (class 1). As for the negative class (class -1), the precision shows that 92% of predictions were correct, and the recall shows that 81% of actual instances were correctly classified. The value of 0.86 of the F1-score shows the harmonic mean of precision and recall, indicating strong but slightly lower recall for the negative class (class -1).

The overall metrics show that the model correctly classified 91% of all instances. The macro average results show the values of 0.91, 0.88 and 0.90 for the precision, recall and F1-score, respectively. The macro average shows the unweighted average of the metrics for

both classes. It treats both classes equally, regardless of their support. As for the weighted average, the results show the values 0.91 for the precision, recall, and the F1-score. This weighted average considers each class's support (number of samples), making it more representative of the actual class distribution.

Based on the classification report, the model performs very well overall, with an accuracy of 91%. The positive class (class 1) has slightly lower precision but higher recall, indicating that the model effectively captures most positive cases (96%). The negative class (class -1) has higher precision but lower recall, meaning some negative instances are not classified as positives. The F1 score shows a good balance between precision and recall, particularly for the positive class (class 1). The classification report reflects strong performance for both classes. However, in the future, the model could be further improved for the negative class (class -1) to increase recall (reduce false negatives). This might involve balancing the dataset, fine-tuning the model, or adjusting classification thresholds.

Hold-out Method

The hold-out method is a straightforward and widely used technique for assessing the performance of machine learning models. It involves dividing the dataset into distinct subsets for training and testing, allowing evaluation of the model's ability to generalize new, unseen data. In classification problems, different training and testing data sizes usually can affect the classifier's performance. Therefore, it is necessary to compare the ratio of data splits through the hold-out method. Table 2 shows the accuracy, precision, F1-score and recall rates when the data are divided into 60:40, 70:30 and 80:20 ratios.

Table 2
Comparison between values of evaluation metrics with different ratios of data splitting

Evaluation Metrics	Training and Testing Ratio		
	60:40	70:30	80:20
Accuracy	86%	87%	91%
Precision	88%	88%	91%
F1-Score	83%	85%	90%
Recall	81%	84%	88%

Table 2 shows a slight difference in the evaluation metrics values between the ratios. However, when the data are divided into 80% training and 20% testing, the results could exceed 90%. From the table, it can be seen that the higher the amount of testing data, the better the results will be. Thus, the best data split for this project is 80% for data training and 20% for data testing. The accuracy and precision obtained are 91%, which shows how well the model could classify the sentiments correctly. The high F1-score of 90% represents

the harmonic means between the precision and recall results. The accuracy result in this study is also higher than the result of the SVM classification (82.9%) in one of the similar works (Ruz et al., 2020). The accuracy of SVM in this study has shown that the algorithm could generate good and reliable performance in this classification problem.

ROC Curve

The receiver operating characteristic (ROC) curve represents a classification model's performance across various thresholds. It plots two key metrics: true and false positive rates. Figure 20 shows the ROC curve results for the best model with a split data ratio of 80:20.

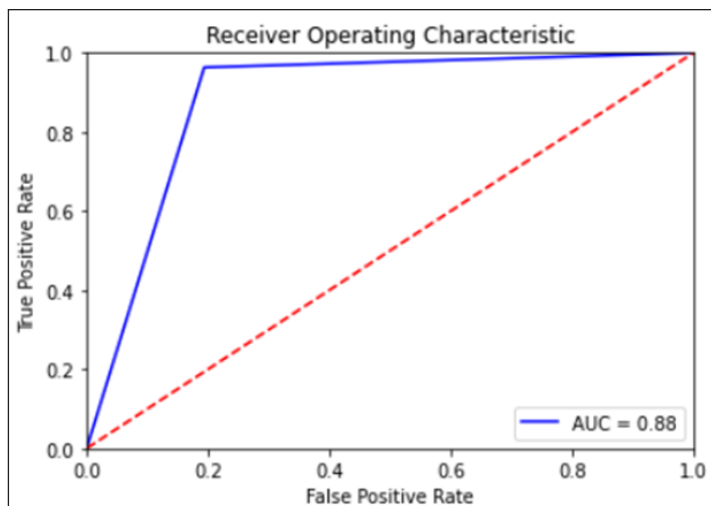


Figure 20. ROC Curve for the best model

In a ROC curve, a higher X-axis value indicates a higher number of FP than TN. Meanwhile, a higher Y-axis value shows a higher number of TP than FN. The area under the ROC curve (AUC) provides the information needed to compute the points in an ROC curve. Based on Figure 20, the ROC curve rises steeply towards the top-left corner of the graph, indicating a high True Positive Rate (TPR-sensitivity) with a low False Positive Rate (FPR). The steep rise in the curve suggests that the model achieves a high TPR while keeping the FPR low. The SVM model has an 88% probability of correctly differentiating between randomly selected positive and negative instances. The model performs much better than random guessing (AUC = 0.5). The value 0.88 indicates that the SVM model performs very well distinguishing between positive and negative classes. The AUC for this SVM classifier with a data split of 80:20 has shown good performance with a 0.88 value. Bhandari (2022) states that a higher AUC indicates better model performance in distinguishing between the two classes.

The ROC curves for the other two models based on the data split of 60:40 and 70:30 are shown in Figure 21. Based on the figure, the green curve represents the data split of 70:30, while the red curve represents the 60:40 data split. The green curve shows that the classifier model performs slightly better than the other model, meaning it has a higher true positive rate for a given false positive rate. The **green curve is slightly higher than the red curve**, indicating better classification performance with more training data (70% training vs 60% training). In this research, increasing the training data ratio has **improved classification performance**. This can be proven by the performance of the best model (AUC 0.88), which has more training data with an 80:20 data split. Based on Figure 21, the **AUC values** confirm that the 70:30 model (AUC 0.788) has a slightly better overall performance than the 60:40 model (AUC 0.730).

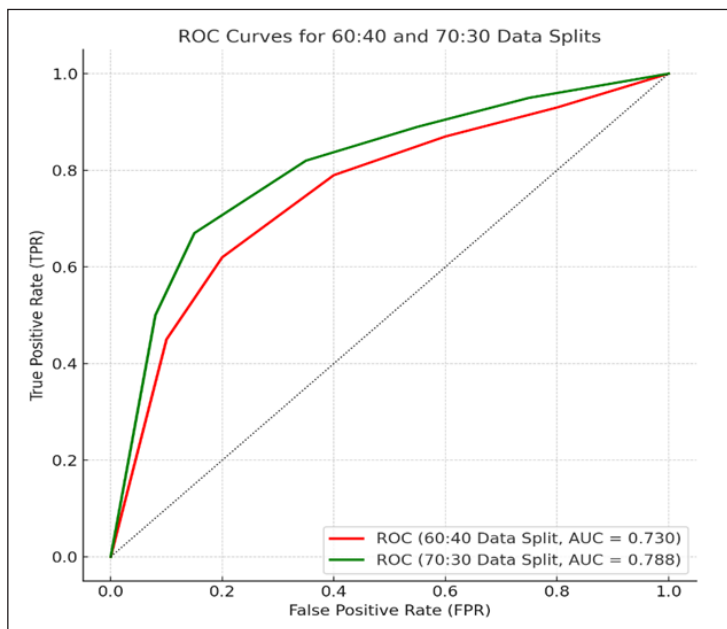


Figure 21. ROC Curve for the other two models

Word Cloud

A word cloud is an electronic image showing the collection of words in different sizes or series of texts. The words' size differs according to how often they are found in the text (Boost Labs, 2020). A word cloud is an excellent option for quickly gaining insight into the most used words and helps to interpret the text visually. The word cloud is generated for this project to give additional information about the dataset. Figure 22 shows the word cloud for the positively labeled tweets. The figure highlights the word 'climate action' since this word appeared in most of the text. In Figure 22, words such as 'solutions,' 'save' and

Based on Table 3, the research carried out by Anoop et al. (2024) and Ruz et al. (2020) has generated good performances with an accuracy of more than 80% for the SVM classifier. As for research done by Thenmozhi et al. (2024) and Anhsori and Shidik (2024), the SVM classifier has also generated more than 70% acceptable accuracies. This similar research has analyzed the public sentiments on climate change based on Twitter data. In the research by Ruz et al. (2020), the dataset has been divided into two datasets. In dataset 1, the SVM algorithm gives the best accuracy score compared to other algorithms that have been implemented. Meanwhile, in dataset 2, the SVM algorithm still scores a high accuracy of more than 80%. Also shown in the table, the proposed system achieved a score of 91%, which is higher accuracy than other comparable works carried out using different algorithms. In light of this, it can be shown that the suggested project is more effective and superior in categorizing tweets about climate change awareness.

Discussion

The evaluation parameters used to evaluate the performance of this project's SVM classifier model are the accuracy score, confusion matrix, classification report, and ROC curve. This section elaborates on the evaluation results and discusses the possible outcomes if the training and test sizes differ. The first evaluation parameter used in this project is accuracy. Accuracy is defined as the ratio of correct predictions to the total dataset size. In this study, the model achieved an accurate score of 91%. As Barkved (2022) stated, accuracy above 70% indicates an optimal model performance. High accuracy indicates how well the model correctly predicts all labels. However, as noted by Khalid (2021), higher accuracy does not necessarily mean exceptional model performance, as accuracy considers only the overall correct predictions without accounting for the performance of individual labels. Accordingly, a confusion matrix, classification report, and ROC curve were generated to assess the machine learning model's performance quantitatively. In accordance with the results obtained in this section, the SVM classifier model in this project is excellent and reliable in classifying the sentiment on awareness of climate change among the public.

Contribution of Study

It is important to make the public realize the consequences if no action is taken to prevent climate change. This study applies data mining on Twitter to find the sentiment on awareness of climate change for the targeted users for this project, which are authorities such as governments and non-governmental organizations (NGOs), to help them tackle the climate change issue. The realization of creating a society that is very aware is vital to ensure they practice the initiatives to sustain the environment. Therefore, this study highlights how the targeted users can use Twitter for beneficial use, especially in finding a small quantity of awareness to address climate change issues. Besides that, this study also contributes to

knowing the trending words that Twitter users use to crusade about climate change. With this study, society can also launch an awareness campaign and educate the people who tweet ignorant comments about climate change.

As for the machine learning algorithm implemented in this study, SVM showed good performance with a high accuracy of 91%. For several reasons, researchers in sentiment analysis are still implementing SVMs compared to deep learning models. First, SVM is computationally efficient, requiring less computational power and training time compared to deep learning models, which is particularly advantageous when resources are limited. Second, SVM performs well with smaller datasets, while deep learning typically requires large-scale data to avoid overfitting and achieve high accuracy (Mustapha et al., 2024). Third, SVM is easier to interpret and tune compared to the complex architectures of deep learning models, making them suitable for studies focusing on simplicity and transparency (Thenmozhi et al., 2024). Additionally, in some sentiment analysis tasks with well-structured features, SVM can achieve comparable performance to deep learning, providing a robust baseline for comparison (Maada et al., 2022). This makes SVM a valuable tool for research and applications where simplicity, speed, or data scarcity are concerns.

CONCLUSION

This study successfully analyzed public sentiments on the awareness of climate change based on the Support Vector Machine (SVM) algorithm. The SVM classifier could classify the Twitter data into positive (aware) and negative (not aware) polarities with a good accuracy of 91%. This shows that the SVM classifier is capable and reliable in solving this sentiment classification problem. The exploratory data analysis found that more people were aware of climate change situations from the tweets. The significance of the study is that the government could use the study's results and non-governmental organizations (NGOs) to help them increase public awareness and tackle the climate change issue. In Malaysia, the Ministry of Natural Resources, Environment and Climate Change is responsible for handling environmental problems. Environmental NGOs are vital in raising climate change awareness within communities and supporting governments in formulating and implementing adaptive measures. The public needs to be alerted to act before it is too late to save themselves from climate consequences. The increasing impacts of climate change have made humanity and nature suffer from extreme weather, worst storms, unusually heavy rain, more flooding, melting glaciers, and rising sea levels. Preventing climate change is beneficial to humans, wildlife, and nature. As for the SVM classifier, the recommendation for future work is to make an option for a language other than English or to create a multilingual classifier model. Currently, the classifier is able to process tweets in English only. Another suggestion is to use word ambiguity approaches such as SentiWordNet to define polarity based on the sentence context, due to the incorrectly classified tweets if the

users use sarcasm or double-meaning words. Future works also include comparing SVM with other well-known classification algorithms for sentiment analysis, namely the Naive Bayes, Random Forest, and deep learning algorithms such as CNN and RNN.

ACKNOWLEDGEMENT

Special thanks to Universiti Teknologi MARA Cawangan Terengganu for its unwavering support in advancing research at the university. The authors also thank everyone involved, directly or indirectly, for their insightful and constructive feedback.

REFERENCES

- Ahuja, R., Chug, A., Kohli, S., Gupta, S., & Ahuja, P. (2019). The impact of features extraction on the sentiment analysis. *Procedia Computer Science*, 152, 341-348. <https://doi.org/10.1016/j.procs.2019.05.008>
- Alkhatib, M., Barachi, M. El, Samuel Mathew, S., & Oroumchian, F. (2020). Using artificial intelligence to monitor the evolution of opinion leaders' sentiments: Case study on global warming. In *2020 5th International Conference on Smart and Sustainable Technologies (SpliTech)* (pp. 1-6). IEEE. <https://doi.org/10.23919/SpliTech49282.2020.9243726>
- Anhsori, K., & Shidik, G. F. (2024). Comparison performance of SVM, Naïve Bayes and XGBoost Classifier on climate change issue. In *2024 International Seminar on Application for Technology of Information and Communication (iSemantic)* (pp. 1-6). IEEE. <https://doi.org/10.1109/iSemantic63362.2024.10762214>
- Anoop, V. S., Krishnan, T. K. A., Daud, A., Banjar, A., & Bukhari, A. (2024). Climate change sentiment analysis using domain specific bidirectional encoder representations from transformers. *IEEE Access*, 12, 114912-114922. <https://doi.org/10.1109/access.2024.3441310>
- Arora, S. (2020, February 4). SVM: Difference between Linear and Non-Linear Models. *AITUDE*. <https://www.aitude.com/svm-difference-between-linear-and-non-linear-models/>
- Baguio, J. D. S., Lu, B. A., & Peña, C. F. (2023). Text classification of climate change tweets using artificial neural networks, fasttext word embeddings, and latent dirichlet allocation. In *2023 International Conference in Advances in Power, Signal, and Information Technology (APSIT)* (pp. 688-692). IEEE. <https://doi.org/10.1109/APSIT58554.2023.10201782>
- Barkved, K. (2022, March 9). How to know if your machine learning model has good performance. *Obviously AI*. <https://www.obviously.ai/post/machine-learning-model-performance>
- Bhandari, A. (2022, June 14). AUC-ROC curve in machine learning clearly explained. *Analytics Vidhya*. <https://www.analyticsvidhya.com/blog/2020/06/auc-roc-curve-machine-learning/>
- Boost Labs. (2020, November 3). What are word clouds? The value of simple visualizations. *Boost Labs*. [https://boostlabs.com/blog/what-are-word-clouds-value-simple-visualizations/#:%7E:text=Word%20clouds%20\(also%20known%20as,words%20depicted%20in%20different%20sizes](https://boostlabs.com/blog/what-are-word-clouds-value-simple-visualizations/#:%7E:text=Word%20clouds%20(also%20known%20as,words%20depicted%20in%20different%20sizes)
- Brownlee, J. (2020, August 15). What is a confusion matrix in machine learning? *Machine Learning Mastery*. <https://machinelearningmastery.com/confusion-matrix-machine-learning/>

- Chan, C. (2020, December 9). What is a ROC curve and how to interpret it. *Displayr*. <https://www.displayr.com/what-is-a-roc-curve-how-to-interpret-it/>
- Chorev, S. (2021, August 9). What is data cleaning: A practical guide. *Deepchecks*. <https://deepchecks.com/what-is-data-cleaning/>
- Joseph, V., Lora, C. P., & Narmadha, T. (2024). Exploring the application of natural language processing for social media sentiment analysis. In *2024 3rd International Conference for Innovation in Technology (INOCON)* (pp. 1-6). IEEE. <https://doi.org/10.1109/INOCON60754.2024.10511841>
- Khalid, I. A. (2021, December 14). Greater accuracy does not mean greater machine learning model performance. *Medium*. <https://towardsdatascience.com/greater-accuracy-does-not-mean-greater-machine-learning-model-performance-771222345e61>
- Kharwal, A. (2021, July 7). Classification report in machine learning. *Thecleverprogrammer.com*. Article 1774. <https://thecleverprogrammer.com/2021/07/07/classification-report-in-machine-learning/>
- Kumar, S. (2020, February 4). SVM: Difference between Linear and Non-Linear Models. *AITUDE*. <https://www.aitude.com/svm-difference-between-linear-and-non-linear-models/>
- Loureiro, M. L., & Alló, M. (2020). Sensing climate change and energy issues: Sentiment and emotion analysis with social media in the U.K. and Spain. *Energy Policy*, *143*, 111490. <https://doi.org/10.1016/j.enpol.2020.111490>
- Maada, L., Al Fararni, K., Aghoutane, B., Fattah, M., & Farhaoui, Y. (2022). A comparative study of sentiment analysis machine learning approaches. In *2022 2nd International Conference on Innovative Research in Applied Science, Engineering and Technology (IRASET)* (pp. 1-5). IEEE. <https://doi.org/10.1109/IRASET52964.2022.9738346>
- Markham, K. (2020, February 3). Simple guide to confusion matrix terminology. *Data School*. <https://www.dataschool.io/simple-guide-to-confusion-matrix-terminology/>
- Mohamed, D. M. E. D., & El-din, M. H. N. (2017). Performance analysis for sentiment techniques evaluation perspectives. In *Proceedings of the International Conference on Advanced Intelligent Systems and Informatics 2017* (pp. 448-457). Springer International Publishing. https://doi.org/10.1007/978-3-319-64861-3_42
- Mustapha, W. N. A. W., Sabri, N. M., Abu Bakar, N. A. A., Nik Daud, N. M., & Azizan, A. (2024). Detection of harassment toward women in Twitter during pandemic based on machine learning. *International Journal of Advanced Computer Science and Applications*, *15*(3), 1035-1043. <https://doi.org/10.14569/IJACSA.2024.01503103>
- Narkhede, S. (2021, June 15). Understanding AUC - ROC curve - Towards data science. *Medium*. <https://towardsdatascience.com/understanding-auc-roc-curve-68b2303cc9c5>
- National Geographic Society. (2019, March 27). *Climate Change*. <https://www.nationalgeographic.org/encyclopedia/climate-change/>
- Otero, P., Gago, J., & Quintas, P. (2021). Twitter data analysis to assess the interest of citizens on the impact of marine plastic pollution. *Marine Pollution Bulletin*, *170*. <https://doi.org/10.1016/j.marpolbul.2021.112620>

- Pai, A. (2022, June 21). What is Tokenization in NLP? Here's all you need to know. *Analytics Vidhya*. <https://www.analyticsvidhya.com/blog/2020/05/what-is-tokenization-nlp/>
- Ram, N. R., Gautum, S., Jadeja, A., Joisar, H., & Rathore, N. (2024). Social media sentiment analysis using Twitter dataset. In *2024 1st International Conference on Cognitive, Green and Ubiquitous Computing (IC-CGU)* (pp. 1-5). IEEE. <https://doi.org/10.1109/IC-CGU58078.2024.10530694>
- Ramanathan, V., Al Hajri, H., & Ruth, A. (2024). Conceptual level semantic sentiment analysis using Twitter data. In *2024 International Conference on Advances in Data Engineering and Intelligent Computing Systems (ADICS)* (pp. 1-8). IEEE. <https://doi.org/10.1109/ADICS58448.2024.10533498>
- Ray, S., & Kumar, A. M. S. (2023). Prediction and analysis of sentiments of reddit users towards the climate change crisis. In *2023 International Conference on Networking and Communications (ICNWC)* (pp. 1-7). IEEE. <https://doi.org/10.1109/ICNWC57852.2023.10127496>.
- Reddy, M. B. K., Vani, B., & Babu, C. N. K. (2022). A comparative analysis for the detection of hit rate of popular music videos in social network using logistic regression over support vector machine algorithm. In *2022 3rd International Conference on Intelligent Engineering and Management (ICIEM)* (pp. 544-549). IEEE. <https://doi.org/10.1109/ICIEM54221.2022.9853055>
- Ruz, G. A., Henríquez, P. A., & Mascareño, A. (2020). Sentiment analysis of Twitter data during critical events through Bayesian networks classifiers. *Future Generation Computer Systems*, *106*, 92-104. <https://doi.org/10.1016/j.future.2020.01.005>
- Shofiya, C., & Abidi, S. (2021). Sentiment analysis on COVID-19-related social distancing in Canada using twitter data. *International Journal of Environmental Research and Public Health*, *18*(11), 5993. <https://doi.org/10.3390/ijerph18115993>
- Singh, G., Singh, J., & Tripathy, B. (2024). Significance of sentiment analysis approaches using Machine Learning (ML) techniques. In *2024 2nd International Conference on Computer, Communication and Control (IC4)* (pp. 1-6). IEEE. <https://doi.org/10.1109/IC457434.2024.10486310>
- Singhal, G. (2020, October 5). Importance of text pre-processing. *Pluralsight*. <https://www.pluralsight.com/guides/importance-of-text-pre-processing>
- Singleton, S., Kumar, S. A. P., & Li, Z. (2019). Twitter analytics-based assessment: Are the United States coastal regions prepared for climate change. In *Proceedings of the International Symposium on Technology and Society (ISTAS)* (pp. 150-155). IEEE. <https://doi.org/10.1109/ISTAS.2018.8638266>
- Siong, T. G. (2019, December 13). What are w and b parameters in SVM? *Cross Validated*. <https://stats.stackexchange.com/users/128610/siong-thye-goh>
- Sudhir, P., & Suresh, V. D. (2021). Comparative study of various approaches, applications and classifiers for sentiment analysis. *Global Transitions Proceedings*, *2*(36), 205-211. <https://doi.org/10.1016/j.gltp.2021.08.004>
- Thenmozhi, M., Shubigsha, G., Sindhuja, G., & Dhinakar, V. (2024). Sentiment analysis on climate change using Twitter data. In *2024 2nd International Conference on Networking and Communications (ICNWC)* (pp. 1-6). IEEE. <https://doi.org/10.1109/icnwc60771.2024.10537404>

- Varshney, H., Shishodiya, P., & Sriramulu, S. (2022). Classifying tweets based on climate change. In *2022 3rd International Conference on Intelligent Engineering and Management (ICIEM)* (pp. 956-960). IEEE. <https://doi.org/10.1109/ICIEM54221.2022.9853094>.
- Wali, K. (2022, May 4). Explained: Stemming vs lemmatization in NLP. *Analytics India Magazine*. <https://analyticsindiamag.com/explained-stemming-vs-lemmatization-in-nlp>
- Wang, J., Obradovich, N., & Zheng, S. (2020). A 43-million-person investigation into weather and expressed sentiment in a changing climate. *One Earth*, 2(6), 568-577. <https://doi.org/10.1016/j.oneear.2020.05.016>
- Yogi, K. S., Gowda, V. D., Sindhu, D., Soni, H., Mukherjee, S., & Madhu, G. C. (2024). Enhancing accuracy in social media sentiment analysis through comparative studies using machine learning techniques. In *2024 International Conference on Knowledge Engineering and Communication Systems (ICKECS)* (Vol. 1, pp. 1-6). IEEE. <https://doi.org/10.1109/ICKECS61492.2024.10616441>

Enhancing Leachate Treatment with Electrocoagulation: A Computational Approach Using Response Surface Methodology

Mahmoud A. M. Al-Alwani¹, Alia Atasha Arisucman², Zadariana Jamil² and Azianabiha A Halip Khalid^{2,3*}

¹Department of Biology, College of Education for Pure Sciences/Ibn Al-Haitham, University of Baghdad, 10071 Jadria, Baghdad, Iraq

²School of Civil Engineering, College of Engineering, Universiti Teknologi MARA, 40450 Shah Alam, Selangor, Malaysia

³Bioremediation Research Centre (myBioREC), School of Civil Engineering, College of Engineering, Universiti Teknologi MARA, 40450 Shah Alam, Selangor, Malaysia

ABSTRACT

Malaysia's growing population and industrialisation have increased solid waste accumulation in landfills, leading to a rise in leachate production. Leachate, a highly contaminated liquid from landfills, poses environmental risks and affects water quality. Conventional leachate treatments are costly and time-consuming due to the need for additional chemicals. Therefore, the Electrocoagulation process could be used as an alternative method. Electrocoagulation is an electrochemical method of treating water by eliminating impurities by applying an electric current. In the present study, the optimisation of contaminant removal was investigated using Response Surface Methodology. Three parameters were considered for optimisation: the current, concentration of leachate, and the electrodes' distance. The outcome of this study includes ANOVA analysis, mathematical modelling and 3D surface plot modelling. The optimum condition for contaminants removal was obtained at a current of 4 Amp, a concentration of leachate of 90.95%, and an electrode distance of 3 cm. The outcomes obtained under these conditions were about 47.85% and 76.32% removal of COD

and turbidity, respectively. Both percentage COD and turbidity removal models achieved significant results, demonstrating that at least one of the independent variables has a significant impact on the dependent variable.

ARTICLE INFO

Article history:

Received: 22 August 2024

Accepted: 24 February 2025

Published: 24 April 2025

DOI: <https://doi.org/10.47836/pjst.33.S3.08>

E-mail addresses:

mamash73@gmail.com (Mahmoud A. M. Al-Alwani)

aliaatasha.aris@gmail.com (Alia Atasha Arisucman)

zadariana@uitm.edu.my (Zadariana Jamil)

azianabiha@uitm.edu.my (Azianabiha A Halip Khalid)

*Corresponding author

Keywords: Current intensity, electrocoagulation process, electrode distance, leachate treatment, process optimisation, Response Surface Methodology (RSM)

INTRODUCTION

Leachate, a concerning outcome of landfill activity, poses environmental risks, impacting ecosystems and water quality. It is produced when water seeps through other materials or solid waste and collects pollutants that are either suspended or dissolved in the process (Detho et al., 2024). This process occurs when rainwater or other liquids come into contact with waste products within the landfill. This liquid can dissolve and remove a variety of contaminants and materials, such as organic matter, heavy metals, chemicals, and pathogens, as it moves through the waste (Hussein et al., 2021). Leachate will not be directly discharged to a municipal wastewater treatment plant since it is a complicated and extremely contaminated liquid (Rangga et al., 2024). Municipal wastewater treatment plants may not be suited to handle the pollutants in leachate because they are primarily intended to treat domestic and industrial sewage. Thus, leachate is often treated in on-site treatment systems or specialised leachate treatment facilities.

Current leachate treatment methods still have some drawbacks in terms of time and cost. Standard physico-chemical procedures are inadequate for treating leachate due to high operational costs and recalcitrant matter in the leachate (Bandala et al., 2021). Among the emerging methods, electrocoagulation (EC) has shown great potential as a sustainable alternative for effective leachate treatment. The electrocoagulation (EC) process is an electrochemical method for treating water using a direct electric current without adding chemicals, where tiny particles of the contaminants are removed from the water. EC treatment for wastewater operates through electrochemical reactions when an electric current is applied between electrodes. At the anode, metal ions such as Al^{3+} are released and form metal hydroxides that act as coagulants, destabilising and aggregating suspended particles into larger flocs (Salim et al., 2024). Water electrolysis produces hydrogen gas and hydroxyl ions at the cathode, further aiding coagulation by raising the pH value (Sharma et al., 2021). The process has demonstrated the ability to effectively remove contaminants such as fluoride, arsenic, heavy metals, dyes, and oils from residual, surface, and underground water (López-Guzmán et al., 2021). Despite the established potential of EC to remove pollutants from leachate, challenges remain in optimising the process for high efficiency. For more than two decades, researchers have investigated the use of EC for leachate treatment (Ding et al., 2021; Galvão et al., 2020; Rookesh et al., 2022); however, significant gaps persist in understanding optimal operating conditions, particularly in the context of diverse and complex leachate compositions (Guo et al., 2022).

Response Surface Methodology (RSM) offers a powerful statistical and mathematical tool for optimising research studies. It enables the analysis and description of interactions between factors (independent variables) and responses (dependent variables) (Tay et al., 2023). In the context of EC, RSM facilitates the identification of ideal conditions for contaminant removal while accounting for variable interactions. Previous studies, such

as those by Sediqi et al. (2021) have utilised RSM to optimise EC processes, focusing on minimising energy and resource consumption while treating landfill leachate. Recent works, including Faheem et al. (2022) and Apaydin and Özkan (2020) examined factors such as initial COD, initial pH, applied current, and electrolysis time using central composite design (CCD), while others such as Ameli et al. (2024) and Gautam et al. (2022) optimised current density, electrolysis time, and inter-electrode distance. However, the influence of leachate concentration on the electrocoagulation treatment process has received limited attention in the existing literature.

This study addresses existing gaps by investigating the optimisation of COD and turbidity removal, focusing on the specific interactions between initial leachate concentration, applied current and electrode distance. The research also develops a mathematical model to illustrate these interactions and identify optimal conditions that maximise efficiency. By doing so, this work advances the application of EC in leachate treatment, addressing limitations in previous studies and offering a framework for future innovations in the field.

MATERIALS AND METHODS

Sample Collection

Leachate was collected at Jeram Sanitary Landfill (3°11'20"N, 101°21'50"E), located in Selangor, Malaysia. Table 1 shows the characteristics of raw leachate generated at Jeram Sanitary Landfill obtained from a previous study (Kamaludin et al., 2021).

The landfill began operation in 2007, receiving 3400 tonnes of waste daily. The design lifespan for this landfill is 20 years. Jeram Sanitary Landfill receives many kinds of waste, including domestic, food, market, wood pallets, and green waste. At Jeram Sanitary Landfill, raw leachate will go to the anaerobic lagoon before proceeding to the next process. There are three biological process stages in the three different SBR lagoons. The leachate will be aerated for 22 hours, and the aerator will be off for 2 hours. The leachate will be transferred to the next SBR stage during the off period. Later, it will be transferred to the settling tank before proceeding with the physical process.

Electrocoagulation Process

The electrocoagulation process uses direct current to break down the contaminants existing in the leachate as either dissolved or suspended particles (Das et al., 2022). In the present study, aluminium (Al) electrodes were used for both anode and cathode. Electrodes

Table 1
Characteristics of raw leachate from Jeram Sanitary Landfill

Parameter	Sunny Day	Rainy Day
pH	7.35	7.35
COD (mg/L)	1168.96	598.54
DO (mg/L)	8.41	8.32

were submerged in 1 L of leachate diluted with distilled water according to the desired concentration. The electrodes' dimensions were 6.0 cm x 15.0 cm x 0.1 cm, with a total surface area of 360 cm². The dimension of the 1 L glass beaker was 21.0 cm in height with an 8.5 cm inner diameter and 9.0 cm outer diameter. The electrodes produced Al ions, Al³⁺, during the EC process, which ions were essential for forming aluminium hydroxide, Al(OH)₃, to remove the leachate's impurities. Additionally, a previous study has shown that Al electrodes removed 70% more COD than Fe electrodes (Tahreen et al., 2020). When direct current (DC) is applied at the electrodes, electrochemical reactions assist the coagulant production in situ without any chemical additions. The reactions of both electrode surfaces follow Equations 1 and 2 (Das et al., 2022).

Electrochemical reactions at anode:

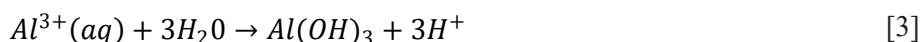


Electrochemical reactions at the cathode:



The chemical reactions at the electrodes acted as coagulation, as shown in Equation 3, and initiated the flocculation process. The flocs settled for 20 minutes. The treated sample was then separated from the flocs using a cloth strainer before laboratory testing.

Formulation of coagulant:



Rubber bands with different diameters were used to measure the distance between a pair of electrodes. The rubber bands were tied to ensure they did not move when submerged in the leachate. The crocodile clips were clipped on the spring clips to avoid direct contact with the liquid, and the crocodile clips were connected to the DC power supply.

Parameter for Leachate Treatment

In this study, two parameters were selected, namely, COD and turbidity. These two parameters are important criteria in the discharge standard. They are regulated by the Environmental Quality Act 1974 and its subsequent amendments and regulations, particularly focusing on the Environmental Quality (Control of Pollution from Solid Waste Transfer Station and Landfill) Regulations 2009, as shown in Table 2.

COD and turbidity were chosen as dependent variables because they are key indicators of leachate contamination and are affected by EC. COD measures dissolved organic matter, while turbidity tracks suspended particles. Therefore, both of these parameters are good indicators for assessing the effectiveness of EC in treating leachate, as they represent both dissolved and suspended contaminants.

Table 2
Parameters and limits for leachate discharge in Malaysia

Parameter	Limit
Chemical Oxygen Demand (COD)	≤ 20 mg/L
Turbidity	5 NTU
pH	6.0–9.0

Pollutant Removal Analysis

The sludge generated after the EC process was removed from the treated sample using a cloth strainer before conducting the Chemical oxygen demand (COD) and Turbidity testing. The COD was measured by the HACH method-reactor Digestion Method (Method 8000) digestion in the 0–1500 mg/L range, and the turbidity was determined using a Hach 2100Q portable turbidity meter.

Based on the obtained result, the removal percentage of the pollutant was calculated using the expression in Equation 4 as follows:

$$Removal (\%) = \frac{C_i - C_f}{C_i} \quad [4]$$

Where C_i and C_f are the COD and turbidity concentration at the treatment's beginning and end, respectively.

Response Surface Methodology (RSM)

Response surface methodology is one of the methods used in the Design of Experiments (DOE) software that helps optimise the electrocoagulation process. Three parameters or factors were used as input in this study, which included the concentration of leachate, applied current, and the electrodes' distance. Initial leachate concentration is critical as it represents the amount of organic matter that needs to be oxidised. It directly influences adjustments to other operational factors, such as current intensity, to achieve effective removal. Electrode distance, on the other hand, affects the strength of the electric field. A shorter distance creates a stronger electric field, improving the rate of electrolysis. However, if the distance is too short, it can result in excessive current density, leading to increased power consumption, overheating, or electrode degradation (Hanif et al., 2022). Additionally, applied current impacts energy consumption, which is critical in optimising the process for efficiency and cost-effectiveness (Faheem et al., 2022). Table 3 shows the range values of DC, concentration of leachate, and electrode distance that were input in the software.

The applied current ranged from 1.5A to 4.0A, considering the high contamination level of the leachate and referring to the optimum conditions suggested by Galvão et al. (2020).

Table 3
Range values for parameters

Parameter	Current, Amp	Concentration of Leachate, %	Electrodes' Distance, cm
Range Value	1.5–4.0	50–100	0.8–3.0

The electrodes' distance between the anode and the cathode was set between 0.8 cm and 3.0 cm (Ameli et al., 2024). A shorter distance between the anode and the cathode can result in a higher electric field intensity. 0.8 cm is considered practical for rapid treatment and efficient contaminants removal, while 3.0 cm is the maximum value to reduce electrode wear (Guo et al., 2022). Therefore, based on these ranges, 13 different values with varying combinations of each factor and level were carried out, as shown in Table 4.

Table 4
Parameters generated by RSM

Std	Run	Factor 1	Factor 2	Factor 3
		A: Current (Amp)	B: Concentration (%)	C: Electrodes' Distance (cm)
1	5	4	100	0.80
2	10	4	50	3
3	9	1.50	100	3
4	3	1.50	50	0.80
5	4	0.98	75	1.90
6	11	4.52	75	1.90
7	13	2.75	39.65	1.90
8	12	2.75	110.36	1.90
9	6	2.75	75	0.34
10	2	2.75	75	3.46
11	8	2.75	75	1.90
12	1	2.75	75	1.90
13	7	2.75	75	1.90

The model's goodness of fit was assessed using the coefficient of determination (R^2), where a value close to 1 indicates strong agreement between experimental and predicted outcomes. The significant factors and interactions influencing COD and turbidity removal percentages were identified through analysis of variance (ANOVA). Statistical significance was determined by examining p -values. Factors with p -values less than 0.05 (indicating a probability higher than 95%) were considered significant for the removal

process. Subsequently, three-dimensional plots along with contour plots were generated to visualise the effects of these significant factors on both parameters. The optimal ranges for each factor to achieve effective COD and turbidity removal were determined using desirability functions. The quadratic mathematical model was employed to predict the optimal conditions for the treatment process.

Three trial experiments were conducted based on the optimised conditions suggested by the Response Surface Methodology (RSM) to verify their accuracy. Data in triplicates were expressed as mean \pm standard deviation. The experimental results were verified by comparing them to the predicted outcomes from the RSM model. A less than 10% deviation between the predicted and experimental results was considered acceptable, confirming the model's validity.

RESULTS AND DISCUSSIONS

ANOVA Analysis

The analysis of variance (ANOVA) statistics for the percentage of COD and turbidity removal are shown in Tables 5 and 6, respectively. The associated p -value for each model was below 0.05, suggesting that the corresponding model terms are significant. The terms

Table 5
ANOVA for a fitted quadratic polynomial model for COD removal

Parameter	Sum of Squares	df	Mean Square	F-value	p-value	
Model	2535.46	9	281.72	148.53	0.0008	significant
A	870.70	1	870.70	459.07	0.0002	
B	56.82	1	56.82	29.96	0.0120	
C	1.73	1	1.73	0.9120	0.4100	
AB	62.61	1	62.61	33.01	0.0105	
AC	231.5	1	231.50	122.05	0.0016	
BC	78.03	1	78.03	41.14	0.0077	
A ²	11.61	1	11.61	6.12	0.0897	
B ²	19.33	1	19.33	10.19	0.0496	
C ²	320.86	1	320.86	169.17	0.0010	
Residual	5.69	3	1.90			
Lack of Fit	0.7836	1	0.7836	0.3194	0.6289	not significant
Pure Error	4.91	2	2.45			
Cor Total	2541.15	12				

A, B, AB, AC, BC, B², and C² are significantly illustrated by $p < 0.05$ for COD removal. Meanwhile, terms A, B, AB, BC, and C² are significant for turbidity removal. The insignificant term represented by p -values above 0.05 was removed from further analysis. Reducing the number of insignificant terms can improve the model's performance.

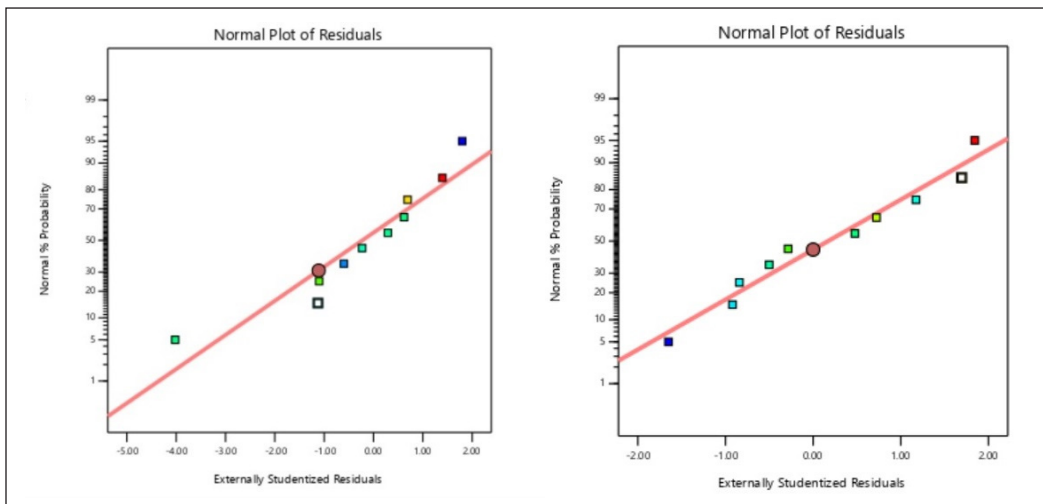
Table 6
ANOVA for a fitted quadratic polynomial model for turbidity removal

Parameter	Sum of Squares	df	Mean Square	F-value	p-value	
Model	862.74	7	123.25	10.80	0.0093	significant
A	129.93	1	129.93	11.38	0.0198	
B	181.26	1	181.26	15.88	0.0105	
C	4.03	1	4.03	0.3533	0.5781	
AB	121.03	1	121.03	10.60	0.0225	
AC	20.57	1	20.57	1.80	0.2372	
BC	240.21	1	240.21	21.05	0.0059	
C ²	203.55	1	203.55	17.83	0.0083	
Residual	57.07	5	11.41			
Lack of Fit	51.19	3	17.06	5.80	0.1505	not significant
Pure Error	5.88	2	2.94			
Cor Total	919.81	12				

The R² were 0.99 and 0.93 for the COD and turbidity models, highlighting the high correlation between experimental and predicted values. Additional evaluation to validate the suitability of the proposed models was conducted using additional diagnostic tools within RSM, including a normal plot of residuals illustrated in Figure 1. The linear relationship between students' residuals and the normal probability plot indicated a strong correlation between predicted and observed data.

The statistical model was then used to generate the quadratic model regression. In terms of their coded factors, the final regression model is expressed by the following second-order polynomial in Equations 5 and 6, respectively. It represents the relationship between input variables and a response variable using quadratic terms.

$$\begin{aligned}
 & \text{COD Removal, \%} \\
 & = +21.37 + 14.75A - 3.77B - 0.6576C - 5.60AB \\
 & \quad + 10.76AC + 6.25BC + 1.31A^2 - 1.69B^2 + 6.87C^2 \qquad [5]
 \end{aligned}$$



(a)

(b)

Figure 1. Normal plot of residuals for (a) COD removal and (b) Turbidity removal

Turbidity Removal, %

$$= +60.29 + 5.70A + 6.73B - 1.00C - 7.78AB + 3.21AC + 10.96BC + 5.36C^2 \quad [6]$$

The mathematical model generated in RSM offers significant benefits for optimising the removal of COD and turbidity from leachate. It helps identify the best combination of process variables to maximise the efficiency of COD and turbidity removal. Additionally, it allows for accurate prediction of the removal efficiency under various conditions, reducing the need for extensive experimentation. Furthermore, the model provides a quantitative basis for decision-making, enabling the selection of the most effective parameters to enhance the removal process from leachate.

3D-plot Surface Modelling

COD Removal

The interaction effect of leachate concentration and current on COD removal is shown in Figure 2. It became evident from the figure that the current had a more pronounced effect on COD removal compared to the concentration of leachate. The percentage of COD removal increased proportionately with higher Amp, with the maximum removal of 45% achieved at 4.5 Amp. Conversely, there were no notable changes in COD removal percentage throughout the different ranges of leachate concentration. According to Shahedi et al. (2020), a high current level stimulates increased COD removal by accelerating the formation rate of coagulants, thereby enhancing contaminant removal efficiency.

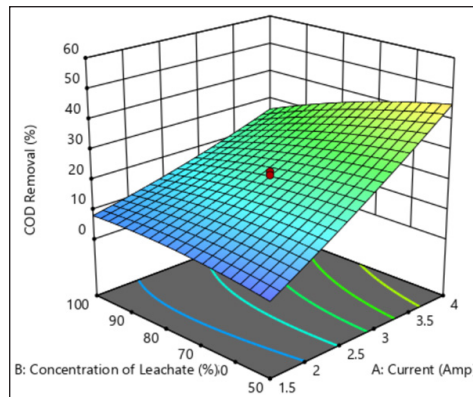


Figure 2. 3D response surface plot of the interaction effect of current and concentration of leachate on COD removal

COD removal during the EC process primarily occurs through coagulation and subsequent flocculation mechanisms facilitated by the *in situ* formation of coagulants. When a direct current is applied, the anodic dissolution of aluminium electrodes generates Al^{3+} ions, which hydrolyse to form aluminium hydroxide, $Al(OH)_3$. These hydroxides serve as effective coagulants, adsorbing organic contaminants responsible for the COD load (Gasmi et al., 2022). Therefore, increased current strengthens the electric field, accelerating the dissolution of aluminium and the formation of hydroxides as illustrated in Figure 2.

The surface plot in Figure 3 illustrates the response of COD removal efficiency based on the interaction between the current and the distance between the electrodes. As the current increases from 0.8 to 3.5 Amp, the COD removal efficiency tends to rise, suggesting that higher currents enhance the COD removal process by providing more electrical energy. Conversely, as the distance between the electrodes decreases from 2.45 cm to 1.35 cm, the COD removal efficiency also increases significantly, indicating that a smaller electrode distance favours more effective interaction and, thus, higher COD removal efficiency.

The plot demonstrates a non-linear interaction between current and electrode distance, with the highest COD removal efficiencies achieved at higher currents and shorter electrode distances. The red dot on the plot represents the optimal point, indicating the specific combination of current and electrode distance that maximises efficiency. Based on the surface plot, it can be concluded that while both factors significantly influence COD removal efficiency, electrode distance appears to be the more significant factor. This differs from the findings from Nasrullah et al. (2022), who reported that electrode distance had less effect on treatment at high current intensities, likely due to the higher current range (15–20 A) used in their study. Nevertheless, compared to the change along the current axis, the steep increase in COD removal efficiency with decreasing electrode distance suggests that optimising electrode spacing is crucial for achieving higher COD removal rates in the present study.

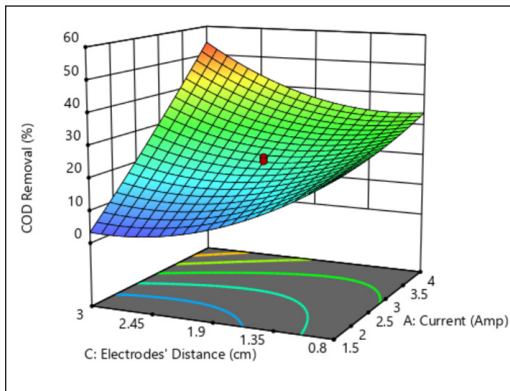


Figure 3. 3D response surface plot of the interaction effect of current and electrodes' distance on COD removal

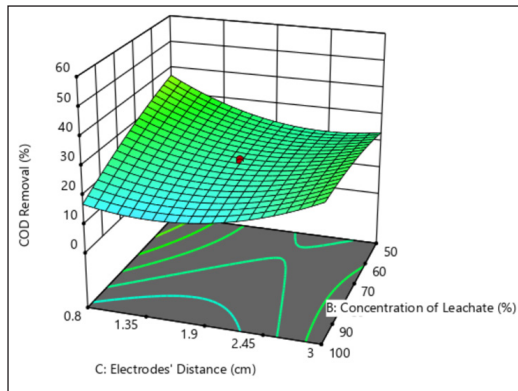


Figure 4. 3D response surface plot of the interaction effect of leachate's concentration and electrodes' distance on COD removal

Figure 4 shows the response of COD removal efficiency based on the interaction between leachate concentration and the distance between the electrodes. From the findings, when the distance between the electrodes decreases from 3 cm to 0.8 cm, the COD removal efficiency gradually increases, suggesting that a smaller electrode distance enhances COD removal efficiency. At a fixed current at 2.75 Amp and 75% leachate, the 0.34 cm electrode distance produced 35% COD removal compared to the 1.9 cm distance that achieved only 19.87%. This trend is consistent with a previous study by Rookesh et al. (2022) that reported 44.1% and 40.6% COD removal with 0.66 cm and 1.5 cm electrode distance, respectively.

According to Ameli et al. (2024), a narrower inter-electrode distance will form more gas bubbles, which increases the possibility of collisions between coagulants and pollutants. Furthermore, shorter electrode distances intensify the electric field, promoting more uniform coagulant dispersion and faster aggregation of suspended particles, as depicted in Figure 4. Nonetheless, overly close electrode spacing can lead to electrode passivation or gas bubble shielding, reducing process efficiency. Thus, as per the present study, RSM is crucial for optimising electrode spacing to achieve efficient COD removal.

The COD removal percentage varies with the concentration, from 50% to 100%, with higher leachate concentrations generally showing a slight decrease in efficiency. Under 3 Amp current, 100% concentration achieved 10.03% COD removal and increased considerably to 56.1% using 50% leachate. The concentration of leachate directly determines the pollutant load in the solution. Higher concentrations typically mean a greater variety and number of contaminants, which can saturate or overwhelm the treatment system, reducing efficiency. From the results, it can be concluded that leachate concentration is the more significant factor in this interaction. Compared to the more gradual response to changes in electrode distance, the more pronounced change in COD removal efficiency with varying leachate concentrations suggests that optimising leachate concentration is

crucial for achieving higher COD removal rates. While electrode distance influences the operational efficiency of the EC process, leachate concentration fundamentally dictates system performance in terms of COD removal. The chemical interactions between coagulants and organic contaminants primarily drive COD reduction, highlighting leachate concentration as the more critical parameter.

Turbidity Removal

Figure 5 illustrates the interaction between current and leachate concentration on turbidity removal percentage. The plot indicates that turbidity removal efficiency increases with higher current levels up to a certain optimal point, after which the effect may remain unchanged or decrease.

When the leachate concentration is maintained at 75%, the lowest current at 0.98 Amp produced 51.33% turbidity removal, increasing to 73.77% at 1.5 Amp. However, it was reduced to 67.45% removal efficiency when the current increased further to 4.52 Amp. Conversely, higher leachate concentrations tend to decrease turbidity removal efficiency, indicating an inverse relationship. The turbidity removal decreased from 62.31% to 55.81% when the concentration increased from 50% to 100% with a 4 Amp current supply. Lower leachate concentrations can improve mass transfer conditions, as the driving force for pollutant migration toward the electrodes is less hindered. This leads to improved contact between the pollutants and the active electrode surface. Notably, the current is the more significant factor affecting turbidity removal, as its increase leads to a substantial improvement in removal efficiency compared to the more detrimental effect of increased leachate concentration.

Figure 6 illustrates how the distance between electrodes and the leachate concentration interact to remove the turbidity.

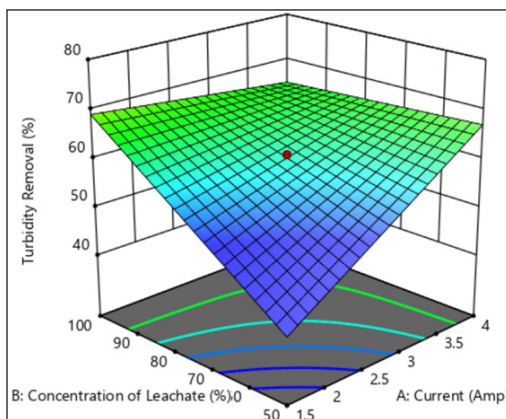


Figure 5. 3D response surface plot of the interaction effect of current and concentration of leachate on turbidity removal

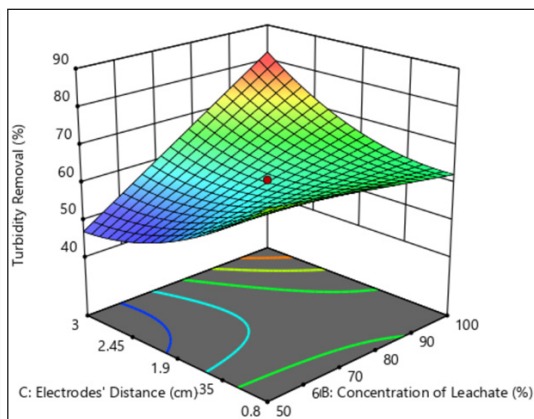


Figure 6. 3D response surface plot of the interaction effect of concentration of leachate and electrodes' distance on turbidity removal

The interaction shows that the turbidity removal was determined to be more influenced by the electrodes' distance than the concentration of leachate. 73.94% turbidity but reduced to 62.31% at 3 cm. The result is supported by a study by Gautam et al. (2022) that reported 37.9% COD removal at a 3.0 cm electrode distance, while 43.3% was achieved at a 1.5 cm electrode distance. Turbidity is primarily caused by suspended solids rather than dissolved contaminants. Therefore, the concentration of leachate, which primarily reflects dissolved pollutants, has a lesser impact on turbidity removal. While dilution lowers the overall load of dissolved pollutants, it has minimal effect on the suspended solids, causing turbidity. This makes electrode distance a more critical factor for turbidity removal efficiency.

Optimum Conditions for COD and Turbidity Removal from Leachate Using EC Process

The optimisation process was conducted to determine the optimum COD and turbidity removal using Design of Expert 13 software. During the optimisation step, the operational conditions (current, leachate concentration, and electrode distance) were set "within the range." In contrast, the responses (COD and turbidity removal percentages) were set to "maximum" to achieve the highest performance. The optimum working conditions and their respective removal efficiencies were identified and are presented in Table 7.

Table 7
Optimum condition for COD and turbidity removal

Result	Current, Amp	Leachate, %	Electrodes' Distance, cm	Removal %	
				COD	Turbidity
Model prediction	4	90.95	3	51.73 ± 4.39	79.88 ± 6.91
Verification				47.85 ± 3.2	76.32 ± 5.11

Under the optimal conditions of the EC process (current: 4 Amp; leachate concentration: 90.95%; and electrode distance: 3 cm), COD removal efficiency reached 51.73%, while turbidity removal achieved 79.88%. These outcomes were identified as the best performance using a desirability function value of 1.0, indicating a perfect compromise between the multiple response variables. The high desirability score highlights the robustness of the optimisation methodology in predicting conditions that maximise treatment efficiency.

A validation experiment was conducted under the same conditions to verify these results. The validation experiment recorded 47.48% COD removal and 76.32% turbidity removal. The percentage differences between the predicted and experimental results were calculated to be 8.11% and 4.66% for COD and turbidity, respectively. These discrepancies are relatively minor and fall within an acceptable range of below 10%, affirming the reliability and accuracy of the model used for process optimisation. The narrow gap between

the predicted and experimental results underscores the reliability of the statistical model and optimisation approach. The observed variations might arise from operational factors such as electrode wear, slight current density fluctuations, or the leachate matrix's inherent heterogeneity. These findings emphasise the importance of thorough experimental design and statistical validation in ensuring the reproducibility and scalability of EC processes.

The COD removal efficiency under optimal conditions reflects the EC process's ability to oxidise and coagulate organic matter in the leachate. However, the moderate efficiency (51.73%) suggests that a portion of the organic load comprises recalcitrant compounds resistant to degradation (Lebron et al., 2021). These chemical substances, such as compounds, include certain pesticides, synthetic polymers, or complex organic molecules like polycyclic aromatic hydrocarbons (PAHs) that are resistant to degradation or breakdown by natural biological, chemical, or physical processes (Bandala et al., 2021). This aligns with the known limitations of EC, particularly for treating complex organic matrices such as leachate, where a combination of advanced oxidation processes or biological treatment might be necessary for complete COD removal (Sharma et al., 2021). On the other hand, the turbidity removal efficiency of 79.88% indicates the effective destabilisation and aggregation of colloidal particles in the leachate through coagulation mechanisms (Hanif et al., 2022). The higher turbidity removal compared to COD removal suggests that the EC process preferentially targets high-molecular-weight particulate and colloidal impurities over dissolved organic matter (Ogedey & Ogunz, 2024).

Overall, the results demonstrate the potential of EC as a viable treatment technology for leachate, particularly in reducing turbidity and partially mitigating COD. However, further process enhancement, such as optimising electrode material, introducing hybrid treatment systems, or employing sequential treatments, could be investigated to achieve higher removal efficiencies and broader pollutant coverage. In addition, future scope could include investigating the treatment of specific pollutants found in leachate, such as heavy metals, focusing on lead, mercury, cadmium, and chromium. Removal of organic pollutants such as volatile organic compounds and pesticides, biochemical oxygen demand (BOD), and specific hydrocarbons such as petroleum hydrocarbons could be explored using EC. Based on the result of the present study, understanding how EC addresses these diverse contaminants will help refine the process for different leachate compositions.

Additionally, scaling up EC to industrial applications will require overcoming challenges such as ensuring consistent treatment efficiency, minimising energy consumption, managing electrode degradation, and maintaining long-term system stability (Hanif et al., 2022) managing electrode degradation, and maintaining long-term system stability (Das et al., 2022). Exploring alternative electrode materials, such as titanium, platinum (Sadaf et al., 2024), or carbon-based electrodes (Guo et al., 2022) may offer improved performance and durability compared to traditional materials like iron or aluminium. Finally, conducting

detailed economic and environmental impact assessments will provide insights into the long-term feasibility and sustainability of EC as a treatment solution for leachate at larger scales (Gasmi et al., 2022).

CONCLUSION

This study offers a novel contribution to leachate treatment by focusing on optimising leachate concentration in the EC process. Previous studies have primarily concentrated on factors such as applied current and electrode distance, often overlooking the significant influence of leachate concentration on treatment efficiency. The optimum conditions for the input factors were identified: current at 4 Amperes, leachate concentration at 90.95%, and electrode distance at 3 cm. Under these conditions, the actual results achieved were 47.85% COD removal and 76.32% turbidity removal. The R^2 values were 0.99 for COD and 0.93 for turbidity, indicating a high correlation between the experimental and predicted values. The results demonstrate that higher leachate concentrations generally reduced COD removal efficiency, as expected, due to the increased complexity and contamination load. This insight is particularly valuable for scaling up the EC process in real-world applications, where leachate concentration can vary significantly.

ACKNOWLEDGEMENTS

This work was supported by the School of Civil Engineering, College of Engineering, Universiti Teknologi MARA, Shah Alam, Malaysia.

REFERENCES

- Ameli, F., Hashemi, H., Samaei, M. R., Asgari, E., & Mohammadian Fazli, M. (2024). Enhanced reducing leachate pollution index through electrocoagulation using response surface methodology. *Heliyon*, *10*(18), e38134. <https://doi.org/10.1016/j.heliyon.2024.e38134>
- Apaydin, Ö., & Özkan, E. (2020). Landfill leachate treatment with electrocoagulation: Optimization by using Taguchi method. *Desalination and Water Treatment*, *173*, 65-76. <https://doi.org/10.5004/DWT.2020.24719>
- Bandala, E. R., Liu, A., Wijesiri, B., Zeidman, A. B., & Goonetilleke, A. (2021). Emerging materials and technologies for landfill leachate treatment: A critical review. *Environmental Pollution*, *291*, 118133. <https://doi.org/10.1016/J.ENVPOL.2021.118133>
- Das, P. P., Sharma, M., & Purkait, M. K. (2022). Recent progress on electrocoagulation process for wastewater treatment: A review. *Separation and Purification Technology*, *292*, 121058. <https://doi.org/10.1016/J.SEPPUR.2022.121058>
- Detho, A., Kadir, A. A., & Azhar, M. A. (2024). Comparative analysis of contaminant levels in leachate and soil from young and old landfills. *Pertanika Journal of Science and Technology*, *32*(5), 2299-2312. <https://doi.org/10.47836/pjst.32.5.20>

- Ding, J., Jiang, M., Zhao, G., Wei, L., Wang, S., & Zhao, Q. (2021). Treatment of leachate concentrate by electrocoagulation coupled with electro-Fenton-like process: Efficacy and mechanism. *Separation and Purification Technology*, 255, 117688. <https://doi.org/10.1016/j.seppur.2020.117668>
- Faheem, K., Khan, S. U., Washeem, M., & Khan, S. U. (2022). Energy efficient removal of COD from landfill leachate wastewater using electrocoagulation: Parametric optimization using RSM. *International Journal of Environmental Science and Technology*, 19(5), 3625-3636. <https://doi.org/10.1007/s13762-021-03277-3>
- Galvão, N., de Souza, J. B., & de Sousa Vidal, C. M. (2020). Landfill leachate treatment by electrocoagulation: Effects of current density and electrolysis time. *Journal of Environmental Chemical Engineering*, 8(5), 104368. <https://doi.org/10.1016/j.jece.2020.104368>
- Gasmi, A., Elboughdiri, N., Ghernaout, D., Hannachi, A., Halim, K. S. A., & Khan, M. I. (2022). Electrocoagulation process for removing dyes and chemical oxygen demand from wastewater: Operational conditions and economic assessment – A review. *Desalination and Water Treatment*, 271, 74-107. <https://doi.org/10.5004/DWT.2022.28792>
- Gautam, P., Kumar, S., Vishwakarma, S., & Gautam, A. (2022). Synergistic optimization of electrocoagulation process parameters using response surface methodology for treatment of hazardous waste landfill leachate. *Chemosphere*, 290, 133255. <https://doi.org/10.1016/j.chemosphere.2021.133255>
- Guo, Z., Zhang, Y., Jia, H., Guo, J., Meng, X., & Wang, J. (2022). Electrochemical methods for landfill leachate treatment: A review on electrocoagulation and electrooxidation. *Science of The Total Environment*, 806, 150529. <https://doi.org/10.1016/J.SCITOTENV.2021.150529>
- Hanif, M. H. M., Kamaruddin, M. A., Norashiddin, F. A., Niza, N. M., Shadi, A. M. H., Sabri, M. N. I. M., & Zawawi, M. H. (2022). Landfill leachate treatment technology via electrocoagulation: A review of operating parameters, intensification, and modelling. *Desalination and Water Treatment*, 260, 77-101. <https://doi.org/10.5004/dwt.2022.28456>
- Hussein, M., Yoneda, K., Mohd-Zaki, Z., Amir, A., & Othman, N. (2021). Heavy metals in leachate, impacted soils and natural soils of different landfills in Malaysia: An alarming threat. *Chemosphere*, 267, 128874. <https://doi.org/10.1016/J.CHEMOSPHERE.2020.128874>
- Kamaludin, M., Bohari, H., & Ponachi, N. S. (2021). Characteristics of raw leachate of Jeram sanitary landfill. *Politeknik & Kolej Komuniti Journal of Life Long Learning*, 5, 71-78.
- Lebron, Y. A. R., Moreira, V. R., Brasil, Y. L., Silva, A. F. R., Santos, L. V. de S., Lange, L. C., & Amaral, M. C. S. (2021). A survey on experiences in leachate treatment: Common practices, differences worldwide and future perspectives. *Journal of Environmental Management*, 288, 112475. <https://doi.org/10.1016/J.JENVMAN.2021.112475>
- López-Guzmán, M., Flores-Hidalgo, M. A., & Reynoso-Cuevas, L. (2021). Electrocoagulation process: An approach to continuous processes, reactors design, pharmaceuticals removal, and hybrid systems—A review. *Processes*, 9(10), 1831. <https://doi.org/10.3390/pr9101831>
- Nasrullah, M., Ansar, S., Krishnan, S., Singh, L., Peera, S. G., & Zularisam, A. W. (2022). Electrocoagulation treatment of raw palm oil mill effluent: Optimization process using high current application. *Chemosphere*, 299, 134387. <https://doi.org/10.1016/J.CHEMOSPHERE.2022.134387>

- Ogedey, A., & Oguz, E. (2024). Application of electrocoagulation process for the disposal of COD, NH₃-N and turbidity from the intermediate sanitary landfill leachate. *Environmental Science and Pollution Research*, 31(7), 11243-11260. <https://doi.org/10.1007/s11356-024-31937-7>
- Rangga, J. U., Ismail, S. N. S., Rasdi, I., & Karuppiah, K. (2024). Estimation of leachate volume and treatment cost avoidance through waste segregation programme in Malaysia. *Pertanika Journal of Science and Technology*, 32(1), 339-364. <https://doi.org/10.47836/pjst.32.1.19>
- Rookesh, T., Samaei, M. R., Yousefinejad, S., Hashemi, H., Derakhshan, Z., Abbasi, F., Jalili, M., Giannakis, S., & Bilal, M. (2022). Investigating the electrocoagulation treatment of landfill leachate by iron/graphite electrodes: Process parameters and efficacy assessment. *Water*, 14(2), 205. <https://doi.org/10.3390/w14020205>
- Sadaf, S., Roy, H., Fariha, A., Rahman, T. U., Tasnim, N., Jahan, N., Sokaan-Adeaga, A. A., Safwat, S. M., & Islam, M. S. (2024). Electrocoagulation-based wastewater treatment process and significance of anode materials for the overall improvement of the process: A critical review. *Journal of Water Process Engineering*, 62, 105409. <https://doi.org/10.1016/J.JWPE.2024.105409>
- Salim, A., El Bouari, A., Tahiri, M., & Tanane, O. (2024). Elimination of copper from wastewater arising from metal plating through electrocoagulation. *Analytical and Bioanalytical Electrochemistry*, 16(9), 817-829. <https://doi.org/10.22034/abec.2024.716156>
- Sedqi, S., Bazargan, A., & Mirbagheri, S. A. (2021). Consuming the least amount of energy and resources in landfill leachate electrocoagulation. *Environmental Technology & Innovation*, 22, 101454. <https://doi.org/10.1016/J.ETI.2021.101454>
- Shahedi, A., Darban, A. K., Taghipour, F., & Jamshidi-Zanjani, A. (2020). A review on industrial wastewater treatment via electrocoagulation processes. *Current Opinion in Electrochemistry*, 22, 154-169. <https://doi.org/10.1016/J.COEELEC.2020.05.009>
- Sharma, L., Prabhakar, S., Tiwari, V., Dhar, A., & Halder, A. (2021). Optimization of EC parameters using Fe and Al electrodes for hydrogen production and wastewater treatment. *Environmental Advances*, 3, 100029. <https://doi.org/10.1016/J.ENVADV.2020.100029>
- Tahreen, A., Jami, M. S., & Ali, F. (2020). Role of electrocoagulation in wastewater treatment: A developmental review. *Journal of Water Process Engineering*, 37, 101440. <https://doi.org/10.1016/j.jwpe.2020.101440>
- Tay, K. W. W., Chin, S. F., Wasli, M. E., & Musa, Z. (2023). Response Surface Methodology: A versatile tool for the optimization of particle sizes of cellulose beads. *Pertanika Journal of Science and Technology*, 31(6), 2805-2822. <https://doi.org/10.47836/pjst.31.6.10>

Elucidation of *Chromolaena odorata* Extract's Pharmacological Potential Through Integration of Network Pharmacology and Molecular Docking Study

Nur 'Ainun Mokhtar¹, Fatahiya Mohamed Tap^{2*}, Iswaibah Mustafa²,
Mohd Shahrul Nizam Salleh², Norzila Mohd², Nurhannani Ahmad Rozani² and
Norazlan Mohamad Misnan³

¹Faculty of Pharmacy, Universiti Teknologi MARA Cawangan Pulau Pinang, Kampus Bertam, 13200 Kepala Batas, Pulau Pinang, Malaysia

²School of Chemical Engineering, College of Engineering, Universiti Teknologi MARA Cawangan Terengganu, Kampus Bukit Besi, 23200 Dungun, Terengganu, Malaysia

³Herbal Medicine Research Center (HMRC), Institute for Medical Research (IMR), National Institutes of Health (NIH), Persiaran Setia Murni, Setia Alam, 40170 Shah Alam, Selangor, Malaysia

ABSTRACT

Network pharmacology, an interdisciplinary field that combines principles from pharmacology, systems biology, and network science, provides a robust framework for exploring the intricate relationship between biological systems and pharmacologically active compounds. This study focuses on the herbal medicine *Chromolaena odorata*, known as “*Daun kapal terbang*” in Malaysia. This plant, renowned for its diverse medicinal properties, underwent thorough analysis, revealing its anti-inflammatory, antimicrobial, anticancer, antidiabetic, and wound-healing attributes. However, a deeper understanding of its pharmacological mechanism of action remains unclear. This study addresses this gap by conducting network pharmacology analysis and molecular docking studies on

C. odorata. In this current work, three identified compounds from *C. odorata*, namely squalene, linolenic acid and hexadecanoic acid, were subjected to compound-target identification via SwissTargetPrediction and Cytoscape 3.10.1 visualization tools. Subsequently, Gene Ontology enrichment was performed to analyze gene clusters within the network. Finally, AutoDOCK tools were employed to elucidate the protein-ligand interaction among selected targets. PPARA was identified as the most important target among all the key proteins based on the binding affinity and GO enrichment

ARTICLE INFO

Article history:

Received: 22 August 2024

Accepted: 24 February 2025

Published: 24 April 2025

DOI: <https://doi.org/10.47836/pjst.33.S3.09>

E-mail addresses:

nurain2942@uitm.edu.my (Nur 'Ainun Mokhtar)

fatahiya@uitm.edu.my (Fatahiya Mohamed Tap)

norzi085@uitm.edu.my (Norzila Mohd)

shahrulnizam@uitm.edu.my (Mohd Shahrul Nizam Salleh)

iswaibahmustafa@uitm.edu.my (Iswaibah Mustafa)

nurh4nnani@gmail.com (Nurhannani Ahmad Rozani)

norazlan.misnana@moh.gov.my (Norazlan Mohamad Misnan)

*Corresponding author

analysis. PPARA displayed the strongest binding affinities: -9.6 kcal/mole for squalene, -7.6 kcal/mole for linolenic acid, and -7.0 kcal/mole for hexadecanoic acid, surpassing the affinities observed for PGR and RORA. This comprehensive study not only emphasizes the significance of network pharmacology in delineating herbal remedy potentials but also underscores its implications for advancing drug development, particularly in designing novel therapeutics based on targeted mechanisms.

Keywords: *Chromolaena odorata*, gene ontology, herbal medicine, KEGG, molecular docking, network pharmacology

INTRODUCTION

Network pharmacology is an increasingly interdisciplinary field integrating principles from pharmacology, systems biology, and network science. It offers a powerful framework for comprehensively searching the complex relationship between biological systems and pharmacologically active compounds, thereby shedding light on the complex mechanisms of drug actions. Within the field of herbal medicine and pharmaceutical development, network pharmacology emerges as a pivotal player, presenting a systematic and data-driven approach to unveil the pharmacological potential inherent in herbal remedies (Hopkins, 2008). Its value in modern drug discovery has been demonstrated through case studies where herbal medicine findings have been successfully translated into therapeutics. For example, the application of network pharmacology in the study of traditional Chinese medicine has led to significant advancements in identifying multi-target drug candidates (Zhou et al., 2020). Notably, compounds such as imatinib, a tyrosine kinase inhibitor for chronic myeloid leukemia, and zanamivir, an antiviral drug for influenza, have been successfully developed from Computer-Aided Drug Design (CADD), showcasing the synergy of computational approaches with network pharmacology in modern drug discovery (Andrews et al., 2000; Sliwoski et al., 2014).

Herbal medicines, often composed of a collection of bioactive compounds, possess the capacity to interact with diverse targets within the human body. The compound-target network empowers researchers to recognize and characterize these multi-target effects, providing profound insights into the involved mechanisms that underscore the efficacy of herbal remedies. Such insights, in turn, promise to inform the design of more effective and safer drugs. Through the detailed mapping of interactions between herbal compounds and their molecular targets, researchers can identify key proteins and pathways essential to the therapeutic effects of these phytochemicals (Li & Zhang, 2013).

Throughout history, small molecular compounds derived from natural sources have played a significant role in combating diseases and serving as valuable starting points for drug development. Natural products possess the unique ability to interact with multiple

targets within these intricate disease systems, aligning with this multifaceted therapeutic approach. As the utilization of natural products continues to evolve as promising candidates for drug discovery, it has become increasingly imperative to thoroughly assess the range of interactions these small molecules have with multiple biological targets. Nevertheless, the lack of a comprehensive understanding of the pharmacological mechanisms governing the actions of these drugs has hindered their broader integration into the field of drug development (Sun et al., 2022).

In this study, we aimed to evaluate the pharmacological potential of *C. odorata*, a traditional herbal medicine locally known as “Daun kapal terbang” in Malaysia, using a network pharmacology-based approach. This botanical species has a well-documented array of medicinal properties, encompassing anti-inflammatory, antimicrobial (Olawale et al., 2022), anticancer, antidiabetic, and wound-healing (Sirinthipaporn & Jiraungkoorskul, 2017). Our study contributes to the understanding of the key target proteins and therapeutic potential of this plant.

In our study, we conducted network pharmacology analysis and molecular docking studies on *C. odorata*, verifying and enhancing the findings. These approaches highlight network pharmacology's significance in identifying this herbal remedy's therapeutic potential. Our research sheds light on the compound-target network of *C. odorata*. It contributes valuable insights to herbal medicine and drug development, with potential implications for developing novel therapeutics.

MATERIALS AND METHODS

Plant Verification, Plant Extraction and GS-MS Analysis

The plant was collected, verified, extracted, and submitted for GC-MS analysis as described in our prior work (Mokhtar et al., 2023). In brief, GCMS analysis was performed on an Agilent 7890B gas chromatography system (Agilent, CA, USA) coupled with Agilent 5975C (Agilent, CA, USA) mass selective detector and fitted with DB-1MS column (30 m x 0.25mm x 0.25 µm). Helium was used as the carrier gas at a flow rate of 1.0 mL/min under the following operating conditions: 2ml initial injection volume, split injection ratio of 1:10, initial oven temperature stabilization at 60°C for 4 min and ramping to 230°C at a rate of 6°C/min, detector temperature of 260°C, injector temperature of 230°C and ionization voltage of 70 eV. The chemical components in the extract were identified and quantified by comparing the mass spectra to the NIST library database.

Construction of Compound-target Network

The bioactive compounds of *C. odorata* (squalene, linolenic acid, and hexadecanoic acid) were analyzed to establish a compound-target network. Potential target proteins for each compound were identified using SwissTargetPrediction (<https://www.swisstargetprediction>).

ch/) (Daina et al., 2019). The identified targets were then visualized using Cytoscape 3.10.1, a software tool for constructing interaction networks (Shannon et al., 2003). To further understand the protein-protein interactions (PPI) within the network, the targets were imported into the STRING database (<https://string-db.org/>) with the interaction confidence threshold set to "medium confidence," restricted to the "Homo sapiens" species. Nodes without network connections were excluded. This methodology enables a detailed exploration of the molecular interactions and pathways associated with the pharmacological potential of *C. odorata*.

Gene Ontology (GO) Enrichment Analysis

Gene Ontology (GO) enrichment and Kyoto Encyclopedia of Genes and Genomes (KEGG) pathway analyses were conducted to investigate the potential mechanisms of *C. odorata* in therapeutic applications using ClueGO, an additional Cytoscape plug-in. The analyses were performed to elucidate insights into the biological processes, molecular functions, and pathways associated with the identified targets. This approach facilitated a deeper understanding of the pathways and mechanisms through which the bioactive compounds of *C. odorata* may contribute to its pharmacological activities, particularly in wound healing (Thomas, 2017).

Molecular Docking on Selected Target Protein

Protein Data Bank (PDB) (<https://www.rcsb.org/>) was used to retrieve the 3D structure of all protein targets. Subsequently, AutoDock Tools was employed to prepare the docking input files and parameters at the binding pocket of PGR (PDB ID: 1SQN), PPARA (PDB ID:5HYK) (Madauss et al., 2004) and RORA (PDB ID:1N83) (Kallen et al., 2002). Then, the grid box dimensions of the active site were constructed at 28 Å on each side. A docking procedure was carried out to find the affinity of the squalene, linolenic acid and hexadecanoic acid by docking them against the receptors PGR, PPARA and RORA using Assisted Molecular Docking AMDock (Valdés-Tresanco et al., 2020), a software integrated with AutoDock Vina. Finally, complex details of the protein-ligand interactions were visualized using tools such as PyMOL and Discovery Studio Visualizer.

RESULTS

Compound Analysis of *Chromolaena odorata*

Based on Mokhtar et al. (2023), the ethanolic extract of *C. odorata* contains a diverse array of secondary metabolites, encompassing terpenoids, steroids, flavonoids, alkaloids, saponins, and tannins. The presence of these significant phytochemicals was substantiated through gas chromatography-mass spectrometry (GC-MS) analysis, confirming the

prominence of linolenic acid, squalene, and hexadecanoic acids as the primary compounds, as shown in Table 1. Therefore, in this current work, we explored the therapeutic potential of *C. odorata* based on these identified compounds.

Table 1

Major compound of ethanolic extract of *Chromolaena odorata* based on GC-MS based on prior work (Mokhtar et al., 2023)

Compound Name	Molecular Formula	Area (%)	Quality (%)
Squalene	C ₃₀ H ₅₀	3.53	99
Linolenic acid	C ₂₀ H ₃₄ O ₂	8.07	99
Hexadecanoic acid	C ₁₈ H ₃₆ O ₂	9.40	98

Construction of Compound-target Network

Identification of the target protein of these compounds was conducted through SwissTargetPrediction, which gave a total of 98, 99 and 99 targets for squalene, linolenic acid and hexadecanoic, respectively. These protein targets were further used to construct a compound-target network using Cytoscape 3.10, consisting of three compounds (squalene, linolenic acid and hexadecanoic acid) and 296 interactive target proteins (Figure 1). Based on this network analysis, a total of 10 targets shown overlapping among the three

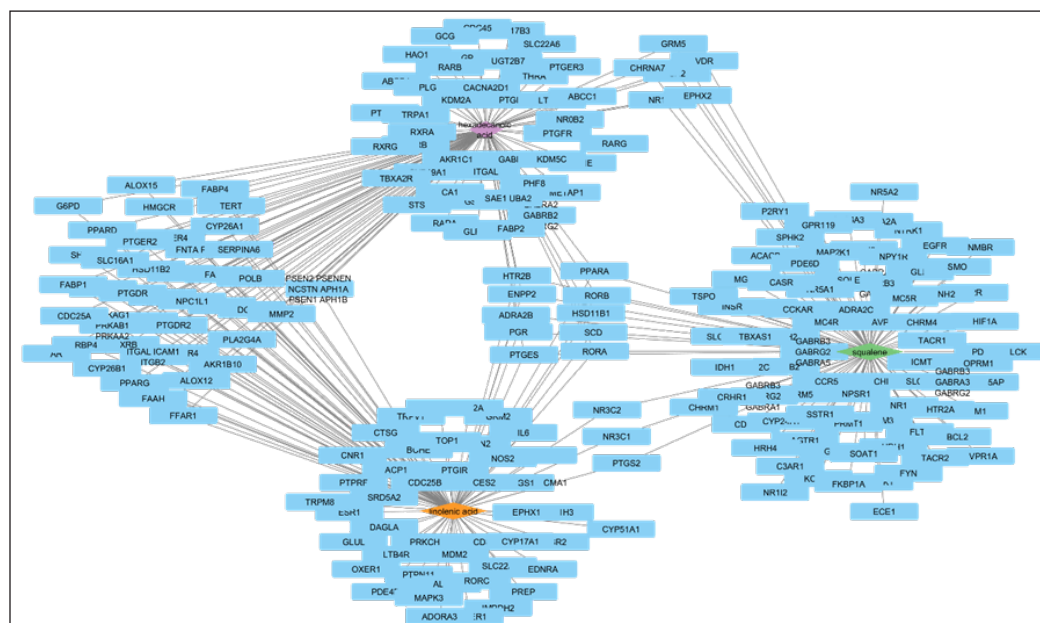


Figure 1. Compound-targets network of squalene, linolenic acid and hexadecanoic acid. The compounds were represented in a diamond shape, and each compound was differentiated using color coding: squalene (green), linolenic acid (orange), and hexadecanoic acid (purple)

compounds, which are identified as HTR2B, ENPP2, ADRA2B, PGR, PPARA, PTGES, RORB, HSD11B1, SCD and RORA. This means that the highest-degree genes are greatly linked to each other; thus, all of these genes might be hub targets (Batool et al., 2022).

Gene Ontology and KEGG Pathway Analysis

GO enrichment analysis was carried out to analyze these 10 hit target proteins. The selection of the 10 overlapping targets was based on their central roles within the constructed compound-target network, as these targets represent shared nodes with high connectivity among the three studied compounds, as depicted in Figure 1. Focusing on these targets enables a network-driven approach to understanding the pharmacological mechanisms of *C. odorata*. The analysis was performed using the ClueGO plugin according to KEGG pathways based on biological processes, cellular processes, and molecular function. The GO term fusion was restricted to $pV \leq 0.005$, which is based on the false discovery rate (Bindea et al., 2009). Based on the GO enrichment analysis, nuclear receptor activity and regulatory activity of Small Ubiquitin-like Modifier (SUMO) protein pathways were found to be associated with studied compounds (Figure 2).

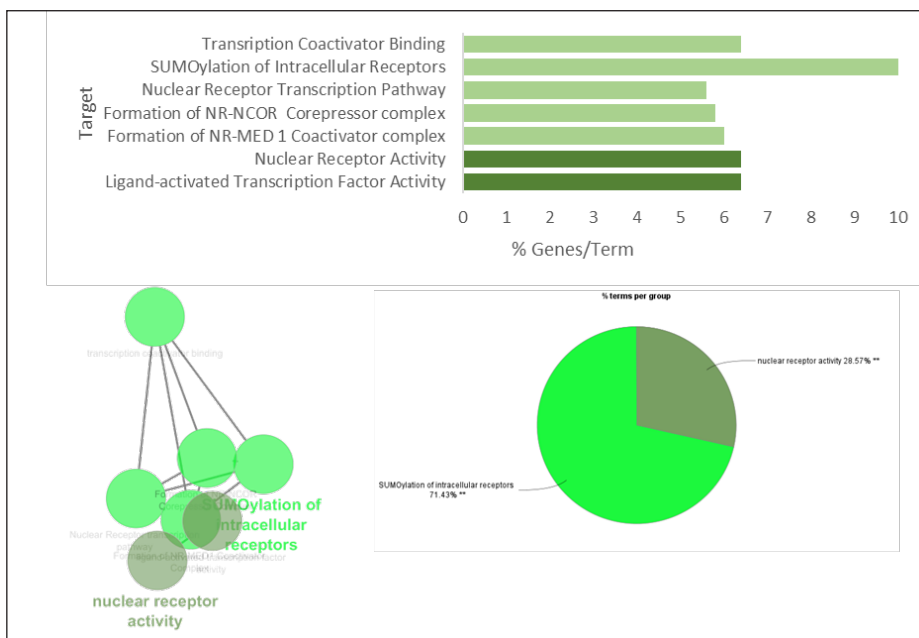


Figure 2. GO enrichment analysis is based on ten selected target genes

Through GO enrichment analysis, it was found that these associated genes (PGR, PPARA and RORA) are the nuclear receptors that have main roles in regulating gene expression and various physiological processes, as shown in Table 2.

Table 2

GO functional group analysis with associated genes

GO ID	GO Term	Associated Genes Found
GO:0098531	Ligand-activated transcription factor activity	[PGR, PPARA, RORA, RORB]
GO:0004879	Nuclear receptor activity	[PGR, PPARA, RORA, RORB]
R-HSA:376419	Formation of NR-MED1 Coactivator Complex	[PGR, PPARA, RORA]
R-HSA:382096	Formation of NR-NCOR Corepressor Complex	[PGR, PPARA, RORA]
R-HSA:383280	Nuclear Receptor transcription pathway	[PGR, PPARA, RORA]
R-HSA:4090294	SUMOylation of intracellular receptors	[PGR, PPARA, RORA]
GO:0001223	Transcription coactivator binding	[PGR, PPARA, RORA]

Molecular Docking Evaluation

Table 3 and Figure 3 provide details on the docking scores and binding poses of specific compounds (squalene, linolenic acid, and hexadecanoic acid) against three distinct proteins, which are PGR (PDB ID: 1SQN), PPARA (PDB ID: 5HYK), and RORA (PDB ID: 1N83).

Table 3

Docking score of target protein and compounds

Receptor Target	Compounds	Binding Affinity (kcal/mol)	Hydrogen Bonding	Hydrophobic Bond
PGR	Squalene	-6.6	-	Val 379, Met 368, Val 403, Ala 330, Ala 371, Phe 391, Ile 400, Val 364, Arg 367, Tyr 380, Cys 288, Leu 295
	Linolenic Acid	-6.6	Gln 277, Val 270	Ile 447, Phe 278, Val 4444, Ile 354 His 440 Leu 460, Leu 456 and Ala 454
	Hexadecanoic acid	-6.2	Leu 718 and Arg 370	Leu 887, Leu 797, Cys 891, Met 759, Phe 778, Met 801, Val 760, Leu 763, and Tyr 890
PPARA	Squalene	-9.6	-	Cys 891, Met 801, Leu 763, Leu 797, Leu 887, Leu 218, Leu 721, Met 759, Phe 778, and Val 760.
	Linolenic Acid	-7.6	Arg 766, Phe 778	Met 759, Leu 718, Met 801, Leu 797, Cys 891, Leu 715, Tyr 890, Met 756, and Leu 887
	Hexadecanoic acid	-7.0	-	Val 274, Phe 273, Val 444, Ile 447, Ile 354, and Leu 456
RORA	Squalene	-9.0	-	Ala 454, Val 270, Ile 447, Ile 354, Phe 273, Cys 276, Phe 318, Leu 321, Met 220, Val 324, Phe 218 and Met 320
	Linolenic Acid	-6.6	-	Leu 394, Phe 273, Val 444, Ile 354, His 440, Leu 460, Leu 456, and Ala 454
	Hexadecanoic acid	-5.8	Tyr 290 and Gln 289	Arg 367, Ala 371, Val 364, Ala 330, and Ala 454,

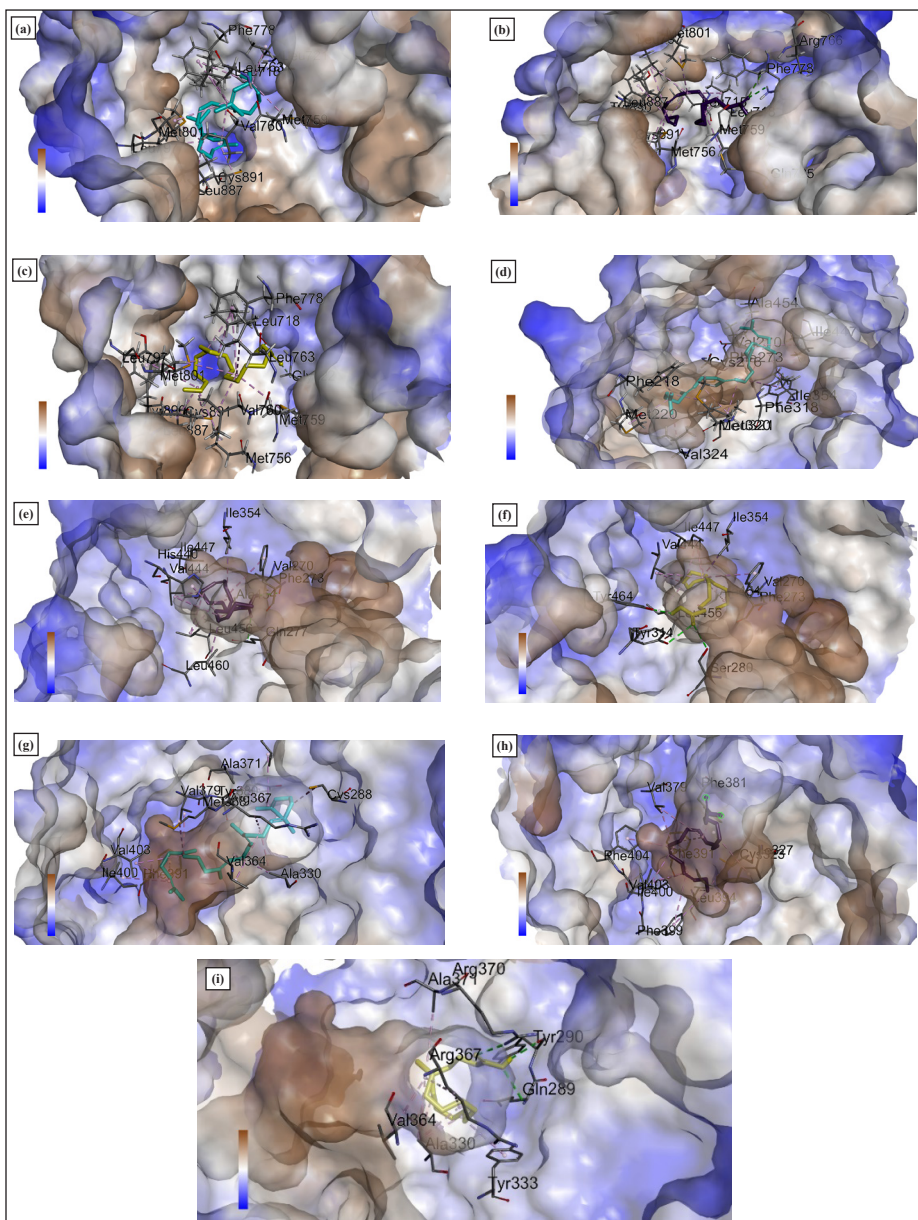


Figure 3. The docking of squalene (cyan), linolenic acid (purple) and hexadecanoic acid (yellow) in the binding site of key target proteins (a) (b) (c) PGR, (d) (e) (f) PPARα and (g) (h) (i) RORA. The representation of amino acid residues is the interactions in the binding site. The representation of brown and blue showed high hydrophobicity and less hydrophobicity, respectively

The results from docking simulations elucidate the proficient binding capabilities of these compounds within the active sites of their respective target proteins, underscoring their potential as either inhibitors or agonists. Notably, among these three proteins investigated,

Based on this molecular docking prediction, the binding affinity of these compounds is mostly attributed to hydrophobic interactions rather than hydrogen bonding between the compounds and residues within the active site vicinity of the targeted protein.

DISCUSSION

Many studies have been conducted to evaluate the medicinal potential of *C. odorata* despite its status as an invasive weed. Its notable pharmacological activity, such as wound healing, anti-inflammatory, anticancer, antidiabetic, and antifungal properties, has been well documented (Olawale et al., 2022). However, a deeper understanding of its pharmacological mechanism of action remains unclear. Hence, this study aims to address this gap by conducting network pharmacology analysis and molecular docking studies on *C. odorata*. Specifically, we are interested in defining which protein target *C. odorata* might have an interaction with that greatly influenced its therapeutic activity. The network pharmacological approach offers a comprehensive overview of uncovering novel therapeutic applications by mapping connections between its properties and diseases. Moreover, understanding its pharmacological network could facilitate the development of new drugs, considering its wide-ranging medicinal activities, while providing essential insights into the safety and efficacy crucial for its integration into modern medicine.

We begin by selecting three prominent compounds of ethanolic extract of *C. odorata*, which are squalene, linolenic acid and hexadecanoic acid, as these three compounds were shown to be abundantly present through GCMS analysis. Then, the gene targets associated with these compounds were retrieved using the compound target database tool SwissTargetPrediction (<https://www.swisstargetprediction.ch/>). To further understand how these gene targets relate to particular pathways or target diseases, which might further be used to unravel their pharmacological potential, gene ontology (GO) was carried out. GO follows what could be called the “molecular biology paradigm,” in which a gene encodes a gene product, and that gene product carries out a molecular-level process or activity (molecular function) in a specific location relative to the cell (cellular component). This molecular process contributes to a larger biological objective (biological process) comprised of multiple molecular-level processes (Thomas, 2017). In this context, gene ontology analysis aims to identify those biological processes, cellular locations and molecular functions impacted by the condition studied. Based on the GO enrichment analysis of this current work, we have found that PGR, PPARA, and RORA are nuclear receptors that mainly regulate gene expression and various physiological processes associated with *C. odorata*'s prominent compounds.

The progesterone receptor, encoded by the PGR gene, is found in various tissues in the body, including the uterus, breast, and other reproductive organs. Its main function is to bind to progesterone, which triggers a series of cellular responses essential for various

physiological processes (Grimm et al., 2016). On the other hand, Peroxisome Proliferator-Activated Receptor Alpha (PPARA) plays an important role in regulating lipid metabolism, particularly fatty acid oxidation in the liver and other tissues (Kersten & Stienstra, 2017). A recent study indicates that downregulation of PPARA plays an important role in the impaired mitochondrial function in the corneal epithelium and delayed corneal wound healing in diabetes (Liang et al., 2023). The study also suggested that based on their finding, PPARA agonists might have therapeutic potential for treating diabetic keratopathy. In our work, we found that all three ligands tested (squalene, linolenic acid and hexadecanoic acid) have shown the most stable binding affinity towards PPARA, which gives the idea that *C. odorata*'s prominent phytoconstituents possess the potential to be one of the PPARA agonists candidates.

Additionally, Retinoic Acid Receptor-Related Orphan Receptor Alpha (RORA) has been implicated in lipid metabolism regulation, immune system modulation, and inflammatory responses, making it a crucial player in various physiological processes and potentially affecting multiple aspects of health and disease. Its role in inflammatory responses means that RORA can affect how the body responds to injury and stress, which can have implications for conditions like heart disease and arthritis (Franczyk et al., 2022). In a study by Jiang et al. (2020), RORA overexpression inhibited the proliferation and tumorigenesis of glioma cell lines and glioma stem cells (GSCs) by inhibiting the TNF- α mediated NF- κ B signaling pathway. This suggested that RORA inhibition would be a potential treatment target for tumor disease. In this context, it could be suggested that *C. odorata* anticancer and antitumoral activity might be driven by the regulation of RORA in the same manner.

After analyzing the pathways related to these genes, a molecular docking study was conducted to further support the finding through structure-based analysis, including predicting the ability of squalene, linolenic acid and hexadecanoic acid to bind at the appropriate target binding site of PGR, PPARA and RORA. The docking results demonstrated that all the compounds effectively bound to the active site of their target proteins. PPARA exhibited the highest binding affinity among these three key proteins studied compared to PGR and RORA. These findings accentuate the preferential interaction and stronger affinity of the studied compounds towards PPARA, signifying its pivotal role as a primary target for these ligands and suggesting their potential therapeutic relevance in modulating PPARA-associated pathways, including metabolic syndrome, neurodegenerative and heart disease (Lin et al., 2022).

Using a molecular docking approach, we further elucidate the structure-based interactions potentially established between specific gene targets and the compounds under investigation. This step holds significant importance as it substantiates the preliminary predictions derived from the gene ontology analysis. According to the findings of the

molecular docking study, it was determined that squalene primarily engages with PGR, PPARA, and RORA through hydrophobic interactions, with the lack of any observed hydrogen bonding with these gene targets. The specific amino acid residues implicated in these hydrophobic interactions were identified as follows: Val 379, Met 368, Val 403, Ala 330, Ala 371, Phe 391, Ile 400, Val 364, Arg 367, Tyr 380, Cys 288, and Leu 295 for PGR; Cys 891, Met 801, Leu 763, Leu 797, Leu 887, Leu 218, Leu 721, Met 759, Phe 778, and Val 760 for PPARA; and residues Ala 454, Val 270, Ile 447, Ile 354, Phe 273, Cys 276, Phe 318, Leu 321, Met 220, Val 324, Phe 218, and Met 320 for RORA. Structurally, squalene is composed of six double bonds, suggesting that this feature may contribute significantly to the observed hydrophobic interactions.

Conversely, the second compound under investigation, namely linolenic acid, demonstrated the formation of two hydrogen bonds with residues Gln 277 and Val 270 on the PGR target protein while interacting with residues Arg 766 and Phe 778 through hydrogen bonding in the PPARA protein. Linolenic acid also engaged in hydrophobic interactions with all target proteins. Specifically, residues Ile 447, Phe 278, Val 444, Ile 354, His 440, Leu 460, Leu 456, and Ala 454 formed hydrophobic bonds with the PGR protein, whereas Leu 394, Phe 273, Val 444, Ile 354, His 440, Leu 460, Leu 456, and Ala 454 interacted in a hydrophobic manner with RORA. In the case of the PPARA target protein, hydrophobic interactions were observed with residues Met 759, Leu 718, Met 801, Leu 797, Cys 891, Leu 715, Tyr 890, Met 756, and Leu 887. Considering the structural attributes of linolenic acid, probable interactions with the proteins PPARA, PGR, and RORA through hydrogen bond formation were due to functional groups such as hydroxyl (-OH) or carboxyl (-COOH) groups. Furthermore, due to its lengthy hydrocarbon chain, its hydrophobic nature could potentially cause hydrophobic interactions with the nonpolar domains of the target proteins, which is crucial in stabilizing the complexes formed.

Last, in the sequence, hexadecanoic acid formed hydrogen bonds with Leu 718 and Arg 370 within the PGR target protein, along with Tyr 290 and Gln 289 within the RORA target protein. Additionally, hexadecanoic acid was used to establish hydrophobic contacts. Specifically, residues that are Leu 887, Leu 797, Cys 891, Met 759, Phe 778, Met 801, Val 760, Leu 763, and Tyr 890 participated in hydrophobic interactions with the PGR gene. In the context of hydrophobic interactions with the RORA and PPARA target proteins, distinct residues of Arg 367, Ala 371, Val 364, Ala 330, and Ala 454 for RORA, and Val 274, Phe 273, Val 444, Ile 447, Ile 354, and Leu 456 for PPARA were found to be involved.

The interconnected roles of PPARA, PGR, and RORA in wound healing, as obtained in this study, suggest a multifaceted mechanism through which *C. odorata* exerts its therapeutic potential, particularly in wound healing. GO enrichment analysis identified these nuclear receptors as central to the regulatory network of *C. odorata*'s bioactive compounds. PPARA contributes significantly by regulating lipid metabolism and mitochondrial function,

which are essential for energy production during keratinocyte migration and fibroblast proliferation in tissue regeneration (Briganti et al., 2024). Furthermore, PPARA mitigates oxidative stress through fatty acid oxidation, reducing the accumulation of reactive oxygen species (ROS) and fostering an optimal environment for cellular repair (Lin et al., 2022). RORA complements this role by modulating immune responses via the NF- κ B signaling pathway, suppressing pro-inflammatory cytokines such as TNF- α and IL-6, thereby facilitating inflammation resolution and promoting angiogenesis (Franczyk et al., 2022). This angiogenic role is critical for delivering oxygen and nutrients to the regenerating tissue (Ham et al., 2010). PGR enhances wound healing by mediating progesterone signaling, which supports collagen deposition and angiogenesis during the proliferation phase and by influencing keratinocyte proliferation and differentiation for epidermal layer formation (Barrientos et al., 2008).

These pathways are interconnected through their shared involvement in inflammation resolution, energy metabolism, and oxidative stress reduction. The coordinated actions of PPARA and RORA ensure a balanced inflammatory response and an oxidative stress-free environment, while PGR drives structural tissue repair and vascularization. Together, these findings demonstrate how *C. odorata* bioactive compounds target these pathways to create a multifaceted approach to wound healing, integrating metabolic, inflammatory, and structural processes.

CONCLUSION

This study successfully conducted network pharmacology and docking study of squalene, linolenic acid and hexadecanoic acid against the selected target proteins. Our compound-network interaction revealed that these three studied compounds were associated with nuclear receptor key proteins. Out of the three gene target proteins studied, PPARA stood out as the most crucial target according to the GO enrichment analysis and molecular docking assessment. Specifically, among these three proteins, PPARA displayed the strongest binding affinities: -9.6 kcal/mole for squalene, -7.6 kcal/mole for linolenic acid, and -7.0 kcal/mole for hexadecanoic acid, surpassing the affinities observed for PGR and RORA. This finding demonstrated that at the molecular level, *C. odorata* is most likely modulating the nuclear receptors key protein exerting its pharmacological activities. However, to address the limitations in the computational study, further analysis, such as molecular dynamics simulations and experimental validations, is essential to confirm the active components and elucidate the therapeutic mechanisms of *C. odorata*. These next steps will provide credibility to the findings and further our understanding of their pharmacological potential.

ACKNOWLEDGEMENTS

This work was supported by Research Grant MyRA Universiti Teknologi MARA, Malaysia [600-RMC/GPM ST 5/3 (019/2021)]. We also thank the College of Engineering, UiTM Shah Alam and School of Chemical Engineering, UiTM Cawangan Terengganu, Kampus Bukit Besi, for administrative support.

REFERENCES

- Andrews, C. W., Bennett, L., & Yu, L. X. (2000). Predicting human oral bioavailability of a compound: development of a novel quantitative structure-bioavailability relationship. *Pharmaceutical Research*, *17*(6), 639-644. <https://doi.org/10.1023/a:1007556711109>
- Barrientos, S., Stojadinovic, O., Golinko, M. S., Brem, H., & Tomic-Canic, M. (2008). Growth factors and cytokines in wound healing. *Wound Repair and Regeneration*, *16*(5), 585-601. <https://doi.org/10.1111/j.1524-475X.2008.00410.x>
- Batool, S., Javed, M. R., Aslam, S., Noor, F., Javed, H. M. F., Seemab, R., Rehman, A., Aslam, M. F., Paray, B. A., & Gulnaz, A. (2022). Network pharmacology and bioinformatics approach reveals the multi-target pharmacological mechanism of fumaria indica in the treatment of liver cancer. *Pharmaceuticals*, *15*(6), 654. <https://doi.org/10.3390/ph15060654>
- Bindea, G., Mlecnik, B., Hackl, H., Charoentong, P., Tosolini, M., Kirilovsky, A., Fridman, W. H., Pagès, F., Trajanoski, Z., & Galon, J. (2009). ClueGO: A cytoscape plug-in to decipher functionally grouped gene ontology and pathway annotation networks. *Bioinformatics*, *25*(8), 1091-1093. <https://doi.org/10.1093/bioinformatics/btp101>
- Briganti, S., Mosca, S., Di Nardo, A., Flori, E., & Ottaviani, M. (2024). New Insights into the role of PPAR γ in skin physiopathology. *Biomolecules*, *14*(6), 10-13. <https://doi.org/10.3390/biom14060728>
- Daina, A., Michielin, O., & Zoete, V. (2019). SwissTargetPrediction: Updated data and new features for efficient prediction of protein targets of small molecules. *Nucleic Acids Research*, *47*(W1), W357-W3664. <https://doi.org/10.1093/nar/gkz382>
- Franczyk, B., Gluba-Brzózka, A., Rysz-Górzynska, M., & Rysz, J. (2022). The role of inflammation and oxidative stress in rheumatic heart disease. *International Journal of Molecular Sciences*, *23*(24), 15812. <https://doi.org/10.3390/ijms232415812>
- Grimm, S. L., Hartig, S. M., & Edwards, D. P. (2016). Progesterone Receptor signaling mechanisms. *Journal of Molecular Biology*, *428*(19), 3831-3849. <https://doi.org/https://doi.org/10.1016/j.jmb.2016.06.020>
- Ham, S. A., Kim, H. J., Kim, H. J., Kang, E. S., Eun, S. Y., Kim, G. H., Park, M. H., Woo, I. S., Kim, H. J., Chang, K. C., Lee, J. H., & Seo, H. G. (2010). PPAR δ promotes wound healing by up-regulating TGF- β 1-dependent or -independent expression of extracellular matrix proteins. *Journal of Cellular and Molecular Medicine*, *14*(6B), 1747-1759. <https://doi.org/10.1111/j.1582-4934.2009.00816.x>
- Hopkins, A. L. (2008). Network pharmacology: The next paradigm in drug discovery. *Nature Chemical Biology*, *4*(11), 682-690. <https://doi.org/10.1038/nchembio.118>

- Jiang, Y., Zhou, J., Zhao, J., Hou, D., Zhang, H., Li, L., Zou, D., Hu, J., Zhang, Y., & Jing, Z. (2020). MiR-18a-downregulated RORA inhibits the proliferation and tumorigenesis of glioma using the TNF- α -mediated NF- κ B signaling pathway. *EBioMedicine*, 52, 102651. <https://doi.org/10.1016/j.ebiom.2020.102651>
- Kallen, J. A., Schlaeppli, J. M., Bitsch, F., Geisse, S., Geiser, M., Delhon, I., & Fournier, B. (2002). X-ray structure of the hROR α LBD at 1.63 Å: Structural and functional data that cholesterol or a cholesterol derivative is the natural ligand of ROR α . *Structure*, 10(12), 1697-1707. [https://doi.org/10.1016/S0969-2126\(02\)00912-7](https://doi.org/10.1016/S0969-2126(02)00912-7)
- Kersten, S., & Stienstra, R. (2017). The role and regulation of the peroxisome proliferator activated receptor alpha in human liver. *Biochimie*, 136, 75-84. <https://doi.org/https://doi.org/10.1016/j.biochi.2016.12.019>
- Li, S., & Zhang, B. (2013). Traditional Chinese medicine network pharmacology: Theory, methodology and application. *Chinese Journal of Natural Medicines*, 11(2), 110-120. [https://doi.org/10.1016/S1875-5364\(13\)60037-0](https://doi.org/10.1016/S1875-5364(13)60037-0)
- Liang, W., Huang, L., Whelchel, A., Yuan, T., Ma, X., Cheng, R., Takahashi, Y., Karamichos, D., & Ma, J.-X. (2023). Peroxisome proliferator-activated receptor- α (PPAR α) regulates wound healing and mitochondrial metabolism in the cornea. *Proceedings of the National Academy of Sciences of the United States of America*, 120(13), e2217576120. <https://doi.org/10.1073/pnas.2217576120>
- Lin, Y., Wang, Y., & Li, P. F. (2022). PPAR α : An emerging target of metabolic syndrome, neurodegenerative and cardiovascular diseases. *Frontiers in Endocrinology*, 13(December), 1-13. <https://doi.org/10.3389/fendo.2022.1074911>
- Madauss, K. P., Deng, S. J., Austin, R. J. H., Lambert, M. H., McLay, I., Pritchard, J., Short, S. A., Stewart, E. L., Uings, I. J., & Williams, S. P. (2004). Progesterone receptor ligand binding pocket flexibility: Crystal structures of the norethindrone and mometasone furoate complexes. *Journal of Medicinal Chemistry*, 47(13), 3381-3387. <https://doi.org/10.1021/jm030640n>
- Mokhtar, N. A., Tap, F. M., Hannani, N., Rozani, A., & Bahiyah, N. (2023). Phytochemical profiling , pharmacology prediction , and molecular docking study of *Chromolaena odorata* extract against multiple target proteins in wound healing. *Journal of Herbmedd Pharmacology*, 12(4), 469-482. <https://doi.org/10.34172/jhp.2023.44672>
- Olawale, F., Olofinsan, K., & Iwaloye, O. (2022). Biological activities of *Chromolaena odorata*: A mechanistic review. *South African Journal of Botany*, 144, 44-57. <https://doi.org/10.1016/j.sajb.2021.09.001>
- Shannon, P., Markiel, A., Ozier, O., Baliga, N. S., Wang, J. T., Ramage, D., Amin, N., Schwikowski, B., & Ideker, T. (2003). Cytoscape: A software environment for Integrated Models. *Genome Research*, 13(11), 2498-2504. <https://doi.org/10.1101/gr.1239303>
- Sirinthipaporn, A., & Jiraungkoorskul, W. (2017). Wound healing property review of Siam weed, *Chromolaena odorata*. *Pharmacognosy Reviews*, 11(21), 35-38. https://doi.org/10.4103/phrev.phrev_53_16
- Sliwoski, G., Kothiwale, S., Meiler, J., & Lowe, E. W. (2014). Computational methods in drug discovery. *Pharmacological Reviews*, 66(1), 334-395. <https://doi.org/10.1124/pr.112.007336>
- Sun, D., Gao, W., Hu, H., & Zhou, S. (2022). Why 90% of clinical drug development fails and how to improve it? *Acta Pharmaceutica Sinica B*, 12(7), 3049-3062. <https://doi.org/10.1016/j.apsb.2022.02.002>

- Thomas, P. D. (2017). The gene ontology and the meaning of biological function BT. In C. Dessimoz & N. Škunca (Eds.), *The Gene Ontology Handbook* (pp. 15-24). Springer New York. https://doi.org/10.1007/978-1-4939-3743-1_2
- Valdés-Tresanco, M. S., Valdés-Tresanco, M. E., Valiente, P. A., & Moreno, E. (2020). AMDock: A versatile graphical tool for assisting molecular docking with Autodock Vina and Autodock4. *Biology Direct*, *15*(1), 1-12. <https://doi.org/10.1186/S13062-020-00267-2>
- Zhou, Z., Chen, B., Chen, S., Lin, M., Chen, Y., Jin, S., Chen, W., & Zhang, Y. (2020). Applications of network pharmacology in traditional Chinese medicine research. *Evidence-Based Complementary and Alternative Medicine*, *2020*(1), 1646905. <https://doi.org/10.1155/2020/1646905>

Breast Cancer Prediction: A Random Forest-based System with Expert Validation

Sharifah Nurulhikmah Syed Yasin*, Aiman Azhar and Rajeswari Raju

College of Computing, Informatics and Mathematics, Universiti Teknologi MARA Cawangan Terengganu, Kampus Kuala Terengganu, 21080 Kuala Terengganu, Terengganu, Malaysia

ABSTRACT

Breast cancer (BC) is a fatal invasive disease among women that impacts women globally. It is listed as a significant disease among Malaysian women. Early detection and accurate diagnosis are important to improve the treatment outcome of a patient, as advanced stages of BC can increase fatality rates. The conventional methods of diagnosis are effective, but they face challenges such as high cost, radiation exposure, and the need for specialized operators. Therefore, this study focuses on developing a BC prediction system using a Random Forest (RF) algorithm. It is trained using the "BC Wisconsin (Diagnostic) Data Set" from Kaggle, consisting of 570 records with eight critical attributes selected for prediction. The algorithm and system are developed using Python and evaluated on accuracy, precision, recall, and F1-score, achieving 91.23%, 90.70%, 86.67%, and 88.89%, respectively. The algorithm was integrated with AdaBoost and XGBoost to add the experimental value, resulting in a better result than a single RF. Expert validation by a specialist confirmed the reliability of the dataset and accuracy of the prediction system, highlighting its potential to be a valuable tool for early BC detection. The study concludes that the RF-based system provides robust predictions, making it a promising approach for enhancing BC diagnostic processes.

Keywords: Algorithm, breast cancer, machine learning, prediction, random forest

ARTICLE INFO

Article history:

Received: 22 August 2024

Accepted: 24 February 2025

Published: 24 April 2025

DOI: <https://doi.org/10.47836/pjst.33.S3.10>

E-mail addresses:

nurulhikmah@uitm.edu.my (Sharifah Nurulhikmah Syed Yasin)

aimanazhar377@gmail.com (Aiman Azhar)

rajes332@uitm.edu.my (Rajeswari Raju)

*Corresponding author

INTRODUCTION

Breast cancer (BC) has increasingly become a common invasive disease in women, while it remains rare in men. BC forms the malignant cells within the breast tissue (Kinra, 2019; Minnoor & Baths, 2022). Patients may experience symptoms such as a breast lump, bloody nipple discharge, and alterations in the shape of the nipple or

breast (Kinra, 2019; Minnoor & Baths, 2022). In Malaysia, BC was the most common cancer from the year 2007–2016. The percentage increased from 17.7% in 2007–2011 to 19% in 2012–2016. This type of cancer has also been the most common cancer among Malaysian women, where 34.1% of the cancers reported was BC (National Cancer Registry, 2019). While the number of BC patients has increased in Malaysia, the disease has also impacted women globally. According to the World Health Organization (WHO), 2.3 million women were diagnosed with BC in 2022, with 670,000 of them succumbing to the disease.

Early detection and diagnosis of BC are vital for enhancing patient outcomes. Identifying BC at an early, localized stage greatly increases the likelihood of successful treatment and cure (Breast cancer, 2024). Moreover, an early and accurate diagnosis can increase survival rates, offering a better cure result and reducing the need for aggressive treatments (Li et al., 2024). On the contrary, advanced BC, particularly in stage four, often involves circulating tumor cells that drastically lower survival rates to as low as 40% (Zuo et al., 2017).

The most practical methods to carry out the diagnosis are performing clinical breast tests, mammograms, ultrasound tests, molecular breast imaging (MBI), magnetic resonance imaging (MRI), blood tests, and breast biopsy (He et al., 2020). Nevertheless, these methods have encountered several challenges, such as high cost, radiation exposure, requiring professional operators, long imaging times, and restrictions for patients with metal implants (He et al., 2020; Park et al., 2024). Therefore, there are potential solutions to these problems where a machine learning-based clinical prediction system can fill this gap and assist in the early identification of BC (Duan et al., 2024; Macaulay et al., 2021; Minnoor & Baths, 2022).

Machine learning (ML) can help the BC diagnosis process by predicting and classifying it based on the previous diagnosis data. ML analyses huge amounts of data containing the factors or symptoms of previously diagnosed, labeled data (Duan et al., 2024; Macaulay et al., 2021; Minnoor & Baths, 2022). The popular ML algorithms used in the previous study to predict disease are the decision tree, Support Vector Machine (SVM), K-nearest neighbor, multilayer perceptron, and random forest (RF). Among this algorithm, RF is found to produce the highest accuracy prediction (Mohamed et al., 2023; Rashid et al., 2024; Sumwiza et al., 2023).

The previous studies on RF for BC prediction conclude their research after accuracy testing and rarely extend the research to include expert validation. Therefore, this study seeks to develop and verify a prediction system for BC by adapting RF algorithms. The development is physically carried out using Python language, followed by accuracy testing using accuracy, precision, and recall metrics and result validation by a BC specialist consultant. In addition, the dataset utilized in this study is collected from the Kaggle website the dataset's name is "BC Wisconsin (Diagnostic) Data Set", which has 570 data person which has the BC attributes.

RELATED WORKS

Macaulay et al. (2021) study develops a predictive model for BC risk using an RF Classifier in African women. This study compares the results with the previous work that adopted the Gail model. The data involved in the prediction model are self-reported risk factor data and BMI values. Eleven significant risk factors were identified, including benign breast disease, a history of cancer, pesticide use, age at first child, exercise, and fruit intake. The study emphasizes the importance of these factors in predicting BC risk. The dataset was divided into training (70%) and testing (30%) sets during development. The RF classifier has undergone training using the selected features in the dataset. The output of the developed system shows high accuracy (98.33%) and sensitivity (100%) in predicting BC. This result has shown that the developed algorithm outperformed the previous Gail model. The main contribution of this study is that the algorithm proposed specifically addresses the unique risk profile of African women and has a high accuracy score.

Another study by Minnoor and Baths (2022) focuses on developing an automated system for BC diagnosis using an RF algorithm. This study emphasizes the importance of early diagnosis and aims to create a model to effectively classify malignant and benign tumors. This study utilizes the Wisconsin BC Diagnostic dataset from the UCI Machine Learning Repository, which contains 569 labeled instances of tumors (212 malignant and 357 benign) to train the RF engine. The dataset is imbalanced and needs to be fixed using upscaling techniques. Initially, the dataset contained seventeen key factors; however, this study chose eleven factors to use. The factors are diagnosis, symmetry, concavity, area, texture, compactness, radius, smoothness, concave points, perimeter, and fractal dimension. The reduction of the key factors is done to enhance computational efficiency. Consequently, the RF model surpasses the other machine learning algorithms evaluated, attaining a high accuracy rate of 99.3% in diagnosing malignant tumors.

Duan et al. (2024) conducted a study that created a machine learning-based prediction model for distant metastasis in BC. Distant metastasis refers to the spread of cancer cells from the primary tumor to other body parts. This study aims to identify the potential of biomarkers related to distant metastasis by using various bioinformatics techniques like weighted gene co-expression network analysis (WGCNA), differential expression analysis, and LASSO regression analysis. Therefore, 21 biomarkers related to distant metastasis were labeled and derived from a dataset analysis. Some machine learning models were trained using the recognized biomarkers, including logistic regression, RF, gradient boosting decision trees (GBDT), support vector machines (SVM), and XGBoost. The result shows that the RF model was the best-performing model for predicting distant metastasis, with a 93.6% accuracy score.

Yifan et al. (2021) recommended a method to improve the accuracy of BC diagnosis by combining two machine learning algorithms: RF and AdaBoost. This study aims to create

a classification model able to differentiate between benign and malignant breast tumors by using ML algorithms. This study applies to the Wisconsin Diagnostic BC Database, involving 569 samples (212 malignant and 357 benign) with 32 attributes relating to tumor characteristics. StandardScaler is employed to confirm a stable and standardized dataset. RF and AdaBoost are integrated to improve accuracy and effectively convert the classifier. As a result, the integrated model showed impressive results, with an accuracy of 98.6%. Therefore, this study concludes that integrating two ML algorithms (RF and AdaBoost) enhances the accuracy of prediction for BC diagnosis. Similarly, integrating RF with XGBoost has enhanced the imbalance dataset handling, as reported by Natras et al. (2022). XGBoost has shown an improvement of 6% in the overall performance of RF, where XGBoost leverages gradient boosting and regularization techniques. The purpose is to improve predictive accuracy while mitigating overfitting. Overall, the hybrid approach enhances model performance and addresses some limitations of RF, like vulnerability to class imbalance and challenges in interpretability.

The reviewed studies have revealed that RF has the capacity to predict BC in a patient very well. Nevertheless, none of the studies have shown expert validation of the results. Hence, this study works on developing a prediction system for BC, followed by validation of the results by a medical specialist. Table 1 provides a comparative analysis of the reviewed studies, detailing the datasets used and their respective percentages of accuracy.

Table 1
Comparative analysis of the related works

Author	Year & Publication	Dataset	Accuracy
Macaulay et al. (2021)	2021 Cancer Treatment and Research Communications	180 subjects of African women in Lagos State, Nigeria, with 90 confirmed as BC cases and 90 benign cases	Accuracy: 91.67% Sensitivity: 87.10% Specificity: 96.55% Area Under Curve (AUC): 92%
Minnoor & Baths (2022)	2022 International Conference on Machine Learning and Data Engineering	Wisconsin BC Diagnostic dataset of UCI Repository. 569 instances (samples) of tumors, with 212 classified as malignant and 357 classified as benign.	Initial dataset with 16 features: 100% Minimal dataset with eight features: 99.3%
Duan et al. (2024)	2024 Computers in Biology and Medicine	Gene Expression Omnibus (GEO) GSE9893 Dataset: 155 samples, 48 developed distant metastasis, while 107 did not. GSE43837 Dataset: 38 samples with 19 patients had developed distant metastasis, and 19 had not.	Accuracy: 93.6% F1-score: 88.9% Area Under Curve (AUC): 91.3%.

Table 1 (continue)

Author	Year & Publication	Dataset	Accuracy
Yifan et al. (2021)	2021 IEEE 3rd International Conference on Communications, Information System and Computer Engineering (CISCE 2021)	Wisconsin BC Diagnostic dataset, UCI Machine Learning Repository. 569 samples of tumors, with 212 labeled as malignant and 357 labeled as benign.	Accuracy: 98.6%

Bootstrapping is widely used in random forests, particularly for breast cancer prediction. It creates multiple subsets of the original dataset through resampling, which helps reduce variance and improve overall prediction stability. Multiple studies show that this approach can also lessen the risk of overfitting by allowing more accurate uncertainty estimates (Ishwaran & Lu, 2019; Mentch & Zhou, 2020).

At the same time, bootstrapping can increase computational requirements, especially in high-dimensional settings or when data is limited (Ishwaran & Lu, 2019). Despite these challenges, it remains a valuable method for building random forest models to detect subtle patterns in breast cancer data and provide more reliable predictions.

Comparative Analysis of Machine Learning Models in Breast Cancer Prediction

This study further explores RF and compares it with other machine learning algorithms to deepen understanding. The main models explored in this study include Support Vector Machine (SVM), Logistic Regression (LR) and Random Forest (RF). Each model has its unique strengths and limitations, which must be understood in relation to each other to choose the optimal model for a given task. Rashidi et al. (2019) and Shehab et al. (2022) explain Artificial Intelligence (AI) and Machine Learning (ML) in their study, outlining the basic concepts, types, and applications across healthcare, finance, and transportation. The explanation covers key ML techniques, including supervised, unsupervised, and reinforcement learning, focusing on their use in predictive modeling. The study also highlights challenges such as data quality, model interpretability, and bias and looks at the future potential of AI/ML. The summary of this study is sorted in Table 2.

Based on Table 2, each machine learning model—Random Forest (RF), Support Vector Machine (SVM), and Logistic Regression (LG)—offers unique advantages and limitations in breast cancer prediction. Random Forest excels in performance and feature interpretation but is limited by its lower interpretability and computational intensity. SVM is effective for high-dimensional and non-linear data but requires significant hyperparameter tuning and may struggle with large datasets. Logistic Regression is simple and computationally efficient but often underperforms in complex scenarios and is sensitive to outliers. Therefore, model selection should align with the dataset's characteristics, interpretability needs, and available computational resources (Rashidi et al., 2019; Shehab et al., 2022).

Table 2
Comparative table of strengths and limitations of ML models in breast cancer prediction

Model	Strength	Limitation
Support Vector Machine (SVM)	High accuracy, good for non-linear data, effective in high-dimensional spaces, robust to overfitting.	Requires significant computational power, expensive, sensitive to kernel choice and hyperparameter tuning, hard to interpret, limited scalability.
Logistic Regression (LR)	Simple, interpretable, fast to train, effective for linearly separable data.	Struggles with non-linear relationships and data, prone to underfitting with complex data, and sensitive to outliers.
Random Forest (RF)	It is robust against overfitting, handles large and complex datasets well, provides feature importance, high accuracy and robustness, and there is no need for feature scaling.	Computationally intensive, slow to predict, limited interpretability compared to LR and high memory usage.

MATERIALS AND METHODS

This study utilizes the RF algorithm to predict BC in a patient. The approach is designed to process user-inputted data via an interface that receives eight significant attributes to predict the disease's existence. The RF model starts with bootstrapping subsets of the dataset to construct multiple decision trees. Each tree uses information gain entropy to determine the best attribute for splitting the data at each node. This approach guarantees that the model captures complex interactions between tumor characteristics. Predictions are made across all individual trees within the group, and the outcome is determined through a majority voting mechanism. This method enhances the robustness and generalizability of predictions, providing reliable assessments of whether a tumor is malignant or benign. The system framework of this study is shown in Figure 1.

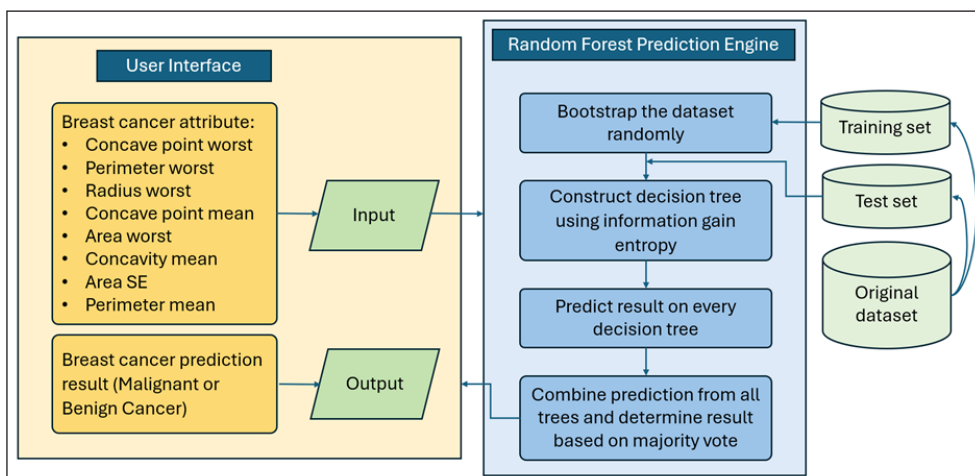


Figure 1. System framework

Dataset Selection and Preparation

Dataset Selection

The first step in the prediction system process is to gather the dataset. The dataset for this study is employed from the Kaggle platform: the BC Wisconsin (Diagnostic) Data. The dataset encompasses 570 medical records, each derived using the Fine Needle Aspiration (FNA) technique. FNA is a quick and straightforward procedure that involves extracting fluid or cells from a breast lesion or cyst using a thin needle, like those used for blood draws. The dataset was compiled by a physician at the University of Wisconsin Hospital, Dr William H. Wolberg. The dataset records BC diagnoses in 30 dimensions. This dataset is already cleaned up in the aspect of missing data by the creator of the dataset. The initial attributes are 30 and are reduced to 8, the top important attributes contributing to the algorithm learning. This study discovered

Principal Component Analysis (PCA) as an extra feature selection method. PCA converts the dataset into a set of orthogonal components ranked by the amount of variance they capture, thus lowering dimensionality while retaining the most critical information. This method enhanced the RF model's computational effectiveness and predictive ability. It can recognize and prioritize key patterns within the 30-dimensional dataset. Using PCA, the system could effectively recognize the most informative features and eliminate redundancies. However, for this study, the manual selection of eight features was believed to be optimal based on their domain relevance and statistical importance. Figure 2 shows the importance of each attribute among many contributing factors between all 30 attributes (Dai et al., 2018).

The blue line in Figure 2 represents the significance of auxiliary diagnosis, implying the attributes that impact the prediction. For instance, the "concave point worst" has numerous blue lines, indicating a greater impact on the prediction result than the "concavity mean," which has fewer blue lines. After knowing the top 8 importance attributes, the original dataset is copied to create a new set encompassing 570 sets of data with only eight important

Variable	Score	
CONCAVE_POINTS_WORST	100.00	
PERIMETER_WORST	79.32	
RADIUS_WORST	71.99	
CONCAVE_POINTS_MEAN	63.48	
AREA_WORST	56.40	
CONCAVITY_MEAN	30.88	
AREA_SE	28.75	
PERIMETER_MEAN	28.23	
AREA_MEAN	25.19	
CONCAVITY_WORST	24.13	
RADIUS_MEAN	18.60	
PERIMETER_SE	7.63	
RADIUS_SE	7.30	
COMPACTNESS_MEAN	4.85	
COMPACTNESS_WORST	3.55	
TEXTURE_WORST	3.36	
SYMMETRY_WORST	2.78	
CONCAVITY_SE	2.56	
SMOOTHNESS_WORST	2.04	
TEXTURE_MEAN	1.57	
FRACTAL_DIMENSION_WORST	1.31	
TEXTURE_SE	.56	
SMOOTHNESS_MEAN	.50	
SYMMETRY_SE	.48	
FRACTAL_DIMENSION_MEAN	.46	
CONCAVE_POINTS_SE	.42	
SMOOTHNESS_SE	.41	
FRACTAL_DIMENSION_SE	.39	
SYMMETRY_MEAN	.34	
COMPACTNESS_SE	.19	

Figure 2. Level of importance for each attribute

attributes, which are concave point worst, perimeter worst, radius worst, concave point mean, area worst, concavity mean, area standard error (SE), perimeter mean and target. The dataset has also been labeled with 1 for malignant cancer and 0 for benign cancer.

Import Dataset to Python

Several predefined Python libraries are employed to preprocess the dataset. Pandas and NumPy are the libraries used for data preprocessing. Panda is a library used to import and manage datasets. NumPy is a library used for arrays, matrices, and various tools for working with arrays, which is very useful for machine learning. After these predefined libraries are installed, the dataset is brought in through the `read_csv()` function of the Pandas library from the dataset file `data.csv` (Table 3).

Table 3
Imported dataset

No	Concave Point Worst	Perimeter Worst	Radius Worst	Concave Point Mean	Area Worst	Concavity Mean	Area Standard Error	Perimeter Mean	Target
1	0.2654	184.6	25.38	0.1471	2019	0.3001	153.4	122.8	1
2	0.186	158.8	24.99	0.07017	1956	0.0869	74.08	132.9	1
3	0.243	152.5	23.57	0.1279	1709	0.1974	94.03	130	1
:	:	:	:	:	:	:	:	:	:
568	0.1418	126.7	18.98	0.05302	1124	0.09251	48.55	108.3	1
569	0.265	184.6	25.74	0.152	1821	0.3514	86.22	140.1	1
570	0	59.16	9.456	0	268.6	0	19.15	47.92	0

It is crucial in machine learning to differentiate the feature matrix, consisting of independent and dependent variables in the dataset. In the `data.csv` dataset, the independent variables are the eight features: the concave point worst, perimeter worst, radius worst, concave point mean, area worst, concavity mean, area standard error (SE), and perimeter mean. The dependent variable is the target, referred to in the last column in Table 3. The `iloc[]` method of the Pandas library will be used to extract an independent variable. The method's function is to extract the first eight columns in the dataset, which are the independent variables, and store them into a NumPy array variable named 'X' as shown in Figure 3(a). A NumPy array variable 'Y' is applied for dependent variables (diagnosis results in the dataset), as shown in Figure 3(b).

Random Bootstrap Dataset

In an RF, bootstrapping means randomly picking data points (with the chance of picking the same one multiple times) from the original dataset to form smaller training sets for each tree. This way, each tree learns from a slightly different set of examples, which helps the whole forest make more accurate and stable predictions.

Based on Table 4, the dataset has been bootstrapped to allow each decision tree in the forest to be trained on a different data set and reduce overfitting. Moreover, Table 4 shows only one bootstrap dataset. The number of bootstrapped datasets depends on the number of trees constructed in the RF. If there are 100 trees, there will be 100 bootstrap datasets created from the original dataset. Figure 5 shows the code for bootstrapping the dataset.

```
Determine the total number of samples in X (n_samples).
Generate n_samples random indices (idxs) from the range [0..n_samples - 1] with replacement
Extract the rows in X corresponding to idxs, store in X_boot.
Extract the rows in y corresponding to idxs, store in y_boot.
Return X_boot, y_boot.
```

Figure 5. Bootstrap pseudocode

This function is called *bootstrap_samples*, which creates a bootstrapped sample of the input data represented by *X* and *y*. This bootstrapped sample is created by randomly selecting elements from *X* and *y* from the dataset with replacement, forming a smaller dataset. This function calculates the number of samples in *X* and then generates an array of indices using the NumPy function *np.random.choice* randomly. Finally, the function returns the *X* and *y* elements corresponding to the selected indices forming the bootstrapped sample.

Table 4
Bootstrap dataset

No	Concave Point Worst	Perimeter Worst	Radius Worst	Concave Point Mean	Area Worst	Concavity Mean	Area Standard Error	Perimeter Mean	Target
1	0.2654	184.6	25.38	0.1471	2019	0.3001	153.4	122.8	1
3	0.243	152.5	23.57	0.1279	1709	0.1974	94.03	130	1
202	0.108	92.15	14.44	0.04107	638.4	0.04187	27.24	78.54	0
548	0.02381	71.12	11.25	0.005495	384.9	0.01012	12.97	65.31	0
:	:	:	:	:	:	:	:	:	:
1	0.2654	184.6	25.38	0.1471	2019	0.3001	153.4	122.8	1

Construct Decision Trees Using Information Gain Entropy

The decision tree in the RF is constructed using entropy information gain as the impurity measure. Entropy measures the impurity or randomness within a dataset. It serves as a criterion for constructing decision trees to divide the data into homogeneous groups. Figure 6 shows the code for the decision tree construct using entropy information gain.

```

Calculate the parent entropy using the function entropy(y).
Split the data using split(X_column, threshold), which returns:
- left_idxes : indices for the left subset
- right_idxes : indices for the right subset
If either left_idxes or right_idxes is empty, return 0.
(No information gain can be obtained if a split results in an empty set.)
Determine the total number of samples, n = length(y).
Compute the size of each split:
- n_l = length(left_idxes)
- n_r = length(right_idxes)
Calculate the entropy of each child set:
- e_l = entropy(y[left_idxes])
- e_r = entropy(y[right_idxes])
Compute the weighted average of these child entropies:
- child_entropy = (n_l / n) * e_l + (n_r / n) * e_r
Subtract the child entropy from the parent entropy to get the information gain:
- information_gain = parent_entropy - child_entropy
Return information_gain.

```

Figure 6. Decision tree construct using entropy information gain pseudocode

In this code, the function created is named `_information_gain`, which calculates the information gain to create the decision tree. The first line of the method assigns the parent entropy, which is the entropy of the target variable, before splitting. Next, the data is split based on the feature `X_column` and threshold value using the `_split` method, which returns two arrays of indices `left_idxes` and `right_idxes` corresponding to the decision tree's left and right branches. Then, the method calculates the entropy of each group and takes a weighted average to obtain the child entropy. The weight of each group is related to the number of samples in each group. Finally, the method calculates the information gain by subtracting the weighted average entropy of the children from the parent entropy.

Make a Prediction on Every Decision Tree

Many decision trees are created in the RF algorithm, each producing a prediction output regarding whether a given sample is malignant or benign. Each tree produces a prediction output indicating whether a given case is malignant or benign. This prediction process occurs for every tree in the RF algorithm. Figure 7 shows the code for prediction on every decision tree created.

```

Initialize an empty list, predictions.
For each instance x in X:
  a. Use the function traverse_tree(x, root_of_decision_tree) to obtain a prediction.
  b. Append this prediction to the predictions list.
Convert the predictions list to an array.
Return the array of predictions.

```

Figure 7. Prediction on every decision tree pseudocode

This code predicts every decision tree created based on the bootstrap dataset. The prediction's result is stored in an array of X .

Combine Predictions from All Trees and Determine the Result Based on the Majority Vote

Lastly, this RF engine determines the prediction based on the majority result, calculated by tallying the results from all decision trees. The prediction is obtained by determining which category (malignant or benign) has more occurrences, which involves summing up all the 1s and 0s and selecting the category with the greater count. Figure 8 shows the code used to combine tree predictions and determine the result.

This code will take a set of inputs (X) and run the prediction function for each decision tree in the set of trees stored in the model. It then collects the predictions for each sample, switches the axis to group the predictions for each sample, and finally chooses the one with majority votes from the tree predictions for each sample as the final prediction.

```

Initialize an empty list called tree_predictions.
For each tree in trees:
  a. Obtain the tree's predictions for all instances in X, call this partial_preds.
  b. Append partial_preds to tree_predictions.
Convert tree_predictions to a 2D array with shape (#trees, #instances).
Swap its axes to have shape (#instances, #trees), so each row now corresponds to a
single instance and contains predictions from each tree.
For each row (set of predictions for one instance):
  a. Determine the majority-vote label (e.g., using a function most_common_label).
  b. Add this label to a new list of final_predictions.
Convert final_predictions to an array.
Return final_predictions.

```

Figure 8. Combine prediction from all trees pseudocode

Hybrid Model Development

To further evaluate the robustness and performance of the prediction system, hybrid models were developed by integrating Random Forest (RF) with boosting algorithms such as AdaBoost and XGBoost (Refer Table 5). For the RF-AdaBoost hybrid, misclassified occurrences from RF were iteratively reweighted to enhance prediction accuracy. At the same time, XGBoost was used for its gradient-boosting capabilities and effective handling of imbalanced datasets. Both models were trained using the same dataset, with hyperparameters optimized through grid search to ensure fair comparisons. Each hybrid model's performance metrics, including accuracy, precision, recall, and F1-score, were calculated to assess their improvements over standalone RF.

Table 5
Configurations for hybrid models

Model	Algorithm Description	Key Parameters	Optimization Technique
RF (Standalone)	Ensemble of decision trees using majority voting.	Number of trees: 100, Max depth: 10	Random Search
RF + AdaBoost	Boosting misclassified instances iteratively with RF as a base.	Learning rate: 0.1, Number of estimators: 50	Grid Search
RF + XGBoost	Gradient boosting with RF as a base.	Learning rate: 0.1, Max depth: 6, Subsampling: 0.8	Grid Search

RF + AdaBoost

AdaBoost refines the Random Forest (RF) base estimator in this hybrid approach by iteratively adjusting the weights of misclassified instances. This process enables the model to concentrate on more challenging samples in subsequent iterations. The aggregated predictions are derived through a weighted majority voting mechanism, where greater weight is assigned to trees with higher accuracy, enhancing the final output. Key hyperparameters, including the number of estimators and the learning rate, were optimized through grid search to balance computational efficiency and predictive accuracy.

RF + XGBoost

The integration with XGBoost leverages its advanced gradient-boosting capabilities to further refine Random Forest (RF) predictions. XGBoost is particularly effective in handling imbalanced datasets, utilizing regularization techniques and tree pruning to reduce overfitting while maintaining robust predictive performance. RF serves as the base learner in this framework, with XGBoost applied iteratively to enhance its predictions. Key hyperparameters, such as the learning rate, maximum tree depth, and subsampling ratio,

were optimized using grid search to achieve superior model performance. Both hybrid models were trained and tested on the same dataset as the standalone Random Forest (RF) model to ensure direct comparability. Their effectiveness was evaluated using standard performance metrics, including accuracy, precision, recall, and F1-score.

User Interface

The user interface is created using *Streamlit*, an open-source framework mainly used to build data science or machine learning web apps. In this user interface, the user needs to input eight BC attributes: the concave point worst, perimeter worst, radius worst, concave point mean, area worst, concavity mean, area standard error (SE), and perimeter mean. Then, the user can click the Predict button to get the cancer result. Figure 9 shows the user interface.

Accuracy Evaluation

Accuracy assessment is vital in determining machine learning algorithms' efficiency. The process entails comparing the predicted outputs to the actual results and calculating the proportion of correct predictions. The outcome of this evaluation provides valuable information on the model's strengths and weaknesses and enables identifying areas for improvement. In this study, a comprehensive analysis of the model's accuracy is performed to determine its suitability for its intended purpose and make any necessary modifications to enhance its performance. There are four important things for accuracy testing: accuracy, precision, recall, and f1 score. The formulas for each of the tests are as follows.

$$\text{Accuracy} = \frac{(TP + TN)}{(TP + TN + FP + FN)} \quad [1]$$

$$\text{Precision} = \frac{TP}{(TP+FP)} \quad [2]$$

$$\text{Recall} = \frac{TP}{(TP+FN)} \quad [3]$$

$$F1 - \text{Score} = 2 \times \frac{PRECISION \times RECALL}{PRECISION + RECALL} \quad [4]$$

Accuracy measures the proportion of correct predictions made by the model out of the total predictions. Precision is the ratio of true positive predictions to all positive predictions made by the model. Recall, or sensitivity, is the proportion of true positive predictions relative to the total number of actual positive samples. The F1 score, the harmonic mean

of precision and recall, provides a balanced metric that considers both. A high F1 score indicates a well-balanced model in terms of precision and recall. In the formulas, TP stands for True Positive, TN for True Negative, FP for False Positive, and FN for False Negative. These values are all represented in the confusion matrix, a table used in machine learning to assess a classifier's performance by showing the counts of true positive, true negative, false positive, and false negative predictions.

Figure 9. User interface of the prediction system

Expert Evaluation

Selecting a qualified medical expert was a critical step to ensure accurate evaluation. (Moosavi et al., 2024; Vazquez-Zapien et al., 2022) and validation of the research objectives.

The following criteria guided the identification and recruitment of the medical professional for this study, adopted and modified from (Moosavi et al., 2024):

a. Clinical Expertise in Breast Oncology

The medical expert was required to have specialized training in breast oncology and demonstrate extensive experience in diagnosing and treating breast cancer. This encompassed expertise typically found among oncologists, breast cancer surgeons, or radiologists focusing on breast imaging. These qualifications ensured the evaluator's capability to provide detailed and clinically relevant insights.

b. Familiarity with Diagnostic Standards

The expert needed to be well-versed in clinical guidelines, diagnostic criteria, and screening protocols for breast cancer to ensure alignment with current medical practices. This knowledge was necessary to ensure that the feedback and assessments were grounded in present standards.

c. Comfort with Data Analysis and Technology

Although advanced technical expertise was not a requirement, the expert was expected to have a basic understanding of computer predictive algorithms and associated performance metrics. This foundational knowledge enabled the evaluator to engage meaningfully with the study's model validation and effectively interpret its outputs.

d. Objective and Independent Perspective

The expert was selected with careful consideration of potential conflicts of interest to maintain the integrity and neutrality of the evaluation process. Preference was given to candidates without involvement in developing the predictive model, ensuring unbiased assessments and recommendations.

This systematic selection process was critical in identifying a qualified medical expert who could provide high-quality, evidence-based evaluations and contribute to the robustness of the study outcomes.

Figure 10 illustrates a streamlined Expert Validation Process for Clinical Model delineated into six sequential phases: Preliminary Briefing, Dataset Review, Case-Based Evaluation, Model Explainability Tools, Performance Metrics Discussion, Feedback Session, and Iterative Consultation.

The expert validation workflow begins with the Preliminary Briefing, which summarizes the clinical model's objectives, scope, and intended applications. This phase

ensures that stakeholders have a shared understanding of key concepts and expectations. The second phase, Dataset Review, involves a detailed evaluation of the data used for training and validating the model. Experts examine critical aspects such as data quality, representativeness, and potential biases to assess the reliability of the dataset.

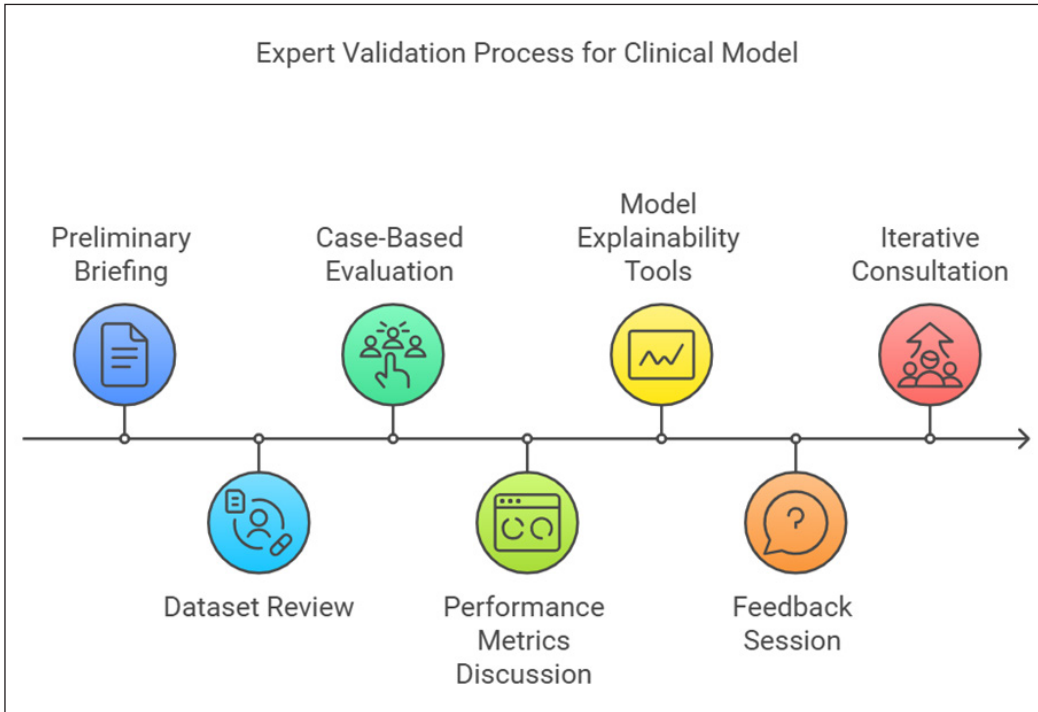


Figure 10. Expert evaluation process

The workflow then progresses to Case-Based Evaluation, where domain-specific test cases are analyzed to assess the model's performance in practical, real-world scenarios. This phase relies on clinical expertise to explore the complex situation that generic metrics may overlook. Next, the Model Explainability Tools phase focuses on interpreting the model's decision-making processes through visualization or analytical techniques. This step enhances transparency and allows experts to confirm that the model's logic aligns with clinical reasoning.

In the Performance Metrics Discussion, the expert reviews quantitative performance indicators tailored to the clinical context, such as accuracy. This phase ensures that the model meets the necessary performance standards for clinical implementation. Additionally, after the initial models are developed, the expert shares her evaluation in the Rating and Sharing stage. This step facilitates reflection on different approaches and quality assessments of the random forest model for breast cancer prediction.

The final stages, Feedback Session and Iterative Consultation, integrate insights from previous phases and refine the model based on expert input. This iterative approach promotes continuous improvement and alignment with clinical needs. The workflow integrates technical analysis with domain expertise to validate clinical models, ensuring they are reliable, interpretable, and suitable for their intended purpose.

RESULTS

This study aims to measure the accuracy of the RF algorithm in predicting BC and get the expert's validation on the dataset and the results produced by the developed system. The list of inputs in as shown in Table 6 illustrates the prediction. After going through all the procedures, the output for this input is “Benign Cancer,” which means non-cancerous growth cells.

Table 6
System input samples

Attributes	Values
Concave Points Worst (0.0–0.291)	0.0000
Perimeter Worst (50.41–251.2)	50.410
Radius Worst (7.93–36.04)	7.930
Concave Point Mean (0.0–0.201)	0.000
Area Worst (185.2–4245.0)	185.200
Concavity Mean (0.0–0.427)	0.000
Area SE (6.802–542.2)	6.802
Perimeter Mean (43.79–188.5)	43.790

Next, the accuracy testing for this BC prediction system is calculated using confusion matrix accuracy. The formulas involved in this calculation are the accuracy formula [1], precision formula [2], recall formula [3], and F1 score formula [4]. Table 7 shows the confusion matrix output and table, and Table 8 shows the calculation for accuracy, precision, recall and F1 Score.

Table 7
Confusion matrix scores

	Predicted No	Predicted Yes
Actual No	TN = 65	FP = 4
Actual Yes	FN = 6	TP = 39

As indicated by the calculations in Table 8, the algorithm's accuracy is 91.23%, indicating that this percentage of predictions made by the model is correct. The algorithm's

precision is 90.70%, meaning that this proportion of positive predictions is accurate. Additionally, the model's recall is 86.67%, showing that the algorithm correctly identifies this percentage of actual positive samples. Finally, the algorithm's F1 score is 88.89%, reflecting a well-balanced performance between precision and recall.

Table 8
Calculation and scores for accuracy, precision, recall and F1

	Calculation	Answer	Percentage
Accuracy	$(39 + 65) / (39 + 65 + 4 + 6)$	0.9123	91.23%
Precision	$39 / (39 + 4)$	0.9070	90.70%
Recall	$39 / (39 + 6)$	0.8667	86.67%
F1 Score	$2 * (0.9123 * 0.8667) / (0.9123 + 0.8667)$	0.8889	88.89%

Additional experiments that combined RF with AdaBoost and XGBoost were conducted to assess the performance of hybrid models. The RF-AdaBoost model achieved an accuracy of 95.4%, a precision of 92.8%, and an F1-score of 91.7%. In comparison, the RF-XGBoost model demonstrated better results, with an accuracy of 96.8%, precision of 94.2%, and an F1-score of 93.5%. These findings highlight that hybrid models performed better than standalone RF by reducing false positives and improving overall robustness. The detailed comparative results are summarized in Table 9.

Table 9
Performance comparison of standalone and hybrid RF models

Model	Accuracy (%)	Precision (%)	Recall (%)	F1-Score (%)
RF (Standalone)	91.23	90.70	86.67	88.89
RF + AdaBoost	95.40	92.80	90.50	91.70
RF + XGBoost	96.80	94.20	92.70	93.50

Expert Evaluation

To ensure the reliability of the validation process, a medical expert who has specialized in breast cancer diagnosis for more than 20 years was selected. The expert selection was based on predefined standards, including clinical expertise in public health, the highest academic qualifications of PhD in public health, and knowledge of machine learning applications.

The first evaluation was on the dataset utilized in this study, derived from Fine Needle Aspiration (FNA) procedures. It is found to be significant and clinically relevant for breast cancer prediction. FNAs are a widely accepted diagnostic tool for assessing suspicious breast lesions, offering minimally invasive means to gather cytological data. Utilizing this dataset for machine learning model development aligns with contemporary diagnostic approaches, where predictive algorithms enhance the accuracy and efficiency of clinical

workflows. An expert reviewed the algorithm results to ensure the credibility of the RF algorithm and its real-world applicability.

While recall, precision, and F1-score indicate how well the machine learning model performs from a computational standpoint, expert review ensures these results are meaningful in actual clinical settings. A seasoned medical professional can interpret whether the model’s high recall reduces missed diagnoses without overburdening the healthcare system or whether strong precision realistically minimizes unnecessary follow-ups. By aligning the model’s metrics with real-world workflow constraints and patient needs, expert input helps confirm that the system excels on paper and holds tangible benefits for clinical decision-making, patient safety, and healthcare efficiency.

The expert's second evaluation assessed the prediction produced by the RF system. The expert was appointed to review the results based on the criteria and indicators in Table 10.

Table 10
Expert rating scale

Criterion	Excellent (5/5)	Good (4/5)	Acceptable (3/5)	Not Acceptable (<3/5)
Model Sensitivity (Recall)	Recall \geq 90%	Recall \geq 85%	Recall \geq 80%	Recall < 80%
Model Precision	Precision \geq 90% (Minimizes false positives, aligns with efficient resource use and patient confidence)	Precision \geq 85%	Precision \geq 80%	Precision < 80%
Overall Balance (F1-Score)	F1 \geq 90%	F1 \geq 85%	F1 \geq 80%	F1 < 80%
Clinical Interpretability and Relevance	Key features and reasoning steps align strongly with medical knowledge; easy integration into workflows	Mostly aligns with standard clinical factors; minor gaps in transparency or complexity	Some clinical alignment may require additional explanation or data refinement	Not clinically interpretable or relies heavily on non-clinical features
Population and Generalizability	The dataset will represent typical patient populations and disease variability	Mostly representative, with minor known biases	Some representativeness concerns that may limit generalizability	Significant concerns about bias or lack of generalizability

Table 11 shows the medical expert's evaluation results. The expert's evaluation was based on standalone RF and hybrid RF performance. The expert also thoroughly reviewed all the inputs given to the system and the predictions produced.

Table 11
Expert evaluation results

Criterion	Standalone RF	RF + XGBoost	Rationale
Model Sensitivity (Recall)	Good (4/5) – (86.67%)	Excellent (5/5) – (92.7%)	Standalone RF misses about 13% of cases, which is acceptable but not ideal. The hybrid model's higher recall significantly reduces missed cancers.
Model Precision	Excellent (5/5) – (90.7%)	Excellent (5/5) – (94.2%)	Both models exhibit high precision, minimizing false positives and unnecessary interventions.
Overall Balance (F1-Score)	Good (4/5) – (88.89%)	Excellent (5/5) – (93.5%)	The hybrid model shows a well-balanced performance, indicating a strong synergy between precision and recall.
Clinical Interpretability and Relevance	Good (4/5)	Good (4/5)	Features used (e.g., FNA-related attributes) are clinically meaningful. Additional explainability details would be helpful for a higher rating.
Population and Generalizability	Acceptable (3/5)	Acceptable (3/5)	Although the dataset is relevant, more information on diversity, sample size, and representativeness is needed to confidently rate higher.

DISCUSSION

This study demonstrates the potential of Random Forest (RF)-based systems for improving breast cancer prediction. The standalone RF model performed well, achieving 91.23% accuracy and an F1-score of 88.89%. Enhancements to the RF algorithm, such as integrating boosting techniques like AdaBoost and XGBoost, further improve prediction accuracy and robustness. These hybrid approaches address the limitations of standalone RF models, such as susceptibility to overfitting and challenges with class imbalances. AdaBoost prioritizes misclassified instances to refine predictions, while XGBoost employs efficient parallel processing to handle large and complex datasets. However, these enhancements require greater computational resources and extensive hyperparameter tuning. These findings highlight the importance of combining algorithms to enhance prediction accuracy and reduce false positives. Expert validation was vital in confirming that the model's predictions were reliable and aligned with real-world clinical needs.

Incorporating expert validation has become a uniqueness of this study, introducing critical qualitative insights. Beyond statistical measures, expert input provides clinical credibility, ensuring the model's predictions align with real-world diagnostic practices. Experts also enhance contextual accuracy, interpreting patterns and assessing their clinical significance. Importantly, their feedback identifies hidden biases, such as systematic underperformance in specific subgroups, thereby promoting fairness in medical AI applications. This is aligned with the findings of a scoping review study by Moosavi et

al. (2024) that highlights the importance of executing an expert review of AI or machine learning clinical algorithms to build robust evidence of their applications.

However, there are still challenges to address. While effective, the dataset used in this study may not reflect the full diversity of breast cancer cases, which could limit its reliability for certain groups. Additionally, the advanced computing needs of hybrid models like RF + XGBoost might make it hard to use in places with fewer resources. Clinical experiments are also needed to see how well the system works in real healthcare environments.

Future work should focus on using more diverse datasets and making hybrid models more efficient and easier to use in actual settings. Expert feedback will continue to play an important role, ensuring the system is practical and fair and meets the needs of healthcare providers.

CONCLUSION

This study developed and validated a breast cancer prediction system based on the Random Forest (RF) algorithm, further enhanced with hybrid models integrating AdaBoost and XGBoost. The standalone RF achieved 91.23% accuracy, while the RF + XGBoost hybrid improved performance to 96.8% accuracy and an F1-score of 93.5%. This hybrid work highlights the system's strength in reducing false positives and enhancing diagnostic reliability. A key novelty of this work is the integration of expert validation in RF for breast cancer prediction, ensuring clinical relevance and alignment with real-world practices. Using clinically significant attributes and robust evaluation metrics underscores its potential as a practical early detection tool. However, limitations such as dataset diversity and computational demands remain. Future research should focus on diverse datasets and efficiency optimization to enhance usability in medical settings.

ACKNOWLEDGEMENTS

This work was supported by Universiti Teknologi MARA, Malaysia.

REFERENCES

- Breast cancer. (2024). *World Health Organization*. <https://www.who.int/news-room/fact-sheets/detail/breast-cancer>
- Dai, B., Chen, R.-C., Zhu, S.-Z., & Zhang, W.-W. (2018). Using Random Forest Algorithm for breast cancer diagnosis. In *International Symposium on Computer, Consumer and Control (IS3C)* (pp. 449-452). IEEE. <https://doi.org/10.1109/IS3C.2018.00119>
- Duan, H., Zhang, Y., Qiu, H., Fu, X., Liu, C., Zang, X., Xu, A., Wu, Z., Li, X., Zhang, Q., Zhang, Z., & Cui, F. (2024). Machine learning-based prediction model for distant metastasis of breast cancer. *Computers in Biology and Medicine*, 169(January), 107943. <https://doi.org/10.1016/j.compbiomed.2024.107943>

- He, Z., Chen, Z., Tan, M., Elingarami, S., Liu, Y., Li, T., Deng, Y., He, N., Li, S., Fu, J., & Li, W. (2020). A review on methods for diagnosis of breast cancer cells and tissues. *Cell Proliferation*, 53(7), 1-16. <https://doi.org/10.1111/cpr.12822>
- Ishwaran, H., & Lu, M. (2019). Standard errors and confidence intervals for variable importance in random forest regression, classification, and survival. *Statistics in Medicine*, 38(4), 558-582. <https://doi.org/10.1002/sim.7803>
- Kinra, P. (2019). Market analysis of breast cancer. *Oncology & Cancer Case Reports*, 6(1), 1-5. <https://www.ioncworld.org/open-access/market-analysis-of-breast-cancer.pdf>
- Li, X., Li, X., Zhang, K., Guan, Y., Fan, M., Wu, Q., Li, Y., Holmdahl, R., Lu, S., Zhu, W., Wang, X., & Meng, L. (2024). Autoantibodies against Endophilin A2 as a novel biomarker are beneficial to early diagnosis of breast cancer. *Clinica Chimica Acta*, 560(March), 119748. <https://doi.org/10.1016/j.cca.2024.119748>
- Macaulay, B. O., Aribisala, B. S., Akande, S. A., Akinnuwesi, B. A., & Olanjo, O. A. (2021). Breast cancer risk prediction in African women using Random Forest Classifier. *Cancer Treatment and Research Communications*, 28, 100396. <https://doi.org/10.1016/j.ctarc.2021.100396>
- Mentch, L., & Zhou, S. (2020). Randomization as regularization: A degrees of freedom explanation for random forest success. *Journal of Machine Learning Research*, 21, 1-36.
- Minnoor, M., & Baths, V. (2022). Diagnosis of Breast cancer using random forests. *Procedia Computer Science*, 218(2022), 429-437. <https://doi.org/10.1016/j.procs.2023.01.025>
- Mohamed, E. S., Naqishbandi, T. A., Bukhari, S. A. C., Rauf, I., Sawrikar, V., & Hussain, A. (2023). A hybrid mental health prediction model using Support Vector Machine, Multilayer Perceptron, and Random Forest algorithms. *Healthcare Analytics*, 3(March), 100185. <https://doi.org/10.1016/j.health.2023.100185>
- Moosavi, A., Huang, S., Vahabi, M., Motamedivafa, B., Tian, N., Mahmood, R., Liu, P., & Sun, C. L. F. (2024). Prospective human validation of artificial intelligence interventions in cardiology: A scoping review. *JACC: Advances*, 3(9), 101202. <https://doi.org/10.1016/j.jacadv.2024.101202>
- Natras, R., Soja, B., & Schmidt, M. (2022). Ensemble machine learning of Random Forest, AdaBoost and XGBoost for vertical total electron content forecasting. *Remote Sensing*, 14(15), 1-34. <https://doi.org/10.3390/rs14153547>
- National Cancer Registry. (2019). *National Cancer Registry Report 2012-2016*. [https://www.moh.gov.my/moh/resources/Penerbitan/Laporan/Umum/2012-2016 \(MNCRR\)/Summary_MNCR_2012-2016_-_06112020.pdf](https://www.moh.gov.my/moh/resources/Penerbitan/Laporan/Umum/2012-2016 (MNCRR)/Summary_MNCR_2012-2016_-_06112020.pdf)
- Park, K. H., Loibl, S., Sohn, J., Park, Y. H., Jiang, Z., Tadjoeidin, H., Nag, S., Saji, S., Md. Yusof, M., Villegas, E. M. B., Lim, E. H., Lu, Y. S., Ithimakin, S., Tseng, L. M., Dejthevaporn, T., Chen, T. W. W., Lee, S. C., Galvez, C., Malwinder, S., ... Harbeck, N. (2024). Pan-Asian adapted ESMO clinical practice guidelines for the diagnosis, treatment and follow-up of patients with early breast cancer. *ESMO Open*, 9(5), 102974. <https://doi.org/10.1016/j.esmoop.2024.102974>
- Rashid, M. M., Yaseen, O. M., Saeed, R. R., & Alasaady, M. T. (2024). An improved ensemble machine learning approach for diabetes diagnosis. *Pertanika Journal of Science and Technology*, 32(3), 1335-1350. <https://doi.org/10.47836/pjst.32.3.19>

- Rashidi, H. H., Tran, N. K., Betts, E. V., Howell, L. P., & Green, R. (2019). Artificial intelligence and machine learning in pathology: The present landscape of supervised methods. *Academic Pathology*, 6, 2374289519873088. <https://doi.org/10.1177/2374289519873088>
- Shehab, M., Abualigah, L., Shambour, Q., Abu-Hashem, M. A., Shambour, M. K. Y., Alsalibi, A. I., & Gandomi, A. H. (2022). Machine learning in medical applications: A review of state-of-the-art methods. *Computers in Biology and Medicine*, 145(November 2021), 105458. <https://doi.org/10.1016/j.combiomed.2022.105458>
- Sumwiza, K., Twizere, C., Rushingabigwi, G., Bakunzibake, P., & Bamurigire, P. (2023). Enhanced cardiovascular disease prediction model using random forest algorithm. *Informatics in Medicine Unlocked*, 41(March), 101316. <https://doi.org/10.1016/j.imu.2023.101316>
- Vazquez-Zapien, G. J., Mata-Miranda, M. M., Garibay-Gonzalez, F., & Sanchez-Brito, M. (2022). Artificial intelligence model validation before its application in clinical diagnosis assistance. *World Journal of Gastroenterology*, 28(5), 602-604. <https://doi.org/10.3748/wjg.v28.i5.602>
- Yifan, D., Jialin, L., & Boxi, F. (2021). Forecast model of breast cancer diagnosis based on RF-AdaBoost. In *2021 IEEE 3rd International Conference on Communications, Information System and Computer Engineering (CISCE)* (pp. 716-719). IEEE. <https://doi.org/10.1109/CISCE52179.2021.9445847>
- Zuo, T., Zeng, H., Li, H., Liu, S., Yang, L., Xia, C., Zheng, R., Ma, F., Liu, L., Wang, N., Xuan, L., & Chen, W. (2017). The influence of stage at diagnosis and molecular subtype on breast cancer patient survival: A hospital-based multi-center study. *Chinese Journal of Cancer*, 36(1), 1-10. <https://doi.org/10.1186/s40880-017-0250-3>

REFEREES FOR THE PERTANIKA JOURNAL OF SCIENCE & TECHNOLOGY

Vol. 33 (S3) 2025

The Editorial Board of the *Pertanika* Journal of Science and Technology wishes to thank the following:

Azlan Ismail
UiTM, Malaysia

Mohamed Othman
UPM, Malaysia

Azlin Ahmad
UiTM, Malaysia

Mohd Fadzli Marhusin
USIM, Malaysia

Azliza Mohd Ali
UiTM, Malaysia

Noor Hafhizah Abd Rahim
UMT, Malaysia

Azwa Abdul Aziz
UniSZA, Malaysia

Norshakirah Ab Aziz
UTP, Malaysia

Fitri Maya Puspita
Sriwijaya University, Indonesia

Nur Syarafina Mohamed
UTM, Malaysia

Haryati Jamaluddin
UTM, Malaysia

Sarahani Harun
UKM, Malaysia

Israa Abdulwahab Al-Baldawi
University of Baghdad, Iraq

Siti Nurul Ain Md Jamil
UPM, Malaysia

Jafreezal Jaafar
UTP, Malaysia

Siti Shilatul Najwa Sharuddin
UKM, Malaysia

Lee Tin Sin
UTAR, Malaysia

Wan Lutfi Wan Johari
UPM, Malaysia

Megat Usamah Megat Johari
UPM, Malaysia

Zolidah Kasiran
UiTM, Malaysia

Mohamad Anuar Kamaruddin
USM, Malaysia

UiTM - Universiti Teknologi MARA
UKM - Universiti Kebangsaan Malaysia
UMT - Universiti Malaysia Terengganu
UniSZA - Universiti Sultan Zainal Abidin
UPM - Universiti Putra Malaysia

USIM - Universiti Sains Islam Malaysia
USM - Universiti Sains Malaysia
UTAR - Universiti Tunku Abdul Rahman
UTM - Universiti Teknologi Malaysia
UTP - Universiti Teknologi PETRONAS

While every effort has been made to include a complete list of referees for the period stated above, however if any name(s) have been omitted unintentionally or spelt incorrectly, please notify the Chief Executive Editor, *Pertanika* Journals at executive_editor.pertanika@upm.edu.my

Any inclusion or exclusion of name(s) on this page does not commit the *Pertanika* Editorial Office, nor the UPM Press or the university to provide any liability for whatsoever reason.

Enhancing Leachate Treatment with Electrocoagulation: A Computational Approach Using Response Surface Methodology <i>Mahmoud A. M. Al-Alwani, Alia Atasha Arisucman, Zadariana Jamil and Azianabiha A Halip Khalid</i>	123
Elucidation of <i>Chromolaena odorata</i> Extract's Pharmacological Potential Through Integration of Network Pharmacology and Molecular Docking Study <i>Nur 'Ainun Mokhtar, Fatahiya Mohamed Tap, Iswaibah Mustafa, Mohd Shahrul Nizam Salleh, Norzila Mohd, Nurhannani Ahmad Rozani and Norazlan Mohmad Misnan</i>	141
Breast Cancer Prediction: A Random Forest-based System with Expert Validation <i>Sharifah Nurulhikmah Syed Yasin, Aiman Azhar and Rajeswari Raju</i>	157

Pertanika Journal of Science & Technology

Vol. 33 (S3) 2025

Content

Preface	i
<i>Mohd Sobri Takriff, Mazidah Puteh and Norulhidayah Isa</i>	
Full Factorial Design for Formulation and Optimisation of Polyvinyl Alcohol with Starch Composite Using Conventional Injection Moulding	1
<i>Mohd Shahrul Nizam Salleh, Roshafima Rasit Ali, Norzila Mohd, Fatahiya Mohamed Tap, Iswaibah Mustafa and Zatil Izzah Tarmizi</i>	
Weeds Detection for Agriculture Using Convolutional Neural Network (CNN) Algorithm for Sustainable Productivity	15
<i>Khairun Nisa Mohammad Nasir, Hasiyah Mohamed, Norshuhani Zamin and Rajeswari Raju</i>	
Mathematical Modelling for Performance Prediction of Ex-Mining Lake Water Phytoremediation by <i>Scirpus Grossus</i>	37
<i>Norhaslina Mohd Sidek, Siti Rozaimah Sheikh Abdullah and Sarifah Fauziah Syed Draman</i>	
Modelling Heterogeneous Traffic Performance During Non-Recurrent Congestion (NRC): A Case Study of Tugu Bundaran Sweta Intersection	49
<i>Ahmad Muharror, Wardati Hashim, Noor Azreena Kamaluddin, Nor Izzah Zainuddin, Nur Ilya Farhana Md Noh and Ekarizan Shaffie</i>	
Enhancing Yolov8 Backbone Using Gradient Descent-based Method for Dental Segmentation	65
<i>Dhiaa Mohammed Abed, Shuzlina Abdul-Rahman and Sofianita Mutalib</i>	
Enhancing Recycling Collection Point Coverage in Seremban City, Malaysia: A Comprehensive Study on Adapting Integer Linear Programming Models with Fixed Capacity Levels	81
<i>Muhammad Zulhazwan Rosni, Zati Aqmar Zaharudin and Adibah Shuib</i>	
Public Sentiment on Awareness of Climate Change Based on Support Vector Machine	97
<i>Norlina Mohd Sabri, Izzatul Syahirah Ismail, Nik Marsyahariani Nik Daud and Nor Azila Awang Abu Bakar</i>	



Pertanika Editorial Office, Journal Division,
Putra Science Park,
1st Floor, IDEA Tower II,
UPM-MTDC Center,
Universiti Putra Malaysia,
43400 UPM Serdang,
Selangor Darul Ehsan
Malaysia

<http://www.pertanika.upm.edu.my>
Email: executive_editor.pertanika@upm.edu.my
Tel. No.: +603- 9769 1622

PENERBIT
UPM
UNIVERSITI PUTRA MALAYSIA
P R E S S

<http://penerbit.upm.edu.my>
Email: penerbit@upm.edu.my
Tel. No.: +603- 9769 8855

